SYNTHETIC METAL CONDUCTORS

A thesis submitted by

Jonathan Charles Fitzmaurice B.Sc., A.R.C.S.,

for the

DEGREE OF DOCTOR OF PHILOSOPHY

UNIVERSITY OF LONDON

AND

THE DIPLOMA OF IMPERIAL COLLEGE

Department of Chemistry

Imperial College of Science, Technology and Medicine

London

SW7 2AY

November 1990

to my parents and sister..

Abstract

The one–dimensional tetracyanoplatinate systems e.g., $K_2Pt(CN)_4Br_{0.3}(H_2O)_3$ (Krogmann salts) and square–planar bis–1,2–dithiolene transition metal complexes with Group 1 cations e.g., $Cs_{0.82}[Pd(mnt)_2].1/2H_2O$ are known to exhibit metallic behaviour to low temperatures.

High yield routes to the potassium and alkyl ammonium (arsonium) salts of $[Pt(dithiolene)(CN)_2]^{2-}$ are reported, by displacement of cod (cod: 1,5–cyclooctadiene) by KCN from Pt(cod)(dithiolene) (dithiolene: mnt, maleonitriledithiolate, $C_2S_2(CN)_2^{2-}$; edt, ethylenedithiolate, $C_2S_2H_2^{2-}$; QDT, quinoxaline–2,3–dithiol), and represents a combination of the two features mentioned above. However, attempts to obtain the partially oxidised salt of $[Pt(mnt)(CN)_2]^{2-}$ by electrosynthetic techniques proved unsuccessful.

Reaction of Au(mnt)(tht)Br (tht: tetrahydrothiophene) and KCN proceeds with reduction of the gold(III) complex to K[18–crown–6][$Au(CN)_2$], as opposed to the intended $[Au(mnt)(CN)_2]^-$. The synthesis of Pt(phenylenediamide)(cod) is reported (phenylenediamide: $C_6H_4(NH)_2^{2-}$) and reaction with KCN yields $K_2Pt(CN)_4$ and $[Pt(C_6H_4(NH)_2)_2]^0$.

An investigation into reactions of metal dithiolene complexes led to the isolation of complexes of the type $Pt(PR_3)_2$(dithiolene) (PR_3: PMe_2Ph, PEt_3) (dithiolene: mnt, edt, QDT). Reaction of $[Bu_4N][Au(mnt)Br_2]$ with $S_4N_4H_4$/base or $1/2[Me_2SnS_2N_2]_2$ led to the preferential formation of $[Bu_4N][Au(mnt)_2]$, as opposed to the intended gold dithiolene sulphur–nitrogen complex.

Synthetic organic metal conductors include the BEDT–TTF salts (BEDT–TTF: bis(ethylenedithio)–tetrathiafulvalene or ET) with a variety of anions with electrical properties ranging from semiconducting

to superconducting (at low temperatures) e.g., β–$[ET]_2X$ (X^-: I_3, AuI_2, IBr_2) and κ–$[ET]_2Cu[N(CN)_2]Br$.

The synthesis and crystal structure of $[ET]_3AuBr_4$ is reported, with semiconducting properties (σ_{rt}: 0.25 Scm^{-1}) and a semiconductor–insulator transition at 125K. The compounds $[ET]_4[Pt(mnt)(CN)_2]$ and $[HMTTeF]_3[Pt(mnt)(CN)_2]$ behave as semiconductors at room temperature ($\sigma_{rt} \sim 10^{-1}$ Scm^{-1}) with activation energies of 90 and 40meV, respectively.

Electrocrystallisation of ET and $[Bu_4N][Au(mnt)Br_2]$ in thf yields α'–$[ET]_2AuBr_2$. It is difficult to ascertain the identity of the product from ET and $[Bu_4N][AuBr_4]$ in benzonitrile; while $[ET]_3AuBr_4$ is a possibility (from elemental analysis), conductivity data suggests otherwise– a possibility being δ–$[ET]_2AuBr_2$.

The crystal structure of $[ET]_3NiCl_4.H_2O$ is reported and was obtained by electrochemical oxidation of ET and $[Ph_4As]_2[Ni(CS_3)_2]$ in 1,1,2–trichloroethane. The $NiCl_4^{2-}$ anion exists in an unusually distorted tetrahedral geometry (∠Cl–Ni–Cl 150°). The salt behaves as a metal (σ_{rt}: 20 Scm^{-1}) to low temperatures (120K) and shows sample dependency.

Electrochemical oxidation of ET and $K[Hg(CN)_2Br]$/18–crown–6 ether in benzonitrile yields $[ET]_5HgBr_3$ and $[ET]_5Hg_3Br_{11}$. $[ET]_5HgBr_3$ behaves as a semicondutor (σ_{rt}: 0.3 Scm^{-1}, E_a = 75meV); $[ET]_5Hg_3Br_{11}$ has already been reported.

The infra–red absorption spectra of compressed pellets and structural/property correlations of the ET salts are discussed.

Contents

		Page
Abstract		..3
Contents		..5
List of Tables and Figures		..8
Acknowledgements		..13
Abbreviations		..14
Part 1		
Transition metal dithiolene compounds		
and their Potential as quasi-1D Conductors		
1.1.1.	Properties of Electron Energy Band Systems	..19
1.1.2.	Peierls Distortion	..24
1.1.3.	Metal-1,2-dithiolene Complexes	..27
1.1.4.	Integral Oxidation States	..29
1.1.5.	Non-integral Oxidation States	..31
1.1.6.	Dmit complexes	..32
1.1.7.	Charge Transfer Salts of Transition Metal-1,2-dithiolene Complexes	..34
1.2.1.	Introduction	..36
1.2.2.	Experimental: Bis(phosphine) Platinum Dithiolene Complexes	..37
1.2.3.	$[Bu_4N][Au(mnt)_2]$	..40
1.2.4.	Crystallographic Data:	
	$Pt(PMe_2Ph)_2mnt$	..41
	$[Bu_4N][Au(mnt)_2]$	..41
1.2.5.	Discussion	..43

1.3.1. Mixed Ligand Platinum Dithiolene Complexes ..51

1.3.2. Experimental:
Bis(cyano) Platinum Dithiolene Complexes ..53
1.3.3. Discussion ..63

1.4.1. References ..70

Part 2

Synthetic Organic Metal Conductors

2.1.1. Introduction ..79

2.2.1. Experimental:
Synthetic Routes to ET ..95
2.2.2. Electrocrystallisations ..98

2.3.1. Conductivity Measurements ..107

2.4.1. FT–IR Absorption Spectra of Polycrystalline
Pressed Samples of Organic Metals ..138

2.5.1. Crystal Structures of $[ET]_3NiCl_4.H_2O$ and ..157
2.5.2. $[ET]_3AuBr_4$ ..163
2.5.3. Structural Characteristics of Donor Molecules ..168
2.5.4. Crystallographic Data:
$[ET]_3NiCl_4.H_2O$ ..170
$[ET]_3AuBr_4$ ..171
2.5.5. Discussion ..185

2.6.1. Appendix 1 ..194

2.7.1. References ..195

List of Tables

Part 1		Page
1.2.1.	Bond lengths and angles for $Pt(PMe_2Ph)_2mnt$	..46
1.2.2.	Bond lengths and angles for $[Bu_4N][Au(mnt)_2]$	..48
1.3.1.	Infra–red assignments for $[Pt(dithiolene)(CN)_2]^{2-}$ salts	..66
1.3.2.	Comparison of the IR assignments for metal–QDT complexes with $[Pt(QDT)(CN)_2]^{2-}$	..67
Part 2		
2.5.1.	Bond lengths for $[ET]_3[NiCl_4].H_2O$	..173
2.5.2.	Bond angles for $[ET]_3[NiCl_4].H_2O$	..175
2.5.3.	Torsion angles for $[ET]_3[NiCl_4].H_2O$	..177
2.5.4.	Bond lengths for $[ET]_3AuBr_4$	..180
2.5.5.	Bond angles for $[ET]_3AuBr_4$	..181
2.5.6.	Torsion angles for $[ET]_3AuBr_4$	..183

List of Figures

Part 1		
1.1.1.	Band structure diagram for a 1–D chain with the effects of lattice (Peierls) distortion shown	..25
1.1.2.	Representation of the bidentate dithiolene ligand	..27
1.1.3.	Spatial extension of the $^3b_{2g}$ molecular orbitals for a square planar transition metal bis–dithiolene complex	..29

1.1.4. Representation of the $M(dmit)_2^{z-}$ complex ..33

1.2.1. Structure of the quinoxaline–2,3–dithiol ligand ..43
1.2.2. Crystal structure of $Pt(PMe_2Ph)_2mnt$ ..46
1.2.3. Crystal structure of $[Bu_4N][Au(mnt)_2]$ and packing of the anions in the unit cell ..47

1.3.1. ^1H nmr assignment for (phenylenediamide)Pt(nbd) ..55
1.3.2. ^1H nmr assignment for QDT ..56
1.3.3. Isotopic abundance calculations for parent ion peaks of: (a) $Pt(edt)(CN)_2^{2-}$ ..
(b) $Pt(mnt)(CN)_2^{2-}$ ..
(c) $Pt(QDT)(CN)_2^{2-}$ ..68
1.3.4. Isotopic abundance calculations for parent ion peaks of: (a) Me_2SnQDT ..
(b) $C_6H_4(NH)_2Pt(cod)$ ..69

Part 2

2.1.1. Structures of organic donor molecules ..81
2.1.2. Projection views of donor dimers in:
(a) κ–$[ET]_2Cu(NCS)_2$ ..
(b) κ–$[ET]_2I_3$ ..
(c) κ–$[MDT–TTF]_2AuI_2$ ..
(d) κ–$[BMDT–TTF]_2Au(CN)_2$ ..86

2.2.1. 1,3–dithiole–2–thione–4,5–dithiolate anion ..95
2.2.2. Synthetic scheme for BEDT–TTF (ET) ..96
2.2.3. Structure of thiapendione ..97
2.2.4. 2–oxo–1,3–dithiole dianion ..97

2.2.5. Elongated plates of α'-$[ET]_2AuBr_2$ grown by electrocrystallisation of $[Bu_4N][Au(mnt)Br_2]$ and ET in thf ..102

2.3.1. Plot of $\ln(\sigma/\sigma_{rt})$ versus temperature for $[ET]_4[Pt(mnt)(CN)_2]$ ..112

2.3.2. Plot of $\ln(\sigma/\sigma_{rt})$ versus 1000/T for $[ET]_4[Pt(mnt)(CN)_2]$ ..113

2.3.3. Plot of $\ln(\sigma/\sigma_{rt})$ versus temperature for $[HMTTeF]_3[Pt(mnt)(CN)_2]$ ..114

2.3.4. Plot of $\ln(\sigma/\sigma_{rt})$ versus 1000/T for $[HMTTeF]_3[Pt(mnt)(CN)_2]$ ..115

2.3.5. Estimation of the average activation energy from $d(\ln\sigma)/d(1/T)$ over the temperature range 290–90K for $[HMTTeF]_3[Pt(mnt)(CN)_2]$ ..116

2.3.6. Plot of $\ln\sigma$ versus $1/T^2$ for $[HMTTeF]_3[Pt(mnt)(CN)_2]$ ..117

2.3.7. Plot of $\ln(\sigma/\sigma_{rt})$ versus temperature for $[ET]_3AuBr_4$ (thf) ..118

2.3.8. Plot of $\ln(\sigma/\sigma_{rt})$ versus 1000/T for $[ET]_3AuBr_4$ (thf) ..119

2.3.9. Plot of $d(\ln\sigma)/d(1/T)$ versus temperature for $[ET]_3AuBr_4$ (thf) ..120

2.3.10. Plot of $\ln(\sigma/\sigma_{rt})$ versus temperature for $ET/AuBr_4$ (benzonitrile) ..121

2.3.11. Plot of $\ln(\sigma/\sigma_{rt})$ versus 1000/T for $ET/AuBr_4$ (benzonitrile) ..122

2.3.12. Plot of $\ln(\sigma/\sigma_{rt})$ versus temperature for $[ET]_3[NiCl_4].H_2O$ (crystal {a}) ..123

2.3.13. Plot of $\ln(\sigma/\sigma_{rt})$ versus 1000/T for

$[ET]_3[NiCl_4].H_2O$ (crystal {a}) ..124

2.3.14.1. Plot of $\ln(\sigma/\sigma_{rt})$ versus temperature for $[ET]_3[NiCl_4].H_2O$ (crystal {b}) ..125

2.3.14.2. Combined conductivity plots for crystals {a} and {b} of $[ET]_3[NiCl_4].H_2O$ ..126

2.3.15. Plot of $\ln(\sigma/\sigma_{rt})$ versus 1000/T for $[ET]_3[NiCl_4].H_2O$ (crystal {b}) ..127

2.3.16. Plot of $d(\ln\sigma)/d(1/T)$ versus temperature for $[ET]_3[NiCl_4].H_2O$ (crystal {b}) ..128

2.3.17. Plot of σ versus temperature for $[ET]_3[NiCl_4].H_2O$ (crystal {b}) and best fit to the expression $\exp(-\Delta_H/K_BT).T^{-\alpha}$ ..129

2.3.18. Plot of $\ln(\sigma/\sigma_{rt})$ versus temperature for $[ET]_3[NiCl_4].H_2O$ (crystal {b} after phase change) ..130

2.3.19. Plot of $\ln(\sigma/\sigma_{rt})$ versus 1000/T for $[ET]_3[NiCl_4].H_2O$ (crystal {b} after phase change) ..131

2.3.20. Plot of $\ln\sigma$ versus $1/T^2$ for $[ET]_3[NiCl_4].H_2O$ (crystal {b} after phase change) ..132

2.3.21. Plot of $\ln(\sigma/\sigma_{rt})$ versus temperature for $ET/NiCl_4$ (benzonitrile) ..133

2.3.22. Plot of $\ln(\sigma/\sigma_{rt})$ versus 1000/T for $ET/NiCl_4$ (benzonitrile) ..134

2.3.23. Plot of $d(\ln\sigma)/d(1/T)$ versus temperature for $ET/NiCl_4$ (benzonitrile) ..135

2.3.24. Plot of $\ln(\sigma/\sigma_{rt})$ versus temperature for $[ET]_5HgBr_3$ ..136

2.3.25. Plot of $\ln(\sigma/\sigma_{rt})$ versus 1000/T for $[ET]_5HgBr_3$ ..137

2.4.1. Absorption spectra for $[ET]_4[Pt(mnt)(CN)_2]$, $[HMTTeF]_3[Pt(mnt)(CN)_2]$ and $[ET]_5HgBr_3$ ..151

2.4.2. Absorption spectra for $[TTF]_5AuBr_4$ and $[TTF]_2[Pt(mnt)(CN)_2]$ ..152

2.4.3. Absorption spectra for α'-$[ET]_2AuBr_2$, $ET/AuBr_4$ (benzonitrile) and ET_3AuBr_4 (thf) ..153

2.4.4. Absorption spectra for $[ET]_3[NiCl_4].H_2O$, $ET/NiCl_4$ (benzonitrile) and $ET/CoCl_4$ ..154

2.4.5. Absorption spectra for $ET/Pd_2Cl_6^{2-}$, $ET/Pd_2Br_6^{2-}$ and $ET/Pt_2Cl_6^{2-}$ ..155

2.4.6. Vibrational assignments of neutral TTF ..156

2.5.1. Structure of ET molecule and numbering scheme ..158

2.5.2. View down crystallographic a axis in $[ET]_3[NiCl_4].H_2O$ ..159

2.5.3. View down crystallographic b axis in $[ET]_3[NiCl_4].H_2O$ ..160

2.5.4. View down crystallographic c axis in $[ET]_3[NiCl_4].H_2O$ ..161

2.5.5. Graphical representation of the ratio b/a (C–S/C=C bond lengths for the central TTF portion of ET) versus e (charge) for known ET salts ..162

2.5.6. View down crystallographic a axis in $[ET]_3AuBr_4$ ..164

2.5.7. View down crystallographic b axis in $[ET]_3AuBr_4$ ..165

2.5.8. View down crystallographic c axis in $[ET]_3AuBr_4$ ..166

2.5.9. Perspective views of $[ET]_3AuBr_4$ in the unit cell ..167

2.5.10. The π–framework of neutral ET and ethylene conformations of the six–membered ethylenedithiolate ring ..168

2.5.11. Packing arrangements of donor molecules in β–$[ET]_2X$ and β–$[ET]_2AuCl_4$ salts ..186

Acknowledgements

I would like to thank my supervisor Dr J D Woollins for his help during the past three years. I am indebted to Alexandra Slawin (Woollins) and Dr D J Williams for X-ray crystallographic structure determinations. Similarly, I am grateful to 3M, Harlow for sponsorship and collaboration with Dr A J Lindsay.

A vital contribution was provided by Prof. A E Underhill's research group at Bangor, through the use of their conductivity apparatus. Special mention is reserved for Stephen Edge and Charlie Wainwright for their advice, friendship and help in obtaining conductivity measurements.

Thanks to past (Paul, nee' Reg, Ivan and Yogi) and present members (Mark, Julia, Vanessa and Paul (PFK)) of 551 for enduring my presence for the past three years. Indeed, knowing Dr P F Kelly has been an experience one is unlikely to forget– incidents ranging from wet paper towel fights, cardice battles, corridor football games and rubber glove fights to name but a few (i hope this does not indicate a more vehement side to my personality). Richard Wickham also deserves a mention for "enlightening" topics of conversation (football, golf and Viz) over the summer.

Other people who deserve a mention are Dr Andy Dengel, especially for organizing cricket, Dr Edmond Magner, Chris Leahy, Philip Clapp, Victor Christou *et al.*

Thanks also to Patrick Johnston for producing the tables and for house sharing (also included, Jim and Jon) over the past few years.

List of Abbreviations

Å	Angström unit, 10^{-10}m
a,b,c,α,β,γ	Crystallographic lattice parameters
a,b,c mode	Intrastacking modes
a_g	Totally symmetric (gerade) stretching vibration
ab initio	From first principles
asym	Asymmetric stretching vibration
β^*	Refers to higher superconducting temperature, due to application of pressure
BCS	Superconducting mechanism (Bardeen, Cooper and Schrieffer)
bdt	Benzenedithiolate
BEDT–TTF	Bis(ethylenedithio)–tetrathiafulvalene
BEDO–TTF	Bis(ethylenedioxy)–tetrathiafulvalene
BMDT–TTF	Bis(methylenedithio)–tetrathiafulvalene
Bu	Butyl (superscript ^{t}, tertiary)
CDW	Charge density wave
cod	Cycloocta–1,5–diene
CT	Charge transfer
dbu	1,8–Diazabicyclo[5.4.0]undec–7–ene
DMET	Dimethyl(ethylenedithio)–diselenadithiafulvalene
dmit	4,5–dimercapto–1,3–dithiole–2–thione
dmso	Dimethylsulphoxide
ϵ_F	Fermi energy
E_a	Activation energy
E_g	Band gap energy
edt	Ethylenedithiolate

e–mv	Electron molecular vibrational
esr	Electron spin resonance
Et	Ethyl
FT	Fourier transform
h	Planck's constant, 6.626×10^{-34} Js ($\hbar = h/2\pi$)
HMTTeF	Hexamethylenetetratellurafulvalene
IR	Infra–red
K_B	Boltzmann's constant, 1.381×10^{-23} JK^{-1}
K_F	Fermi wavevector ($\AA^{-1}$)
λ	Electron phonon coupling constant
L,Z,W mode	Interstacking packing modes
μ	Mobility of charge carriers ($\propto T^{-\alpha}$)
MDT–TTF	Methylenedithio–tetrathiafulvalene
MI	Metal–insulator transition
mnt	Maleonitriledithiolate
ν	frequency, Hz $\equiv$ cm^{-1}
nbd	2,5–norbornadiene
NMP	N–methylphenazinium
QDT	Quinoxaline–2,3–dithiol
ρ	Resistivity (Ωcm $\equiv$ S^{-1}cm)
σ_{rt}	Conductivity ($= \rho^{-1}$) at room temperature
SCF–MO/MP2	Self–consistent field, molecular orbital and second–order Mosser Plesset calculations
SDW	Spin density wave
sym	Symmetrical vibration
synmetal	Synthetic Metal
T_c	Superconducting transition temperature
T_{MI}	Metal–insulator transition temperature
tcdt	Tetrachlorobenzene dithiolate

tce	1,1,2–trichloroethane
TCNQ	7,7,8,8–tetracyanoquinodimethane
tfd	Trifluorodithiolate
TMTSF	Tetramethyltetraselenafulvalene
TTF	Tetrathiafulvalene
TTT	Tetrathiatetracene

Part 1:
Transition metal dithiolene compounds and their potential as quasi-1D conductors.

Introduction

Considerable interest has focused on the chemical and physical properties of one–dimensional materials and the observation of phenomena such as metal–insulator transitions and cooperative magnetic interaction.

Both inorganic and organic examples of one–dimensional materials have been studied. They have been the subject of a number of excellent reviews: one–dimensional inorganic systems have been reviewed by Krogmann[1], Thomas and Underhill[2] and several short reviews by Underhill[3] and Gomm[4]. The electrical properties have been reviewed recently by Underhill[5]. The design, synthesis and physical properties of organic metals have been detailed by Garito and Heeger[6], Yagubskii and Khidekel'[7] and Williams et al[8].

This review concentrates on inorganic materials which exhibit or potentially exhibit a columnar structure, in particular square–planar third row transition metal complexes which exhibit the properties of anisotropic electrical conductivity and the first–row transition metal complexes which exhibit anisotropic cooperative magnetic behaviour.

The materials included in this review are crystalline solids with a common configuration of well defined molecules stacked in linear parallel rows or strands to form one–dimensional columns or chains. One–dimensionality refers to a "gross" (a factor of 100 or greater) anisotropy in the value of at least one intensive variable of the system, for example, conductivity or magnetic susceptibility along a preferred direction. The anisotropy factor is never infinite and may be modified by three–dimensional effects.

The electrical properties have been summarized by Miller and Epstein[9], with emphasis placed on the one electron band theory (which assumes all electrons move independently of each other in a perfect

uniform lattice) in relation to understanding the effects of lattice distortion and the Peierls transition. More sophisticated models are outlined, based on cooperative interactions (e.g., electron–phonon coupling and electron–electron correlation).

1.1.1. Properties of Electron Energy Band Systems

(a) Metals and semimetals: Partial filling of the electron energy band characterises a metal– a semimetal has two or more partially filled bands. Infinitesimal separation of the unoccupied and occupied energy levels by wavevector k allows a net change in electron momentum ($\hbar k$) when an electric field is applied– as a result metals are good conductors with resistivity decreasing to a residual value as the temperature is lowered (e.g., the "ideal" 3–D metal sodium)[10], unless a transition to a semiconducting/insulating state occurs, such as in the one–dimensional partially oxidised tetracyano–platinate systems (i.e., $K_2Pt(CN)_4Br_{0.3}.3H_2O$)[1].

Metals are also characterised by:

(1) Temperature independent Pauli spin susceptibility given by $\chi = 2\mu_B^2\rho(\varepsilon_F)$ where μ_B is the Bohr magneton and $\rho(\varepsilon_F)$ is the density of states per unit energy per spin at maximum occupied energy (Fermi energy, ε_F)

(2) A specific heat term C, where $C = \alpha T + \beta T^3$ (readily observed at liquid helium temperatures)

(3) A characteristic plasma frequency dependence of reflectivity, conductivity and dielectric constant.

(b) Semiconductors and insulators: A material with an energy gap E_g between filled and empty energy bands. If the energy gap is small enough, thermal excitation of a significant number of "free" electrons can occur into the lowest energy band i.e., a semiconductor, otherwise it is termed an insulator. Semiconductors have accepted conductivities of 10^{-9} to 10^{-2} Scm^{-1} ($\Omega^{-1}cm^{-1}$) at room temperature. At the upper end the conductivity is the order of a poor metallic conductor, below, that of an insulator (e.g., phthalic acid, $\sigma \sim 10^{-15}$ Scm^{-1}) with an activation energy (E_a) greater than 5eV. Conductivities in insulators is frequently interpreted in terms of models other than the band model.

Semiconductor properties are dominated by the number of free charge carriers. Intrinsic semiconductors are those whose free carriers are predominately electrons thermally excited across the energy gap from the filled energy band and the holes (empty states in otherwise filled valence band) thereby created.

In the simplest approximation, the conductivity σ, is a function of E_g:

$$\sigma \propto \exp [- Eg/2K_BT]$$

where K_B is Boltzmann's constant. A plot of $In\sigma$ versus 1/T may be used to determine E_g. The activation energy is related to E_g by $E_a = E_g/2$.

An alternative model is represented by "carrier" hopping between localised centres on individual molecules– conduction is dependent on an activation energy[11] and the temperature dependence of the conductivity may depend on the dimensionality of the system[12].

The phenomenological model proposed by Epstein *et al*[13]. assumes the mobility to be strongly temperature dependent and the concentration of mobile charge carriers assumed to be thermally

activated resulting in $\sigma(T) \propto \exp[-\Delta_H/K_BT].T^{-\alpha}$ where μ (mobility of charge carriers) $\sim T^{-\alpha}$ (α: sample dependent constant).

Intrinsic properties are determined by the host material; extrinsic is where the conductivity is governed by chemical impurities and becomes significant at low temperatures.

(c) Design of a Metallic Band system

To obtain a metallic state, one requires planar molecules without bulky substituents that stack in one–dimensional chains, have a close approach to their nearest neighbours in the chain (for large orbital overlap), and possess a non–even number of electrons per crystallographic repeat unit. Partial oxidation of the π–molecular orbital and/or the d_z^2 orbital would aid band formation by (1) greater extension of the molecular orbital and (2) small molecular orbital overlap in directions perpendicular to the chain increasing the anisotropy. The filled d_z^2 orbital is not the highest occupied molecular orbital, but partial oxidation depletes electron density from the orbital with the formation of a band of energy states which become the highest occupied electron energy levels.

In addition, the molecules should be uniformly spaced to avoid splitting of the electron energy bands and the presence of electron withdrawing groups attached to the molecules forming the chain is useful in reducing coulombic repulsion between the mobile electrons.

The degree of orbital overlap of wavefunctions on adjacent molecules determines if there is formation of delocalised electron energy bands.

The current picture of highly conducting inorganic one–dimensional systems has been established through the exhaustive study of $K_2Pt(CN)_4X_{0.3}.3H_2O$ (X = Cl or Br) (see reviews by Underhill[5] and

Miller and Epstein[9]) and to a lesser extent through the study of other complexes. The $Pt(CN)_4^{1.7-}$ ions form a columnar stacked structure with a short intrachain Pt–Pt separation of 2.88Å. Overlap of $5d_z^2$ and $6p_z$ orbitals of adjacent Pt atoms leads to a delocalised partially filled (~ 7/8) band structure resulting in one–dimensional metallic properties (optical, magnetic and transport) at room temperature.

Emphasis is placed on square–planar third–row transition metal complexes where magnetic properties do not dominate and on divalent first–row transition metals complexes with strong one–dimensional interactions. The propensity for metal–metal band formation is greatest for the third–row elements compared to second and first row transition metals. The metals which form square planar complexes belong to the Co(I), Ni(II) and Cu(III) triads– although examples of each are known, the Rh(I), Ir(I), Pd(II), Pt(II) and Au(III) form the most prevalent square planar complexes.

The importance of ligand field strength is uncertain. Strong field monodentate ligands are associated with the partially oxidized tetracyanoplatinate and halocarbonyliridate[14] systems. In contrast, the partially oxidized bis(oxalato)platinate[5] has a weaker field bidentate ligand, oxalate.

Only the third row d^8 transition metals have clearly formed conducting systems. These metals form square–planar complexes which allow stacking in one–dimensional chains. The larger spatial extent of the $5d_z^2$ orbital relates with stronger intermolecular interactions in the solid. Within a row, as the net charge on the metal is increased, the electron density of the valence orbitals is contracted. Thus the spatial extent of the $5d_z^2$ orbitals decreases through the series Os(O) > Ir(I) > Pt(II) > Au(III). Osmium (O) exhibits the largest spatial extent of the $5d_z^2$ orbitals and forms clusters, whereas Ir(I), Pt(II) and Au(III)

predominately form square planar complexes. Partial oxidation has been reported for several Ir(I) and Pt(II) complexes. Complexes of these metals are easily oxidised to the d^6 Ir(III) and Pt(IV). Two stable oxidation states of a metal complex appear necessary for the existence of a partial oxidised intermediate (this may not be a rigourous condition as band formation may stabilise a previously uncharacterised oxidation state).

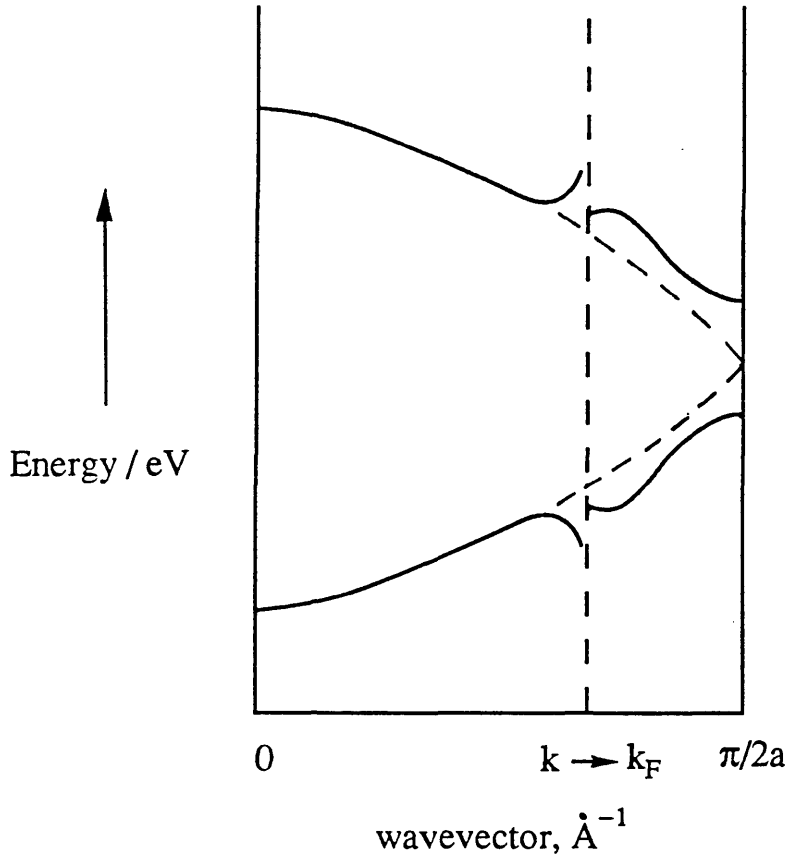
1.1.2. Peierls Distortion[15]

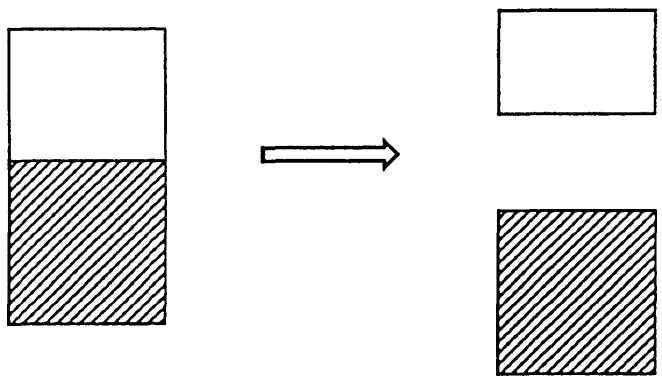
In analogy with the Jahn–Teller effect (F A Cotton and G W Wilkinson)[16], distortion of the symmetry (periodicity) of a chain which has a partially filled electron energy band lowers the total energy of the system.

There is degeneracy and near degeneracy for any partially filled band. The degeneracy is as a result of $E(k) = E(-k)$ for any k in the zone; the near degeneracy is for k's just above or just below the specified Fermi level. If the energy gap which results, coincides with the wavevector of the highest occupied state k_F (k_F is the Fermi wavevector), the occupied states are displaced downwards and empty states raised upwards in energy, resulting in a net reduction of energy (*fig.*, 1.1.1.). The transition arises dynamically through the interaction between the electrons and the quantised lattice vibrations of the solid, phonons[17] ("soft" phonons of wavevector $q = 2k_F$ strongly interact with electrons of wavevector k_F, thereby forming a Kohn anomoly[18] (dip) in the phonon spectrum). The term "soft phonon modes" refers to phonons of lowered energy. The differentiation between a dynamical (Kohn anomoly) or static (Peierls) lattice distortion can be established using inelastic neutron scattering studies[19]. At lower temperatures, the energy (frequency) of the $2k_F$ mode tends to zero and distortion becomes static (Peierls distortion).

The distortion of the lattice (i.e., dimerization) leads to localisation of charge in the one dimensional chain forming a charge density wave which at low temperatures lock together as a result of coulombic attraction, with a resultant large drop in the conductivity. Increasing the dimensionality of the system can couple adjacent chains so that the charge density wave is suppressed.

The Peierls distortion is temperature dependent leading to the





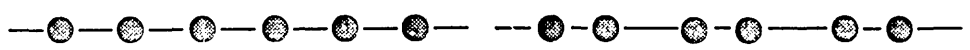


fig., 1.1.1. Allowed energy levels for the uniform chain (dashed line) and distorted chain (solid line). The discontinuity represents an opening of a band gap near the Fermi level, ϵ_F

transition from a band metal to a band semiconductor/insulator as the temperature is lowered below the transition temperature, T_p. A perfect one–dimensional system can only undergo a phase change at 0K; the result of weak 3D intermolecular interactions allows the transition to occur at finite temperatures.

Experimentally, the Peierls distortion may be studied by diffuse X–ray scattering (DXS)[20] experiments in which one–dimensional distortion of chains (or charge density wave) results in weak continuous lines on the layer lines of strong Bragg spots.

1.1.3. Metal–1,2–dithiolene complexes

1,2–dithiolene complexes may be obtained from combination of the appropriate metal atom with the ligand:

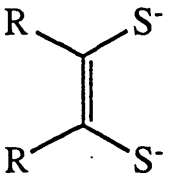


fig., 1.1.2.

in which R = H, CF_3, CN, C_6H_5, CH_3 and C_2H_5 (the RC=CR unit may be part of a benzene ring).

Comprehensive reviews by McCleverty[21], Schrauzer[22], Hoyer *et al*[23], Eisenberg[24] and Underhill[25] detail the synthetic routes towards dithiolenes and their metal complexes.

The ligand in which R = CN was originally obtained by Bähr and Schleitzer in 1955[26] and is usually designated maleonitriledithiolate (mnt). A series of square planar $[M(mnt)_2]^{z-}$ complexes with M = Ni, Cu, Pd, Pt and Au and z = −1 and −2 were prepared and studied in detail in 1962[27]. Since then these complexes have been thoroughly investigated and many others prepared, including those with R = CF_3, H, CH_3, C_6H_5 etc.

Two or three ligands can be associated with the metal atom resulting in different structures. Square planar complexes with two ligands were obtained for M = Ni, Cu, Zn, Pd, Pt and Au[28] and in some cases Fe and Co, with the molecules being associated in dimer pairs[29]. Tris complexes were obtained for $[M(mnt)_3]^{z-}$ where M = V, Cr, Mn, Ge, Mo, Rh, In, Re and Tl[30,31,32,33] with structures intermediate between trigonal prismatic and distorted octahedral.

The bis–1,2–dithiolene square planar complexes, collectively referred to as $[M(S_2C_2R_2)_2]^z$, will be concentrated on, as they can only form linear chain compounds. A variety of oxidation states exist for these compounds, with z = 0, –1 and –2 common and –3 and –4 ionic species have been detected. As a result, facile redox properties are observed in solution suggesting the possibility of charge transport in the solid state.

Interesting electrical and magnetic properties are exhibited by $[M(S_2C_2R_2)_2]^z$ molecules when stacked in metal over metal or metal over sulphur arrays. Evidence suggests the highest occupied molecular orbital is highly delocalised with very low electron density on the metal but considerable spatial extent perpendicular to the plane, which can account for interactions along the chain.

The d^8 dithiolenes are characterised by stable planar radical anions which allow intermolecular interactions through metal–metal (distances of less than 3Å are necessary to allow sufficient overlap of the orbitals to give metallic properties)[34] or metal–sulphur bonds. This is in contrast to TTF–TCNQ and related metals where metallic properties are observed with the closest interatomic distances between adjacent sulphur atoms. Extensive electrochemical properties of the dithiolenes allow the formation of non–integral oxidation states, essential in many, but not all cases to avoid a temperature dependent phase transition between conducting and semiconducting or insulating states and for high conductivity.

There is a great variety of known structures from regular segregated stacks to alternate stacks. In segregated stacks there is the possibility of intermolecular interactions along the chain through overlap of the out of plane $^3b_{2g}$ molecular orbitals (*fig.*, 1.1.3.).

In general, formation of segregated or alternate stacks give rise to cooperative electrical and magnetic behaviour.

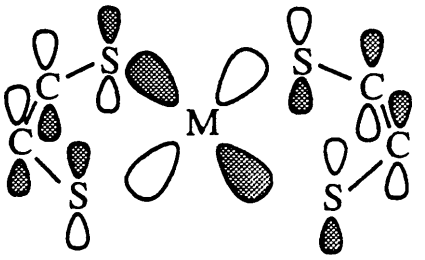


fig., 1.1.3. Spatial extension of the $^3b_{2g}$ molecular orbitals for square planar transition metal bis–dithiolene complexes

1.1.4. Integral oxidation states

Conductivities of various neutral[35,36,37], monoanionic[35,38,39–43] and dianionic[44] complexes have been studied[21,53,65]. The tetraalkylammonium salts (R_4N^+) generally exist in a 2:1 or 1:1 stoichiometry. In the 2:1 salts, the transition metal components are isolated from each other (d(M–M) > 5Å); this does not however prevent interaction between the transition metal components or the presence of interesting properties, e.g., $[Bu_4N]_2[Cu(mnt)_2]$ with regular slipped stacks of $Cu(mnt)_2^{2-}$ anions and d(Cu–Cu) 9.4Å[45,46,47]. The 1:1 systems are all very similar with slipped stacks of metal–dithiolene anions that are associated in pairs with the stacks surrounded by non–interacting cations. $[Et_4N][Ni(mnt)_2]$[48] reveals a columnar structure with molecules stacked as dimers and a large Ni–S overlap consistent with the observed low conductivity and spin–triplet magnetic behaviour. The use of bulky alkyl ammonium cations has resulted in semiconducting compounds with relatively low conductivities at room temperature ($\sigma \sim 10^{-8}$ Scm^{-1}). Weak dimerization is also found to occur for $[Ph_3MeP][M(mnt)_2]$ (M = Ni or Pt)[49] through either the d_{xz} or d_{xy} orbital, which are higher in energy than the d_z^2 orbital.

Dimerization can also be strong as in $[Bu_4N][Co(tcdt)_2]$ and $[Ph_3PCl][Au(tfd)_2]$[50,51]: in each of these cases the distance between the dimers is much greater than the distance within them i.e., d(Co–Co) 10Å. In more tightly bound dimers, the metal atom is displaced by 0.3Å[50,52] out of the plane of the four sulphur atoms; the effect of dimerization, whether weak or strong is limited to minor deviations of the MS_4 unit from planarity[24]. The monoanion complexes have been shown to be more conducting than neutral or dianionic complexes[53,54].

$[NH_4][Ni(mnt)_2].H_2O$[55] was found to be a semiconductor at room temperature (5×10^{-2} Scm^{-1}) with a Ni–Ni spacing of 3.92Å and phase transition occuring between 220–180K which is observed in magnetic susceptibility and conductivity measurements. Conductivities of compressed discs were reported for $Na[M(mnt)_2].1.15H_2O$[48] (M = Ni or Pd) ($\sigma\sim 10^{-1}$ Scm^{-1}) and salts of smaller cations. The dimeric eclipsed $Rb[Pt(mnt)_2].2H_2O$[56] has a conductivity along the metal chain direction (d(M–M) 3.356 and 3.512Å) of 2.5×10^{-5} Scm^{-1}.

Renewed interest has centred upon $[M(S_2C_2(CN)_2]^-$ monoanions (M = Pd or Pt) with small Group 1 cations or NH_4^+. The structure was found to be metal dependent; whereas $[NH_4][Ni(mnt)_2].H_2O$ and $K[Pd(mnt)_2].H_2O$ possesses an equidistant anion stack, $Rb[Pt(mnt)_2].2H_2O$, $[H_3O][Pt(mnt)_2].H_2O$ and $[NH_4][Pd(mnt)_2].H_2O$ exhibit dimer pairs of anions in an eclipsed metal–metal arrangement[54,56,57]. $[Et_4N][Pt(mnt)_2]$ ($\sigma\sim 10^{-8}$ Scm^{-1}) shows anion dimers with a Pt over S configuration while $[H_3O]_x[NH_4]_{1-x}[Pt(mnt)_2].2-xH_2O$ ($\sigma\sim 10^{-5}$ Scm^{-1})[57] exists as an eclipsed Pt over Pt arrangement. While the cation size is important, the palladium dithiolenes show structural characteristics of both nickel and platinum analogues.

1.1.5. Non-integral Oxidation State compounds

Underhill and Ahmad have studied the cation deficient $Li_{0.82}[Pt(mnt)_2].2H_2O$[58,59] and showed the room temperature conductivity along the needle axis to be ~ 100 Scm^{-1}. A two-dimensional network[60] is suggested by short intra and intermolecular contacts and the long Pt-Pt intrachain[62] separation indicates that the bonding within the chain cannot be of simple metal orbital overlap. A Peierls metal-semiconductor transition occurs at ~ 220K as supported by XDS[61] and magnetic susceptibility measurements[62]. Variation of the central metal, cation and substituents of the ligand have also been studied but microcrystalline powders have been formed[63,64,65].

Compounds of the type M'[M"$(mnt)_2$].x(solvent) where M' and M" are divalent transition metal cations have been reported with conductivities as high as 5×10^{-2} Scm^{-1} for M' = Cu and M" = Ni[39]. This has been extended to M" = Pd and Pt[66].

Black plates of $Li_{0.5}[Pt(mnt)_2].2H_2O$[67] show semiconductor properties (σ_{rt}~ 1 Scm^{-1}), with $Pt(mnt)_2^-$ stacked irregularly face to face to form a fourfold distorted linear chain.

$Cs_{0.82}[Pd(mnt)_2].1/2H_2O$[68,69,70] was shown to exhibit metallic behaviour under pressure, the structure containing dimers in an eclipsed configuration but not in a columnar stack arrangement (σ_{rt}~ 5 Scm^{-1} at ambient pressure). The conductivity was attributed to the role of the water molecule in bonding the two dimensional sheet network of S···S anion interactions; a similar explanation was used to explain the conductivity (σ~ 100 Scm^{-1}) in $[H_3O]_{0.33}Li_{0.8}[Pt(mnt)_2].1.67H_2O$, the crystal structure of which indicated a long metal-metal distance[58]. A preliminary investigation of high conductivity in the nickel analogue led to the suggestion that the conductivity is at least in part ligand based,

as supported by evidence of a large Ni–Ni distance[64].

Thus the structure and properties of the materials depend on:

(1) Cation size– small Group 1 metal cations allow close approach of the anions.

(2) The nature of the metal influences the solid state properties. In the series $[M(mnt)_2]^-$ (M = Ni, Pd, Pt) with Group 1 cations, the nickel complexes possess an equidistant stack structure with dimerization occuring at low temperatures. The platinum compounds exist as dimerized anions with diamagnetic ground states at room temperature– an exception being $[H_3O]_{0.33}Li_{0.8}Pt(mnt)_2.1.67H_2O$ which is a metal at room temperature but undergoes a phase transition at 215K to a dimerized state. The palladium series display quite different behavior with the Cs^+ salt exhibiting strong intermolecular S···S interactions within the sheets of the anions.

(3) The nature of the ligand and the extent of S···S contacts is important for the formation of two dimensional networks in the solid state. $Cs[Pd(dmit)_2]$ (dmit = dimercaptoisotrithione) behaves as a metal at atmospheric pressure[72].

1.1.6. Dmit complexes

Recent reviews summarising the field have been published by Underhill[25] and Williams *et al*[8]. 1,3–dithiol–2–thione–4,5–dithiolate or dimercaptoisotrithione (dmit) (*fig.*, 1.1.4.) is a very useful synthon for the preparation of organic donors and in the preparation of dianionic, anionic and neutral species. Their structural relationship to dithiolene complexes makes them an important area of research.

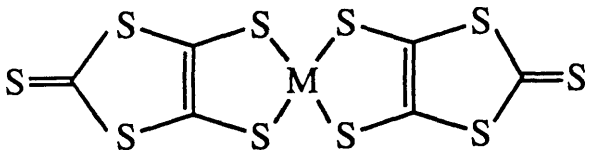


fig., 1.1.4.

The neutral nickel complex was found to be highly conducting; a number of cation deficient $M_x[Ni(dmit)_2]$ complexes[73], charge transfer complexes with various donors[73–78] and Se analogues of the dmit ligand have been published. Structural aspects are modified from the dithiolene case by the formation of a two dimensional S···S network. $[Et_4N]_{0.5}[Ni(dmit)_2]$[79] shows a face–to–face stacking and side by side arrangement of $Ni(dmit)_2$ molecules with $\sigma_{max} = 4.5\times10^{-2}$ Scm^{-1} along the stacking direction. A similar, but more extended network exists for $[Bu_4N]_{0.29}[Ni(dmit)_2]$[76] with $\sigma \sim 10$ Scm^{-1}.

Of particular note is the $TTF[Ni(dmit)_2]_2$[80,81,82] complex which is a superconductor (T_c = 1.62K, 7Kbar) with extended three dimensional interactions, α–$[TTF][Pd(dmit)_2]_2$ (T_c = 6K, 19kbar) and $[Me_4N][Ni(dmit)_2]_2$ (T_c = 5K, 7kbar) which contains the spectator anion Me_4N and therefore the superconducting properties of this latter salt must only involve the metal complexed anion.

Previous TTF charge transfer salts of $[M(dmit)_2]$ have exhibited a 1:2 stoichiometry where M = Ni[80], Pd[80,83] or 1:3 stoichiometry where M = Pt[80,83].

Recent developments[84] have centred on obtaining the alkali metal and donor (e.g., ET, TTF and TMTSF) salts of $[M(dmit)_2]^z$ (M = Ni, Pd, Pt and Au). The Na and K salts of $[Ni(dmit)_2]^{n-}$ exhibit metallic behaviour, while the alkali metal salts of $[Pd(dmit)_2]^{n-}$ are

semiconductors with high conductivities at room temperature ($\sigma \sim$ 1–$10^2 Scm^{-1}$); the Cs salt remains metallic to 60K and then undergoes a transition to a semiconductor. The Pt salts are semiconductors regardless of cation. The Na salt of $[Au(dmit)_2]$ has a room temperature conductivity of $\sigma \sim 10^2 Scm^{-1}$ and undergoes a transition to a semiconductor at 180K. The donor complexes $[TTF]_3[Au(dmit)_2]_2$, $[TMTSF]_3[Au(dmit)_2]_2$ and $[ET][Au(dmit)_2]$[85] were found to be semiconductors ($\sigma \sim$ 0.1, 0.05 and $2\times10^{-4} Scm^{-1}$ respectively) with activation energies E_a = 60, 30 and 230meV.

1.1.7. Charge transfer salts of dithiolenes

Charge transfer salts between large, delocalised organic molecules and a dithiolene were first reported in 1969 and 1971 by Maki[44,86,87,88]. Wudl reported a highly conducting complex involving TTF (tetrathiafulvalene)[40].

Crystallographic data on stacked metal complexes comprising of donor and acceptor molecules has been compiled by Ibers *et al*[89]. The electron acceptor consisted of a large number of 1,2–dithiolene complexes (ML_2; M = Fe, Co, Ni, Pt, Cu or Au; L = edt, mnt, tfd or bdt). A similar review by Alcacer and Novais was extended to early transition metals and heavier main group elements and additional dithiolene substituents[90].

$[TTF]_2[Ni(edt)_2]$[41,42,91] has reasonably high conductivities along two crystallographic directions (σ: 7.4×10^{-3} and 2.7×10^{-4} Scm^{-1}) indicating a 2D character of the arrangement of the TTF molecules. There are three crystallographically distinct types of TTF molecules; two form a columnar stack, the third lies perpendicular to both TTF molecules. $[TTT]_{1.2}[Ni(edt)_2]$[92,93] (TTT = tetrathiatetracene) exhibits metallic like conductivity ($\sigma\sim$ 30 Scm^{-1}) along the 1D chain of stacked

TTT[5/6] units, similar to $K_2Pt(CN)_4Br_{0.3}.3H_2O$. Semiconductors were found for $[TTT]_x[M(mnt)_2]$ (x = 2, M = Pd, Pt; x = 1, M = Ni, Pt)[94,95] with $10^{-4} < \sigma < 10^{-1}$ Scm^{-1}. $[TTF][M(S_2C_2(CF_3)_2)_2]$ (M = Ni, Cu, Pt or Au)[41,96,97,98] are fully transferred 1:1 donor:acceptor salts ($\sigma_{rt} < 10^{-9}$ Scm^{-1}) with the donor and acceptor molecules forming alternating stacks with equal spacing and spin lattice dimerization occuring below the transition temperature. Semiconducting compounds were found for $[TTF]_x[M(mnt)_2]$ (M = Ni, Cu, Pd, Pt; x = 1 or 2)[40,94,95,99,100] with $10^{-7} < \sigma < 10^{-4}$ Scm^{-1}. Complexes of the donor TMTTF have been reported for $[TMTTF]_2[M(mnt)_2]$ (M = Ni, Pd or Pt) and $[TMTTF][Ni(edt)_2]$ with conductivities of 10^{-8} and 10^{-6} Scm^{-1} respectively. Conductivities as high as 10^{-2} Scm^{-1} have been reported for $[TMTTF][M(bdt)_2]$ and $[TTF]_x[Ni(bdt)_2]$ (x = 1 or 2)[100,101,102].

Later developments focused on ET and TMTSF salts of $[M(mnt)_2]$ (M = Ni, Pd, Pt) which were found to be semiconductors ($10^{-6} < \sigma < 10^{-3}$ Scm^{-1})[103]. The crystal structure of $[ET][Ni(mnt)_2]$ indicated that there were no S···S contacts between donor and acceptor molecules[104].

1.2.1. Introduction

Phosphines are able to add to a vacant coordination site in planar dithiolenes to form five-coordinate species (e.g., $Fe(mnt)_2(PBu_3)$[105,106] and $(Ph_3P)Ni(S_4C_4Ph_4)$[107] or displace certain dithiolene ligands to form four coordinate dithiolato complexes (e.g., $Ni(mnt)(PPh_3)_2$)[108]. The infra-red and electronic spectra of the six coordinate complexes, $(Bu_3P)_2NiS_4C_4Ph_4$, $(Ph_2PCH_2)_2PtS_4C_4Ph_4$ and $(Bu_3P)_2PtS_4C_4Ph_4$[109] indicate the ligands have not lost their "dithiolate" character and the metal can be considered to be in the +4 oxidation state.

Complexes of the type $Pt(dithiolene)(PR_3)_2$ were prepared in comparison to $[Pt(S_2N_2H)(PR_3)_2]X$[121] (X^- = Cl, BF_4, PF_6), which is known to form columnar stacks in the solid state. Attempts to prepare transition metal dithiolene sulphur-nitrogen complexes were unsuccessful.

Experimental

Unless otherwise stated, all manipulations were carried out under an inert atmosphere (N_2 or Ar). Solvents were dried and distilled prior to use; ether, thf and hexane from sodium/benzophenone, CH_2Cl_2 from calcium hydride. Acetone and methanol were dried over 4Å and 3Å sieves respectively.

$^{31}P\{^1H\}$ nmr spectra were recorded using a Jeol FX90 Q machine, operating at 36.21MHz and referred to external 85% H_3PO_4; proton nmr spectra were recorded on a Bruker WM-250 machine.

Ir spectra were recorded as KBr discs using a Perkin Elmer FT-1720X spectrometer. Elemental analyses were performed by the departmental microanalytical service. Mass spectra were obtained on a VG 2020 instrument operating in EI (electron impact) and FAB (fast atom bombardment) modes.

Na_2mnt[110], Na_2edt[111] and quinoxaline–2,3–dithiol (QDT)[112] were prepared as described. 1,5–cyclooctadiene, cod, was used as received. Compounds of the type *cis*–$PtCl_2(PR_3)_2$ were made by stoichiometric amounts of the appropriate free phosphine to $Pt(cod)Cl_2$. $Pt(cod)Cl_2$ was prepared from K_2PtCl_4 and cod in the presence of $SnCl_2.2H_2O$[113]. The procedure used to prepare $S_4N_4H_4$[114] and $[Me_2SnS_2N_2]_2$[115] and $[Bu_4N][Au(mnt)Br_2]$[116] was adopted.

Electrochemical work was performed at ambient pressure and temperature using a Princeton Applied Research (PAR) Model 273 and peripheral equipment on solutions which were deoxygenated by purging with argon. Dichloromethane (distilled from CaH_2) was transferred to a voltammetry cell containing sufficient $[^tBu_4N][PF_6]$ and electroactive compound to make the solution *ca.* 0.1 and 5×10^{-4}M in these compounds, respectively. All potentials are referred to the Ag/Ag^+ electrode. Under these conditions, average $E(Cp_2Fe/Cp_2Fe^+)$= +0.46V, with ΔE= 60meV

1.2.2. *Preparation of $Pt(PR_3)_2mnt$ (PR_3=PEt_3, PMe_2Ph)*

In a typical reaction, $PtCl_2(PMe_2Ph)_2$ (70mg, 0.129mmol) was mixed with an equimolar amount of Na_2mnt (24mg, 0.129mmol) and CH_2Cl_2/MeOH (20ml, 3:1). After 2hrs, the orange–red solution was filtered and evacuated to dryness. The resulting solid was dissolved in $CDCl_3$ (2–3ml). The $^{31}P\{^1H\}$ nmr spectra show singlets with accompanying Pt–P splittings with the ratio of the size of the ^{195}Pt satellites to the central resonances being (33/2):66 i.e., ~ 1:4

The orange solid was recrystallised from hot ethanol to give shiny pink micro–crystals of $Pt(PMe_2Ph)_2mnt$ (51mg, 65%). Layering a CH_2Cl_2 solution of the compound with n–hexane gave crystals suitable for X–ray diffraction.

Found(%): C, 39.20; H, 3.54; N, 4.35. Calcd(%) for $Pt(PMe_2Ph)_2mnt$: C, 39.28; H, 3.63; N, 4.35.

$^{31}P\{^1H\}$ (ppm): δ -19.34(s), $^1J(^{195}Pt-^{31}P)$ 2778Hz.

^1H (ppm): δ 1.71 (s, 12H, Me, $^2J(^{31}P-^1H)$ 10.4Hz, $^3J(^{195}Pt-^1H)$ 28.9Hz), 7.38 (m, 10H, Ph, *o* 7.35, *p* 7.39, *m* 7.42).

Ir/cm^{-1}: 3054w, 2960w, 2915w, 2856w, 2222m, 2205vs, 1492s, 1436vs, 1420s, 1406m, 1385s, 1314w, 1301w, 1287m, 1154s, 1107vs, 946vs, 924vs, 910w, 851m, 807w, 741vs, 719vs, 691vs, 508w, 482s, 445m, 434m, 372w.

Pale pink crystals were obtained for the triethylphosphine derivative: Found(%): C, 33.63; H, 5.21; N, 4.65. Calcd(%) for $Pt(PEt_3)_2mnt$: C, 33.62; H, 5.29; N, 4.90.

$^{31}P\{^1H\}$ (ppm): δ 4.82(s), $^1J(^{195}P-^{31}P)$ 2749Hz.

^1H (ppm): δ 1.12 (t, 3H, Me, $^3J(CH_2-CH_3)$ 8Hz, $^3J(^{31}P-^1H)$ 16Hz), 2.05 (m, CH_2 with Pt–H and P–H couplings, which could not be measured accurately due to the broadness of the peak).

Ir/cm^{-1}: 2969m, 2933m, 2877m, 2221m, 2202vs, 1497vs, 1453s, 1416m, 1384m, 1260m, 1152s, 1110m, 1035vs, 1011m, 870w, 804w, 768s, 752vs, 745s, 726s, 701m, 629m, 508m, 441m, 426m, 387w, 310w.

Preparation of $Pt(PR_3)_2edt$ (PR_3 = PEt_3, PMe_2Ph)

Na_2edt (27mg, 0.2mmol) was added to a stirred solution of $PtCl_2(PEt_3)_2$ (100mg, 0.2mmol) in CH_2Cl_2 (10ml). An immediate yellow colouration forms. After 2hrs, the solution was filtered and evacuated to dryness. The $^{31}P\{^1H\}$ nmr revealed two peaks with accompanying Pt–P splittings; that of the desired product and the starting phosphine(δ 9.13ppm, ^1J 3513Hz). Evaporation of the solvent to 0.5ml resulted in the formation of white needle shaped crystals. Yield 55mg (57%).

Found(%): C, 32.10; H, 6.05. Calcd(%) for $Pt(PEt_3)_2edt$: C, 32.24; H, 6.18.

$^{31}P\{^1H\}$ (ppm): δ 4.35(s), $^1J(^{195}Pt-^{31}P)$ 2732Hz.

Ir/cm^{-1}: 3043w, 2961w, 2930w, 2871w, 1523m, 1453m, 1415m, 1384m, 1376m, 1103w, 1033vs, 811s, 767vs, 760vs, 725vs, 675vs, 634m, 417m, 354w.

Addition of diethyl ether was required to precipitate the dimethylphenylphosphine derivative as a pale yellow solid (63mg, 61%). Found(%): C, 37.95; H, 4.21. Calcd(%) for $Pt(PMe_2Ph)_2edt$: C, 38.50; H, 4.31.

$^{31}P\{^1H\}$ (ppm): δ -19.00(s), $^1J(^{195}Pt-^{31}P)$ 2722Hz.

Ir/cm^{-1}: 3043w, 2971w, 2911w, 1519w, 1475w, 1434m, 1417m, 1400m, 1312w, 1262w, 1155w, 1103vs, 955m, 945s, 905vs, 853w, 839w, 808m, 758m, 748s, 734s, 716m, 697s, 667s, 482m, 447m, 432m, 374w, 366w, 337w, 328w.

Preparation of $Pt(PR_3)_2QDT$ (PR_3 = PMe_2Ph, PEt_3)

To a stirred solution of QDT (30mg, 0.154mmol) in MeOH (5ml) was added sodium (10mg, 0.435mmol). After 10mins, $PtCl_2(PMe_2Ph)_2$ (84mg, 0.154mmol) was added together with CH_2Cl_2 (5ml) and the resulting solution allowed to stir for 2hrs. Evaporation of the solvent to 5ml and addition of Et_2O resulted in precipitation of the orange complex.

Found(%): C, 43.13; H, 3.92; N, 4.19. Calcd(%) for $Pt(PMe_2Ph)_2QDT$: C, 43.44; H, 3.95; N, 4.22.

$^{31}P\{^1H\}$ (ppm): δ -17.9(s), $^1J(^{195}Pt-^{31}P)$ 2835Hz.

Ir/cm^{-1}: 1547w, 1527w, 1496w, 1472w, 1434m, 1414m, 1387w, 1365m, 1328w, 1313w, 1259s, 1172vs, 1121vs, 1105s, 1049w, 1024m, 948s, 907vs,

843w, 805w, 762m, 743m, 717s, 689s, 599m, 489m, 445m, 428m.

Triethylphosphine derivative:

Found(%): C, 38.06; H, 5.43; N, 4.43. Calcd(%) for $Pt(PEt_3)_2QDT$: C, 38.52; H, 5.50; N, 4.49.

$^{31}P\{^1H\}$ (ppm): δ 5.5(s), $^1J(^{195}Pt-^{31}P)$ 2817Hz.

Ir/cm^{-1}: 2968w, 2933m, 2876m, 1550m, 1530w, 1496w, 1480w, 1458m, 1453m, 1417m, 1370w, 1365m, 1254s, 1179vs, 1123vs, 1038vs, 1025s, 1004m, 802w, 768vs, 757vs, 726vs, 638m, 598m, 444m, 426m.

Reaction of $Pt(PMe_2Ph)_2mnt$ with Bu_4NCN

$Pt(PMe_2Ph)_2mnt$ (100mg, 0.164mmol) was dissolved in CH_2Cl_2 (40ml) to which was added dry Bu_4NCN (84mg, 0.328mmol) with stirring. After 24hrs at 60°c, the solution had become a deep red. Removal of CH_2Cl_2 *in vacuo* and recrystallisation of the crude solid from ethanol resulted in the formation of light brown microcrystalline $[Bu_4N]_2[Pt(CN)_4]$, which was filtered, washed with isopropanol and dried (Yield: 35mg, 55%). Further removal of the solvent by slow evaporation gave red needles of $[Bu_4N]_2[Pt(mnt)_2]$[117], which was washed with a small quantity of cold isopropanol and dried (Yield: 50mg, 64%). The two compounds were identified by infra-red (ν(CN): 2150, 2135, 2125 cm^{-1}), elemental analysis and mass spectrometry.

1.2.3. *Reaction of $[Bu_4N][Au(mnt)Br_2]$ with $S_4H_4N_4$/dbu*

$[Bu_4N][Au(mnt)Br_2]$ (59.2mg, 8.01×10^{-5}mol) was dissolved in CH_2Cl_2 (10ml) to which was added $S_4N_4H_4$ (7.5mg, 4.0×10^{-5}mol) and an excess of dbu (1,8-Diazabicyclo[5.4.0.]undec-7-ene) (~5 drops). The solution darkened to an orange-brown colour. After filtration, the solvent was taken off *in vacuo* to 0.5ml. Dark red crystals were formed upon cooling.

Found(%): C, 39.48; H, 5.04; N, 9.65. Calcd(%) for $[Bu_4N][Au(mnt)_2]$: C, 40.04; H, 5.04; N, 9.73.

M^- (FAB): 477 $Au(mnt)_2^-$

Reaction of $[Bu_4N][Au(mnt)Br_2]$ with $[Me_2SnS_2N_2]_2$

$[Bu_4N][Au(mnt)Br_2]$ (87mg, 0.105mmol) and $[Me_2SnS_2N_2]_2$ (28.3mg, 5.25×10^{-5}mol) were combined in a schlenk and degassed CH_2Cl_2 (15ml) added. After 24hrs, the yellow-brown solution was filtered through celite and reduced to ~5ml under vacuum. Ether was added slowly until a dark brown crystalline solid was deposited. Recrystallisation from acetone/ethanol followed by slow hexane diffusion into a dichloromethane solution of the compound gave dark red crystals which analysed as $[Bu_4N][Au(mnt)_2]$.

1.2.4. Crystal Data

Computations were carried out on an Eclipse S140 computer using the SHELXTL program system[118].

$C_{20}H_{22}N_2P_2PtS_2$: M = 611.6, triclinic, a = 9.22(5), b = 11.318(6), c = 11.552(7)Å, α = 84.02(4), β = 84.64(4), γ = 71.73(4)°, U = 1149 Å^3, space group P$\bar{1}$, Z = 2, D_c = 1.77 gcm^{-3}. Pink, air stable prisms, μ(Cu-K_α) = 146 cm^{-1}, λ = 1.54178 Å, F(000) = 592.

$C_{24}H_{36}AuN_5S_4$: M = 719.8, triclinic, a = 13.405(5), b = 13.533(5), c = 17.612(5)Å, α = 75.98(3), β = 79.92(3), γ = 78.37(3)°, U = 3009 Å^3, space group P$\bar{1}$, Z = 4 (2 crystallographically independent molecules), D_c = 1.59 gcm^{-3}, μ(Cu-K_α) = 120 cm^{-1}, λ = 1.54178 Å, F(000) = 1432.

Data collection and processing: Nicolet R3m diffractometer, ω-scan method, ($\theta \leq 50°$ and 58° graphite monochromated Cu-K_α radiation; for

(1) 2662 and for (2) 8126 independent measured reflections, 2559 and 6883 observed [$|\underline{F}_o| > 3\sigma(|\underline{F}_o|)$], corrected for Lorentz and polarisation factors; empirical absorption corrections based on 343 and 360 azimuthal measurements. Maximum and minimum transmission factors for (1) were 0.602 and 0.17 and for (2) 0.131 and 0.042 respectively. Structure analysis and refinement: (1) was solved by the heavy atom method and (2) by direct methods; in both cases all the non-hydrogen atoms were refined anisotropically. The positions of the hydrogen atoms were idealised (C-H = 0.96 Å), assigned isotropic thermal parameters $\underline{U}(H) = 1.2\underline{U}eq(C)$ and allowed to ride on their parent carbons. In (2) the methyl groups were refined as rigid bodies. Refinement was by block-cascade full-matrix least squares to $\underline{R}$ = 0.040, $\underline{R}_w$ = 0.042 ($w^{-1} = \sigma^2(\underline{F}) + 0.0010\underline{F}^2$) for (1) and to $\underline{R}$ = 0.050, $\underline{R}_w$ = 0.055 ($w^{-1} = \sigma^2(\underline{F}) + 0.00144\underline{F}^2$) for (2). The maximum and minimum residual electron densities in the final $\Delta\underline{F}$ map were 1.67, 1.25 and -1.07, -1.77 $e\text{Å}^{-3}$ and the mean and maximum shifts/error in the final refinement cycle were 0.002, 0.008 and 0.018, 0.048 respectively.

1.2.5. Discussion

Reaction of $PtCl_2(PMe_2Ph)_2$ with the sodium salt of the appropiate dithiolene ligand (mnt, edt (*fig.*, 1.1.2.), QDT (*fig.*, 1.2.1.) gives the desired mixed ligand complex in fair yield.

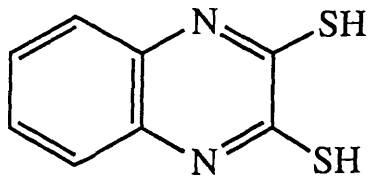


fig., 1.2.1.

The new compounds gave satisfactory microanalyses and had the expected spectroscopic properties. Their ^{31}P nmr spectra consist of singlets with platinum satellites (^1J (^{195}Pt–^{31}P) ca 2800 Hz). Similar derivatives such as $(PPh_3)_2Pt(S_2C_2Ph_2)$[119] have been previously reported.

The IR spectra are as expected (see Schläpfer and Nakamoto[120]). In the case of the mnt complexes the ν(C≡N) and ν(C=C) vibrations increase in frequency by ca 10 and 55 cm^{-1} respectively upon complexation indicating a decrease in bond length whilst the $\nu(C{=}S)_{sym}$ vibration is reduced in frequency consistent with lengthening of the C–S bonds.

Attempts to prepare mixed ligand dithiolene sulphur nitrogen complexes of gold were unsuccessful. Thus reaction of $S_4N_4H_4$ or $[Me_2SnS_2N_2]_2$ with $[Bu_4N][Au(mnt)Br_2]$ was carried out by analogy with previous routes to $S_2N_2^{2-}$ complexes[121]. In both cases the formation of $[Bu_4N][Au(mnt)_2]$ (2) was observed rather than the desired complex. The reaction of auric acid and Na_2mnt has been used to prepare (2)[122].

The cyclic voltammogram for the couple:

$Au(mnt)_2^- + e \rightleftarrows Au(mnt)_2^{2-}/CH_2Cl_2$ vs Ag/Ag^+ agrees with that obtained by Schlupp and Maki[123] ($E^{\cdot}_{\frac{1}{2}(red)} = -0.41V$ vs sce/dmso).

Gold(III) is isoelectronic with Pt(II) (d^8) and it is probable the gold and platinum mnt complexes have similar electronic structures. Schlupp and Maki have calculated that in the formal gold(II) complex $Au(mnt)_2^{2-}$ (d^9), the electron is largely based on the ligand orbital (80% A_g character). Thus, the complex is better described as Au(III) with a radical anion ligand. Geiger *et al.*[124] have noted the difficulty in assigning $Pt(mnt)_2^{3-}$ as Pt(I) (isoelectronic with $Au(mnt)_2^{2-}$) and have concluded that the reduction of the Pt(II) complex could either be metal or ligand based.

The X–ray crystal structures of $Pt(mnt)(PMe_2Ph)_2$ (1) and $[Bu_4N][Au(mnt)_2]$ (2) are shown in *figs.*, 1.2.2. and 1.2.3. with selected bond lengths and angles in Tables., 1.2.1. and 1.2.2.. (1) has the expected square planar geometry with approximate non–crystallographic C_2 symmetry. There is a characteristic slight enlargement of the P–Pt–P angle (92.4(1)°) as a consequence of the bulk of the phosphine ligands. The Pt–P and Pt–S bond lengths are typical for Pt(II). The Pt–S bond length in (1) is slightly longer than in $Pt(mnt)_2^{-}$[57] reflecting the trans effect of sulphur versus phosphorus rather than the difference in formal oxidation state. The transannular S···S distance is 3.23Å. In (2) there are two crystallographically independent molecules. There are no significant differences in their geometries; both anions having approximate non–crystallographically D_{2h} symmetry. The bond lengths and angles are within statistical significance identical to those reported for $[Au(S_2CNBu_2]_2[Au(mnt)_2]$[125]. The metal–sulphur distance in both complexes are nearly identical. The calculated $S(sp^2)$–$C(sp^2)$ distance, assuming sp^2 hybridization on the S atoms is 1.77Å, which implies a

degree of multiple bonding between the sulphur and carbon in $Au(mnt)_2^-$ (S–C(sp^2): 1.75–1.72Å). The transannular S···S distance in (2) (3.27Å) is essentially identical to the cis inter–ring S···S distance (3.28Å) underlining that mnt^{2-} is an almost optimum chelating ligand for the formation of undistorted complexes.

In (1) there are no close contacts and there is no evidence of any intermolecular stacking. In (2) there are no significant intermolecular interactions between the crystallographically independent anions (the planes of the anions are inclined at ca 64°). However centrosymmetrically related pairs of one of the anions pack parallel to each other (*fig*,. 1.2.3.) with an interplanar separation of 3.7Å; the C(5)–C(6) bond lying almost directly over, and parallel to, the S(5)"···S(6)" transannular vector of the symmetry related anion.

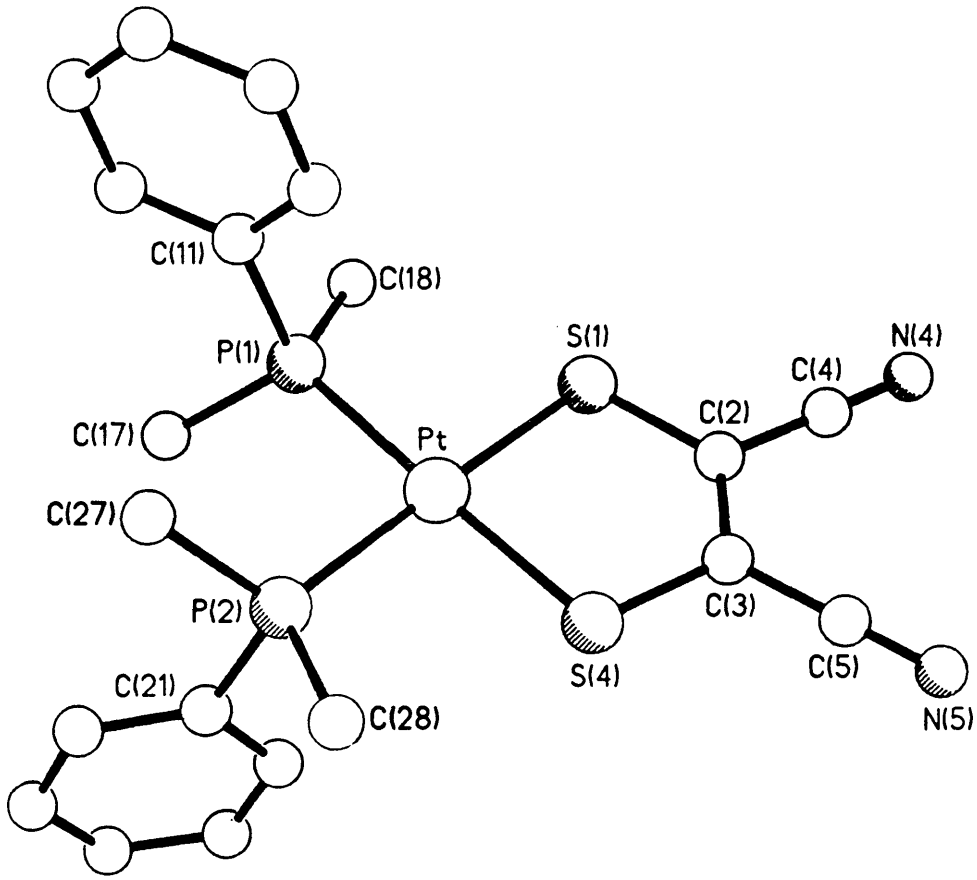


fig., 1.2.2. Crystal structure of $Pt(PMe_2Ph)_2mnt$

Table., 1.2.1.

Selected bond distances and angles: Pt–S(1) 2.309(2), Pt–P(1) 2.278(2), S(1)–C(2) 1.715(8), P(1)–C(17) 1.824(9), P(1)–C(11) 1.828(7), P(2)–C(21) 1.819(7), P(2)–C(28) 1.817(12), C(2)–N(4) 1.440(12), C(4)–N(4) 1.159(13), C(5)–C(3) 1.414(12), Pt–S(4) 2.301(2), Pt–P(2) 2.289(2), S(4)–C(3) 1.741(9), C(2)–C(3) 1.371(14), C(5)–N(5) 1.137(13) Å; S(1)–Pt–P(2) 178.1(1), P(1)–Pt–S(4) 178.3(1), Pt–S(1)–C(2) 102.7(3), Pt–P(1)–C(11) 112.7(3), Pt–P(2)–C(21) 111.7(3), S(1)–C(2)–C(4) 117.4(7), C(4)–C(2)–C(3) 118.5(7), S(4)–C(3)–C(2) 120.9(6), C(2)–C(3)–C(5) 121.6(8), S(1)–Pt–S(4) 88.8(1), Pt–S(4)–C(3) 103.5(3), S(1)–C(2)–C(3) 124.1(6), C(2)–C(4)–N(4) 178.6(10), N(5)–C(5)–C(3) 179.1(9), S(4)–C(3)–C(5) 117.5(8)°.

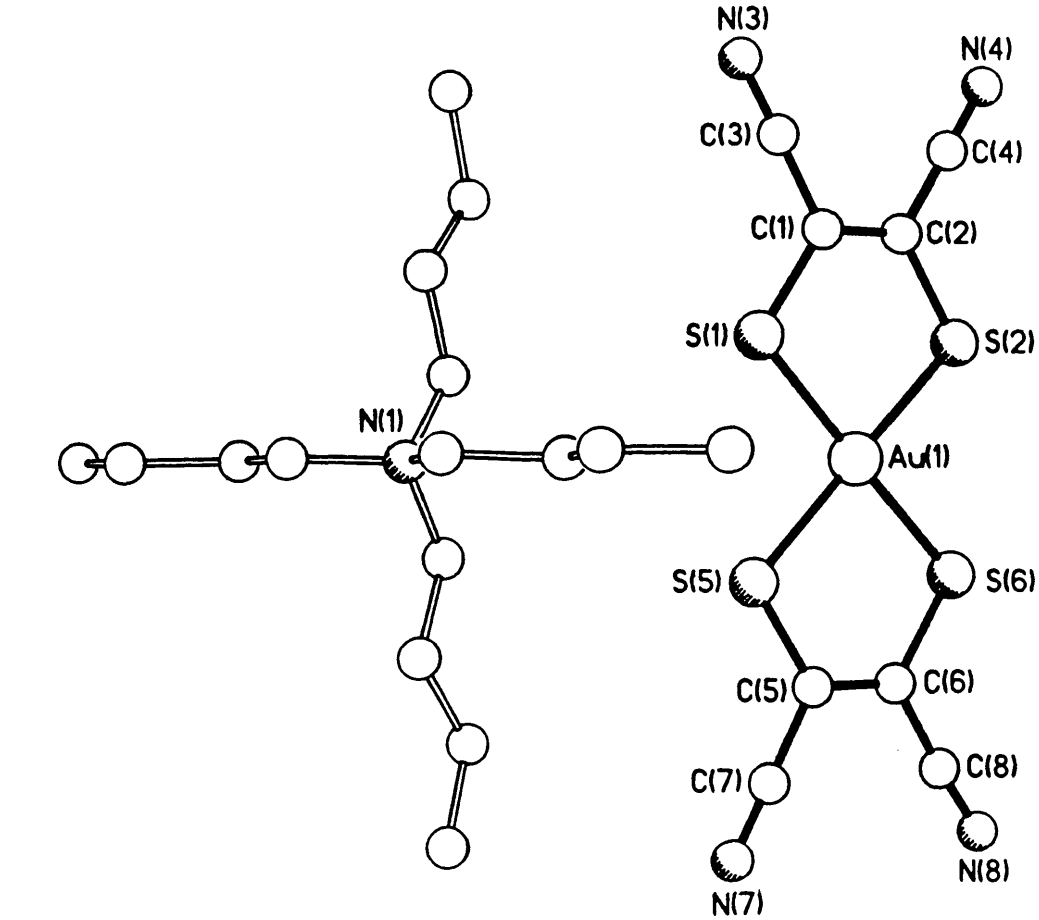


fig., 1.2.3. Crystal structure of $[Bu_4N][Au(mnt)_2]$ and packing of the anions in the unit cell

Table., 1.2.2.

Bond lengths (Å) with e.s.d's in parentheses.

Molecule 1.

Au(1)–S(1)	2.307(3)	Au(1)–S(2)	2.308(3)
Au(1)–S(5)	2.309(3)	Au(1)–S(6)	2.300(3)
S(1)–C(1)	1.749(10)	C(1)–C(2)	1.343(16)
C(2)–S(2)	1.753(10)	C(2)–C(4)	1.389(14)
C(1)–C(3)	1.424(15)	C(3)–N(3)	1.137(16)
C(4)–N(4)	1.142(14)	S(5)–C(5)	1.718(10)
C(5)–C(6)	1.351(15)	C(5)–C(7)	1.445(13)
C(6)–S(6)	1.746(10)	C(6)–C(8)	1.435(4)
C(7)–N(7)	1.148(14)	C(8)–N(8)	1.138(14)

Molecule 2.

Au(1')–S(1')	2.306(3)	Au(1')–S(2')	2.304(3)
Au(1')–S(5')	2.309(3)	Au(1')–S(6')	2.312(2)
S(1')–C(1')	1.731(10)	C(1')–C(2')	1.325(14)
C(2')–S(2')	1.749(10)	C(2')–C(4')	1.421(16)
C(1')–C(3')	1.453(13)	C(3')–N(3')	1.149(13)
C(4')–N(4')	1.162(18)	S(5')–C(5')	1.734(9)
C(5')–C(6')	1.336(13)	C(5')–C(7')	1.452(14)
C(6')–S(6')	1.707(9)	C(6')–C(8')	1.469(15)
C(7')–N(7')	1.160(14)	C(8')–N(8')	1.107(15)

Table., 1.2.3.

Bond angles (°) with e.s.d.'s in parentheses.

Molecule 1.

S(1)–Au(1)–S(2)	90.4(1)	S(1)–Au(1)–S(5)	90.6(1)
S(2)–Au(1)–S(5)	178.9(1)	S(1)–Au(1)–S(6)	178.9(1)
S(2)–Au(1)–S(6)	88.6(1)	S(5)–Au(1)–S(6)	90.4(1)
Au(1)–S(1)–C(1)	101.1(4)	S(1)–C(1)–C(2)	124.1(7)
S(1)–C(1)–C(3)	115.3(9)	C(2)–C(1)–C(3)	120.5(9)
C(1)–C(2)–S(2)	122.8(7)	C(1)–C(2)–C(4)	122.3(10)
S(2)–C(2)–C(4)	114.8(9)	Au(1)–S(2)–C(2)	101.5(4)
C(1)–C(3)–N(3)	179.1(10)	C(2)–C(4)–N(4)	176.4(12)
Au(1)–S(5)–C(5)	101.4(4)	S(5)–C(5)–C(6)	124.4(7)
S(5)–C(5)–C(7)	116.8(8)	C(6)–C(5)–C(7)	119.0(9)
C(5)–C(6)–S(6)	122.9(7)	C(5)–C(6)–C(8)	122.7(9)
S(6)–C(6)–C(8)	114.4(8)	Au(1)–S(6)–C(6)	101.4(4)
C(5)–C(7)–N(7)	177.1(11)	C(6)–C(8)–N(8)	175.8(12)

Molecule 2.

S(1')–Au(1')–S(2')	90.6(1)	S(1')–Au(1')–S(5')	89.2(1)
S(2')–Au(1')–S(5')	179.6(1)	S(1')–Au(1')–S(6')	177.1(1)
S(2')–Au(1')–S(6')	90.1(1)	S(5')–Au(1')–S(6')	90.0(1)
Au(1')–S(1')–C(1')	100.1(3)	S(1')–C(1')–C(2')	125.6(7)
S(1')–C(1')–C(3')	114.7(7)	C(2')–C(1')–C(3')	119.6(9)
C(1')–C(2')–S(2')	122.7(8)	C(1')–C(2')–C(4')	120.3(9)
S(2')–C(2')–C(4')	116.9(8)	Au(1')–S(2')–C(2')	100.8(3)
C(1')–C(3')–N(3')	177.2(12)	C(2')–C(4')–N(4')	177.9(14)
Au(1')–S(5')–C(5')	100.5(3)	S(5')–C(5')–C(6')	124.1(7)
S(5')–C(5')–C(7')	115.1(7)	C(6')–C(5')–C(7')	120.8(9)

C(5')–C(6')–S(6')	124.2(7)	C(5')–C(6')–C(8')	118.5(8)
S(6')–C(6')–C(8')	117.3(7)	Au(1')–S(6')–C(6')	101.1(3)
C(5')–C(7')–N(7')	176.5(12)	C(6')–C(8')–N(8')	176.4(11)

Mixed Ligand Platinum–Dithiolene compounds

1.3.1. Introduction

$Pt(cod)Cl_2$ serves as a suitable starting reagent for the synthesis of a variety of platinum dithiolene compounds, via the tin reagents Me_2Sn(dithiolene) (dithiolene = mnt, edt, QDT), or by reaction with the sodium salts of the dithiolenes.

The dimethyl tin dithiolene reagents[126] have been used to prepare a variety of gold complexes (which are not accessible by the Na_2(dithiolene) route) and also Pt(cod)mnt[111].

Their use has been extended to the synthesis of Pt(cod)edt and Pt(cod)QDT. Me_2SnQDT has not previously been reported and was obtained in an analogous fashion to Me_2Sn(mnt) and Me_2Sn(edt).

It has been found that treatment of the dimeric dianions of iron and cobalt with monodentate ligands such as pyridines, phosphines, phosphites, isonitriles, CN^-, N_3^-, or NCO^- caused dissociation of the complexes and formation of the five–coordinate adducts $[M(L)–S_4]^{1-}$, $[M(CN)–S_4]^{2-}$, etc[127]. ($[M–S_4]^{z-}$ denotes a metal bis–1,2–dithiolene).

The synthesis of Pt(cod)(dithiolene) was considered as a suitable precursor to mixed ligand complexes via displacement of cod. Reaction kinetics between $Pt(mnt)_2^{2-}$ and potassium cyanide suggest the formation of $Pt(mnt)(CN)_2^{2-}$, although the observed rate was very slow[128]. The cyanide ligand, which is noted for producing a strong trans effect and it's high position in the spectrochemical series, acts as a strong nucleophile and is found to displace cod to give K_2[Pt(dithiolene)$(CN)_2$], where dithiolene is represented by mnt, edt and QDT. The degree of back–bonding is considered to be minimal in transition metal cyanide complexes (normal oxidation states i.e., II and III) and is not nearly as extensive as for CO or NO^+. Carbon

monoxide or the thiocyanate ligand were unable to displace cod from Pt(cod)(dithiolene). The fact that the olefin did not appear to be as labile as expected was further supported by reactions carried out with S_4N_3Cl, (with the aim of synthesizing mixed platinum dithiolene sulphur–nitrogen species) in liquid ammonia[129] and S_4N_4 in refluxing xylene, in which no reaction was found to occur. Replacement of cod with norbornadiene (nbd) should increase the lability of the olefin, however no reaction was observed between Pt(nbd)(QDT) and S_4N_3Cl in liquid NH_3 at -78°c.

Transition metal complexes of ligands like *o*–phenylenediamine bear a close analogy to the chemistry of the dithiolenes. The full equivalence of their redox chemistry with that of the dithiolenes suggests a comparable delocalised structure. This class of compound has been explored by Holm[130]. Continuing the theme of Pt olefin complexes, (phenylenediamide)Pt(olefin) has been synthesized where the olefin is 1,5–cyclooctadiene and 2,5–norbornadiene and reaction with KCN studied.

The aim of the present work was to synthesize potassium salts of Group VIII transition metal dithiolene bis–cyanide complexes, in order to attempt partial oxidation of these species. While the potassium, alkyl ammonium and tetraphenylarsonium salts of $[Pt(mnt)(CN)_2]^{2-}$ have been prepared, attempts to prepare $[Pt(C_6H_4(NH)_2)(CN)_2]^{2-}$ and $[Au(mnt)(CN)_2]^-$ were unsuccessful; instead, only $Pt(CN)_4^{2-}$ and $Au(CN)_2^-$ were obtained. It was also disappointing to note that partial oxidation of $K_2[Pt(mnt)(CN)_2]$ could not be achieved.

1.3.2. Experimental

See experimental conditions 1.2.1..

Pt(cod)mnt was obtained via the tin reagent $Me_2Sn(mnt)$[111] and recrystallised from acetone.

Abbreviations:

Mass spectra: $M^{+\cdot}$, M^{-} (parent ion)

Nmr: δ, s, d, t, m, dd (chemical shift (ppm), singlet, doublet, triplet, multiplet, doublet of doublets)

IR: vs, s, m, w, br (intensity– very strong, strong, medium, weak, broad)

Preparation of Pt(cod)edt

An immediate yellow colouration resulted from the addition of Me_2Snedt (142mg, 0.594mmol) to an acetone/dichloromethane solution (1:2, 40ml) of $Pt(cod)Cl_2$ (185mg, 0.495mmol). The resulting mixture was refluxed for 2hrs, filtered and then reduced *in vacuo* until a yellow solid was obtained. After cooling, the yellow solid was filtered, washed with cold acetone (5ml), then diethyl ether (20ml) to give Pt(cod)edt (175mg, 90%).

Found(%): C, 30.25; H, 3.45; S, 16.15. Calcd(%) for Pt(cod)edt: C, 30.53; H, 3.59; S, 16.30.

$M^{+\cdot}$: 393

^1H(ppm)/$CDCl_3$: δ 2.55 (m, 8H, methylene), 5.43 (s, 4H, vinyl H, $^2J(^{195}Pt–^1H)$ 27Hz), 6.71 (s, 2H, vinyl H (edt), $^3J(^{195}Pt–^1H)$ 49Hz).

Ir/cm^{-1}: 3003w, 2958w, 2916w, 2876w, 2828w, 1518s, 1489w, 1474m, 1446m, 1425s, 1339s, 1309w, 1270m, 1178w, 1160w, 1089w, 1073w, 1004s, 898w, 876m, 865s, 824s, 809vs, 769m, 700m, 696vs, 671vs, 460m, 445w, 379m, 370m, 351m.

Preparation of (phenylenediamide)Pt(cod)

$Pt(cod)Cl_2$ (200mg, 0.536mmol) was dissolved in CH_2Cl_2 (15ml) to which was added *o*–phenylenediamine (58mg, 0.536mmol) and stirred for 10mins. Upon addition of dbu (5 drops), the clear solution changed to yellow. After stirring for a further 10mins, the solution was reduced *in vacuo* to 5ml and ethanol (15ml) added with stirring. The resulting solid was filtered, washed with ethanol and cold diethyl ether (5ml) to give $(C_6H_4(NH)_2)Pt(cod)$ as a yellow powder (200mg, 91%).

Found(%): C, 41.00; H, 4.23; N, 6.67. Calcd(%) for $(C_6H_4(NH)_2)Pt(cod)$: C, 41.07; H, 4.43; N, 6.84.

$M^{+}\cdot$: 409

^1H(ppm)/$CDCl_3$: δ 1.56 (br, 2H, NH), 2.48 (m, 8H, methlene), 4.97(9) (s, 4H, ethylene, $^2J(^{195}Pt–^1H)$ 52.4Hz), 6.54 (dd, $2H_{(b,b')}$, ^3J 5.50Hz, ^4J 3.43Hz), 6.67(9) (dd, $2H_{(a,a')}$, ^3J 5.52Hz, ^4J 3.44Hz).

Ir/cm^{-1}: 3347s ν(N–H), 3063w, 3032w, 2998w, 2930w, 2914w, 2874w, 1565m, 1495vs, 1481s, 1460w, 1435w, 1389m, 1329m, 1300vs, 1247w, 1233w, 1213w, 1156m, 1145m, 1017m, 1004m, 990m, 889s, 882s, 865w, 828m, 796m, 724vs, 688vs, 574s, 550vs, 509w, 474m, 456m, 311m.

UV (acetonitrile)/nm: λ 394 (1.70×10^4), 323 (3.72×10^3), 258sh (8.17×10^3), 233 (2.94×10^4). Molar extinction coefficients in parentheses, ϵ ($mol^{-1}dm^3cm^{-1}$).

Preparation of Pt(phenylenediamide)(nbd)

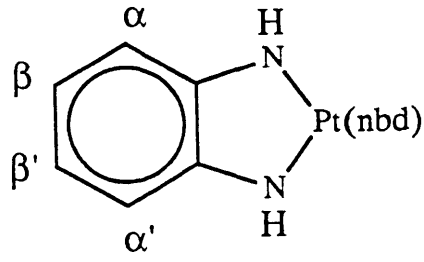
$Pt(nbd)Cl_2$ (300mg, 0.847mmol) was dissolved in CH_2Cl_2 (50ml) to which was added *o*–phenylenediamine (92mg, 0.847mmol) with stirring. The resulting yellow solution was stirred for a further 5mins and then dbu (5 drops) was added. The solution immediately changed to dark green. After 1hr, the solution was filtered, ethanol added (100ml) and

reduced *in vacuo* to 30ml. The fine dark green precipitate was filtered, washed with EtOH/Et_2O (1:10) (50ml) and then Et_2O:pentane (3:1) and dried *in vacuo* to yield Pt($C_6H_4(NH)_2$)(nbd) (252mg, 76%). Found(%): C, 39.20; H, 3.23; N, 6.95. Calcd(%) for Pt($C_6H_4(NH)_2$)(nbd): C, 39.69; H, 3.59; N, 7.12.

$M^{+\cdot}$: 393

^{1}H(ppm)/$CDCl_3$: δ 1.24(3) (t, $2H_\alpha$, ^{3}J 7Hz), 3.44 (m, $2H_\beta$), 4.35(6) (m, $4H_\gamma$, $^2J(^{195}Pt-^1H)$ 53.2Hz), 6.54(9) (dd, $2H_{(b,b')}$ ^{3}J 5.92Hz, ^{4}J 3.25Hz), 6.78(5) (dd, $2H_{(a,a')}$ ^{3}J 5.69Hz, ^{4}J 3.37Hz).

Ir/cm^{-1}: 3352s ν(N–H), 3071w, 3011w, 2925w, 2852w, 1596m, 1568w, 1485s, 1461w, 1373w, 1344w, 1301vs, 1232w, 1207w, 1172w, 1142m, 1099w, 1077m, 1032m, 1021m, 997s, 951s, 920w, 883w, 814w, 798w, 700w, 725s, 691s, 574m, 562m, 487m, 453m.



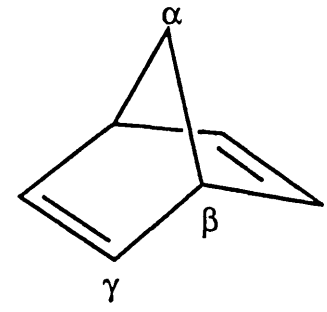


fig., 1.3.1. ^{1}H nmr assignment for (phenylenediamide)Pt(nbd)

Preparation of Me_2SnQDT

Sodium (0.318g, 13.8mmol) was dissolved in ethanol (5ml) to which was added QDT (1.343g, 6.91mmol) in ethanol (25ml). Me_2SnCl_2 (1.519g, 6.91mmol) was then added with stirring to the orange solution. After 4hrs, a fine white suspension had formed which was filtered to leave an orange filtrate. Addition of water (100ml) and subsequent removal of the ethanol *in vacuo* resulted in the formation of the desired product as a yellow precipitate.

This was filtered, washed with water (50ml), cold ethanol (5ml), diethyl ether (3×20ml) and dried *in vacuo*.

Found(%): C, 34.80; H, 2.79; N, 8.08; S, 18.00. Calcd(%) for Me_2SnQDT: C, 35.22; H, 2.96; N, 8.22; S, 18.80.

$M^{+}\cdot$: 342

^1H(ppm)/dmso-d_6: δ 0.94 (s, 6H, $^2J(^{119}Sn-^1H)$ 85.0Hz, $^2J(^{117}Sn-^1H)$ 80.6Hz), 7.44 (dd, $2H_{(a,a')}$, ^3J 6.22Hz, ^4J 3.50Hz), 7.63 (dd, $2H_{(b,b')}$, ^3J 6.33Hz, ^4J 3.39Hz).

Ir/cm^{-1}: 3054w, 2990w, 2964w, 2910w, 1609m, 1560m, 1508s, 1498s, 1477m, 1449m, 1370m, 1338w, 1264s, 1172vs, 1127vs, 1109vs, 1020s, 949w, 891w, 863w, 780s, 757vs, 663w, 606m, 594m, 552m, 517m, 443m, 404m.

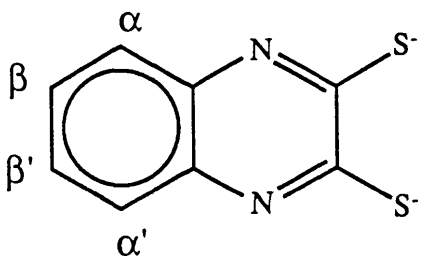


fig., 1.3.2. ^1H nmr assignment for QDT

Preparation of Pt(cod)QDT

The method used to prepare Pt(cod)edt *(see above)* was followed, using $Pt(cod)Cl_2$ (259mg, 0.692mmol) and Me_2SnQDT (236mg, 0.692mmol) to obtain the desired compound as an orange precipitate. Recrystallisation from EtOH yielded orange crystals of Pt(cod)QDT (259mg, 76%).

Found(%): C, 38.10; H, 3.17; N, 5.65; S, 12.78. Calcd(%) for Pt(cod)QDT: C, 38.78; H, 3.25; N, 5.65; S, 12.94.

$M^{+}\cdot$: 495

Ir/cm^{-1}: 3056w, 2964w, 2923w, 2882w, 1558m, 1515s, 1475m, 1451w, 1428w, 1369w, 1333w, 1311w, 1259s, 1249s, 1219m, 1178s, 1166s, 1124vs,

1105vs, 997s, 954w, 901w, 881m, 863m, 826m, 803w, 757vs, 696w, 653w, 599s, 460w, 443w, 428w.

Preparation of Pt(nbd)QDT

Pt(nbd)Cl_2 (190mg, 0.531mmol) and Me_2SnQDT (181mg, 0.531mmol) were combined in a schlenk to which was added acetone/CH_2Cl_2 (1:1) (80ml). After filtering, the solution was stirred for 2hrs. A fine brown precipitate was formed on reducing the solution *in vacuo* to 10ml. Further precipitation was achieved by gradual addition of Et_2O (Yield 183mg, 72%). Recrystallisation from acetone gave Pt(nbd)QDT as reddish-brown crystals.

Found(%): C, 37.29; H, 2.49; N, 5.74; S, 13.12. Calcd(%) for Pt(nbd)QDT: C, 37.57; H, 2.52; N, 5.84; S, 13.37.

$M^{+\cdot}$: 479

Ir/cm^{-1}: 3060w, 3025w, 1547w, 1497w, 1472w, 1417w, 1368m, 1305s, 1256s, 1248s, 1176vs, 1122vs, 1079s, 963w, 947w, 895w, 824w, 802m, 784w, 767m, 759s, 599s, 482w, 425m, 421m.

Preparation of K_2[Pt(mnt)$(CN)_2$]

Pt(cod)(mnt) (0.25g, 0.564mmol) was dissolved in the minimum quantity of CH_2Cl_2 (60ml) to which was added KCN (73mg, 1.12mmol) in methanol (25ml) with stirring. After 1 hour, the yellow solution had faded in colour. The formation of a cream precipitate was achieved by gradual addition of diethyl ether; this was filtered, washed with cold methanol (5ml), dichloromethane (40ml), then ether (40ml) to give K_2[Pt(mnt)$(CN)_2$] (205mg, 78% yield) as a pale pink solid which changes to yellow on exposure to air, presumably due to moisture absorption.

Found(%): C, 15.40; N, 12.00; S, 13.00. Calcd(%) for

$K_2[Pt(mnt)(CN)_2]$: C, 15.48; N, 12.04; S, 13.77.

FAB (dmso/glycerol matrix) M^-: 388

Ir/cm^{-1}: 3630m, 3541m, 2218vs, 2207vs, 2133vs, 2119vs, 1604s, 1488vs, 1159vs, 1112m, 1055m, 1017w, 873m, 806w br, 513s, 453m, 424m, 400m, 366m, 325m.

$K_2[Pt(mnt)(CN)_2]$ (100mg, 0.152mmol) was dissolved in H_2O to which was added an excess of Bu_4NBr (1.25g, 3.82mmol). A cream precipitate formed which was filtered, dried and recrystallised from CH_2Cl_2/benzene to give cream needle–shaped crystals of $[Bu_4N]_2[Pt(mnt)(CN)_2]$ (125mg, 95%).

Found(%): C, 50.52; H, 8.00; N, 9.15; S, 6.91. Calcd(%) for $[Bu_4N]_2[Pt(mnt)(CN)_2].1/2CH_2Cl_2$: C, 50.55; H, 8.04; N, 9.19; S, 7.01.

Ir/cm^{-1}: 2961s, 2932s, 2873s, 2219s, 2193vs, 2138vs, 2130s, 2112s, 1530s, 1488s, 1471s, 1380s, 1365w, 1260w, 1180w, 1152vs, 1116m, 1109w, 1067w, 1052m, 1027m, 883m, 871m, 803m, 748m, 740m, 693s, 515m, 440m, 417w, 394m, 358m, 319m.

The tetraethylammonium and tetraphenylarsonium salts were obtained by the same method described above. Pale pink diamond shaped crystals of $[Et_4N]_2[Pt(mnt)(CN)_2]$ were obtained from dichloromethane/pentane:

Found(%): C, 39.10; H, 5.89; N, 12.10; S, 9.19. Calcd(%) for $[Et_4N]_2[Pt(mnt)(CN)_2].CH_2Cl_2$: C, 39.15; H, 5.99; N, 12.18; S, 9.29.

Ir/cm^{-1}: 2989w, 2949w, 2921w, 2851w, 2217m, 2201vs, 2136vs, 2119vs, 1476vs, 1459vs, 1402m, 1306m, 1262w, 1184s, 1152s, 1114m, 1079w, 1034m, 1006m, 892w, 868m, 794s, 511m, 452m, 421w, 394m, 362m, 321m.

Pale yellow crystals of $[Ph_4As]_2[Pt(mnt)(CN)_2]$ were obtained from ethyl acetate/ethanol:

Found(%): C, 56.00; H, 3.23; N, 4.62; S, 5.20. Calcd(%) for $[Ph_4As]_2[Pt(mnt)(CN)_2]$: C, 56.20; H, 3.49; N, 4.86; S, 5.56.
Ir/cm^{-1}: 3079w, 3056w, 3021w, 2923w, 2221s, 2198vs, 2138vs, 2130vs, 2114m, 1579w, 1539s, 1482s, 1439vs, 1337w, 1311w, 1184m, 1165w, 1152s, 1137m, 1080w, 1072vs, 1021w, 997s, 989w, 845w, 753vs, 746vs, 688vs, 603s, 539s, 530m, 479s, 469s, 464s, 415w, 362m, 345m.

Preparation of $K_2[Pt(edt)(CN)_2]$

Pt(cod)edt (88mg, 0.224mmol) was dissolved in dichloromethane (15ml) to which was added KCN (29mg, 0.45mmol) in methanol (10ml). A further 10ml of CH_2Cl_2 was added and the solution left to stir overnight. The solution faded from it s yellow colour. Addition of CH_2Cl_2 (150ml) and pentane (30ml) resulted in the precipitation of a white solid. This was filtered, washed with CH_2Cl_2 and dried to give $K_2[Pt(edt)(CN)_2]$ (79mg, 85%). The white solid darkened on exposure to air over a period of several days.
Found(%): C, 11.22; H, 0.40; N, 6.72; S, 15.19. Calcd(%) for $K_2[Pt(edt)(CN)_2]$: C, 11.56; H, 0.49; N, 6.74; S, 15.43.
FAB (dmso/glycerol matrix) M^-: 337
Ir/cm^{-1}: 3029w, 2962w, 2927w, 2854w, 2136vs, 2125vs, 2109sh, 1518m, 1166m, 803s, 504w, 409m, 368w, 348w.

Preparation of $[Ph_4As]_2[Pt(edt)(CN)_2]$

$K_2[Pt(edt)(CN)_2]$ (52mg, 0.125mmol) was dissolved in distilled water to which was added an excess of Ph_4AsCl in water, with stirring. An immediate white precipitate resulted, which was filtered, washed with water then isopropanol/Et_2O (1:5). Yield 133mg, 96%.
Found(%): C, 56.50; H, 3.75; N, 2.51; S, 5.68. Calcd(%) for $[Ph_4As]_2[Pt(edt)(CN)_2]$: C, 56.57; H, 3.84; N, 2.54; S, 5.81.

^{1}H(ppm)/dmso–d_6: δ 6.03 (s, 2H, ethylene, ^{3}J(^{195}Pt–^{1}H) 35.9Hz), 7.73–7.93 (m, 40H, tetraphenylarsonium).

Ir/cm^{-1}: 3074w, 3052w, 3036w, 3016w, 2112vs, 2100vs, 1578m, 1509m, 1476m, 1440vs, 1339w, 1321w, 1230w, 1190w, 1166m, 1136w, 1080s, 1042w, 1022w, 997s, 803m, 751vs, 745vs, 689vs, 682m, 674w, 486vs, 470vs, 369m, 351m, 346m.

Preparation of $K_2[Pt(QDT)(CN)_2]$

Pt(cod)(QDT) (200mg, 0.404mmol) was dissolved in dichloromethane (30ml), filtered and KCN (53mg, 0.808mmol) in methanol (15ml) added with stirring. The orange solution was stirred overnight. Addition of CH_2Cl_2 (100ml) and pentane (20ml) resulted in the formation of an orange precipitate, which was filtered, washed with CH_2Cl_2 and dried to give $K_2[Pt(QDT(CN)_2]$ (186mg, 89%).

Found(%): C, 23.00; H, 0.71; N, 10.78; S, 12.29. Calcd(%) for $K_2[Pt(QDT)(CN)_2]$: C, 23.20; H, 0.78; N, 10.83; S, 12.39.

FAB (dmso/glycerol matrix) M$^-$: 439

Ir/cm^{-1}: 3060w, 2135w, 2124vs, 2105vs, 1617br,s, 1561w, 1491w, 1478w, 1440w, 1370s, 1336w, 1265s, 1178vs, 1126vs, 1032w, 943w, 864w, 751vs, 607s, 454w, 429m, 417m.

Preparation of $[Ph_4As]_2[Pt(QDT)(CN)_2]$

A bright orange precipitate was obtained using the procedure adopted for the edt salt.

Found(%): C, 57.70; H, 3.59; N, 4.62; S, 5.29. Calcd(%) for $[Ph_4As]_2[Pt(QDT)(CN)_2]$: C, 57.76; H, 3.68; N, 4.65; S, 5.32.

^{1}H(ppm)/dmso–d_6: δ 7.57(7) (dd, 2H$_{(b,b')}$ ^{3}J 6.28Hz, ^{4}J 3.40Hz), 7.72–7.93 (m, 40H, tetraphenylarsonium).

The ^1H nmr of the tetrabutylammonium salt revealed the second quartet (doublet of doublets) at δ 7.76ppm (dd, $2H_{(a,a')}$ ^3J 6.30Hz, ^4J 3.40Hz).

Ir/cm^{-1}: 3051w, 3020w, 2920w, 2850w, 2133vs, 1616m, 1597m, 1578w, 1483m, 1438vs, 1370m, 1338w, 1312m, 1288m, 1262w, 1173vs, 1138vs, 1129vs, 1081s, 1022w, 997s, 846w, 800w, 742vs, 689vs, 653s, 611w, 597s, 543w, 478s, 467s, 412w, 361w, 354w.

Reaction of $(C_6H_4(NH)_2)Pt(cod)$ with KCN

To a suspension of (phenylenediamide)Pt(cod) (75mg, 1.83×10^{-4}mol) in ethanol (100ml) was added KCN (23mg, 3.53×10^{-4}mol) with stirring. After 24hrs, the solution had turned to a deep brown colour. Filtration followed by removal of ethanol to 15ml and addition of CH_2Cl_2 resulted in the deposition of a light brown solid which analyses as $K_2Pt(CN)_4$ (Yield: 32mg (99%), based on KCN).

Found(%): C, 13.32; N, 15.54. Calcd(%) for $K_2Pt(CN)_4$: C, 12.73; N, 14.85.

Ir/cm^{-1}: (Ph_4As salt) ν(C≡N) 2136, 2125; ν(C=N) 1617; ν(Pt–C) 504, 408.

The filtrate was still an intense dark green/brown colour and contains $Pt[C_6H_4(NH)_2]_2^0$. A comparison of the cyclic voltammogram of an acetone solution of the dried (*in vacuo*) filtrate with $Pt[C_6H_4(NH)_2]_2^0$ [130] indicates comparable oxidation and reduction steps.

Preparation of Au(mnt)(tht)Br

The gold(III) complex, Au(mnt)(tht)Br (tht= tetrahydrothiophene) may be conveniently prepared by the same route as the chloro complex[111], starting from $[Bu_4N][AuBr_4]$.

Reaction of Au(mnt)(tht)Br with KCN

To a stirred solution of Au(mnt)(tht)Br (150mg, 0.30mmol) in acetone/methanol (40ml, 3:1) was added a methanolic solution (25ml) of KCN (38mg, 0.58mmol). The solution gradually lightens to an orange colour, from an initial dark green. After stirring for 1hr, a small amount of KCN had re–precipitated; this was re–solubilized using 18–crown–6 ether. Removal of methanol *in vacuo* and addition of ether to the solution resulted in the precipitation of a brown solid. Recrystallisation from isopropanol gave light brown crystals of K[18–c–6][$Au(CN)_2$].

Found(%): C, 30.86; H, 4.28; N, 5.14. Calcd(%) for K[18–c–6][$Au(CN)_2$]: C, 30.44; H, 4.38; N, 5.07.

M^-: 249

Ir/cm^{-1}: ν(C≡N) 2152; ν(Au–C) 436; ν_{comb} 2590 cm^{-1}.

(cf., K[$Au(CN)_2$][131]: ν_3(C≡N) 2140, ν_2(Au–C) 446, $\nu_2 + \nu_3$ 2586 cm^{-1}).

Attempted partial oxidation of K_2[Pt(mnt)$(CN)_2$]

The electrochemical growth of non–stoichiometric highly conducting platinum chain complexes such as $K_{1.75}Pt(CN)_4.1.5H_2O$ and $K_2Pt(CN)_4Cl_{0.3}.3H_2O$ has been detailed previously[132].

An aqueous solution (5ml) of K_2[Pt(mnt)$(CN)_2$] (150mg) was electrolysed at a d.c. potential of 1.5V for 2 weeks using platinum wire electrodes. There were no signs of crystal growth at the anode after this period. It has been noted that growth of crystals depends on size and shape of the electrodes, current density, concentration of the Pt species and duration of the electrolysis– while partial oxidation of $K_2Pt(CN)_4$ occurs, the sodium salt does not yield a partially oxidised product under similar conditions.

1.3.3. Discussion

The vibrational spectra of complexes of the type $[Pt(dithiolene)(CN)_2]^{2-}$ (dithiolene = mnt, edt and QDT) are tabulated in tables., 1.3.1. and 1.3.2.. The assignments for the dithiolenes mnt and edt are as previously described in 1.2.5.; the frequencies of the (perturbed) stretching vibrations for C⁚⁚C and C⁚⁚S are in agreement with those observed for transition metal bis–1,2–dithiolenes. The value of ν(C⁚⁚C) was found to be dependent to a small degree on the electron withdrawing ability of the substituent, with a lower frequency observed for edt (H) compared to mnt (CN). Coordination of the ligand QDT to metals through sulphur results in reduction of the double bond character of the C–S bond; the ν(CS) modes are shifted from the ligand (830 and 810 cm^{-1}) to lower frequencies (800 to 750 cm^{-1}) upon complexation. The assignment at 429 and 417 cm^{-1} for ν(Pt–S) is in agreement with previous metal–sulphur vibrations while ligand bands at 1580–1350 and 1180–1120 cm^{-1} are due to ν(NCS) modes. The shift to lower frequencies in these bands, from the free ligand, indicate a reinforcement of the NC double bond character and rigidity of the diaza ring– S,S coordination of the ligand to a metal atom, for the anion complex $Ni(QDT)_2^{2-}$, is confirmed by X–ray diffraction[133].

Cyano complexes can be readily identified by the sharp ν(CN) at 2220–2000 cm^{-1} (the ν(C≡N) of free CN^- is 2080 cm^{-1} in aqueous solution). Since ν(C≡N) for mnt occurs at 2220–2200 cm^{-1}, the frequency of the metal–bonded cyanide in the complexes $[Pt(dithiolene)(CN)_2]^{2-}$ can be identified in the range 2136–2105 cm^{-1}. In comparison, ν(C≡N) for $K_2Pt(CN)_4$[134] occurs at 2150 and 2136 cm^{-1}; the decrease in frequency can be correlated to a donation of electron density from the delocalised dithiolene constituent into the antibonding

$2p\pi^*$ orbital of CN. The cyanide ion acts as a σ–donor by donating electrons to the metal and also as a π–acceptor by accepting electrons from the metal. σ–Donation results in an increase in the ν(C≡N) since electrons are removed from the 5σ orbital (weakly antibonding), while π–back bonding leads to a decrease in ν(C≡N), as described above. Generally, CN^- is a better σ–donor and poorer π–acceptor than carbon monoxide.

In addition to ν(C≡N), the cyano complexes exhibit ν(M–C), δ(M–CN) and δ(C–M–C) bands in the low frequency region. The ν(Pt–C) vibrations for the $[Pt(mnt)(CN)_2]^{2-}$, $[Pt(edt)(CN)_2]^{2-}$ and $[Pt(QDT(CN)_2]^{2-}$ salts were located at 450, 459 and 497 cm^{-1} respectively (all medium to weak intensity). δ(Pt–CN) vibrations were found at 345–320, 351–343 and 361–354 cm^{-1} for the mnt, edt and QDT salts, respectively. δ(C–Pt–C) vibrations are reported[135,136] to occur at 95 cm^{-1} (Raman active) for $Pt(CN)_4^{2-}$.

The proton (^1H) nmr for Na_2edt reveals a single peak at δ 6.8 ppm which is shifted to δ 9.2 ppm (CS_2) on complexing in $[Ni(edt)_2]^0$ and was regarded as evidence for a more "aromatic" nature of the proton nmr in the metal complex when compared to the free dithiolate ligand[137]. The ^1H nmr of the compounds Pt(cod)edt ($CDCl_3$) and $[Ph_4As]_2[Pt(edt)(CN)_2]$ (dmso–d_6) showed singlets at δ 6.71 and δ 6.03 ppm, with accompanying $^3J(^{195}Pt–^1H)$ satellites, which is contary to the "more" aromatic nature described above.

The dianionic Pt(dithiolene)$(CN)_2$ salts were found to be diamagnetic, as expected (c.f., $Pt(mnt)_2^{2-}$; diamagnetic consistent with $4a_g^2\ 3b_{2g}^2$ ground state).

The entire pattern of intensities observed at various values of m/e in the parent ion region is in good agreement with that expected on the basis of isotopic abundance calculations (tables., 1.3.3. and 1.3.4.).

The principle fragmentation pattern for [Pt(dithiolene)$(CN)_2$]$^-$ can be summarised as follows:

[Pt(dithiolene)$(CN)_2$]$^-$ → [Pt(dithiolene)(CN)]$^-$ → [Pt(dithiolene)]$^-$ → [Pt(dithiolene)−S]$^-$ → complex fragmentation

Reaction of Au(mnt)(tht)Br with KCN proceeds with reduction of the gold(III) complex to K[18–crown–6][$Au(CN)_2$], as opposed to the intended [Au(mnt)$(CN)_2$]$^-$ complex. The formation of $Au(CN)_2^-$ can be associated with a very high formation constant and two electron reduction step. The asymmetric ν(C≡N) at 2152 cm^{-1} agrees with K[$Au(CN)_2$], in contrast to $Au(CN)_4^-$, which due to the higher oxidation state (+3) and stronger Au–CN σ–bonding has ν(C≡N) at 2189 cm^{-1}.

Reaction of $(C_6H_4(NH)_2)$Pt(cod) with KCN yields $K_2Pt(CN)_4$ and $[Pt(C_6H_4(NH)_2)_2]^0$, in contrast to the Pt(cod)(dithiolene) reactions. This observation may be viewed in the light that the order of oxidative stability of the ligands, *viz.*, $C_6H_4(NH)_2^{2-} < C_6H_4O_2^{2-} < C_2S_2(CN)_2^{2-}$, as measured from half–wave potentials, and the observation[130] that free ligands (i.e., mnt) which are most stable in the anionic form tend to stabilize the z = −2, −1 and possibly 0 members of the electron transfer series, whereas free ligands most stable in the neutral form tend to stabilize the z = 0, +1, +2 members. Thus dianionic complexes of *o*–phenylenediamine are likely to be unstable in an oxidative sense.

λ/cm^{-1}	$\nu(C\equiv N)_{mnt}$	$\nu(C\equiv N)_{Pt}$	$\nu(C\ddot{-}C)$	$\nu(C\ddot{-}S)_{asym}$	$\pi(C-CN)$	$\nu(C\ddot{-}S)_{sym}$	Ring def $+\delta(CCN)$	$\nu(Pt-S)$ + ring def
$K_2[Pt(mnt)(CN)_2]$	2218vs 2119vs	2133vs 2207vs	1488s	1159s	1112m	806w,br	513s	366m
$[Et_4N]_2[Pt(mnt)(CN)_2]$	2217vs 2201vs	2136vs 2130s,2119vs	1525m	1152vs	1114m	794m	511m	362w
$[Bu_4N]_2[Pt(mnt)(CN)_2]$	2219vs 2193vs	2138vs 2130vs,2112s	1530s 1482s	1152vs	1116m	802m	515m	358m
$[Ph_4As]_2[Pt(mnt)(CN)_2]$	2221vs 2198vs	2138vs 2130vs,2114m	1539s	1152s	1114m	803w	520w	362m
$K_2[Pt(edt)(CN)_2]$	—	2136vs 2125vs,2109sh	1518m	1166m	—	803s	—	369w
$[Ph_4As]_2[Pt(edt)(CN)_2]$	—	2112vs 2100vs	1509m	1166m	—	803m	—	369m
$K_2[Pt(QDT)(CN)_2]$	—	2135w 2124vs,2105vs	—	1178vs	—	751vs	—	429m 417m
$[Ph_4As]_2[Pt(QDT)(CN)_2]$	—	2133vs 2123vs	—	1173vs	—	hidden (742vs)	—	412m

Table., 1.3.1. Infra–red assignments for $[Pt(dithiolene)(CN)_2]^{2-}$ salts

λ/cm^{-1}	$\nu(N\ddot{-}C\ddot{-}S)_{asym}$	$\nu(C\ddot{-}C\ddot{-}S)$ $(2,3-R)\beta$ ring str	$\nu(N\ddot{-}C\ddot{-}S)_{sym}$	$\nu(C\ddot{-}S)$	β skel dist	$\delta(N\ddot{-}C\ddot{-}S)$	$\nu(M-S)$
$[Ph_4P]_2[Mo(QDT)_3].H_2O$ (a)	1540m 1360m	1170s	1120s	760s	595s	—	340s
$Na_2[Ni(QDT)_2].H_2O$ (b)	1568w 1550s 1362vs	1170vs	1120vs	792m	599vs	510w	423s
$[Bu_4N]_2[Pt(QDT)_2]$ (c)	1550s 1380w	1165s	1120s	790s	585s	—	400m
$K_2[Pt(QDT)(CN)_2]$	1561w 1370s	1178vs	1126vs	751vs	607s	497w	429,417m
$[Ph_4As]_2[Pt(QDT)(CN)_2]$	1578m 1370m	1173vs	1138vs 1129vs	hidden (742vs)	611w	543w	412m

(a) S Boyde, C D Garner, J H Enemark & R B Ortega, Polyhedron, 1986, 5, 371
(b) A Rignedoli, G Peyronel & W Malavasi, J. Inorg. Nucl. Chem., 1976, 38, 1963
(c) L J Theriot, K K Ganguli, S Kavanos & I Bernal, J. Inorg. Nucl. Chem., 1969, 31, 3133

Table., 1.3.2. Comparison of the IR assignments for metal–QDT complexes with $[Pt(QDT)(CN)_2]^{2-}$

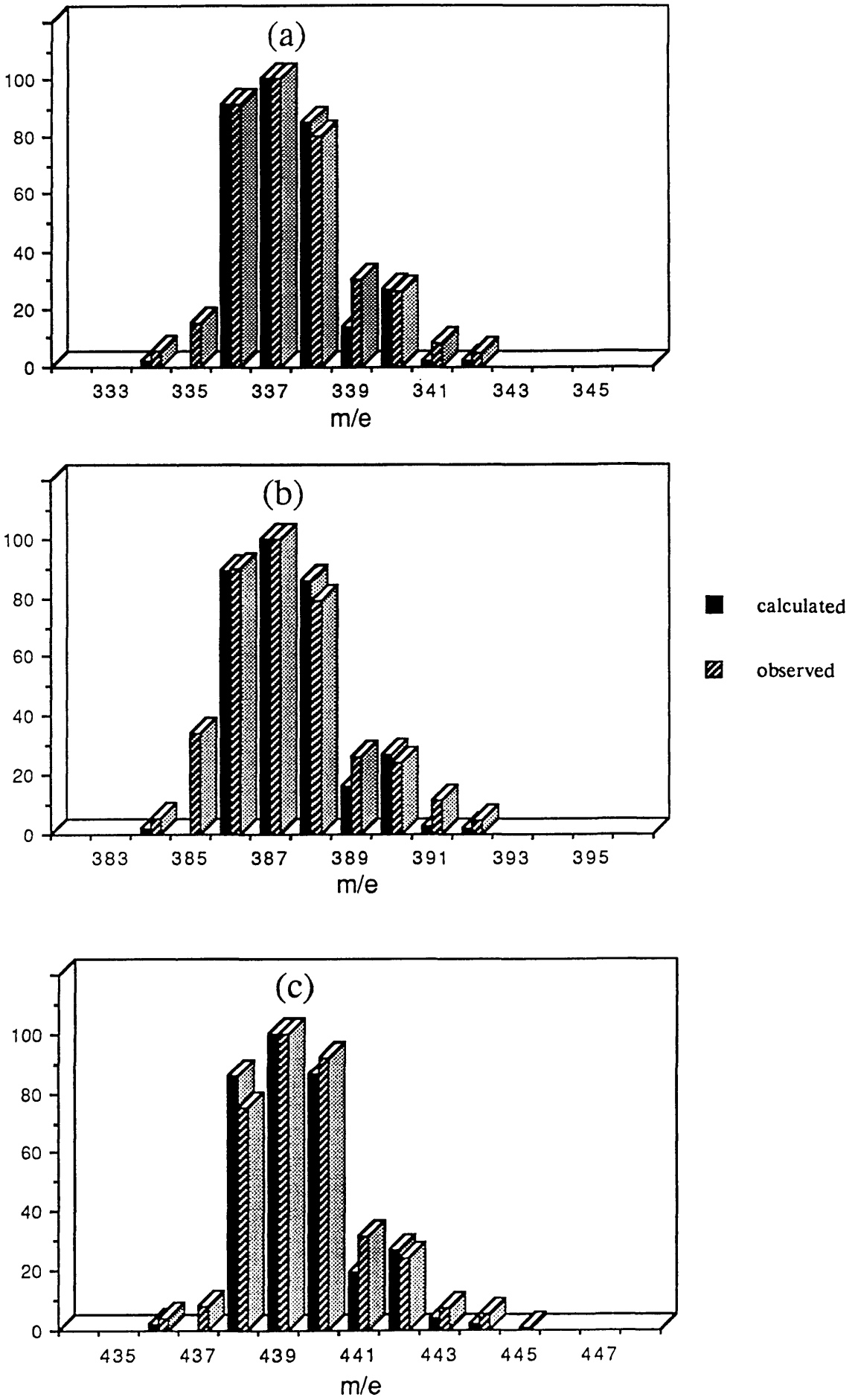


fig., 1.3.3. Isotopic abundance calculations for parent ion peaks of: (a) $Pt(edt)(CN)_2^{2-}$, (b) $Pt(mnt)(CN)_2^{2-}$, (c) $Pt(QDT)(CN)_2^{2-}$

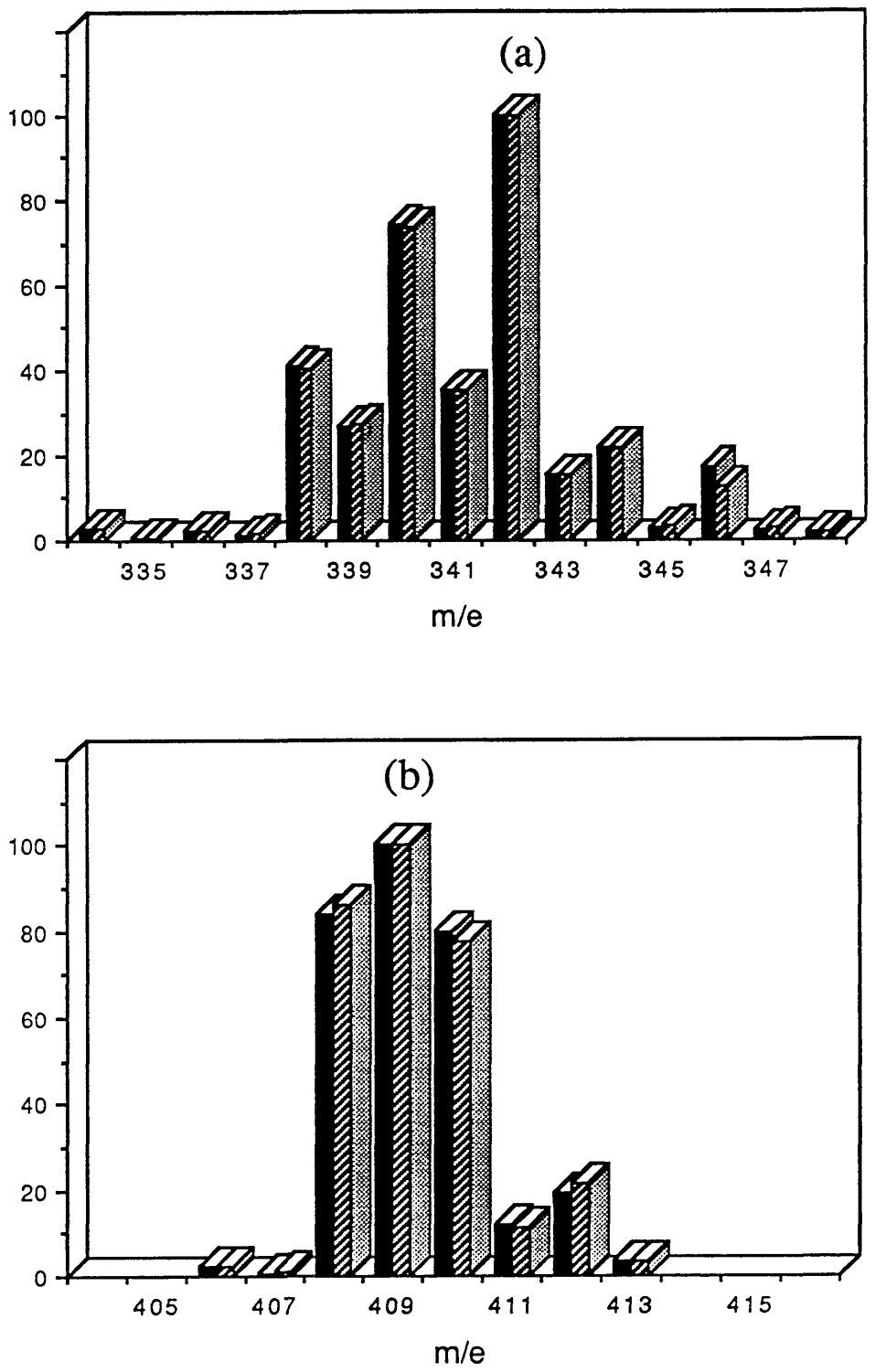


fig., 1.3.4. Isotopic abundance calculations for parent ion peaks of:

(a) Me_2SnQDT, (b) $C_6H_4(NH)_2Pt(cod)$

1.4.1. References

1. K Krogmann, Angew.Chem.Int.Ed.,Engl., 1969, 8, 35

2. T W Thomas and A E Underhill, Chem.Soc.Rev., 1972, 1, 99

3 (a) A E Underhill, 'Low Dimensional Cooperative Phenomena and the Possibility of a High Temperature Superconductor' NATO Advanced Study Institute, Starnberg, Germany, Sept 1974, H J Keller, Ed Plenum Press, NY, 1975, 7A, 237

(b) A E Underhill, Plat.Met.Rev., 1974, 18, 21

4. P S Gomm, Pentacol., 1973, 2

5. A E Underhill, "Compounds Exhibiting Unusual Electrical Properties", Comprehensive Coordination Chemistry, 1987, Ed Pergamon Press, NY, Vol 6, pg 155

6. A F Garito and AJ Heeger, Actt.Chem.Res., 1974, 7, 232

7. E B Yagubskii and M L Khidekel', Russ.Chem.Rev., 1972, 41, 1011

8. J M Williams, H H Wang, T J Emge, U Geiser, M A Beno, P C W Leung, K D Carlson, R J Thorn, A J Schultz and M H Whangbo, Prog.Inorg.Chem., 1987, 35, 51

9. J S Millar and A J Epstein, Prog.Inorg.Chem., 1976, 20, 1

10. D K C MacDonald and K Mendelssohn, Proc.Roy.Soc.London.Ser.A., 1950, 202, 103

11. A N Block, R B Weisman and C M Varma, Phys.Rev.Lett., 1972, 28, 753

12. V Ambegaoker, B I Halperin and J S Langer, Phys.Rev(B)., 1971, 4, 2612

13. A J Epstein and E M Conwell, Solid.State.Commun., 1977, 24, 627

14. A H Reis, Jr in "Extended Linear Chain Compounds", ed. J S Millar, Plenum Press, NY, 1987, vol 1, pg 157

15. R E Peierls, "Quantum Theory of Solids" (Oxford Univ Press), London, 1955, pg 108

16. F A Cotton and G W Wilkinson, "Advanced Inorganic Chemistry– A Comprehensive Text", 4th ed, J Wiley & Sons, NY, 1980, pg 678

17. J M Ziman, "Principles of the Theory of Solids", Cambridge Univ. Press, London, 1964

18. W Kohn, Phys.Rev.Lett., 1959, 2, 393

19. B Renker, H Rietschel, L Pintschovius, W Gläser, P Brüesch, D Kuse and M J Rice, Phys.Rev.Lett., 1973, 30, 1144

20. R Comes and G Shirane in "Highly Conducting One Dimensional Solids", ed J T Devreese, N P Evrard and V E Van Doren, Plenum, NY, 1979, pg 17

21. J A McCleverty, Prog.Inorg.Chem., 1968, 10, 49

22. (a) G N Schrauzer in 'Transition Metal Chemistry', vol 4, R C Carlin, ed., Marcel Dekher, NY, 1968, pg 299

(b) G N Schrauzer, Acc.Chem.Res., 1969, 2, 72

23. E Hoyer, W Dietzsch and W Schroth, Z.Chem., 1971, 11, 41

24. R Eisenberg, Prog.Inorg.Chem., 1970, 12, 295

25. A E Underhill in "Dithiolenes and Related Ligands", Comprehensive Coordination Chemistry, vol 2, ed Pergamon Press, NY, 1987, pg 595

26. (a) G Bähr and H Schleitzer, Chem.Ber., 1955, 88, 1771

(b) G Bähr and H Schleitzer, *ibid.*, 1957, 90, 438

27. H B Gray, R Williams, I Bernal and E Billig, J.Am.Chem.Soc., 1962, 84, 3596

28. A Davison, N Edelstein, R H Holm and A H Maki, J.Am.Chem.Soc., 1963, 85, 2029

29. A L Balch and R H Holm, J.Chem.Soc.,Chem Commun., 1966, 552

30. R Eisenberg and J A Ibers, J.Am.Chem.Soc., 1965, 87, 3776

31. A E Smith, G N Schrauzer, V P Mayweg and W Heinrich, J.Am.Chem.Soc., 1965, 87, 5956

32. R Eisenberg, E I Stiefel, R C Rosenberg and H B Gray, J.Am.Chem.Soc., 1966, 88, 2874

33. E I Stiefel, K Dori and H B Gray, J.Am.Chem.Soc., 1967, 89, 3353

34. J M Williams and A J Schultz, ref. 14, pg 73

35. K W Browall and L V Interrante, J.Coord.Chem., 1973, 3, 27

36. J J Fendley and A K Jonscher, J.Chem.Soc.(Faraday 1)., 1973, 1213

37. E J Rosa and G N Schrauzer, J.Phys.Chem., 1963, 67, 508

38. W E Geiger Jr, J.Phys.Chem., 1973, 77, 1862

39. G Manecke and D Wöhrle, Makromol.Chem., 1968, 116, 36

40. F Wudl, C H Ho and A Nagel, J.Chem.Soc.,Chem.Commun., 1973, 923

41. L V Interrante, K W Browall, H R Hart Jr, I S Jacobs, G D Watkins and S H Wee, J.Am.Chem.Soc, 1975, 97, 889

42. J S Kasper, L V Interrante and C A Secaur, J.Am.Chem.Soc., 1975, 97, 890

43. M G Miles, J D Wilson, D J Dahm and J H Wagenskneckt, J.Chem.Soc.,Chem Commun., 1974, 751

44. L Alcacer and A H Maki, J.Chem.Phys., 1974, 78, 215

45. A Kobayashi and Y Sasaki, Bull.Chem.Soc.Jpn., 1977, 50, 2650

46. K W Plumlee, B M Hoffmann, M T Ratajack and C R Kannewurf, Solid.State.Commun., 1974, 15, 1651

47. K W Plumlee, B M Hoffmann, J A Ibers, Z G Soos, J.Chem.Phys., 1975, 63, 1926

48. E A Perez–Albuerne, L C Isett and R K Haller, J.Chem.Soc.,Chem Commun., 1977, 417

49. C J Fritchie Jr, Acta.Crystallogr., 1966, 20, 107

50. M J Baker–Hawkes, Z Dori, R Eisenberg and H B Gray, J.Am.Chem.Soc., 1968, 90, 4253

51. J H Enemark and J A Ibers, Inorg.Chem., 1968, 7, 2636

52. W C Hamilton and I Bernal, Inorg.Chem., 1967, 6, 2003

53. D R Rosseinsky and R E Malpas, J.Chem.Soc.,Dalton Trans., 1979, 749

54. D I Clemenson, A E Underhill, M B Hursthouse and R L Short, J.Chem.Soc.,Dalton Trans., 1988, 1689

55. L C Isett, D M Rosso and G L Bottger, Phys.Rev.(B)., 1980, 22, 4739

56. M M Ahmad, D J Turner, A E Underhill, A Kobayashi, Y Sasaki and H

Kobayashi, J.Chem.Soc.,Dalton Trans., 1984, 1759

57. P I Clemenson and A E Underhill, J.Chem.Soc.,Dalton Trans., 1989, 67

58. A E Underhill and M M Ahmad, J.Chem.Soc.,Chem Commun., 1981, 67

59. M M Ahmad and A E Underhill, J.Chem.Soc.,Dalton Trans., 1982, 1065

60. A Kobayashi, Y Sasaki, H Kobayashi, A E Underhill and M M Ahmad, J.Chem.Soc.,Chem Commun., 1982, 390

61. A Kobayashi, T Mori, Y Sasaki, H Kobayashi, M M Ahmad and A E Underhill, Bull.Chem.Soc.Jpn., 1984, 57, 3262

62. J R Cooper, M Miljak, M M Ahmad and A E Underhill, J.de.Physique (Colloque)., 1984, 44 (C3), 1391

63. A E Underhill, M M Ahmad, D J Turner, P I Clemenson, K 64. Carneiro, Shen Yueqiuan and K Mortensen, Mol.Cryst.Liq.Cryst., 1985, 120, 369

64. A E Underhill and M M Ahmad, Mol.Cryst.Liq.Cryst., 1982, 81, 223

65. M M Ahmad and A E Underhill, J.Chem.Soc.,Dalton Trans., 1983, 165

66. G Holdcroft and A E Underhill, J.Chem.Soc.,Dalton Trans., 1985, 165

67. A Kobayashi, Y Sasaki, H Kobayashi, A E Underhill and M M Ahmad, Chem.Lett., 1984, 305

68. I D Parker, R H Friend, P I Clemenson and A E Underhill, Nature., London, 1986, 324, 547

69. M B Hursthouse, R L Short, P I Clemenson and A E Underhill, J.Chem.Soc.,Dalton Trans., 1989, 1101

70. I D Parker, R H Friend and A E Underhill, Synth.Met., 1989, 29, F195

71. M M Ahmad, D J Turner, A E Underhill, C S Jacobsen, K Mortensen and K Carneiro, Phys.Rev.B., 1984, 29, 4796

72. R A Clark and A E Underhill, Synth.Met., 1988, 25, 227

73. J Ribas and P Cassoux, C R Hebd.Seances Acad Sci.,Ser B., 1981, 293, 287

74. G C Papavassiliou, Z.Naturforsch.,Teil B., 1981, 36, 1200

75. G C Papavassiliou, Mol.Cryst.Liq.Cryst., 1982, 86, 159

76. L Valade, M Bousseau, A Gleizes and P Cassoux, J.Chem.Soc.,Chem Commun., 1983, 110

77. L Valade, J.-P Legros, M Bousseau, P Cassoux, M Garbauskas and L V Interrante, J.Chem.Soc.,Dalton Trans., 1985, 783

78. P Cassoux, L Valade, M Bousseau, J.-P Legros, M Garbauskas and L V Interrante, Mol.Cryst.Liq.Cryst., 1985, 120, 377

79. R Kato, T Mori, A Kobayashi, Y Sasaki and H Kobayashi, Chem.Lett., 1984, 1

80. M Bousseau, L Valade, J.-P Legros, P Cassoux, M Garbauskas and L V Interrante, J.Am.Chem.Soc., 1986, 108, 1908

81. M Bousseau, L Valade, M.-F Bruniquel, P Cassoux, M Garbauskas and L V Interrante and J S Kasper, Nov.J.Chim., 1984, 8, 3

82. L Brossard, M Ribault, M Bousseau, L Valade and P Cassoux, C R Hebd.Seances Acad Sci.,Ser B., 1986, 302, 205

83. P Cassoux, L Valade, M Bousseau, J.-P Legros, M Garbauskas, L V Interrante, Mol.Cryst.Liq.Cryst., 1985, 120, 377

84. R A Clark and A E Underhill, Synth.Met., 1988, 27, B515

85. I Hawkins, R A Clark, C E Wainwright and A E Underhill, Mol.Cryst.Liq.Cryst., 1990, 181, 209

86. R D Schmidt, R M Wing and A H Maki, J.Am.Chem.Soc., 1969, 91, 4394

87. W E Geiger Jr and A H Maki, J.Phys.Chem., 1971, 75, 2387

88. A Singhabhandhu, P D Robinson, J H Fang and W E Geiger Jr, Inorg.Chem., 1975, 14, 318

89. J A Ibers, L J Pace, J Martinsen and B M Hoffman, Struct.Bonding.(Berlin), 1982, 50, 1

90. L Alcacer and H Novais, "Extended Linear Chain Compounds", 1983, 3, 319

91. L V Interrante, Adv.Chem.Ser., 1976, 150, 1

92. L V Interrante, J W Bray, H R Hart Jr, J S Kasper, P A Piacente, G D Watkins, J.Am.Chem.Soc., 1977, 99, 3523

93. J W Bray, H R Hart Jr, L V Interrante, I S Jacobs, J S Kasper, P A Piacente, and G D Watkins, Phys.Rev., 1977, B16, 1359

94. M G Miles and J D Wilson, Inorg.Chem., 1975, 14, 2357

95. R C Wheland and J L Gillson, J.Am.Chem.Soc., 1976, 98, 3916

96. J W Bray, H R Hart Jr, L V Interrante, I S Jacobs, J S Kasper, G D Watkins, S H Lee and J C Bonner, Phys.Rev.Lett., 1975, 35, 744

97. I S Jacobs, J W Bray, H R Hart Jr, L V Interrante, J S Kasper, G D Watkins, D E Prober and J C Bonner, Phys.Rev., 1976, B14, 3036

98. J S Kasper and L V Interrante, Acta.Crystallogr., 1976, B32, 2914

99. F Wudl, J.Am.Chem.Soc., 1975, 97, 1962

100. C Getten, These, Université des Sciences et Techniques du Languedoc, Académie de Montpellier, 1979

101. P Calas, J M Fabre, M Khalife-el-Saleh, A Mas, E Torreilles and L Giral, Tetrahedron.Lett., 1975, 4475

102. P Calas, J M Fabre, A Mas, M Khalife-el-saleh, E Torreilles, L Cot and L Giral, Mol.Cryst.Liq.Cryst., 1976, 32, 151

103. A E Underhill, J S Tonge, P I Clemenson, Mol.Cryst.Liq.Cryst., 1985, 125, 439

104. W Reith, K Polborn and E Amberger, Angew.Chem.Int.Ed Engl., 1988, 27(5), 699

105. G N Schrauzer, V P Mayweg, H W Fink and W Heinrich, J.Am.Chem.Soc., 1966, 88, 4604

106. A N Balch, Inorg.Chem., 1968, 7, 13

107. G N Schrauzer and V P Mayweg, J.Am.Chem.Soc., 1965, 87, 1483

108. A Davison, N Edelstein, R H Holm and A H Malik, Inorg.Chem., 1964, 3, 814

109. V P Mayweg and G N Schrauzer, Chem.Commun., 1966, 640

110. E I Stiefel, L E Bennett, Z Dori, T H Crawford, C Simo and H B Gray, Inorg.Chem., 1970, 9, 281

111. W Schrath and J Peschel, Chimia., 1964, 18, 171

112. L J Theriot, K F Ganguli, S Kavanos, I Bernal, J.Inorg.Nucl.Chem., 31, 3133

113. J.Chatt, L.M.Vallarino and L.M.Venanzi, J.Chem.Soc., 1957, 2496

114. F Feher, in "Handbook of Preparative Inorganic Chemistry", vol 1, ed G Brauer, Academic Press, NY, 1967, pg 411

115. H W Roesky and H Weiser, Angew.Chem.Int.Ed.Engl., 1973, 12, 674

116. R.Uson, J.Vicente & J.Oro, Inorg.Chim.Acta., 1981, 52, 29

117. E Billig, R Williams, I Bernal, J H Waters and H B Gray, Inorg.Chem., 1964, 3, 663

118. G M Sheldrick, SHELXTL, An Integrated System for Solving, Refining and Displaying Crystal Structures from Diffraction Data. University of Göttingen, F.R.G. (1978); Revision 4.1 (August 1983)

119. G A Bowmaker, P D W Boyd and G K Campbell, Inorg.Chem., 1980, 19, 2679

120. C W Schläpfer and K Nakamoto, Inorg.Chem., 1975, 14, 1338

121. P F Kelly, Ph.D thesis, University of London, 1987

122. A Davison, N Edelstein, R H Holm and A H Malik, Inorg.Chem., 1963, 2, 1227

123. R L Schlupp and A H Maki, Inorg.Chem., 1974, 13, 44

124. W E Geiger Jr, C S Allen, T E Miner and F E Senftleber, Inorg.Chem., 1980, 16, 2003

125. J H Noordik and P T Beurskens, J.Cryst.Molec.Struct., 1971, 1, 33

126. E.W.Abel and C.R.Jenkins, J.Chem.Soc.A., 1967, 1344

127. N G Connelly, J A McCleverty and C J Winscom, Nature., 1967, 216, 999

128. M J Hayes and A E Moran, J.Chem.Soc.A., 1967, 1344

129. I P Parkin, Ph.D thesis, University of London, 1989

130. A.Balch and R.H.Holm, J.Am.Chem.Soc., 1966, 88, 5201

131. L H Jones and R A Penneman, J.Chem.Phys., 1954, 22, 965

132. J S Miller, Inorg.Synth., 1979, 19, 13

133. A Pignedol, G Peyronel and L Antolini, Acta.Cryst., 1974, 30B, 2181

134. G J Kubas and L H Jones, Inorg.Chem., 1974, 13, 2816

135. D M Sweeny, I Nakagawa, S Mizushima and J V Quagliano, J.Am.Chem.Soc., 1956, 78, 889

136. C W F T Pistorius, Z.Phys.Chem., 1960, 23, 197

137. G N Schrauzer and V P Mayweg, J.Am.Chem.Soc., 1965, 87, 3585

Part 2: Synthetic organic metal conductors.

Synthetic Organic Metal Conductors

2.1.1. Introduction

Research on organic donors did not accelerate until after the synthesis of the π–electron acceptor tetracyano–p–quinomethane (TCNQ) in 1960[1] and the sulphur–based electron donor tetrathiafulvalene (TTF) in 1970[2]. The formation of the π donor–acceptor complex TTF–TCNQ in 1973[3,4] resulted in high metallic conductivity to almost $\sim 10^4$ Scm^{-1} around 55K. The formation of a semiconducting/insulating state occurs below the transition temperature owing to the instabilities inherent in the system with one–dimensional or quasi–one–dimensional electron motion (Peierls charge density wave (CDW) or Overhauser spin density wave (SDW) type)[5,6].

Altering the basic TTF framework by substitution of S by Se has resulted in considerable success in reducing the metal–insulator transition. The conducting state of the Se derivative TSF–TCNQ was extended down to 28K[7] and reduced even further to 16K[8] in the hexamethylene derivative HMTSF–TCNQ. In 1978, the conductivity of the 2,5–dimethyl–TCNQ derivative, TMTSF–DMTCNQ was shown to be $\sim 10^5$ Scm^{-1} at 10K under applied pressure[9].

Substitution of sulphur atoms with selenium led to the synthesis of several charge transfer salts of the type $[TMTSF]_2X$, X = charge compensating monovalent anion such as PF_6^-, AsF_6^- or ClO_4^- [10,11,12]. Structural studies indicated that the dimensionality of the system was increased by an infinite "sheet network" of apparently weak, intermolecular donor–donor (Se···Se)[13] interactions which provided a pathway for electron conduction and suppression of a one dimensional Peierls transition. Superconductivity has been observed in many TMTSF salts under applied pressure (to inhibit metal–insulator

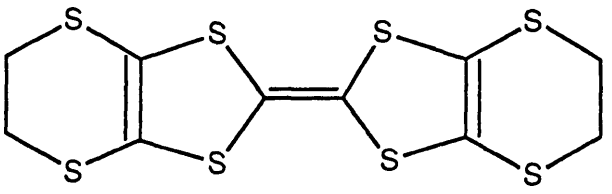
transitions) with $[TMTSF]_2ClO_4$ being a superconductor [T_c~ 1.2K] at ambient pressure[14].

Various approaches have been tried to stabilize the metallic state down to low temperatures. The more diffuse p and d orbitals centered on selenium and tellurium give larger intrachain bandwidths and also favours increased interchain interactions. A large number of Se containing donors are known, but tetratellurafulvalenes are harder to synthesize and are characterised by insolubility in organic solvents.

Organic charge–transfer salts of BEDT–TTF (bis(ethylenedithio)–tetrathiafulvalene, abbreviated ET– see *fig.*, 2.1.1.) were first reported in 1982. The ET salts are of great interest due to the subtle interplay between a rich variety of structural types and the varied solid state properties, most notably superconductivity, that they exhibit. $[ET]_2ClO_4(tce)_{0.5}$ (tce = 1,1,2–trichloroethane) was found to be metallic from room temperature (σ_{max}~ 10^3 Scm^{-1} at 16K) down to 1.4K (σ~ 600 Scm^{-1})[15]. The $[ET]_2X$ systems were also found to contain two–dimensional (2D) "networks" of short S···S interactions which, in effect, increase their "dimensionality" and intermolecular electronic "communication"[16,17]. Shortly after, pressure induced superconductivity (T_c~ 2K, P~ 4Kbar) was found in $[ET]_2ReO_4$[18]. In contrast, the isostructural $[ET]_2BrO_4$ behaves as a metal above 200K (σ~ 600 Scm^{-1}) with a semiconducting state below 100K[19,20].

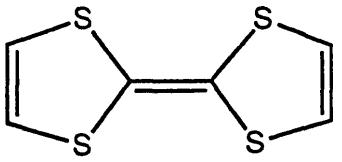
Anions of various types and geometries have been applied in ET salts which include linear, square planar, tetrahedral, octahedral, trigonal planar, polymeric and even cluster–type as in $Mo_6Cl_{14}^{2-}$[21] and $Re_6Se_5Cl_9^-$[22].

Salts of square planar anions include β–$[ET]_2AuCl_4$[23], $[ET]_2Au(CN)_2Cl_2$[23] and the 1:1 salts $[ET]AuCl_2AuCl_4$[24] and $[ET]AuCl_2Br_2$[25]. The crystal and band electronic structure of



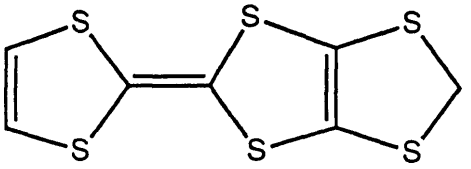
BEDT-TTF

bis(ethylenedithio)-tetrathiafulvalene



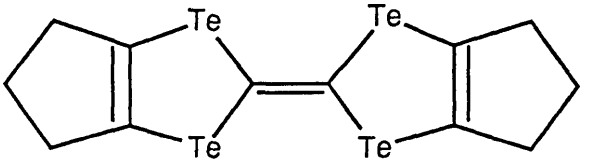
TTF

tetrathiafulvalene



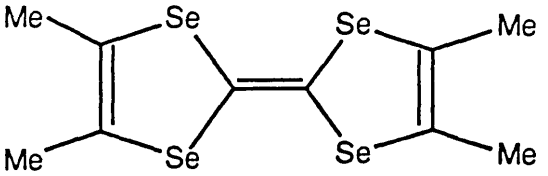
MDT-TTF

methylenedithio-tetrathiafulvalene



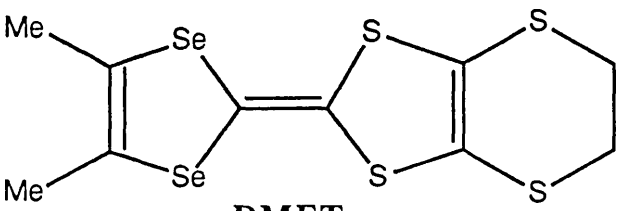
HMTTeF

hexamethylenetetratellurafulvalene



TMTSF

tetramethyltetraselenafulvalene



DMET

dimethyl(ethylenedithio)-diselenadithiafulvalene

fig., 2.1.1. Structures of organic donor molecules

β-$[ET]_2AuCl_4$ is related to the β-phase superconductors, β-$[ET]_2X$ (X^- = I_3, AuI_2, IBr_2) but undergoes a destructive phase transition at 126K. The band electronic structure of $[ET]_2Au(CN)_2Cl_2$ indicates 1D metallic behaviour at room temperature with a broad metal–insulator transition between 250–300K as supported by ESR measurements. Crystals of $[ET]AuCl_2AuCl_4$, obtained by electrocrystallisation of $[Bu_4N][AuCl_4]$ and ET in benzonitrile, were found to be semiconductive ($\sigma_{rt}\sim$ 0.25 Scm^{-1}, E_a= 80 meV). The structure was found to consist of planar $AuCl_4^-$ anions, which form an anion sheet and formally $Au(II)Cl_2^0$ incorporated in the ET sheet. The oxidation state of the $AuCl_2$ species was inferred from the bond lengths of the ET molecule, which indicated ET^+. The anomolous valences was assumed to be stabilized by close interaction beween the ET molecules and sandwiched $AuCl_2$ molecules. In the case of $AuBr_4^-$, the compound of composition $[ET]_2[AuBr_2][AuBr_4].C_6H_5CN$ has been noted. $[ET]AuBr_2Cl_2$ was found to be a narrow band-gap semiconductor ($\sigma_{rt}\sim 3\times10^{-4}$ Scm^{-1}, E_a= 130 meV); the structure consists of stacks of $AuBr_2Cl_2^-$ anions and ET^+ cations which are both slipped and tilted.

Salts of $[ET]_2X$ where X = octahedral anions (PF_6^-, AsF_6^- and SbF_6^-) are either semiconductors (α-$[ET]_2PF_6$: $\sigma\sim$ 0.1 Scm^{-1})[26] or metals (β-$[ET]_2PF_6$: $\sigma\sim$ 10–20 Scm^{-1})[27,28] with metal–insulator transitions occuring near room temperature. In comparison, the $[TMTSF]_2X$ salts (X^- = PF_6^-, AsF_6^- and SbF_6^-)[29] are generally metallic down to ~ 15K with suppression of a metal–insulator transition under applied pressure and a superconducting state near 1K.

ET charge transfer salts containing tetrahedral anions are historically significant, due to the first evidence of metallic conductivity over an extended temperature range ($[ET]_2ClO_4(tce)_{0.5}$)[15], and the first evidence of a superconducting state ($[ET]_2ReO_4$ under applied

pressure[18]) for this class of compound. The 2D extended S···S network in $[ET]_2ClO_4(tce)_{0.5}$ was correlated to isotropic conductivity in the ab-plane (σ_{rt}~ 25:25:10^{-3} Scm^{-1}). The suppression of a metal-semiconductor transition at 81K for $[ET]_2ReO_4$, by applied pressure, results in superconductivity at T_c~ 2K. The tetrahedral oxyanion salts tend to grow multiple phases and include $[ET]_2X$ (X^- = BrO_4[19,20], ReO_4[18]), $[ET]_2X(solvent)_{0.5}$ (X^- = ClO_4[15], BrO_4[30], ReO_4[31]) and $[ET]_3X_2$ (ClO_4[32], BrO_4[30], ReO_4[33,34]). ET derivatives with larger tetrahedral anions include $[ET]_2InBr_4$[35] and $[ET]_2FeCl_4$[36], which are semiconductors (σ_{rt}~ 10^{-2}-10^{-1} Scm^{-1}, E_a≈ 200 meV) with no evidence of a metallic state under applied pressure.

ET salts with trigonal planar anions include $[ET]_2[C(CN)_3]$[37] which exhibits a metal-insulator transition at 180K and room temperature conductivity of 1 Scm^{-1}, and the α,β and γ phases of NO_3^-[38].

There are a wide variety of polymeric anions which include $[ET]Ag_4(CN)_5$[39], $[ET]_3Ag_xI_8$ (x ~ 6.4)[40], κ-$[ET]_2Ag(CN)_2(H_2O)$[41], $[ET]Ag_{1.6}(SCN)_2$[42], $[ET]Cu_2(NCS)_3$[42], $[ET]Ag_{2.4}Br_3$[43] and $[ET]_2Cu_5I_6$[44]. The bis(dicyanamido)cuprate(I) salt, κ-$[ET]_2Cu[N(CN)_2]Br$[45] represents the highest transition temperature at ambient pressure (T_c= 11.6K) for an organic superconductor to date; the isostructural Cl salt, κ-$[ET]_2Cu[N(CN)_2]Cl$[46] has the highest superconducting transition temperature (T_c= 12.5K) accomplished by application of minimal pressure (0.3kbar, dT_c/dP= -3.5K/kbar) following the suppression of a semiconductor-superconductor transition (42K). Both are examples of a series of BEDT-TTF salts with polymeric anions, the latter formed by a (d^{10}) or ($d^{10}s^2$) metal cation (e.g., Ag^+, Au^+, Cu^+, Hg^{2+}, Bi^{3+}) and bridging halide or pseudo-halide anions. Other examples include $[ET]_2HgBr_3(tce)$[47], $[ET]BiI_4$[48], κ-$[ET]_4Hg_{3-x}Br_8$[49] and $[ET]_4Hg_{3-x}Cl_8$[50]. The interweaving

of metal ions with low coordination numbers (2 and 3), and linear bridging ligands with the donor radicals results in unusual 3D networks and avoids the possibility of spin or charge density waves, which drive materials with metallic conductivity to semiconductors or insulators at low temperatures. The polymeric anion ET salts listed show metallic behaviour with room temperature conductivities less than 50 Scm^{-1}.

The anions in these salts, while not directly involved in the electronic conduction, play a vital role in mediating the packing motif of the ET molecules and in governing the lattice (phonon) softness. Therefore the electrical properties of ET salts depend heavily on the symmetry, size and charge of the anion.

Structural–property correlations have been developed for the β–$[ET]_2X$ superconductors (X^- = I_3, T_c: 8K (0.5kbar); AuI_2, T_c: 4.98K and IBr_2, T_c: 2.8K)[51] where both the S···S distances in the corrugated sheet networks and T_c increase concomitantly with linear anion length. Together with the negative pressure dependence of T_c (ca., –1K/kbar) in these materials, led to the suggestion that β–$[ET]_2X$ superconductors with even higher T_c's might be realised by increasing the conducting intermolecular S···S contacts inside the donor lattice by use of anions longer than I_3^- (while maintaining short intradimer contacts). Candidate anions such as $(NC–Ag–CN)^-$ and $(I–Ag–I)^-$ led to the synthesis of the first polymeric anion ET conductors, $[ET]Ag_4(CN)_5$[39] and $[ET]_3Ag_{6.4}I_8$[40].

The discovery of the polymeric anion superconductor, κ–$[ET]_2Cu(NCS)_2$[52,53,54,55] with the highest resistive T_c (10.4K) in an organic superconductor at that time represented a new structural class, entirely different from the β–phase salts, viz., the κ–type salts contain orthogonally arranged molecular dimers such that donor molecule "stacks" do not exist when compared to the corrugated sheet network

of β–phase salts.

There are four classes of organic electron donor molecules which form κ–phase structures, viz., BEDT–TTF, MDT–TTF (methylenedithio–tetrathiafulvalene), DMET (dimethyl(ethylenedithio)–diselenadithiafulvalene) and BMDT–TTF. Superconductivity has been only observed in the first three of these classes, κ–$[ET]_2X$, $X^- = I_3$[56], $Cu(NCS)_2^-$, $Cu[N(CN)_2]Br^-$ and κ–$[ET]_4Hg_{2.89}Br_8$; κ–$[MDT\text{–}TTF]_2AuI_2$ (T_c 4.5K)[57] and κ–$[DMET]_2AuBr_2$ (T_c 1.9K)[58].

An examination of the molecular packing arrangements (*fig.*, 2.1.2.) reveal that superconductivity is related to (i) bond–over–ring intradimer molecular packing and (ii) relatively short (~ 3.35Å) intradimer separations, i.e., considerably shorter than the 3.60–3.70Å spacing in the non–superconducting κ–$[ET]_2Ag(CN)_2.H_2O$[41] and κ–$[BMDT\text{–}TTF]_2Au(CN)_2$[59] and a reason for the lack of ambient pressure superconductivity in $[ET]_4Hg_3Cl_8$[60,61] with an intradimer separation of 3.60Å. The κ–type structure was first observed in the non–superconducting but metallic derivative κ–$[BMDT\text{–}TTF]_2Au(CN)_2$ which has a bond–over–bond arrangement and relatively "hard" $-CH_2\cdots$anion interactions, corresponding to lower T_c's in β–phase BEDT–TTF materials.

The conformation of the ethylene groups in β– and κ–[ET] systems can be correlated to T_c[62]. The "staggered" conformation found in β^*–$[ET]_2I_3$ (T_c~ 8K) and κ–$[ET]_2Cu(NCS)_2$ can be associated with "softer" $-CH_2\cdots$anion contacts[63], and hence a larger electron–phonon coupling constant (λ) and higher T_c, than in β–$[ET]_2X$ ($X^- = AuI_2$, IBr_2) and κ–$[ET]_2I_3$ (T_c= 3.6K)[56] superconductors which possess lower T_c's and eclipsed ethylene group conformations.

A possible correlation between the δ–C–C–H bending frequency

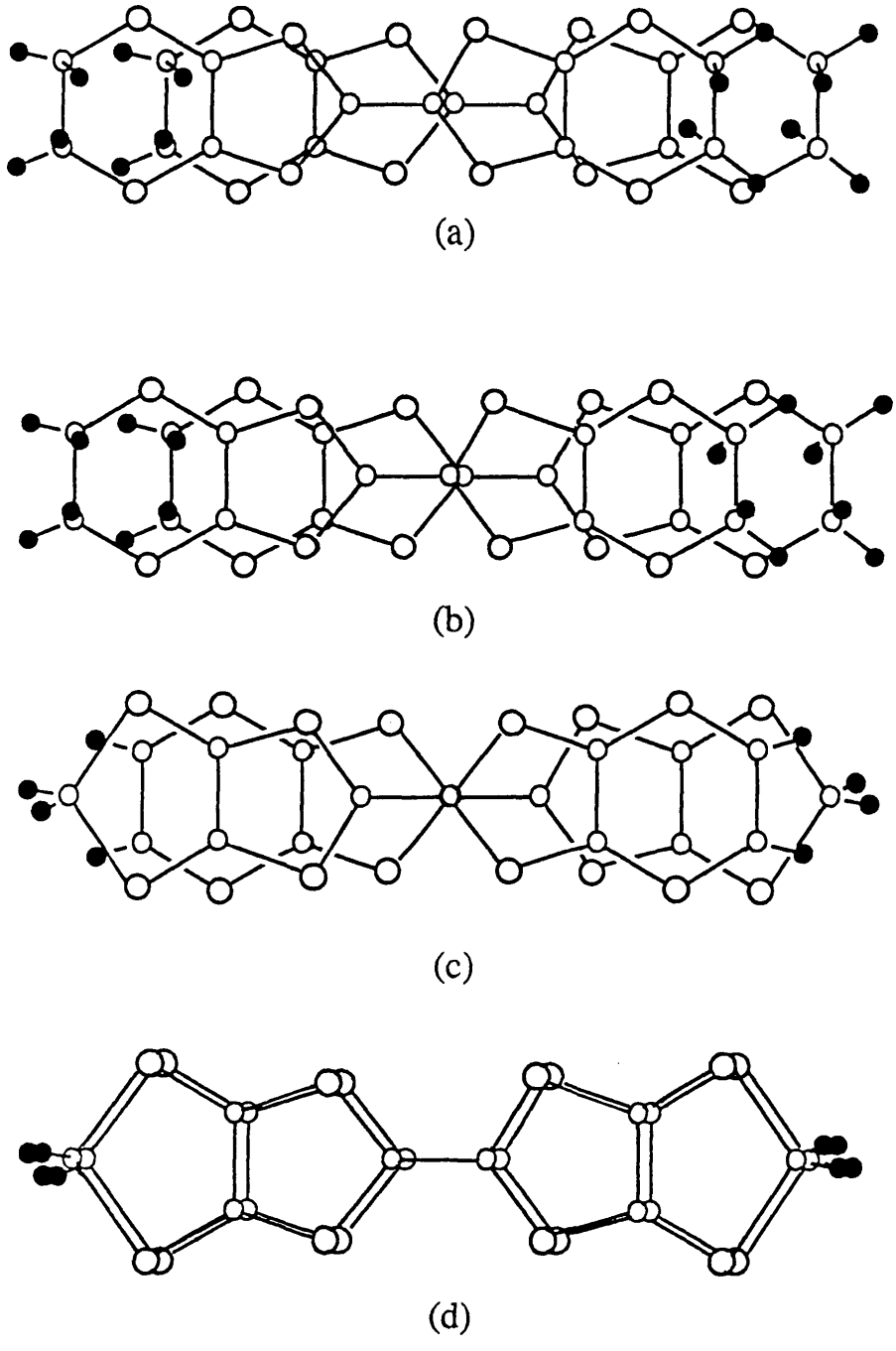


fig., 2.1.2. Projection views of donor dimers in: (a) κ-$[ET]_2Cu(NCS)_2$, (b) κ-$[ET]_2I_3$, (c) κ-$[MDT\text{-}TTF]_2AuI_2$, (d) κ-$[BMDT\text{-}TTF]_2Au(CN)_2$

and "lattice softness" has been postulated[64] (softness of ET molecule–anion interactions with respect to phonon modes such as translational or librational). With an increase in H···X^- distances, the ν(CH) stretching frequencies should increase and δ–C–C–H frequencies should decrease for ET salts, leading to a softening effect in the lattice. The electron–phonon coupling constant (λ) increases as the lattice becomes softer and T_c increases[65]. For the series β–$[ET]_2X$ (X^- = I_3, IBr_2, AuI_2) and β^*–$[ET]_2I_3$, both T_c and λ increase as the H···X^- contacts increase[66] (in length).

All the ET–based ambient pressure superconductors known to date involve: (a) linear anions, e.g., I_3^-[67,68], AuI_2^-[69,70], IBr_2^-[71]; (b) a polymeric network of monovalent (bent) anions, e.g., $Cu(SCN)_2^-$[52,53,54,55] where the packing resembles κ–$[ET]_2I_3$ (a 2D–sheet network composed of paired donor molecules with neighbouring pairs almost perpendicular to each other) and (c) a non–stoichiometric Hg–deficient anion as a polymeric chain network, e.g., $Hg_{2.89}Br_8^{2-}$[49,72].

The ET–based ambient pressure superconductors include β–$[ET]_2I_3$ [T_c~ 1.6K][67,68], γ–$[ET]_3[I_3]_{2.5}$ [T_c~ 2.5K][73,74], ϵ–$[ET]_2I_3[I_8]_{0.5}$ [T_c~ 2.5K][75], θ–$[ET]_2I_3$ [T_c~ 3.6K][76], κ–$[ET]_2I_3$ [T_c~ 3.6K][56], β–$[ET]_2IBr_2$ [T_c~ 2.8K][16,71], β–$[ET]_2AuI_2$ [T_c~ 5.0K][69,70], κ–$[ET]_2Cu(SCN)_2$ [T_c~ 10.4K][52,53], κ–$[ET]_4Hg_{2.89}Br_8$ [T_c~ 4.3K][72] and the highest transition temperature yet observed, in κ–$[ET]_2Cu[N(CN)_2]Br$ [T_c~ 11.6K][45].

Pressure induced superconductivity has been observed in $[ET]_2ReO_4$ [T_c~ 2K, 4Kbar][18], β^*–$[ET]_2I_3$ [T_c~ 8K, 1.3kbar][77,78], $[ET]_4Hg_{2.73}Cl_8$ [T_c~ 1.8K, 12kbar][60,61], $[ET]_3Cl_2(H_2O)_2$ [T_c~ 2K, 16kbar][79,80,81] and κ–$[ET]_2Cu[N(CN)_2]Cl$ [T_c~ 12.5K][46].

ET–based organic metals, though exceedingly poor metals with conductivities less than that of the best known organic conductors and

somewhat less conductive than the $[TMTSF]_2X$ class of organic metals, have a respectible standing as superconductors in comparison to the superconducting elements, with values of T_c between Ga ($T_c \simeq$ 1.1K) and just greater than Nb ($T_c \simeq$ 9.3K), which is the highest T_c for the elements.

It is generally believed that ET–based superconductors are likely BCS superconductors[82]. An energy gap of the order of $E_g \leq$ 4meV at the Fermi energy, ϵ_F, when the temperature is reduced below T_c, is responsible for many of the properties of BCS superconductors, and arises from attractive electron–lattice–electron interactions which allow the electrons to overcome their Coulomb repulsion. In fact, an increasingly large number of ambient pressure superconductors occur as the atomic number of the chalcogen atoms in the electron–donor molecule is decreased from Se to S. As suggested by Wudl and co workers[83], according to BCS theory (isotope effect), a lighter atom (oxygen) than S or Se in otherwise identical organic donor molecules could cause T_c to rise in the lighter atom salt ($T_c \approx 0.18(4t\hbar^2/Ma^2)^{1/2}$)[84] where t is the resonance integral and depends strongly on molecular distortions, a is the length of the order of one a.u., and M, the donor mass. A decrease in metallic bandwidth and increase in density of states at the Fermi level (T_c would be raised) is predicted. For the comparison in new high–T_c superconductors of La–Sr–Cu–O or Y–Ba–Cu–O type the value of t is about ten times larger and M = $16m_p$ (since the O atom vibrations are important). Thus values of T_c as high as 100K may be achieved in principle by the electron–phonon mechanism. The main difference is the frequency of phonons which couple strongly with electrons (large ET molecule vibrations versus light O atom oscillations). Therefore it seems possible to base further work on the electron–phonon mechanism (and higher values of T_c) if a

smaller molecule than ET could be used which would provide the same two or three–dimensional type of motion as the ET molecule does.

Current research has centred upon BEDO–TTF (bis(ethylenedioxy)tetrathiafulvalene) with the anions I_3^-, $AuBr_2^-$, AuI_2^- , $Au(CN)_2^-$, ClO_4^-, BF_4^-, PF_6^- and $Cu_2(NCS)_3^-$[85]. $[BEDO–TTF]_{2.4}I_3$[83] was found to be a wide–band metal (an increase in the metallic band width is observed thus stabilizing the metallic state down to low temperatures, contrary to the above). It is interesting to note that the deuterium isotope effect goes "the wrong way" in κ–d_8–$[ET]_2Cu(NCS)_2$, i.e., T_c increases[52,86]. Deuteration of β–$[ET]_2I_3$ gives rise to T_c, though the difference (1.15K for a protonated sample and 1.43 for a deuterated one) lies within the range of T_c reported by some authors (1.1 to 1.6K)[87]. On the other hand, β^*–$[ET]_2I_3$ seems to show a normal isotope effect[88]. While $[BEDO–TTF]_2PF_6$ is semiconducting and the $[BEDO–TTF]_2X$ salts (X^- = $AuBr_2^-$, $Au(CN)_2^-$ and ClO_4^-) are metallic only near room temperature and semiconducting at low temperatures, $[BEDO–TTF]_2AuI_2$ shows metallic conductivity at low temperature. β–$[BEDO–TTF]_3Cu_2(NCS)_3$[89] is a superconductor [$T_c \sim$ 1.06K] at ambient pressure. Whereas the salts of BEDT–TTF exhibit a great variety in donor molecule packing motifs, the salts of BEDO–TTF reported to date all possess very similar packing motifs with short C–H···O intra and intermolecular hydrogen bonding contacts. The similarity which occurs in the packing implies that the stabilization energy associated with C–H···O interactions is much greater than the associated C–H···S or C–H···C(sp^2) interactions and is comparable in magnitude to the stabilization energy resulting from a C–H···anion contact. Due to slight differences in interstack donor–donor overlap, β–$[BEDO–TTF]_3Cu_2(NCS)_3$ has a two dimensional Fermi surface while $[BEDO–TTF]_2X$ salts have a one–dimensional

Fermi surface.

Short intermolecular contacts can be grouped into three catagories: (a) the chalcogen–chalcogen (e.g., S···S, Se···Se), (b) the C–H···donor, and (c) the C–H···anion contacts. Ab initio SCF–MO/MP2[90] calculations reveal that chalcogen–chalcogen interactions are repulsive although the potential energy surface is soft near Van der Waals contact distances. Therefore the occurence of short X···X contacts in organic donor salts must originate mainly from attractive intermolecular interactions provided by the C–H···donor and C–H···anion contacts. Attractive interactions result from C–H···donor (e.g., C–H···heteroatom, C–H···C(sp^2) and C–H···H) and C–H···anion contacts, which provide the energy needed for the π–framework bending in the neutral donor molecule (to nearly planar in charge transfer salts of BEDT–TTF and BEDO–TTF) and conformational changes in the six membered ring (i.e., staggered or eclipsed). The interaction energies for C–H···X decrease in the order O > S > Se > Te and explains why in molecules such as $[BEDO–TTF]_2X$ (X^- = $AuBr_2$, ClO_4) the donor packing arrangement makes optimum use of C–H···O contacts within a donor stack as well as between adjacent donor stacks. The conformation of the six–membered ring is most stable when staggered but the potential surface for change to the eclipsed conformation is very soft. Hence packing arrangements and thus electronic properties are largely determined by optimum use of attractive C–H···donor and C–H···anion interactions in organic donor salts.

In addition, the increased structural dimensionality compared to quasi–1D systems of at least some of the ET–based metals appears to stabilize the metallic phase over a wide range of temperatures.

The ET molecule is an excellent electron donor for the synthesis of organic metals, due to an almost extended π system (D_{2h} symmetry)

based on a very flat central TTF portion with two pairs of sulphur atoms which have out–of–plane torsion angles of 2 to 8° and terminal carbon atoms extended from the plane (usually one above and one below) by as much as 1.1Å in some cases.

For the $[ET]_2X$ salts, in addition to the S···S intrastack interactions formed when the molecules form loosely stacked columns (via $\pi-\pi$ molecular overlap) there are four outer sulphur atoms which facilitate the formation of extensive interstack interactions (S···S contacts less than sum of Van der Waals radii[91]) and enhances the 2D electrical properties with $\sigma\sim 10^2$–10^3 higher in the sheet rather than the columnar direction. In most cases, a honeycomb network of S···S contacts is formed due to stacks of ET molecules being slightly out of phase and are so tightly packed that no anions or solvent molecules are positioned within the donor layer.

Partial oxidation of ET molecules produces an ET radical cation. An increase in the oxidation state of the ET molecule results in the lengthening of the C=C double bonds and shortening of the C–S bonds[92,93]; this is consistent with extended Hückel calculations which indicate that the highest occupied molecular orbital is bonding with respect to C=C and antibonding with respect to C–S. In addition the conjugated portion of the molecule tends to be more planar in charged species. The spin density for a partially charged ET molecule ($ET^{0.5}$) has been calculated using CNDO/2[35] and found to be twice as large for the sulphur atoms on the inner rings as those on the outer rings. In contrast, the charge density distribution is greater on the outer rings of the molecule. Therefore the inner rings of adjacent ET molecules are more strongly bonded and the outer rings are more strongly repelled. An indication that care must be taken in overinterpreting bonding networks derived by including only S···S bonds less than some

arbitary value (i.e., Van der Waals radii) is provided by the fact that, for the overlap integral for the two inner sulphur atoms to be the same as the two outer sulpur atoms, separated by 3.6Å, a separation of 4Å is required.

Though the ethylene groups of an ET molecule do not interact with any portion of an adjacent ET molecule, there are important interactions with the anions. The anions generally occupy a "layered" arrangement of separate sheets with H···X contacts (where X refers to an atom of the X^- anion) less than the sum of the Van der Waals radii.

Anion size and anion–CH_2 hydrogen interactions are important factors which control the packing of the ET molecule and thus the transport properties of the resulting charge–transfer salt. Alteration of the anion size and hence the donor–to–anion "hydrogen bonding" interactions has been correlated to the lattice softness and phonon frequencies and, therefore, to the superconducting T_c values.

Important intermolecular interactions between the anion and donor molecule were first noted in $[TMTSF]_2X$ salts (X^- = ClO_4^-, BF_4^-, ReO_4^-)[94,95,96] with H···X (H atoms of the methyl group in TMTSF) and Se···X contacts in the anion cavity. Donor–anion interactions depend on (1) the ET network motif (2) the anion layer motif and (3) the environment surrounding the anions. The α and β phases of $[ET]_2I_3$ show important differences in the respective 2D networks; α–$[ET]_2I_3$[97] is a semiconductor (σ_{rt}~ 60–250 Scm^{-1}) with narrow band gap but an insulator below ~ 135K. Among the β–$[ET]_2X$ salts, four are isostructural: the ambient pressure superconductors X^- = I_3^-, AuI_2^- and IBr_2^- (with T_c's ~ 1–8K) and the low temperature metal X^- = I_2Br^-[98] with metallic conductivity (σ_{rt}~ 20 Scm^{-1}) down to 0.5K but no observation of superconductivity even under pressure.

When the anion size is small in β–$[ET]_2X$ salts (X^- = ICl_2, BrICl)[99], the anisotropic contraction of donor–donor distances distorts the ET network to such an extent that the ET molecules are greatly dimerized within each stack. Thus donor–anion interactions (i.e., those indicated by short H···I, H···Br and H···Cl) are not only important for crystal packing but also for the physical properties.

The ET networks in the α–phase salt of $[ET]_2I_3$ have a herringbone pattern of adjacent columns of inclined ET molecules, while the β–phase has a uniform motif of identical ET stacks. Short H···I contacts are observed in both phases with the α–phase also exhibiting short anion–anion contacts.

In the series H···I, H···Br, H···Cl in β–$[ET]_2X$ (X = trihalide anions), the shortest observed contact distances are 2.97, 2.89 and 2.59Å, which are 0.38, 0.26 and 0.41Å less than the corresponding Van der Waals radii sum. The very short H···Cl contact distance in β–$[ET]_2ICl_2$[99] is due to the more electronegative Cl atom and is not strictly isostructural to other β phase salts (short contacts 2.59 to 2.77Å). A narrow range of distances (2.91 to 2.94Å) is observed for X^- = IBr_2 at 120K due to an unusual "trigonal" environment of close H atoms about each Br atom; the three shortest H···X contacts in β–$[ET]_2AuI_2$ (20K) are much larger, at 2.97 to 3.15Å.

The importance of anion length can be related to the expectation of ambient pressure superconductivity in ET salts with X^- intermediate in length between I_3^- (10.1Å) and IBr_2^- (9.3Å). Though the anion I_2Br^- is intermediate in length (9.7Å), the disorder created by the asymmetry of the anion i.e., I–I–Br as opposed to I–Br–I, means that it is not a superconductor[100].

Based on studies of $[TMTSF]_2X$ and β–$[ET]_2X$ organic conductors some structural features can be correlated:

(1) Donor molecules should form stable free radical (open–shell) species enabling the formation of partially filled bands in radical cation–anion salts.

(2) Planar or nearly planar donor molecules with sulphur atoms in the periphery that can pack together to form extended S···S networks are more likely to promote electrical conductivity in a 2D or 3D manner.

(3) Strong coupling in 2D or 3D is necessary to avoid Peierls distortion in quasi 1D metals resulting in metal–insulator transitions.

(4) Anions lacking a centre of symmetry should be avoided since they often introduce disorder into the crystal resulting in random electronic potentials and localisation of electrons in stacks leading to semiconducting or insulating phases.

(5) High purity crystalline synmetals are achieved by use of rigourously purified starting materials and slow electrocrystallisation.

Recent analyses of the structural features of κ–salts, together with the negative pressure dependence of T_c for κ–$[ET]_2Cu(NCS)_2$ (–3 to –3.6K/kbar), which is the largest known for any superconductor suggests that even higher T_c's may be attained by incorporation of even larger polymeric anions resulting in an enlarged unit cell and increased interdimer spacings while maintaining short 3.35Å intradimer distances. Similar arguments based on the effective "volume" of ET have also been put forward by Saito *et al*[101].

Experimental

2.2.1. Syntheses of Organic Donors:

BEDT-TTF (ET) has been known since 1978[102].

(a) *CS_2 route*: the key step involves the isolation of the 1,3-dithiole-2-thione-4,5-dithiolate anion (1) which is generated from the reduction of CS_2 either electrolytically[103] or by use of an alkali metal in DMF[104].

1

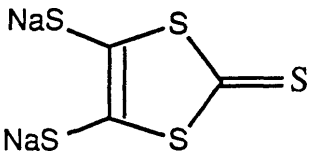


fig., 2.2.1.

The versatile dianion (1) leads to many sulphur-based organic donors, but is air and light sensitive; in addition, the concommitant formation of the trithiocarbonate anion lowers the yield and needs to be separated before reaction with $Br(CH_2)_nBr$. This can be achieved by formation of the bis-chelate zinc complex, $[R_4N]_2[Zn(dmit)_2]$ with subsequent separation of Na_2CS_3. Treatment of the Zn complex with benzoylchloride generates bis(benzoylthio)dithiole-thione, an air stable crystalline solid, which upon stirring with NaOMe, gives the anion (1) in pure form which can be used directly.

Reaction with dibromoalkane ($Br(CH_2)_nBr$, n = 2, 3) gives ethylene (or propylene)-dithio-1,3-dithiole-2-thione (2,5,7,9-tetrathiabicyclo[4.3.0]non-1(6)-en-8-thione!) which upon coupling in neat triethylphosphite gives ET or PT[105] (see *fig.*, 2.2.2.).

The zincate reacts with dibromomethane to produce 4,5-methylenedithio-1,3-dithiole-2-thione. Conversion to the thioxo

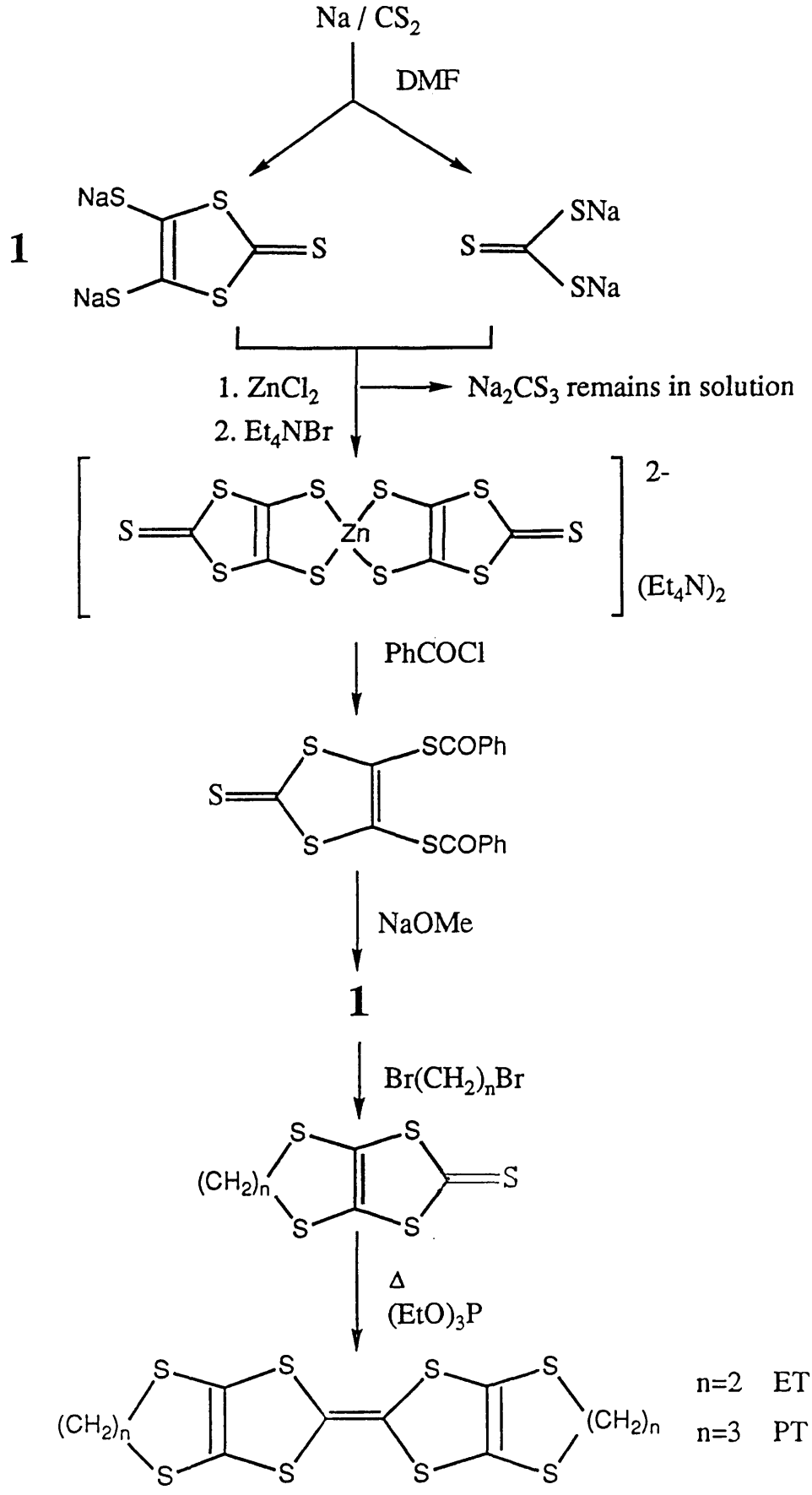
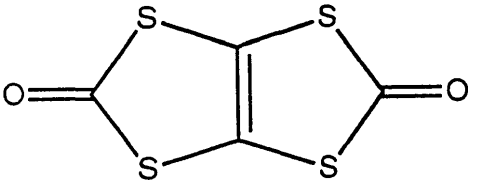


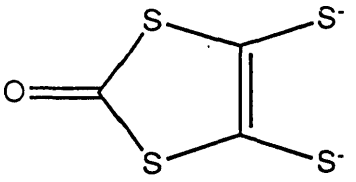
fig., **2.2.2.** Synthetic scheme for BEDT-TTF (ET)

group by $Hg(OAc)_2$ and coupling in neat triethyl phosphite yields bis(methylenedithio)-tetrathiafulvalene, BMDT-TTF or MT[106]. Thiapendione (*fig.*, **2.2.3.**) is a very important building block for donor synthesis and can be reached by treating the zincate with thiophosgene and then mercuric acetate[107], or alternatively refluxing dichloroacetate with potassium O-isopropyldithiocarbonate in acetone followed by acid initiated cyclization[108]. The commercial availability of thiapendione allows a wide variety of TTF analogues to be synthesized.



Thiapendione
fig., **2.2.3.**

The use of a weak base, Na_2CO_3 and a phase-transfer reagent to selectively cleave one carbonyl group generates the dithiolate anion[109]:



2-oxo-1,3-dithiole dianion
fig., **2.2.4.**

MT is conveniently prepared by treating the dithiolate anion with dibromomethane and is significantly shorter than the zincate route (*vide supra*). The 2-oxo-1,3-dithiole half unit in general undergoes facile coupling in neat phosphite and offers higher yields.

General: Microanalyses were provided by the Imperial College Microanalytical service. X-band epr measurements were made with a Varian E12 spectrometer, operating at about 9.2GHz.

Thf was distilled from sodium/benzophenone. 1,1,2-trichloroethane was purified by washing with conc. H_2SO_4 followed by 10% aqueous K_2CO_3, 10% $NaCl_{(aq)}$ and distilling from CaH_2 (b.p. 113.5°C). Benzonitrile was distilled from P_2O_5 (40°c/1mm Hg) and stored over 4Å sieves. Acetonitrile was distilled prior to use from CaH_2.

ET was prepared by the literature method[105] and recrystallised from chloroform. TTF (Aldrich Chem. Co) was recrystallised from CH_2Cl_2/cyclohexane; HMTTeF was used as received (Aldrich Chem.Co). $[Bu_4N][AuBr_4]$[110] and $[Bu_4N][Au(dithiolene)Br_2]$[111] (dithiolene = mnt, edt) were recrystallised from isopropanol. $[Ph_4As]_2[MCl_4]$ (M = Ni[112], Co[113]) were recrystallised from ethanol/ethyl acetate. Crystalline $K[Hg(CN)_2Br]$ was obtained by slow evaporation of an aqueous ethanolic solution of $Hg(CN)_2$ and KBr[114]. $[Ph_4As]_2[M(CS_3)_2]$ salts (M = Ni, Pd, Pt) were prepared as described[115]. $[Ph_4As]_2[M_2Cl_6]$ were obtained by addition of an excess of $[Ph_4As]Cl$ to an aqueous solution of K_2PtCl_4. Similarily, addition of Bu_4NBr to K_2MBr_4 (M= Pt, Pd) resulted in the formation of $[Bu_4N]_2[M_2Br_6]$[116,117].

2.2.2. Electrocrystallisations

Crystals of the highest purity are desired. Slow nucleation and the minimum of disturbances such as temperature variation and intermittent intense light are desired. Extremely clean and dry containers and electrodes, highly purified and dried materials (organic donors, inorganic anions and solvents) are prerequisites for successful crystal growth.

A typical experimental set–up involves dissolving 5–10 mg of the donor compound in the chosen solvent (11 ml) and placing in the anode compartment; 15–30mg of the anionic derivative in 12 ml of solvent is pipetted into cathodic cell retaining 1 ml which is added to the donor solution. The solutions are degassed for 30 s, the platinum wire electrodes placed in the H–cell (solution under argon) and a current density of 1 μAcm^{-2} applied using a constant current source. The H–cells are maintained in a temperature controlled environment (22°C) in the dark (to avoid possible photochemical decomposition of the donor).

Electrical Conductivity studies

Single crystal measurements were made using 4 probe dc techniques with silver/graphite paint as the contact material. Compressed pellet measurements were used for microcrystalline and powdered samples. The sample mounting was similar to that described by Coleman[118], using 25μm diameter 99.99% pure annealed gold wire. All single crystal measurements were along the direction of growth; the isotropic (anisotropic) nature of the crystals could not be established due to their size along the other two axies. Nearly all conductivity measurements of organic conductors show sample dependent variations, as a result of irregular crystal morphologies and crystal imperfections. The use of the term metallic conductivity refers to increasing electrical conductivity (decreasing resistivity) as the temperature is lowered. Forward runs refer to a decrease in the temperature step during conductivity measurements; the obverse is true for reverse runs. Hysteresis effects in the forward and reverse runs indicate the possible development of microcracks during the cooling cycle– see *fig.*, 2.3.21.

Preparation of $[ET]_4[Pt(mnt)(CN)_2]$ and $[HMTTeF]_3[Pt(mnt)(CN)_2]$

Black crystals of $[ET]_4[Pt(mnt)(CN)_2]$ were grown by electrocrystallisation of a solution of 2mM ET and 5mM $[Bu_4N]_2[Pt(mnt)(CN)_2]$ in thf, at a current density of $1\mu Acm^{-2}$. The crystals exhibited a metallic lustre, after washing with acetone and drying *in vacuo*; they were, however, too small and of insufficient quality for X–ray diffraction. Attempts to prepare crystals of better quality from 1,1,2–tce and benzonitrile were unsuccessful.
Found(%): C, 28.23; H, 1.37; N, 2.41. Calcd(%) for $[ET]_4[Pt(mnt)(CN)_2]$: C, 28.69; H, 1.67; N, 2.91.

Black crystalline blocks and clusters of $[HMTTeF]_3[Pt(mnt)(CN)_2]$ were obtained by elecrocrystallisation of 2mM HMTTeF and 5mM $[Bu_4N]_2[Pt(mnt)(CN)_2]$ in thf.
Found(%): C, 21.00; H, 1.52; N, 2.25. Calcd(%) for $[HMTTeF]_3[Pt(mnt)(CN)_2]$: C, 21.13; H, 1.52; N, 2.35

Conductivity measurements for the two salts were made on compressed discs.

A black microcrystalline solid was also obtained from electrocrystallisation of TTF and $[Bu_4N]_2[Pt(mnt)(CN)_2]$ in acetonitrile, with stoichiometry $[TTF]_2[Pt(mnt)(CN)_2]$.
Found(%): C, 27.00; H, 0.90; N, 7.09. Calcd(%) for $[TTF]_2[Pt(mnt)(CN)_2]$: C, 27.16; H, 1.01; N, 7.04.

Preparation of $[ET]_3[AuBr_4]$

Electrocrystallisation of a thf solution of ET (2mM) and $[Bu_4N][AuBr_4]$ (3mM) ($0.5\mu Acm^{-2}$) gave black microcrystalline clusters and blocks.
Found(%): C, 21.54; H, 1.38.

Calcd(%) for $[ET]_3AuBr_4$: C, 21.57; H, 1.45.

A segment cut from one of the blocks was suitable for X-ray diffraction; conductivity measurements were carried out on a compressed disc of the sample. Hexagonal plates and thin elongated platelets formed at the anode using benzonitrile as the solvent. Owing to the small size of the "coffin-like" plates, 2-probe (instead of the usual 4-probe) conductivity measurements were carried out on the plates. It was not possible to salvage the hexagonal plates in-tact. Microanalysis (Found(%): C, 21.28; H, 1.30) does not provide any conclusive evidence as to the identity of the compound and corresponds closely to that calculated for $[ET]_2AuBr_2$ (*vide infra*); the platelets exhibited semiconductive properties at room temperature, with no indication of a phase transition as observed for $[ET]_3AuBr_4$ (thf). It has been suggested that the redox potential for the reaction:

$$AuBr_4^- + 2e^- \rightarrow AuBr_2^- + 2Br^-$$

corresponds closely to the oxidation potential of ET[24], so that compounds of the type $[ET]_2AuBr_2$ are possible, of which there are several phases, i.e., α'-119,120, β''-132, δ-133, ς-134 and t-$[ET]_2AuBr_2$[134].

Electrocrystallisation of HMTTeF with $[Bu_4N][AuBr_4]$ in thf and benzonitrile proved unsuccessful, with only a light brown solid being deposited at the bottom of the anodic compartment, which could not be identified.

A black microcrystalline solid was obtained from electrocrystallisation of TTF and $[Bu_4N][AuBr_4]$ in benzonitrile, with approximate stoichiometry $[TTF]_5[AuBr_4]$.
Found(%): C, 23.86; H, 1.36. Calcd(%) for $[TTF]_5[AuBr_4]$: C, 23.42; H, 1.31.

Preparation of α'-$[ET]_2[AuBr_2]$

Further investigation into donor/anionic complexes containing square planar anions was carried out by electrocrystallisation of ET with $[Bu_4N][Au(mnt)Br_2]$ in thf. After 12 hours, very thin long plates had formed at the anode (*fig.*, **2.2.5.**). Identical lattice parameters and appropriate elemental analyses revealed the donor salt to be the α'-form of $[ET]_2[AuBr_2]$. Variation of the dithiolene to $[Au(edt)Br_2]^-$ and solvent to 1,1,2-tce resulted also in the formation of α'-$[ET]_2[AuBr_2]$[119].

Found(%): C, 21.33; H, 1.41. Calcd(%) for $[ET]_2[AuBr_2]$: C, 21.33; H, 1.43.

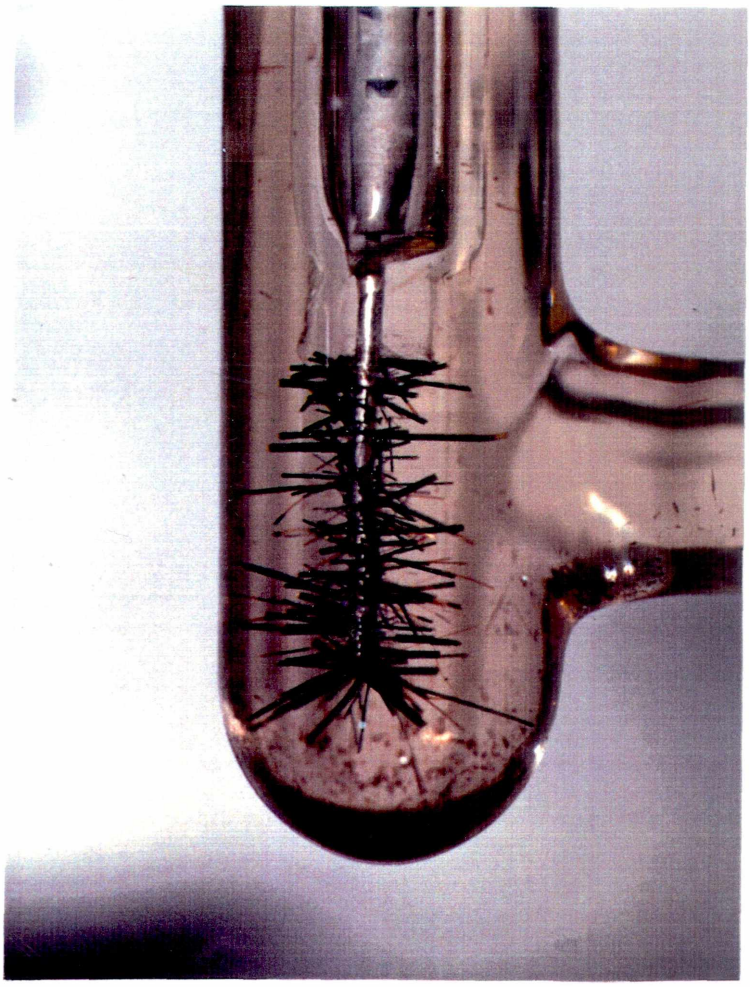


fig., **2.2.5.** Elongated plates of α'-$[ET]_2AuBr_2$ grown by electrocrystallisation of $[Bu_4N][Au(mnt)Br_2]$ and ET in thf

Preparation of $[ET]_3[NiCl_4].H_2O$

Long black needles of $[ET]_3[NiCl_4].H_2O$ were grown by electrocrystallisation of 3mM ET and 5mM $[Ph_4As]_2[Ni(CS_3)_2]$ in 1,1,2–tce at a current density of $1\mu Acm^{-2}$. Black clusters of the compound were also formed at the bottom of the anodic cell. The stoichiometry was determined by X–ray crystallography and confirmed by elemental analyses:

Found(%): C, 26.25; H, 1.90. Calcd(%) for $[ET]_3NiCl_4.H_2O$: C, 26.25; H, 1.91.

The surprise finding is that not only does the structure contain the $NiCl_4^{2-}$ anion (as opposed to the intended $Ni(CS_3)_2^{2-}$ anion), but the crystal structure also contains a water molecule encorporated during electrocrystallisation. The origin of $NiCl_4^{2-}$ may be suggested by HCl present in 1,1,2–tce, while the water may be due to recrystallisation of $[Ph_4As]_2[Ni(CS_3)_2]$ from CH_3NO_2/Et_2O.



"That's Dr. Arnold Moore. He's conducting an experiment to test the theory that most great scientific discoveries were hit on by accident."
(Hoff. © 1957, The New Yorker Magazine, Inc.)

Electrocrystallisation of $[Ph_4As]_2[Pt(CS_3)_2]$ and $[Ph_4As]_2[Pd(CS_3)_2]$ with ET in 1,1,2–tce, at a current density of $1\mu Acm^{-2}$, resulted only in the formation of a black non–crystalline solid (similar in shape to metal turnings) at the anode. Elemental analyses suggests a totally different

stoichiometry;

Found(%): C, 16.61; H, 0.98. Calcd(%) for $[ET]PtCl_4$: C, 16.64; H, 1.12

Found(%): C, 18.56; H, 1.20. Calcd(%) for $[ET]PdCl_4$: C, 18.98; H, 1.27.

The non–crystallinity of the two solids would agree with the 1:1 stoichiometry.

Initial epr measurements in the X–band range (9.120 GHz) at liquid nitrogen temperatures (~ 77K) consisted of a single Lorentzian shaped line. The g value was nearly the same for both the Pt and Pd salts (2.0074 and 2.0076) with similar linewidths (25 and 20 gauss) respectively.

Reaction of ET and $[Ph_4As]_2[NiCl_4]$

Black wafers were grown by electrocrystallisation of 2mM ET and 5mM $[Ph_4As]_2[NiCl_4]$ in benzonitrile.

Elemental analysis did not correspond to any reasonable stoichiometry.

Reaction of ET and $[Ph_4As]_2[CoCl_4]$

Long black thin branches were grown by electrocrystallisation of 1.5mM ET and 3mM $[Ph_4As]_2[CoCl_4]$ in benzonitrile. The solid was not of sufficient quality for X–ray analysis.

Found(%): C, 30.12; H, 1.91; N, 0.67. Calcd(%) for $[ET]_4[CoCl_4].C_7H_5N$: C, 30.64; H, 2.00; N, 0.76.

Similar C,H percentages exist for $[ET]_n[CoCl_4].C_7H_5N$ (n: 3,2), but with increasing percentages of N.

It is pertinent to mention that electrocrystallisation of $[Et_4N]_2[CoCl_4]$ with ET in CH_2Cl_2 results in the formation of the chlorine salt $[ET]_3[Cl_2].2H_2O$[80], which shows superconductivity at 2K under a pressure of 16Kbar[79]. Chlorine abstraction from the solvent

was related to the formation of the complex[81].

Calcd(%) for $[ET]_3[Cl_2].2H_2O$: C, 28.58; H, 2.23.

Reaction of ET and $K[Hg(CN)_2Br]$

Large diamond shaped thin brown platelets formed at the anode from electrocrystallisation of ET (3mM) and $K[Hg(CN)_2Br]$ (20mM) /18–crown–6 in benzonitrile ($1\mu Acm^{-2}$). After 1 week, the solid was retrieved from the solution, washed with acetone and dried. The surface of the brittle platelets was very uneven when viewed under the microscope. Conductivity measurements were carried out on a compressed disc of the sample, since attachment of the gold probes to the platelets resulted in the development of micro–cracks.

Found(%): C, 25.51; H, 1.65; N, 0.00. Calcd(%) for $[ET]_5HgBr_3$: C, 25.41; H, 1.71.

The lack of nitrogen and hence cyanide in the microanalysis is supported by the disappearance of $\nu(C\equiv N)$ in the absorption spectrum ($Na[Hg(CN)_2Br]$, $\nu(C\equiv N)$ 2187 cm^{-1}).

Replacement of the anode, and a current density of $1\mu Acm^{-2}$ maintained for 1 month, resulted in the formation of long black needles suitable for X–ray crystallography.

Unit cell parameters corresponded exactly with those given for $[ET]_5Hg_3Br_{11}$[121].

Found(%): C, 17.51; H, 1.16. Calcd(%) for $[ET]_5Hg_3Br_{11}$: C, 17.64; H, 1.18.

Continuation of the electrocrystallisation process for a further month resulted in the formation of long crystalline plates of $[ET]_5Hg_3Br_{11}$.

Comparable ET–Hg–Br systems have involved electrocrystallisation of ET and $[Bu_4N][HgBr_3]$ in 1,1,2–tce ($0.5\mu Acm^{-2}$) and resulted in the

formation of $[ET]_2HgBr_3$.tce and $[ET]_4Hg_2Br_6$.tce as the major phases, and the superconductor κ-$[ET]_4Hg_{2.89}Br_8$ as a very minor phase.

Reaction of ET with $[Ph_4As]_2[Pd_2X_6]$ (X = Cl, Br) and $[Ph_4As]_2[Pt_2Cl_6]$

Black amorphous solids were obtained by electrocrystallisation of ET (3mM) and $[Ph_4As]_2[M_2X_6]$ (2mM) in 1,1,2-tce. Elemental analyses do not provide any conclusive evidence as to the identity of the products.

ET/Pt_2Cl_6: Found(%): C, 20.15, H, 1.19. Calcd(%) for $[ET]_3Pt_2Cl_6$: C, 20.50; H, 1.38; $[ET]_2PtCl_6$: C, 20.41; H, 1.37.

ET/Pd_2Cl_6: Found(%): C, 23.69; H, 1.27. Calcd(%) for $[ET]_3Pd_2Cl_6$: C, 22.81; H, 1.53; $[ET]_2PdCl_4$: C, 23.61; H, 1.58.

ET/Pd_2Br_6: Found(%): C, 21.06; H, 1.38. Calcd(%) for $[ET]_4Pd_2Cl_6$: C, 21.53; H, 1.44; $[ET]_3PdCl_6$: C, 20.71; H, 1.39.

The absorption spectra for compressed discs of the compounds show e-mv coupling in the relevant regions, symmetric ν(C=C) stretching vibrations and metal halogen stretches in the case of chlorine.

Epr measurements at 9.120 GHz for ET/Pd_2Cl_6 and ET/Pd_2Br_6 at liquid nitrogen temperatures show similar g-values (2.0062 and 2.0058) but differing line widths (10 and 50 gauss) respectively.

The epr measurements are similar to those found for other ET salts[122] ($2.0023 < g < 2.0115$).

The complex $[ET]_4PtCl_6$.bn ($\sigma_{rt} \sim 10^1$ Scm^{-1}; semiconductor, T_{MI}: 245K) has been recently reported[123], obtained by electrocrystallisation of $[Bu_4N]_2PtCl_6$ and ET in benzonitrile; the workers were unable to obtain the salt containing $PtCl_4^{2-}$ by either chemical or electrochemical oxidation of ET using $[Bu_4N]_2PtCl_4$ as the electrolyte.

Materials for the ~~21st~~ 22nd Century!

2.3.1. Conductivity Measurements

Electrical conductivity studies on compressed discs of $[ET]_4[Pt(mnt)(CN)_2]$ (*fig.*, 2.3.1.) and $[HMTTeF]_3[Pt(mnt)(CN)_2]$ (*fig.*, 2.3.3.) indicate semiconductor properties with room temperature conductivities of 0.14 and 0.18 Scm^{-1}, respectively. The electrical conductivities represent a 10^5 fold increase on those reported for ET–metal bis–dithiolene salts and are comparable in magnitude to those reported for $[ET]_4[M(CN)_4]$ (M= Ni or Pt)[124]. $[ET]_x[M(mnt)_2]$ (M= Pt, Pd) and $[ET][Ni(mnt)_2]$[125] were found to be semiconductors with room temperature conductivities in the range 10^{-3} to 10^{-5} Scm^{-1} and activation energies of approximately 300meV; the 1:1 stoichiometry was suggested for the absence of a conducting phase. While a plot of $\ln(\sigma/\sigma_{rt})$ versus $10^3/T$ for $[ET]_4[Pt(mnt)(CN)_2]$ (*fig.*, 2.3.2.) indicates a straight line with activation energy 90meV (band gap energy = $2E_a$), the T^{-1} dependence for $[HMTTeF]_3[Pt(mnt)(CN)_2]$ is variable over the temperature range (*fig.*, 2.3.4.). An estimation of the average activation energy from $\delta(\ln\sigma)/\delta(1/T)$ in the temperature range 290–90K (*fig.*, 2.3.5.) gives $E_a\sim$ 40meV ($E_g\sim$ 80meV). A plot of $\ln\sigma$ versus $1/T^2$ over the temperature range 300–200K reveals a linearity which has been related to two dimensionality in metals (*fig.*, 2.3.6.).

The T^2 dependence of resistivity (T^{-2} dependence of conductivity) in metals down to low temperatures may be described by the effect of disorder on electron–phonon coupling[126] or by electron–electron coulomb scattering[127]. In considering a two dimensional electron system[128] (if Umklapp processes are taken into account– without such

processes, Coulomb scattering gives zero contribution to the resistivity), the T^2 dependence may be explained by electron–electron scattering; calculations show that the coulomb interaction is much larger than electron–phonon scattering even at room temperature. This behaviour would also be expected for 1D metals, but over the whole temperature range. In $[TMTSF]_2X$ compounds, the T^2 contribution is also observed at low temperatures[129,130]. Thus the T^2–dependence of the resistivity testifies in favour of a strong repulsion of quasi–particles.

Compressed disc conductivity measurements for $[ET]_3[AuBr_4]$ obtained by electrocrystallisation, using thf as the solvent, reveals a semiconductor ($\sigma_{rt}\sim$ 0.25 Scm^{-1}) (*fig.*, **2.3.7.**) with low activation energy ($E_a\sim$ 25meV) (*fig.*, **2.3.8.**) which undergoes a Peierls distortion at 125K (*fig.*, **2.3.9.**) to an insulating phase at lower temperatures.

Electrocrystallisation of ET and $[Bu_4N][AuBr_4]$ in benzonitrile gave small thin plates; due to the size, 2–probe conductivity measurements were carried out and the results suggest possibly a different stoichiometry or new phase. The plates exhibited semiconducting properties ($\sigma_{rt}\sim 2.2\times10^{-3}$ Scm^{-1}) (*fig.*, **2.3.10.**) with large activation energies (E_a= 205meV, E_g= 410meV) (*fig.*, **2.3.11.**). The compound behaves as an insulator at temperatures less than 150K. While only X–ray diffraction studies can reveal the stoichiometry (and phase) of the compound, one can draw comparisons with the known phases of $[ET]_2AuBr_2$; α'–$[ET]_2AuBr_2$, which is isostructural with the $Au(CN)_2^-$ and $Ag(CN)_2^-$ salts and resembles β–$[ET]_2PF_6$, is reported to be a 1D metal[119] and suffers a metal–insulator transition at 250K with band gap energies of 230 meV above and 340 meV below the temperature[120]; β''–$[ET]_2AuBr_2$[132], which is regarded as a modification of the superconductive β form, behaves as a 1D metal and undergoes a metal–semiconductor transition at 200K; δ–$[ET]_2AuBr_2$[133] was found to

be a semiconductor (σ_{rt}~ 0.04 Scm^{-1}, E_a= 180 meV), which undergoes a phase transition between 335–320K; the twist phase is reported[134] to be non–metallic in character, while the δ–phase is metallic to low temperatures. Thus the δ– and twist phases bear the closest comparison based on conductivity measurements.

The electrocrystallisation of $[ET]_3[NiCl_4].H_2O$ in 1,1,2–tce (somewhat by accident) provides a useful comparison for ET–metal halide salts and especially $[ET]_3[AuBr_4]$ described within. Since the transition metal halide salts of ET reported to date are all of the stoichiometry $[ET]_2[MX_4]$ and $[ET][MX_4]$[36], the 3:1 ratio is very interesting. Conductivity measurements (4–probe along the needle axis) on single crystals of $[ET]_3[NiCl_4].H_2O$ indicated metallic behaviour with a room temperature conductivity of 20 Scm^{-1}. Initial results on crystal {a} showed metallic behaviour, with the conductivity at 120K twice the room temperature value (*figs.*, 2.3.12. and 2.3.13.). Unfortunately the crystal was subjected to a current surge and therefore lost. A second crystal (denoted {b}) showed slightly different behaviour with a conductivity maximum at 150K, whereupon a slight decrease in the conductivity occurs to a plateau between 140 and 90K (*fig.*, 2.3.16.) and then a decrease in conductivity to semi–metallic behaviour at the lowest temperature measured (20K, σ~ 12 Scm^{-1}) (*figs.*, 2.3.14. and 2.3.15.). The $\ln(\sigma/\sigma_{rt})$ versus T curve can be approximated by the phenomenological model proposed by Epstein *et al*[131]. which assumes the mobility to be strongly temperature dependent ($\mu \propto T^{-\alpha}$; α: sample dependent constant) and the concentration of the mobile charge carriers assumed to be thermally activated. Thus:

$$\sigma(T) = A \cdot \exp(-\Delta_H/KT) \cdot T^{-\alpha}$$

The solid line in the conductivity plot for crystal {b} (*fig.*, 2.3.17.) represents the best fit from regressional analysis using the equation above, with the parameters Δ_H = 19.3(6)meV and α = 1.82, using data for T > 50K. At lower T, electrons in localised states may dominate σ(T). Such a model has been used to fit conductivity data for TCNQ salts, where α = 3–4 implies a more strongly T–dependent mobility; the value of Δ_H is also higher (40–80meV) suggesting an increased activation energy. The transition in the one–dimensional conductor NMP–TCNQ has been related[131] to a Mott–Hubbard metal–insulator transition since electron–electron Coulomb repulsion effects are significant (tight–binding theory and the accompanying Peierls instability assumes all electrons move independently of each other in a perfect uniform lattice).

Upon cooling crystal {b} from room temperature on a repeat run, it was found to have undergone a "permanent" structural phase change, as evidenced by the conductivity plot (*fig.*, 2.3.18.). A plot of $\ln(\sigma/\sigma_{rt})$ versus T indicates semiconducting behaviour with a high room temperature conductivity of 20 Scm^{-1}, decreasing to ~ 6 Scm^{-1} at 55K. The T^{-1} dependence is non–linear (*fig.*, 2.3.19.), implying a two dimensionality to the compound (*fig.*, 2.3.20.). An estimation of the activation energy for the temperature range 290–135K is E_a~ 15meV.

The conductance curves for the 4–probe measurements on the ET/$NiCl_4$ whisker showed strong hysteretic differences between cooling and warming cycles (*fig.*, 2.3.21. and 2.3.22.); resistive jumps are indicative of problems with contact resistances or the development of microcracks, which was not suprising when the surface of the whisker was viewed under the microscope. Electrocrystallisation of ET and $[Ph_4As]_2[NiCl_4]$ in benzonitrile yielded whisker shapes of $[ET]_x[NiCl_4]$ at the anode. The room temperature conductivity was found to be

5 Scm^{-1} with only a slight increase to 250K ($d(\sigma)/d(T) \simeq 1.3\times10^{-3}$ $Scm^{-1}K^{-1}$) (*fig.*, **2.3.23.**); a further decrease in the temperature resulted in a sharp transition at 140K to a semiconducting state with $\sigma\sim 10^{-1}$ Scm^{-1} at 50K.

Conductivity measurements on a compressed disc of the ET/mercuric bromide species ($[ET]_5HgBr_3$) reveals a semiconductor (σ_{rt} = 0.3 Scm^{-1}) (*fig.*, **2.3.24.**) with (low) activation energy, E_a = 75meV (E_g = 150meV) (*fig.*, **2.3.25.**). This compares with crystals of $[ET]_5Hg_3Br_{11}$ obtained later, which are reported to be metallic[121].

fig., 2.3.1.

Plot of $\ln(\sigma/\sigma_{rt})$ versus temperature for $[ET]_4[Pt(mnt)(CN)_2]$ (thf)

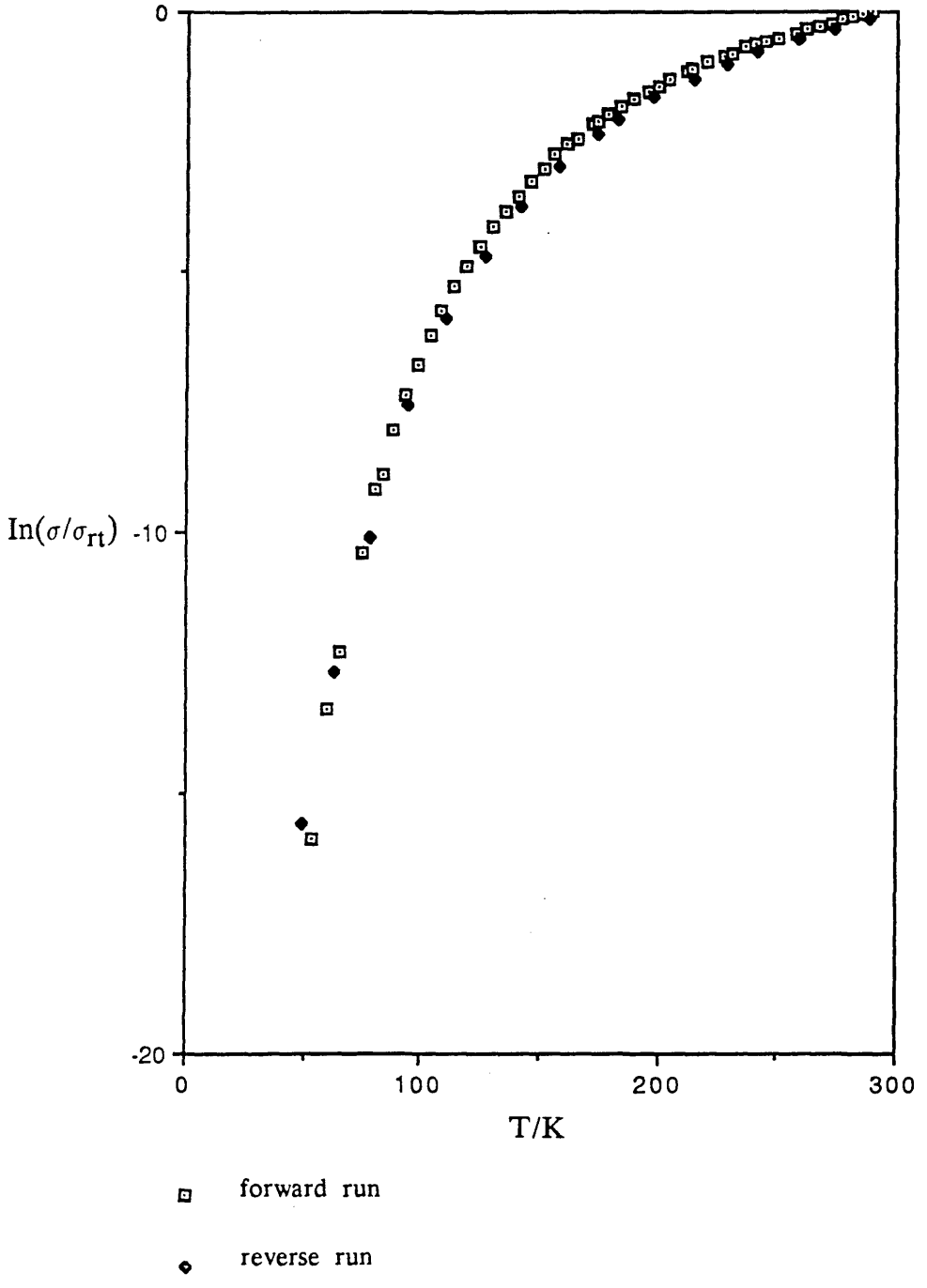


fig., **2.3.2.**

Plot of $\ln(\sigma/\sigma_{rt})$ versus $10^3/T$ for $[ET]_4[Pt(mnt)(CN)_2]$ (thf)

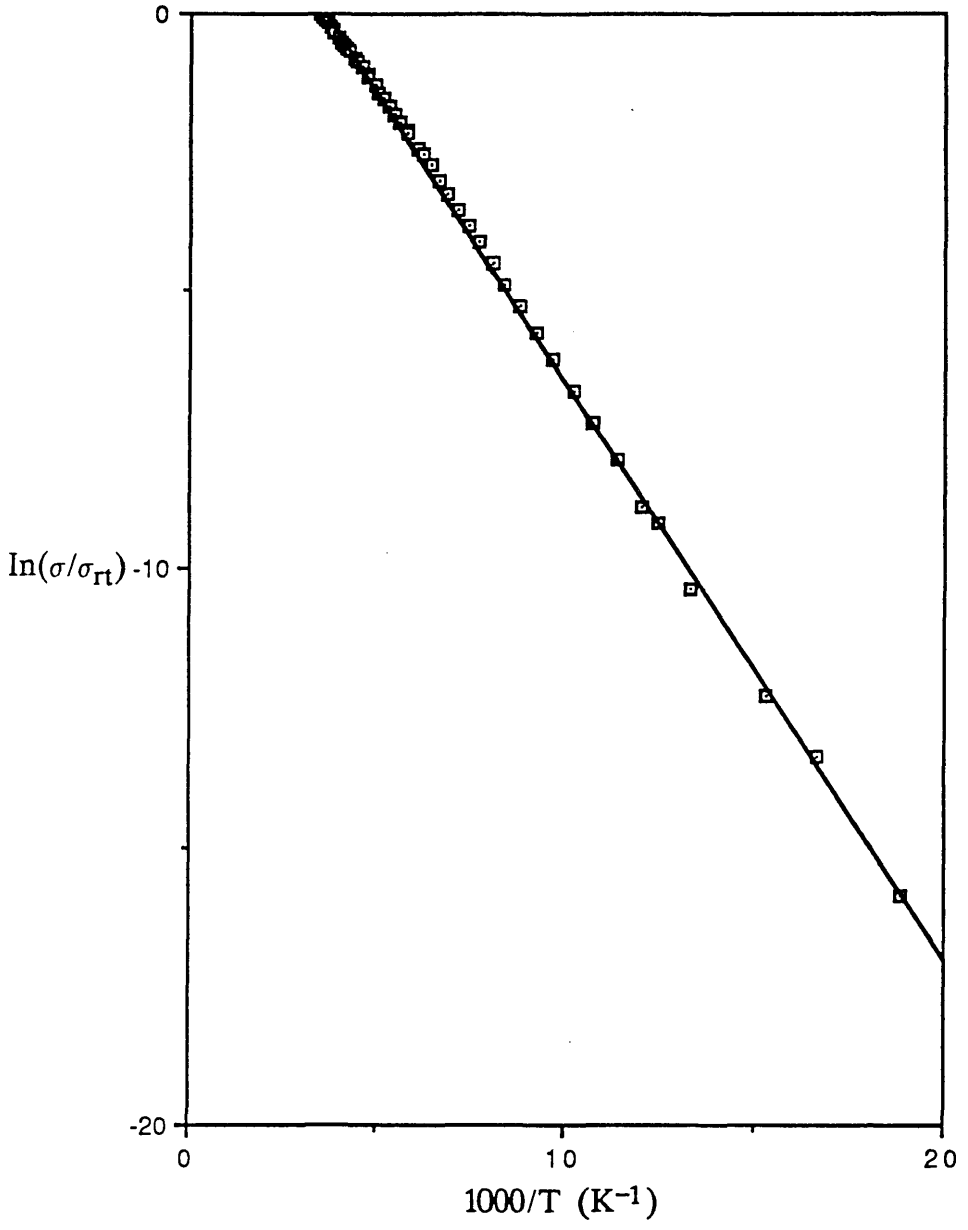


fig., **2.3.3.**

Plot of $\ln(\sigma/\sigma_{rt})$ versus temperature for $[HMTTF]_3[Pt(mnt)(CN)_2]$ (thf)

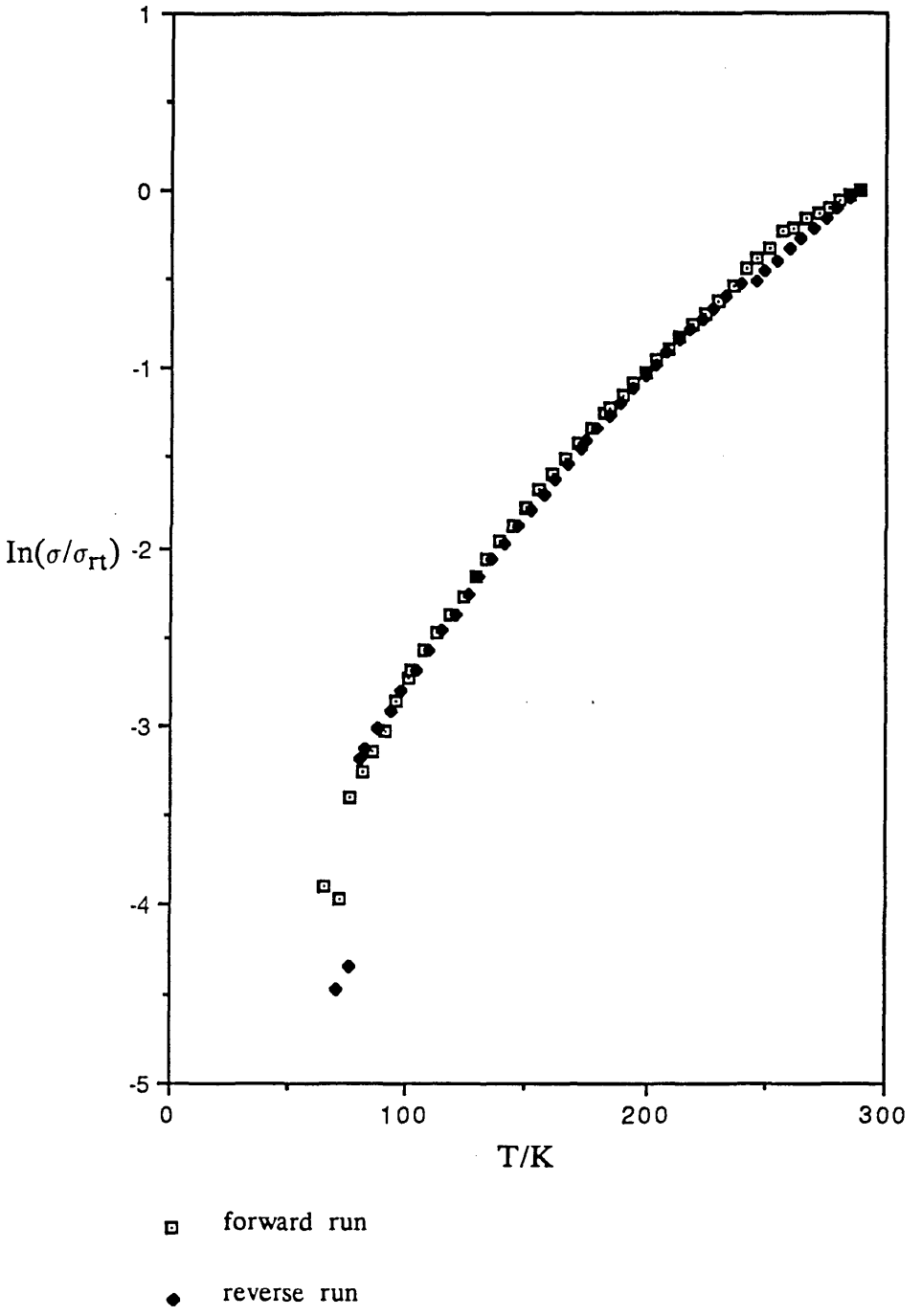


fig., **2.3.4.**

Plot of $\ln(\sigma/\sigma_{rt})$ versus $10^3/T$ for $[HMTTF]_3[Pt(mnt)(CN)_2]$ (thf)

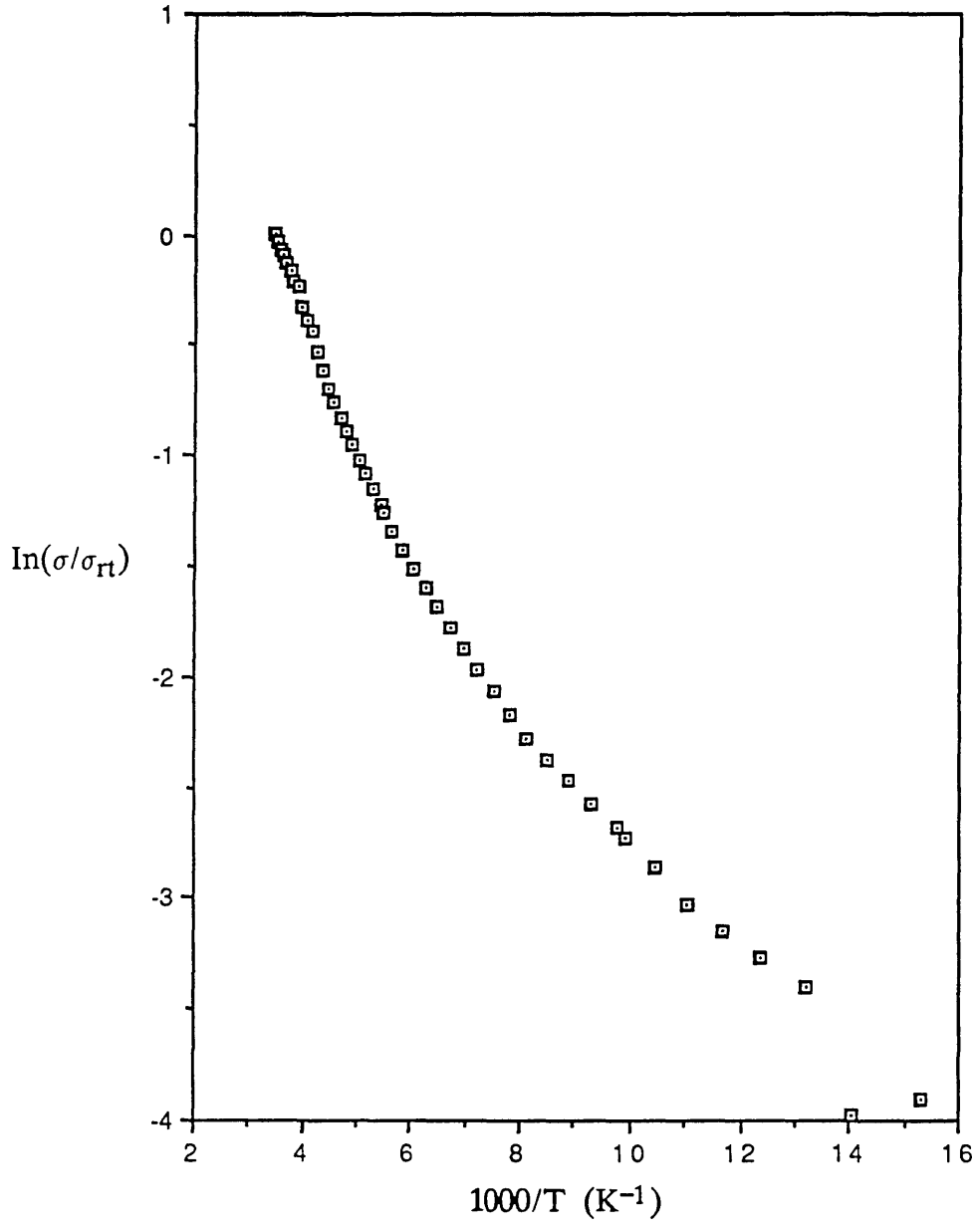


fig., **2.3.5.**

Plot of $d(\ln\sigma)/d(1/T)$ versus $1/T$ to estimate activation energy for $[HMTTF]_3[Pt(mnt)(CN)_2]$

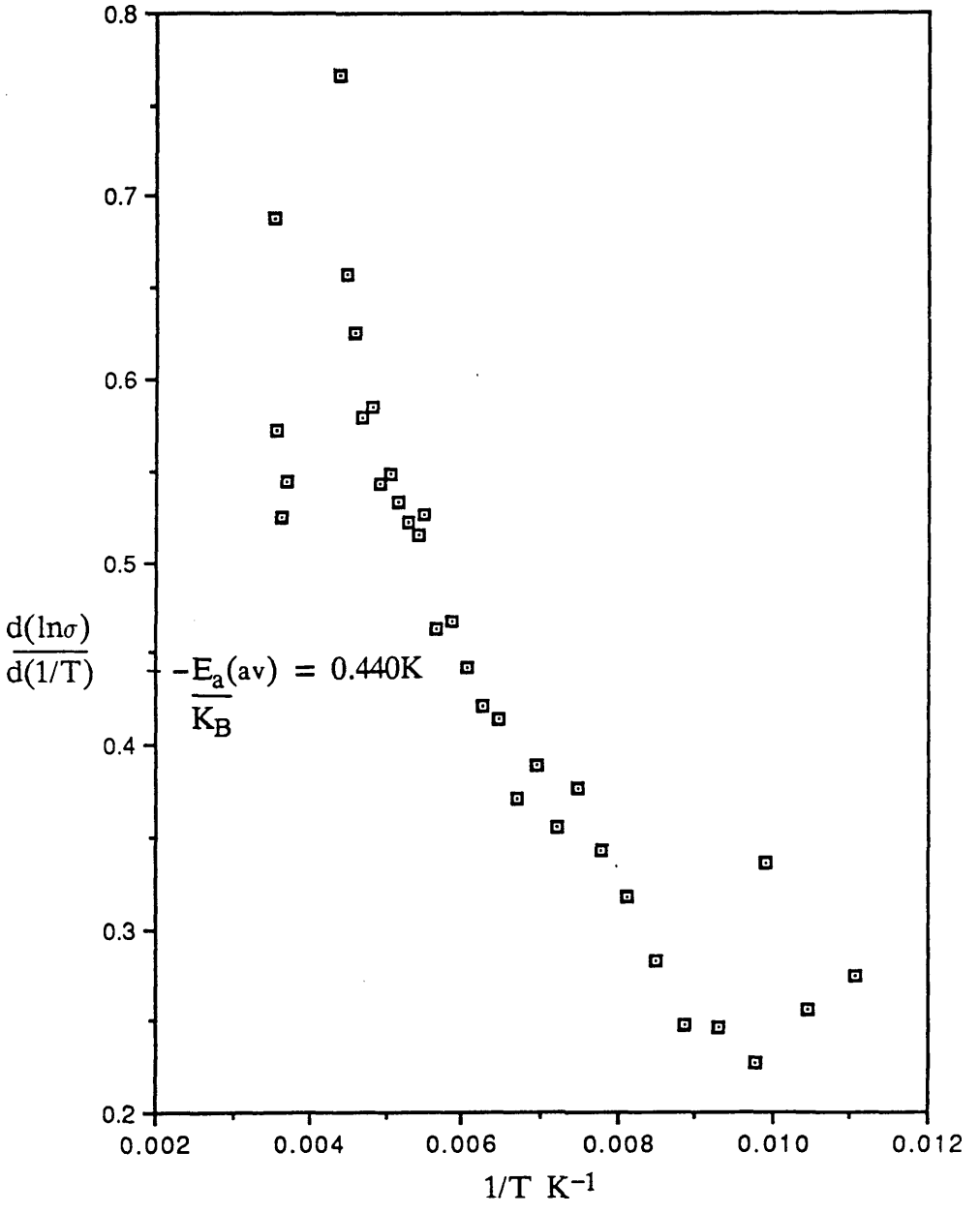


fig., **2.3.6.**

Plot of $\ln\sigma$ versus $1/T^2$ for $[HMTTF]_3[Pt(mnt)(CN)_2]$ to indicate two–dimensionality of the compound

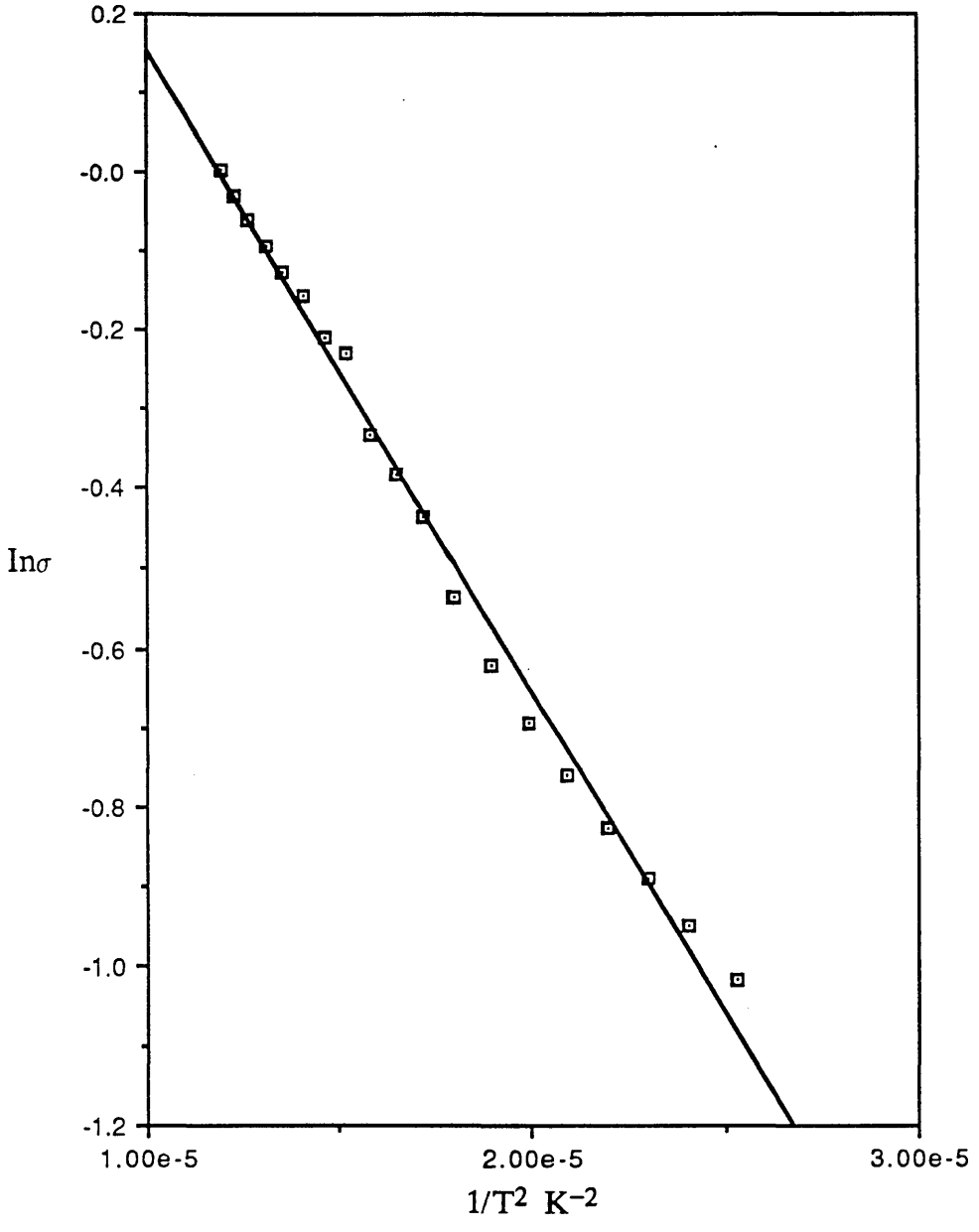


fig., 2.3.7.

Plot of $\ln(\sigma/\sigma_{rt})$ versus temperature for $[ET]_3AuBr_4$ (thf)

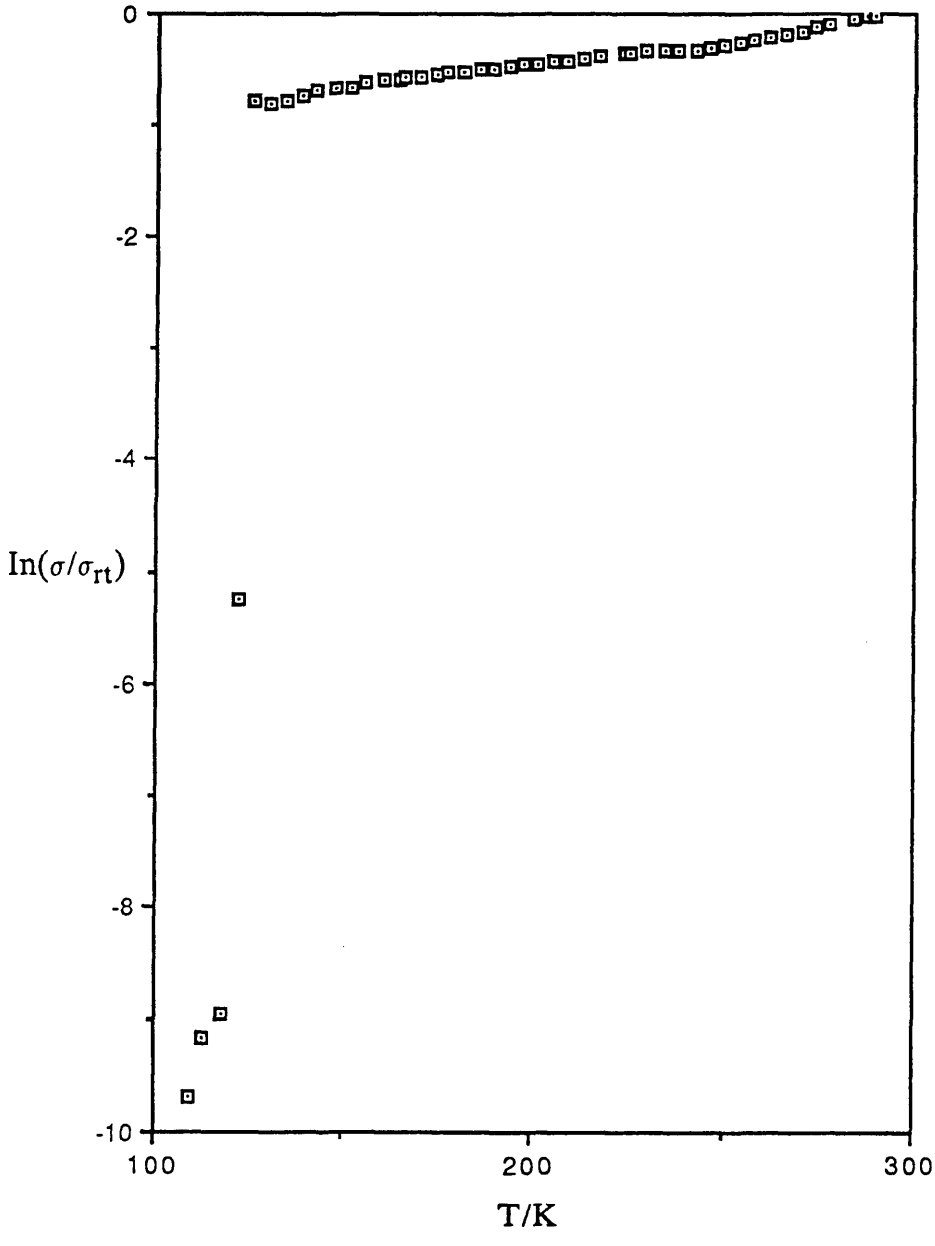


fig., 2.3.8.

Plot of $\ln(\sigma/\sigma_{rt})$ versus $10^3/T$ for $[ET]_3AuBr_4$ (thf)

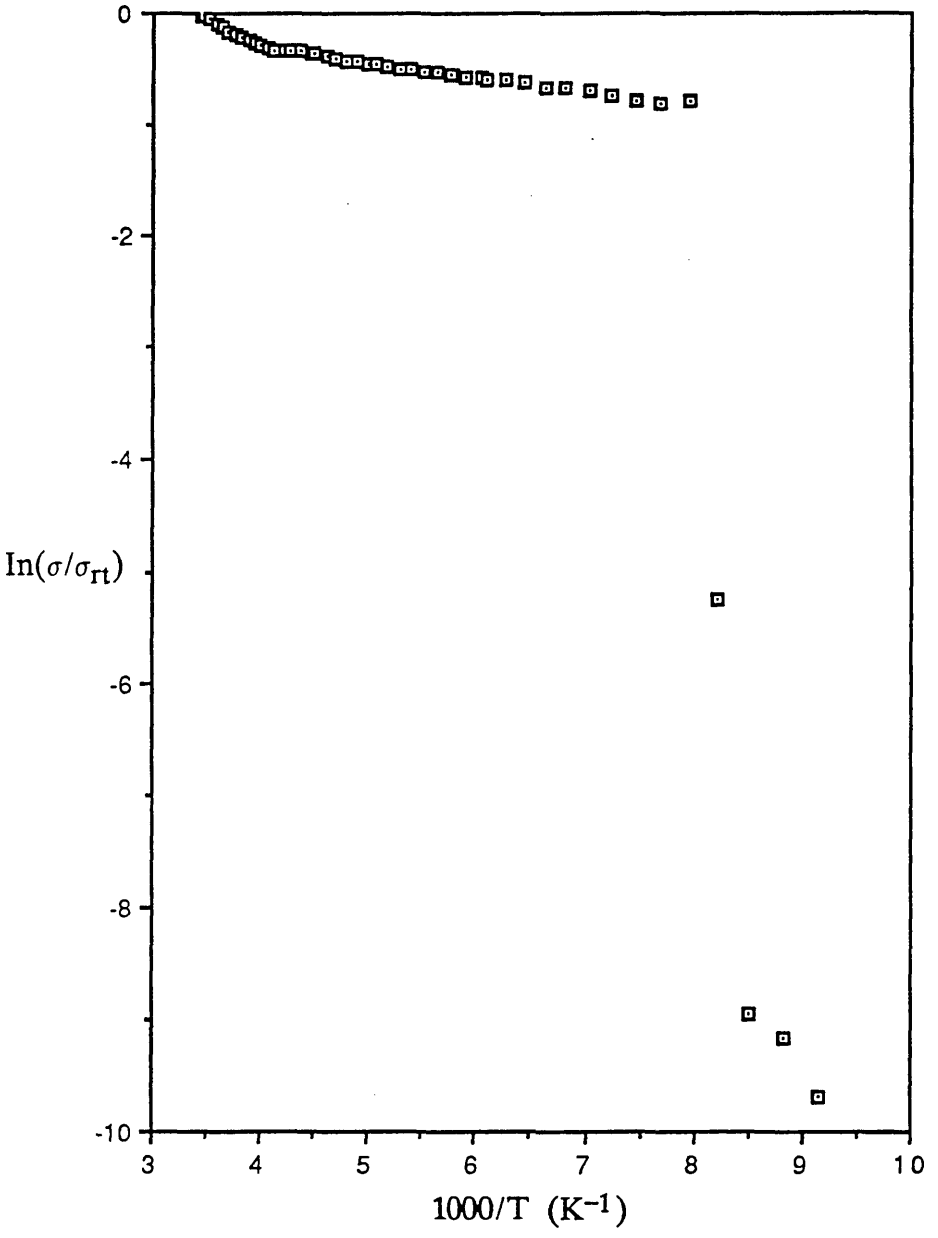


fig., **2.3.9.**

1st Order Derivative plot for $[ET]_3AuBr_4$ to indicate phase change transition temperature

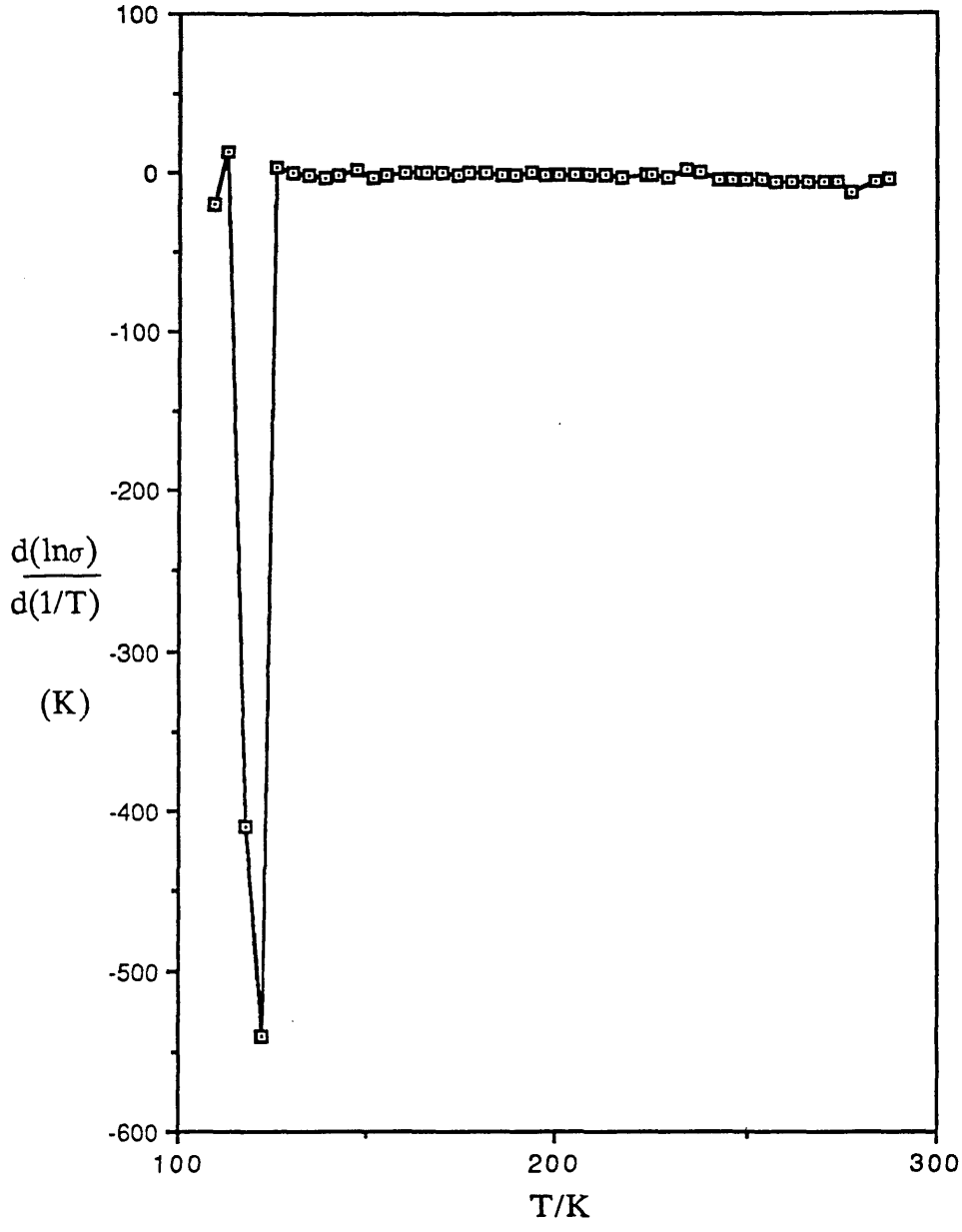


fig., **2.3.10.**

Plot of $\ln(\sigma/\sigma_{rt})$ versus temperature for [ET]/$AuBr_4$ single crystal (benzonitrile)

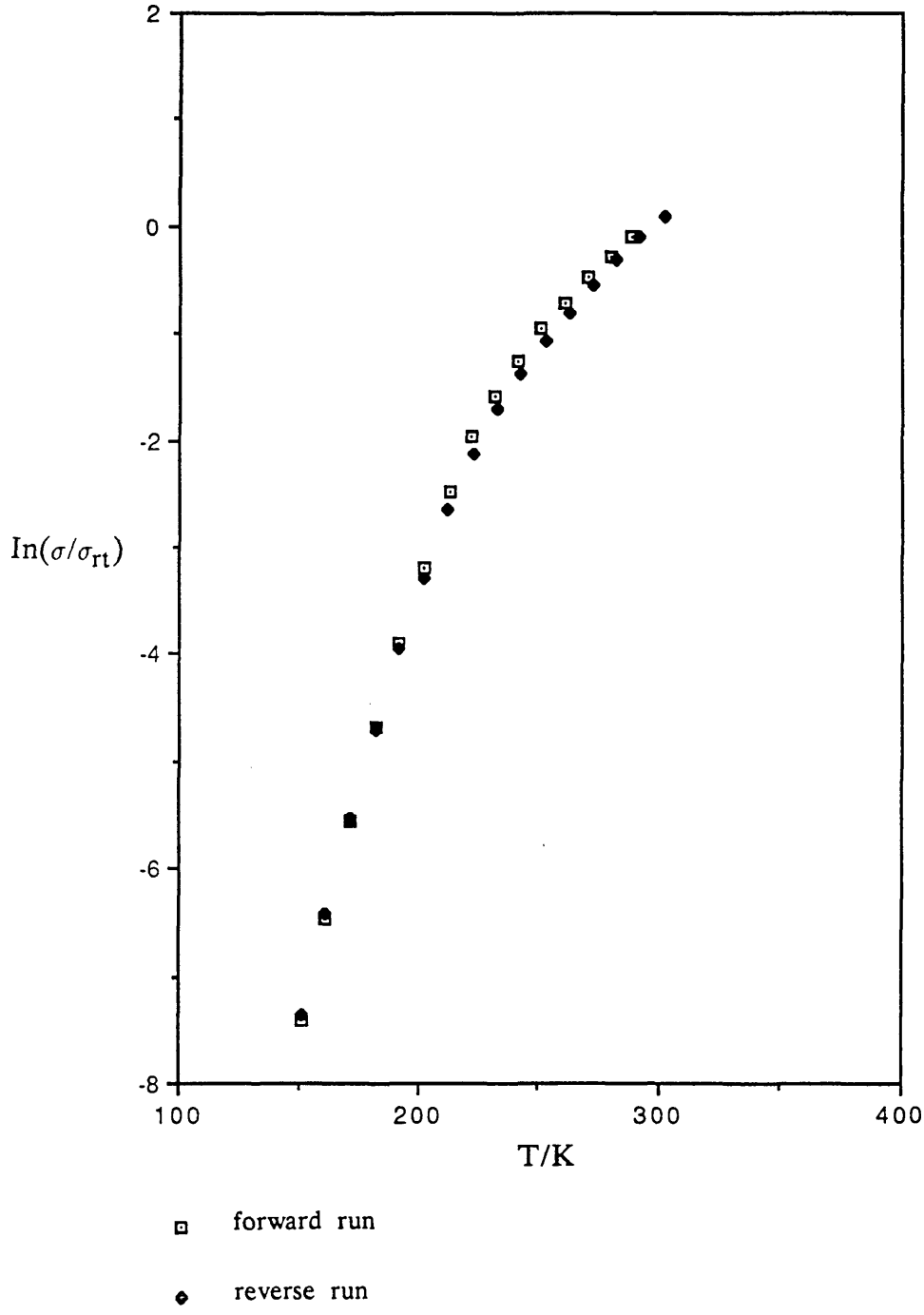


fig., **2.3.11.**

Plot of $\ln(\sigma/\sigma_{rt})$ versus $10^3/T$ for [ET]/$AuBr_4$ single crystal (benzonitrile)

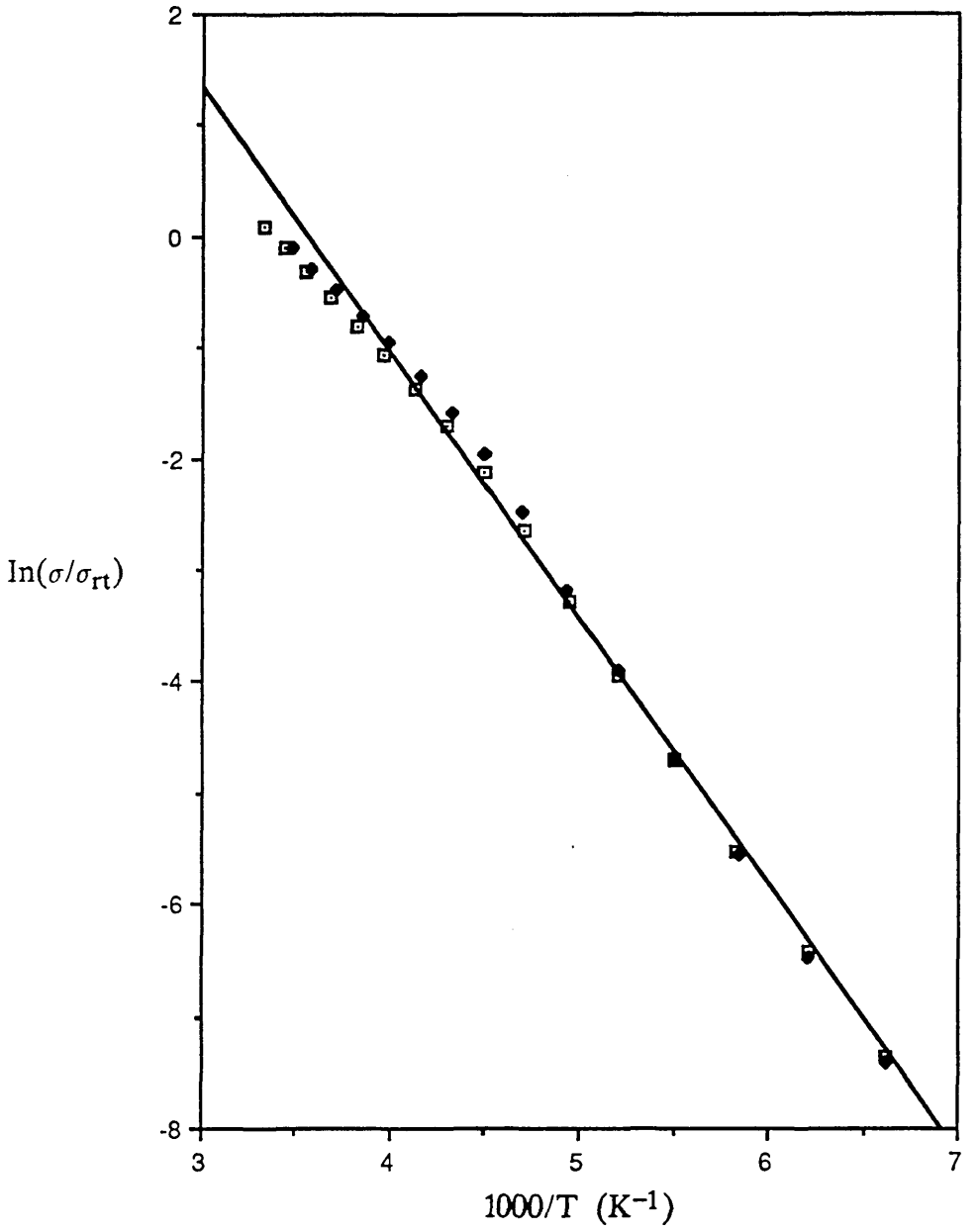


fig., **2.3.12.**

Plot of $\ln(\sigma/\sigma_{rt})$ versus temperature for $[ET]_3NiCl_4.H_2O$ (single crystal {a}, 1,1,2–tce)

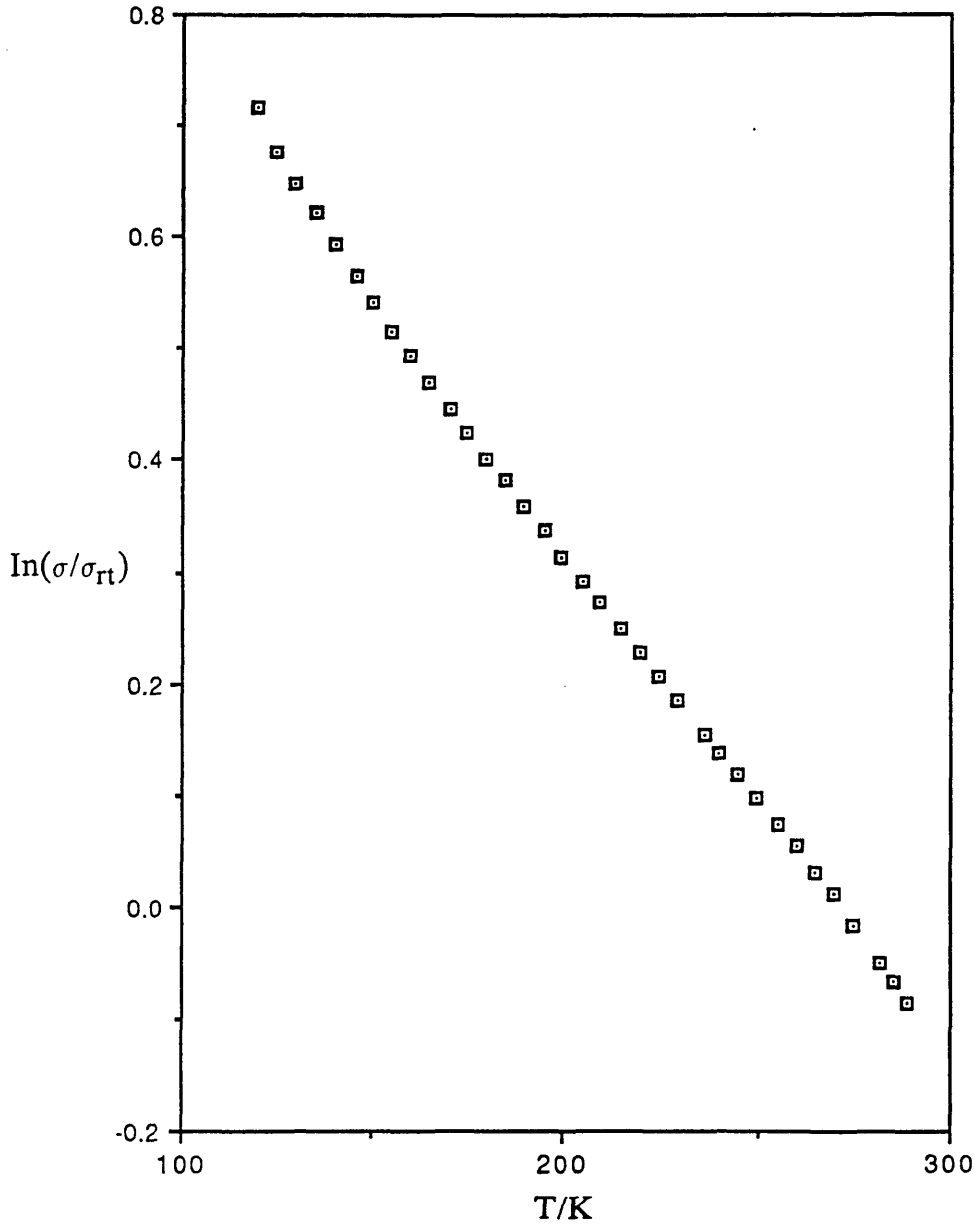


fig., **2.3.13.**

Plot of $\ln(\sigma/\sigma_{rt})$ versus $10^3/T$ for $[ET]_3NiCl_4.H_2O$ (single crystal {a}, 1,1,2-tce)

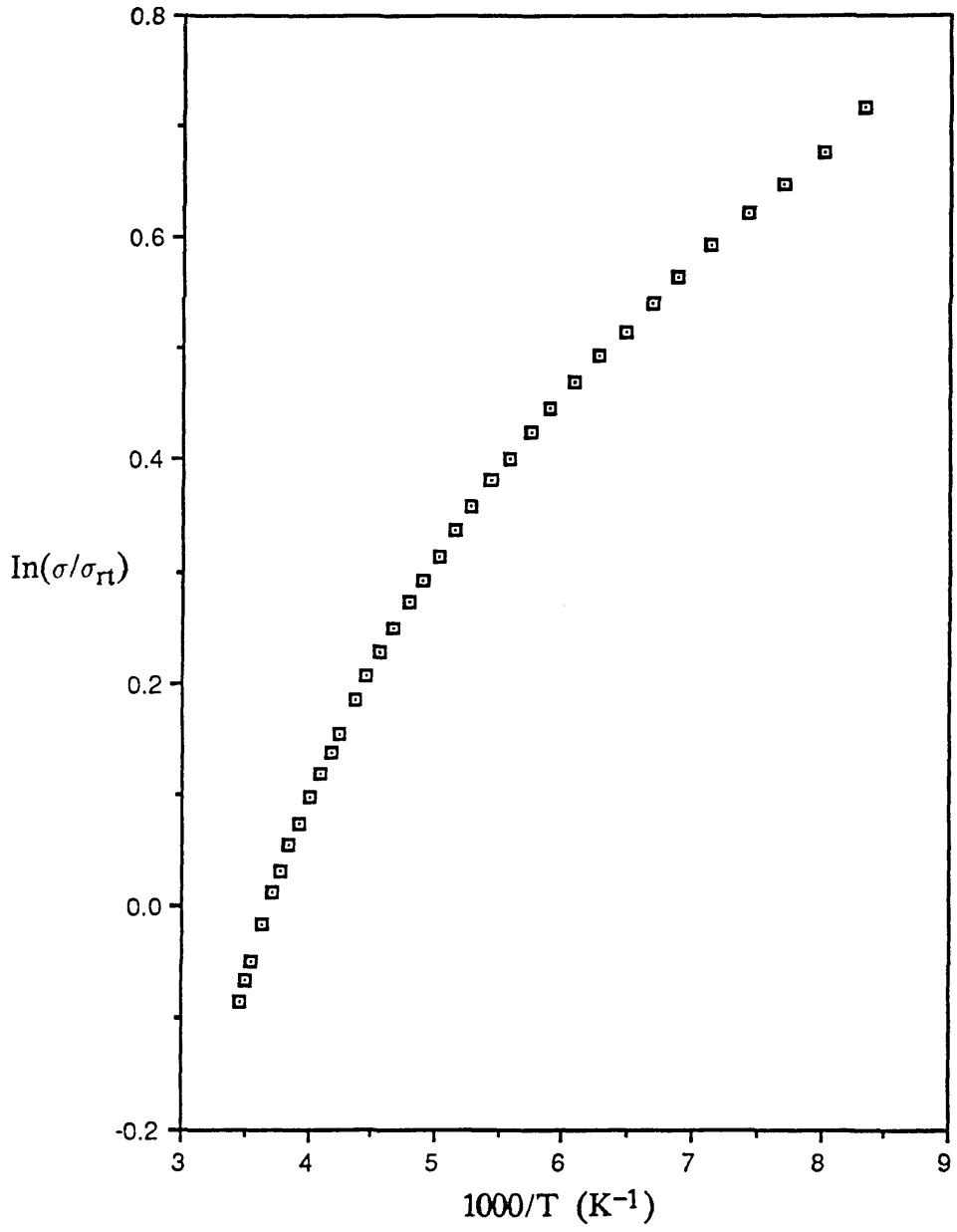


fig., 2.3.14.1.

Plot of $\ln(\sigma/\sigma_{rt})$ versus temperature for $[ET]_3NiCl_4.H_2O$ (single crystal {b}, 1,1,2-tce)

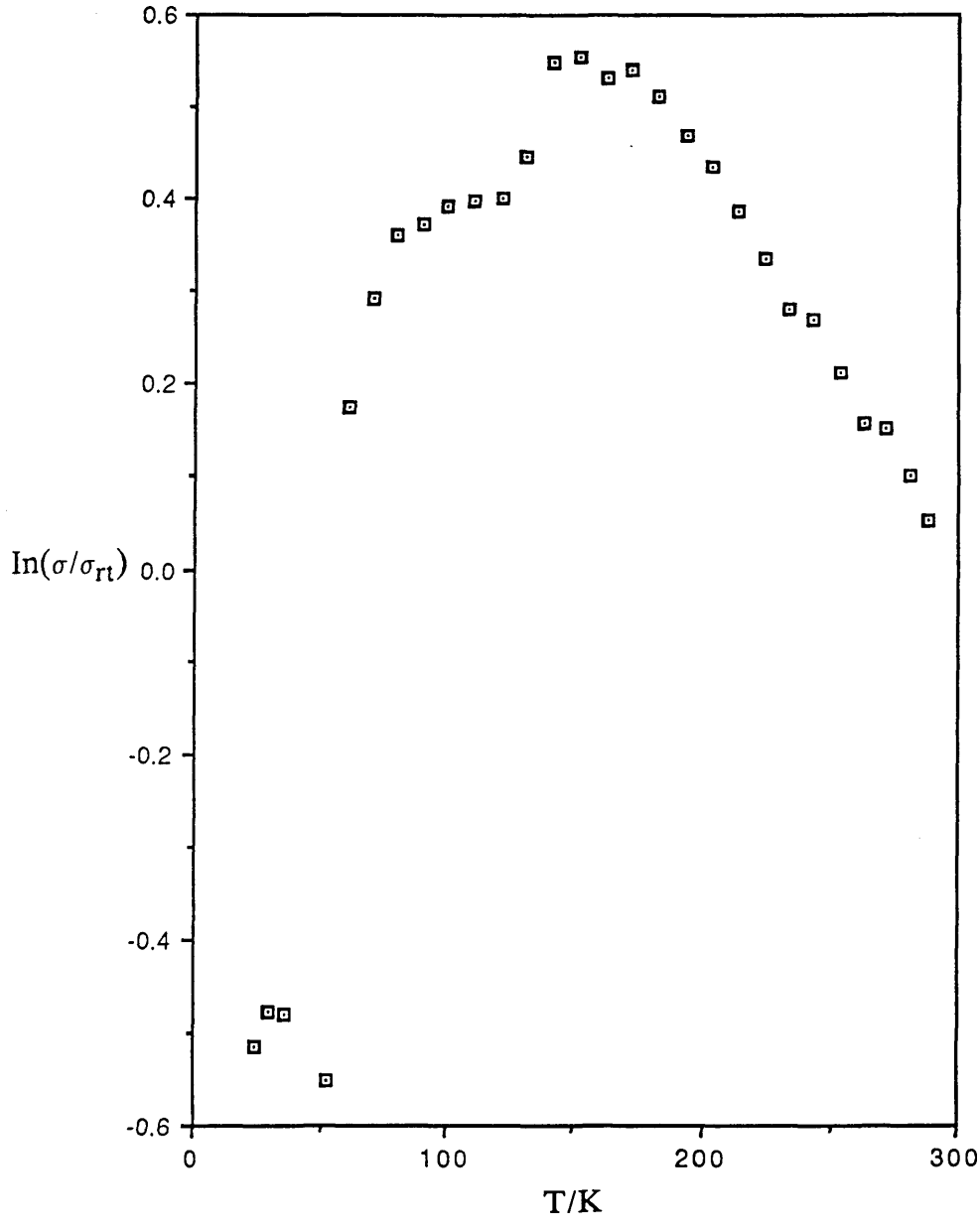


fig., **2.3.14.2.**

Combined conductivity plots for $[ET]_3NiCl_4.H_2O$ (single crystals {a} and {b})

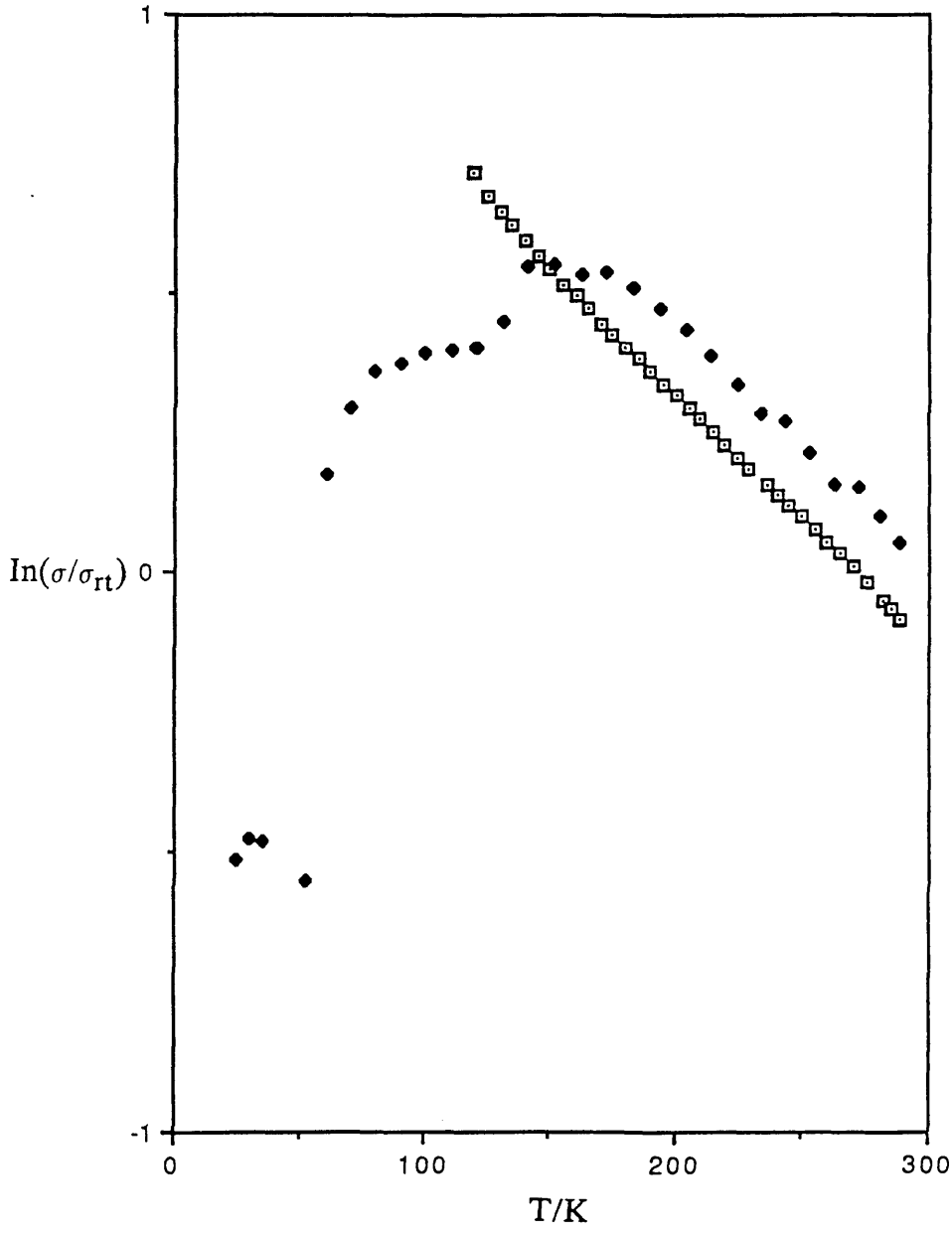


fig., **2.3.15.**

Plot of $\ln(\sigma/\sigma_{rt})$ versus $10^3/T$ for $[ET]_3NiCl_4.H_2O$ (single crystal {b}, 1,1,2–tce)

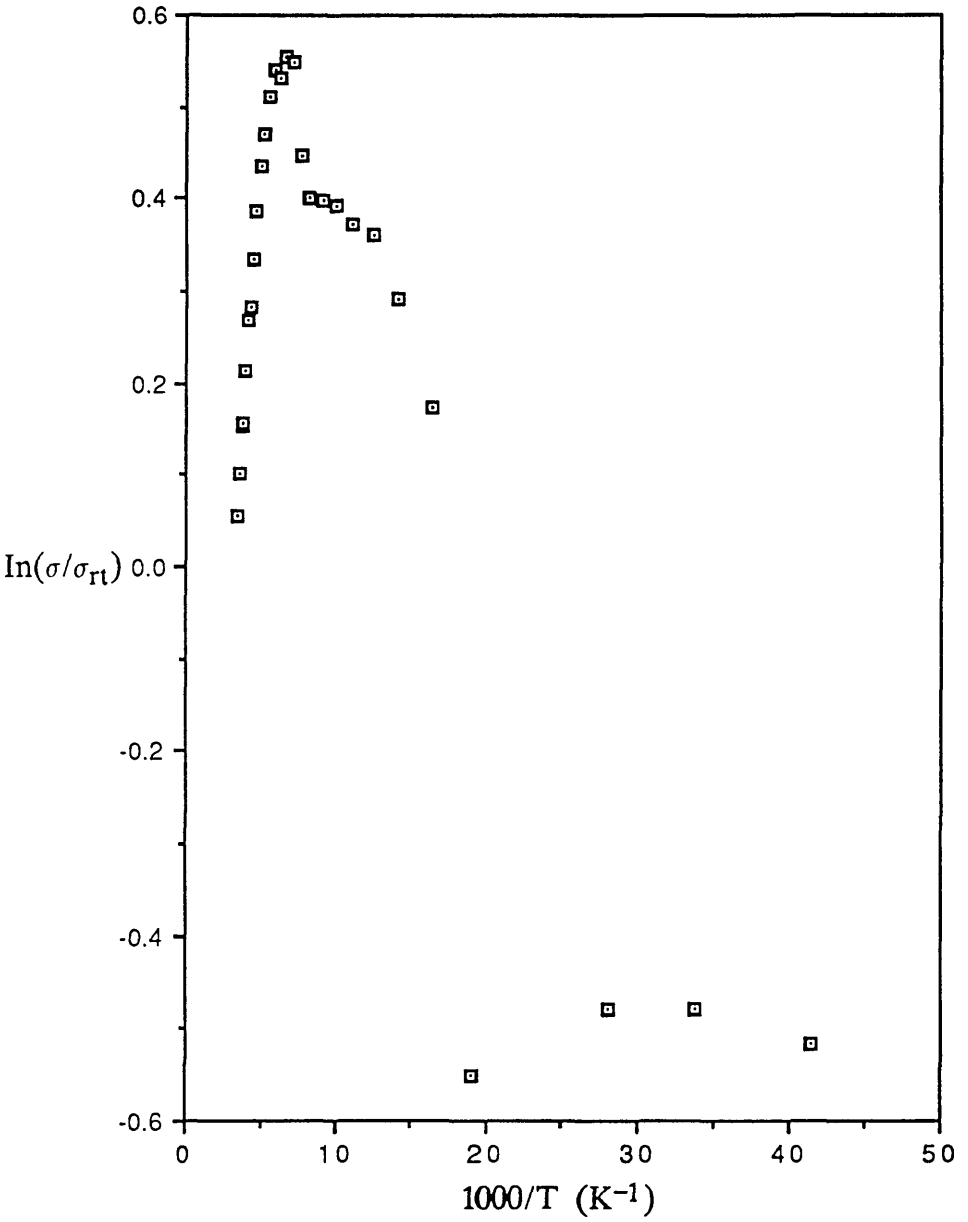


fig., **2.3.16.**

1st Order Derivative Plot for $[ET]_3NiCl_4.H_2O$ (single crystal {b}) to indicate phase change transition temperature(s)

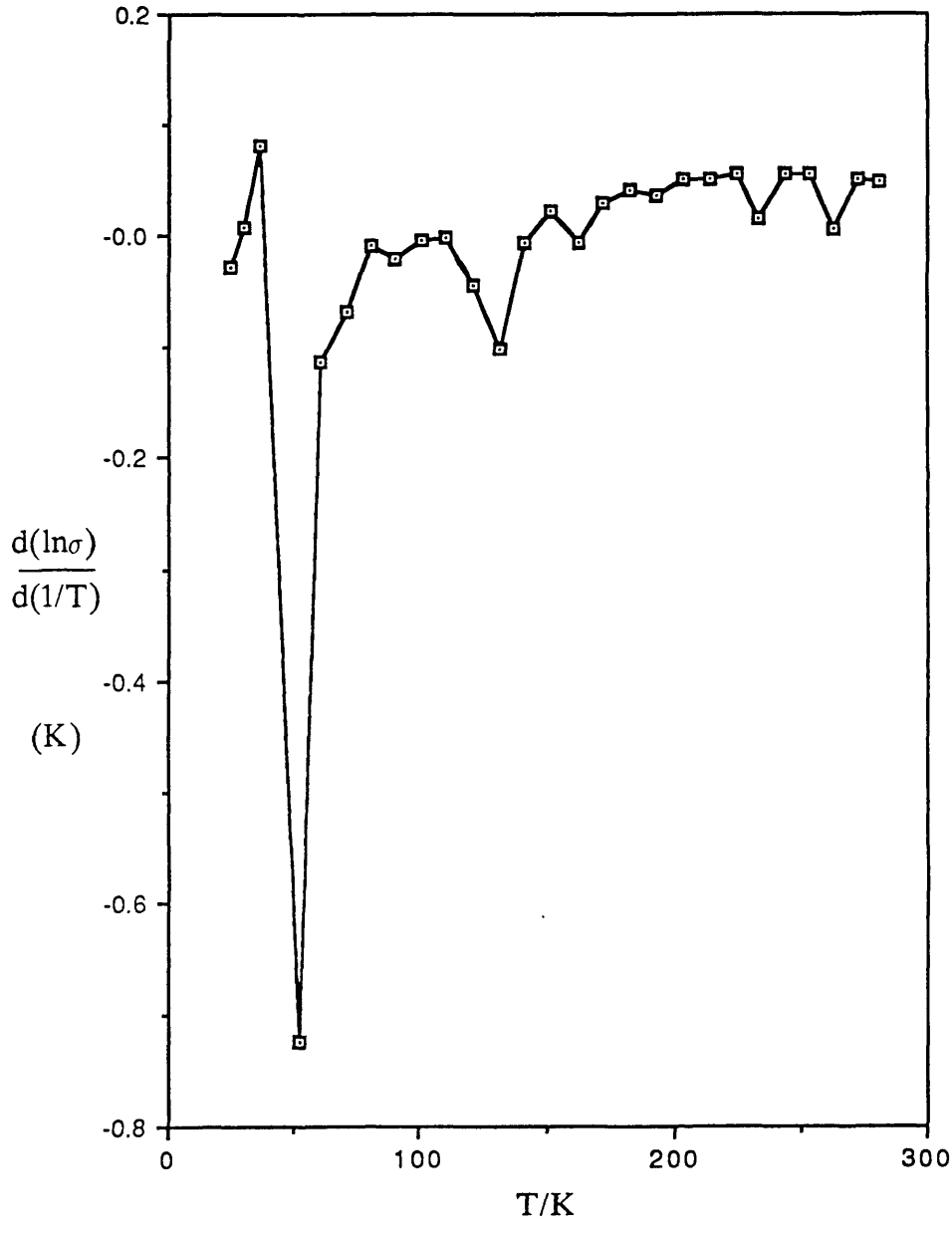
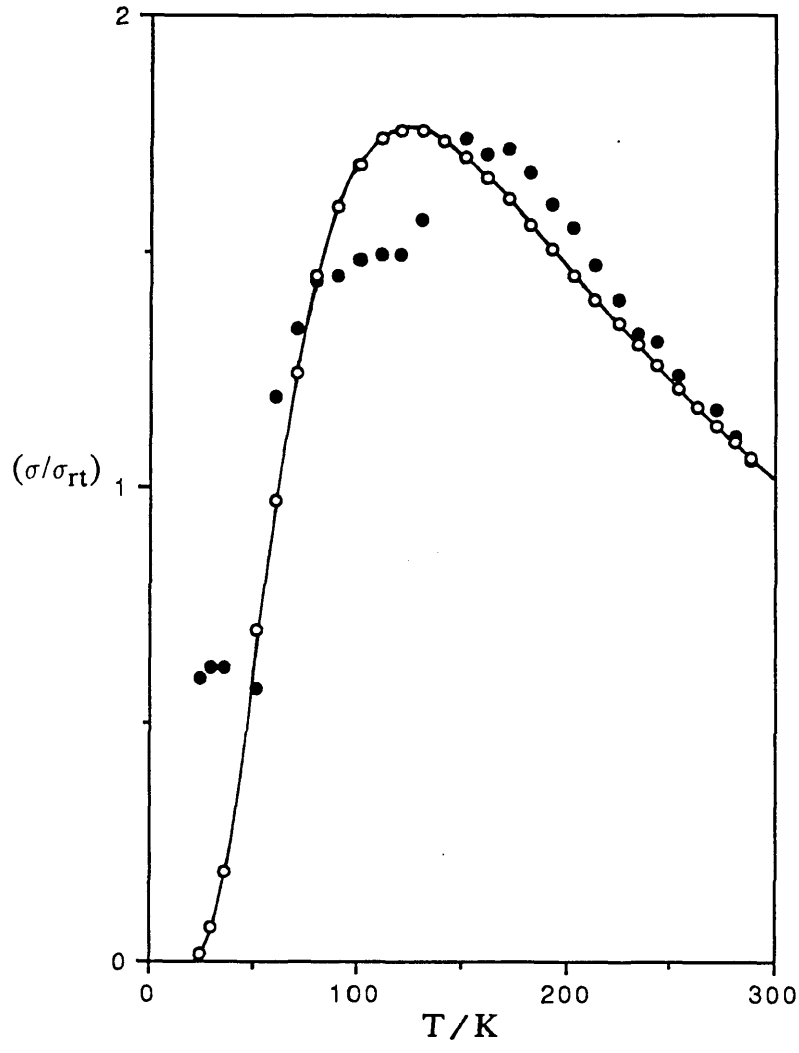


fig., 2.3.17.

Plot of σ versus temperature for $[ET]_3[NiCl_4].H_2O$ (crystal {b}) and best fit to the expression $\exp(-\Delta_H/K_BT).T^{-\alpha}$



● Experimental data

—o— Best fit: Δ_H 19.3meV;

α 1.82

fig., **2.3.18.**

Plot of $\ln(\sigma/\sigma_{rt})$ versus temperature for $[ET]_3NiCl_4.H_2O$ (single crystal {b}, 1,1,2–tce) after phase change

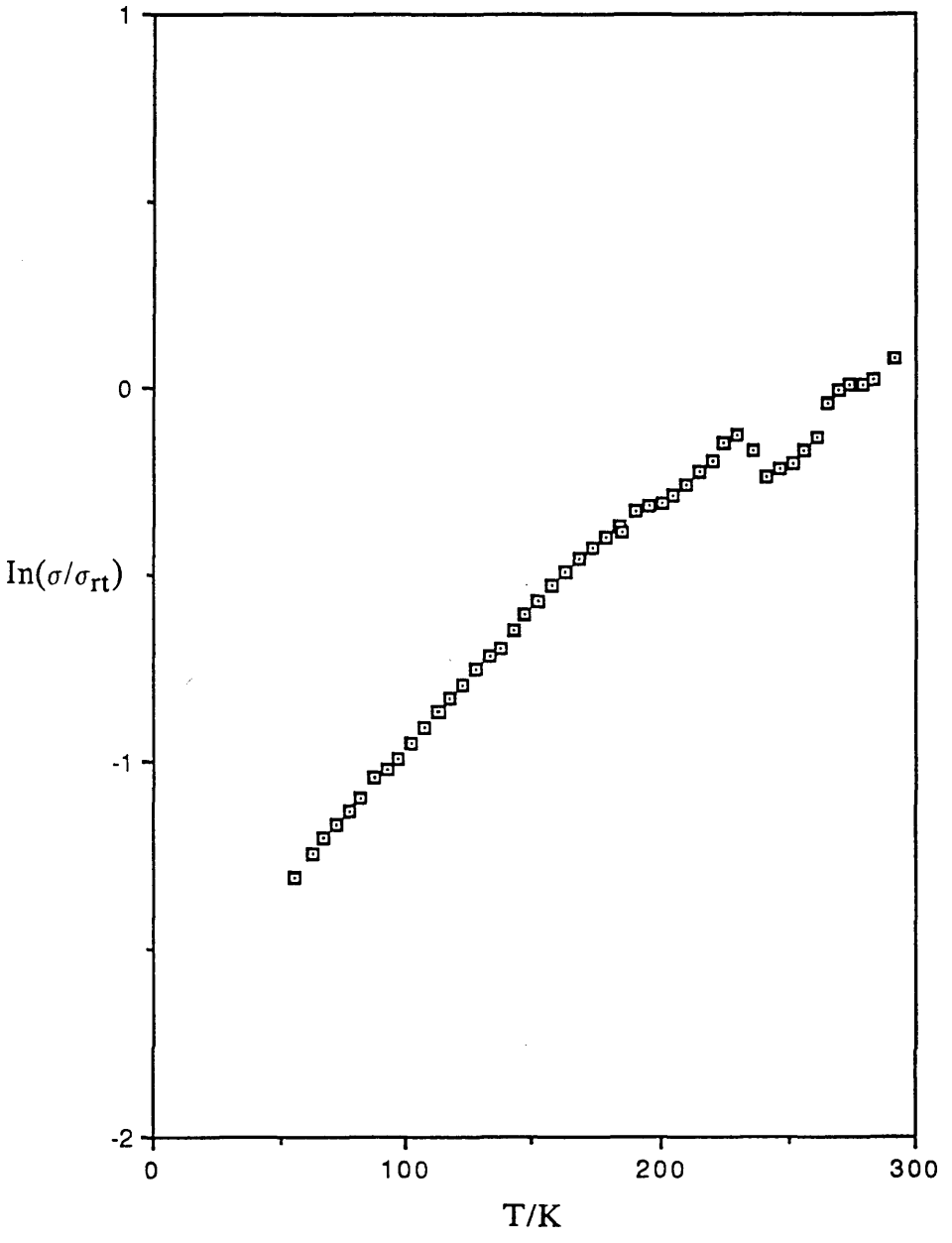


fig., **2.3.19.**

Plot of $\ln(\sigma/\sigma_{rt})$ versus $10^3/T$ for $[ET]_3NiCl_4.H_2O$ (single crystal {b}, 1,1,2–tce) after phase change

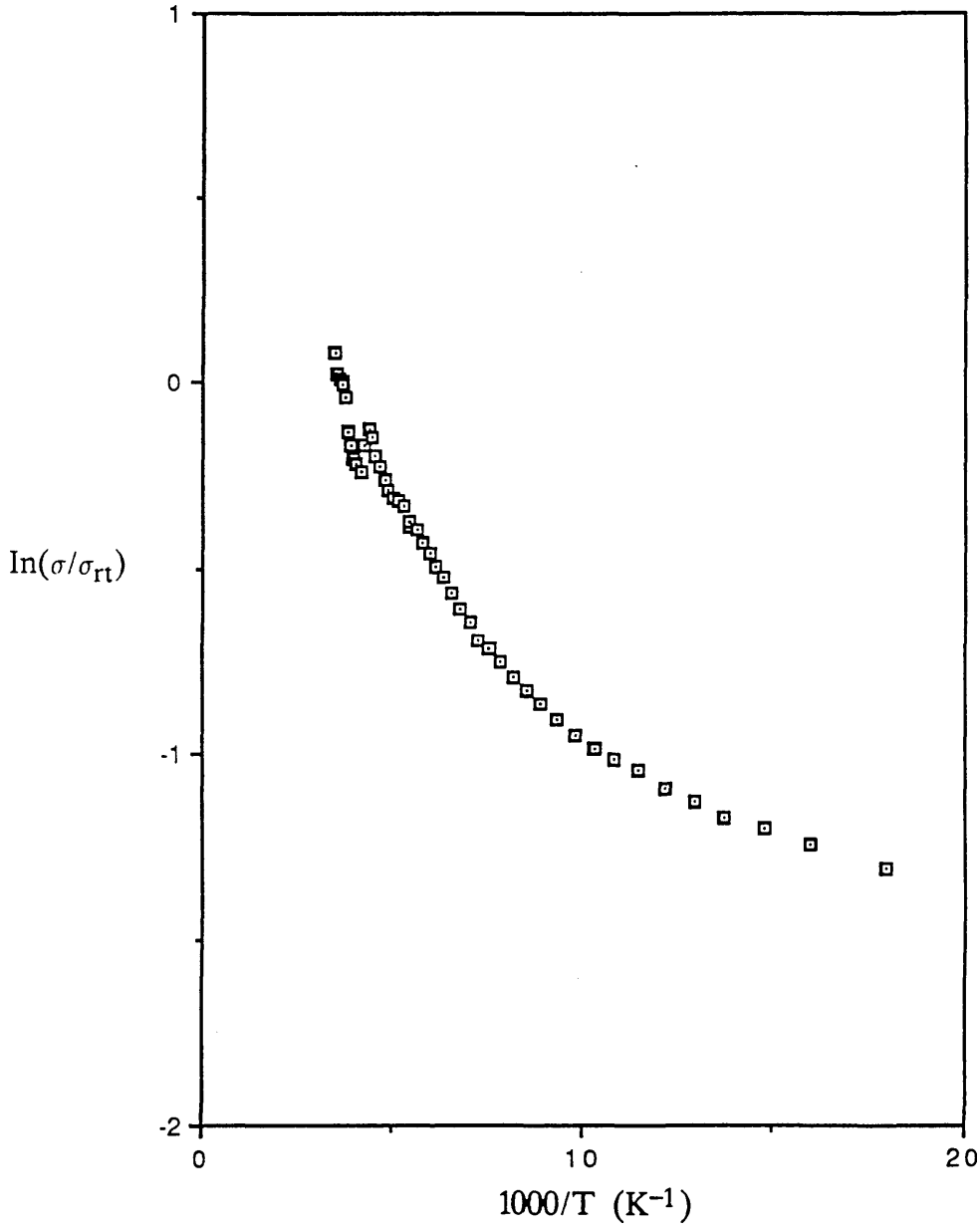


fig., **2.3.20.**

Plot of $\ln\sigma$ versus $1/T^2$ for $[ET]_3NiCl_4.H_2O$ (single crystal {b} after phase change) to show two–dimentionality of the compound

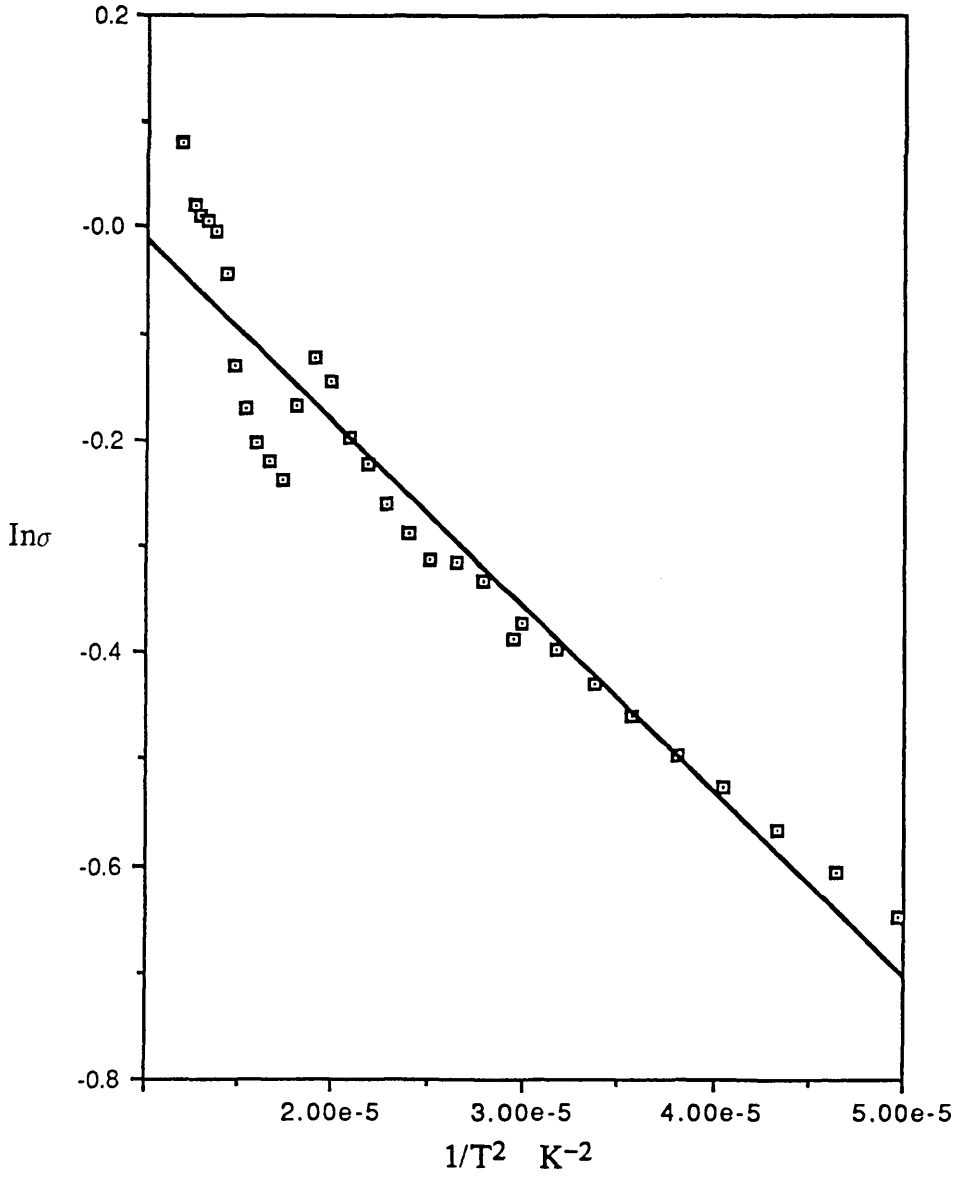


fig., **2.3.21.**

Plot of $\ln(\sigma/\sigma_{rt})$ versus temperature for [ET]/$NiCl_4$ whisker (benzonitrile)

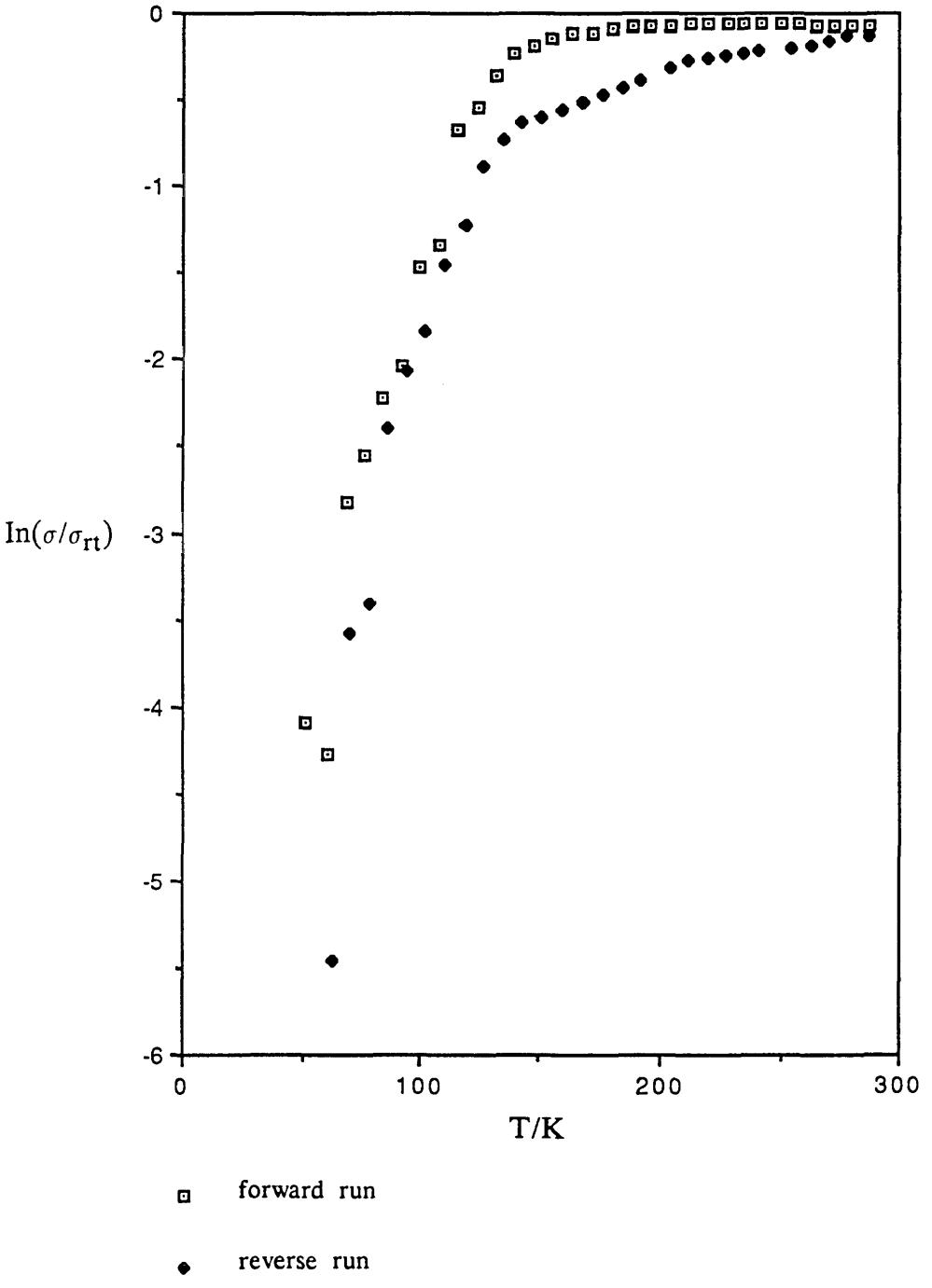


fig., 2.3.22.

Plot of $\ln(\sigma/\sigma_{rt})$ versus $10^3/T$ for $[ET]/NiCl_4$ whisker (benzonitrile)

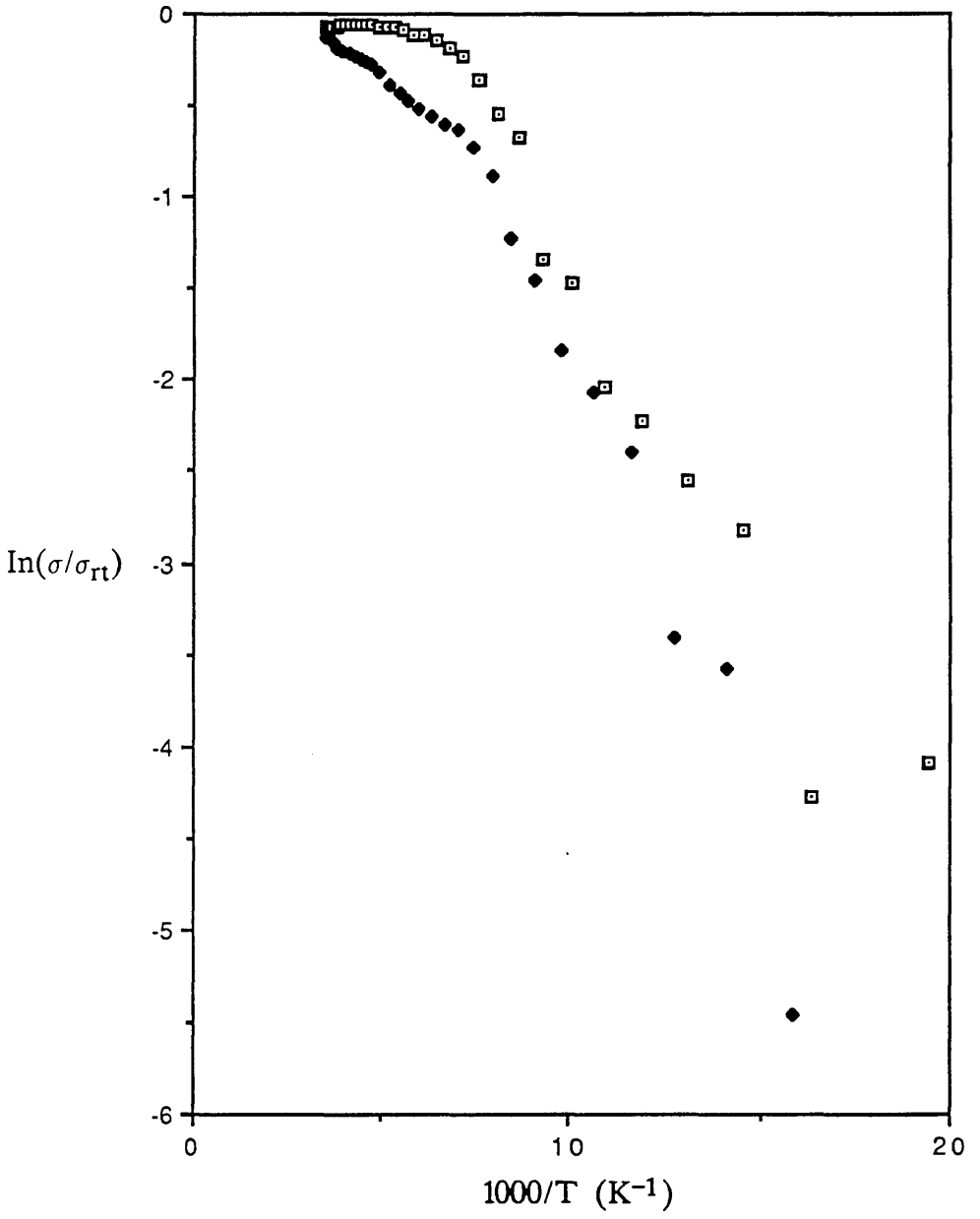


fig., **2.3.23.**

Plot of $d(\ln\sigma)/d(1/T)$ versus temperature for $ET/NiCl_4$ (benzonitrile)

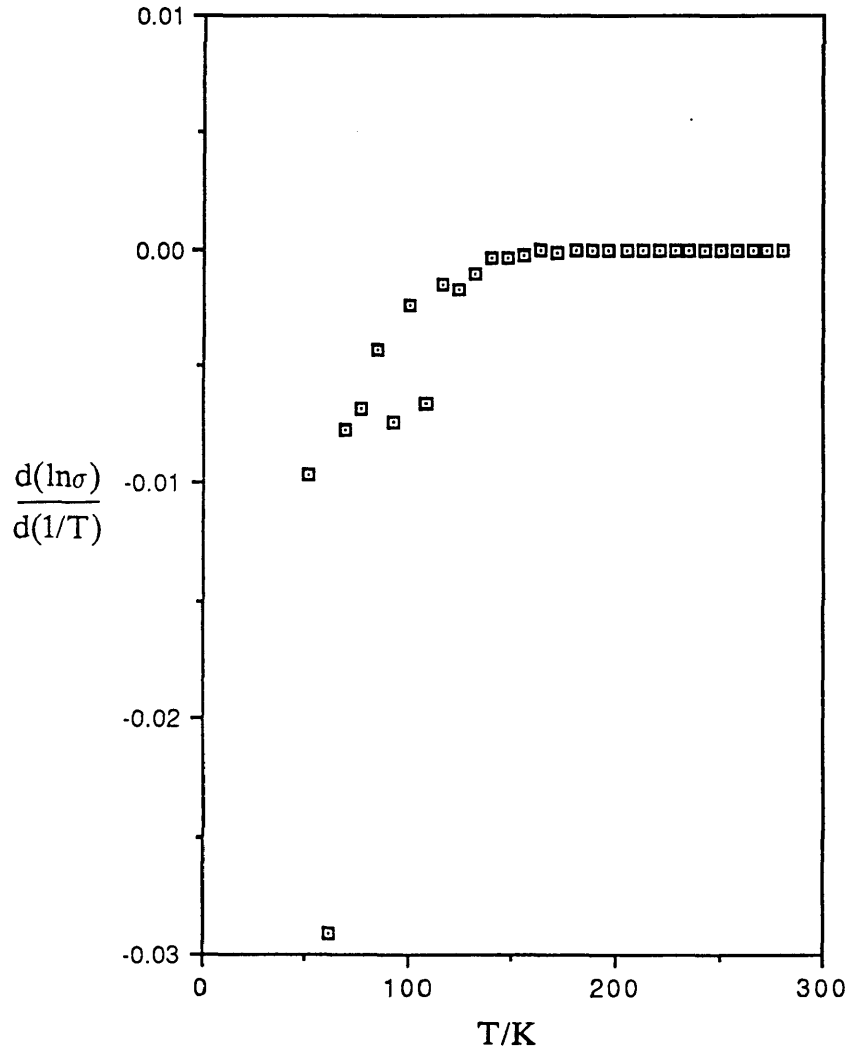


fig., **2.3.24.**

Plot of $\ln(\sigma/\sigma_{rt})$ versus temperature for $[ET]_5HgBr_3$

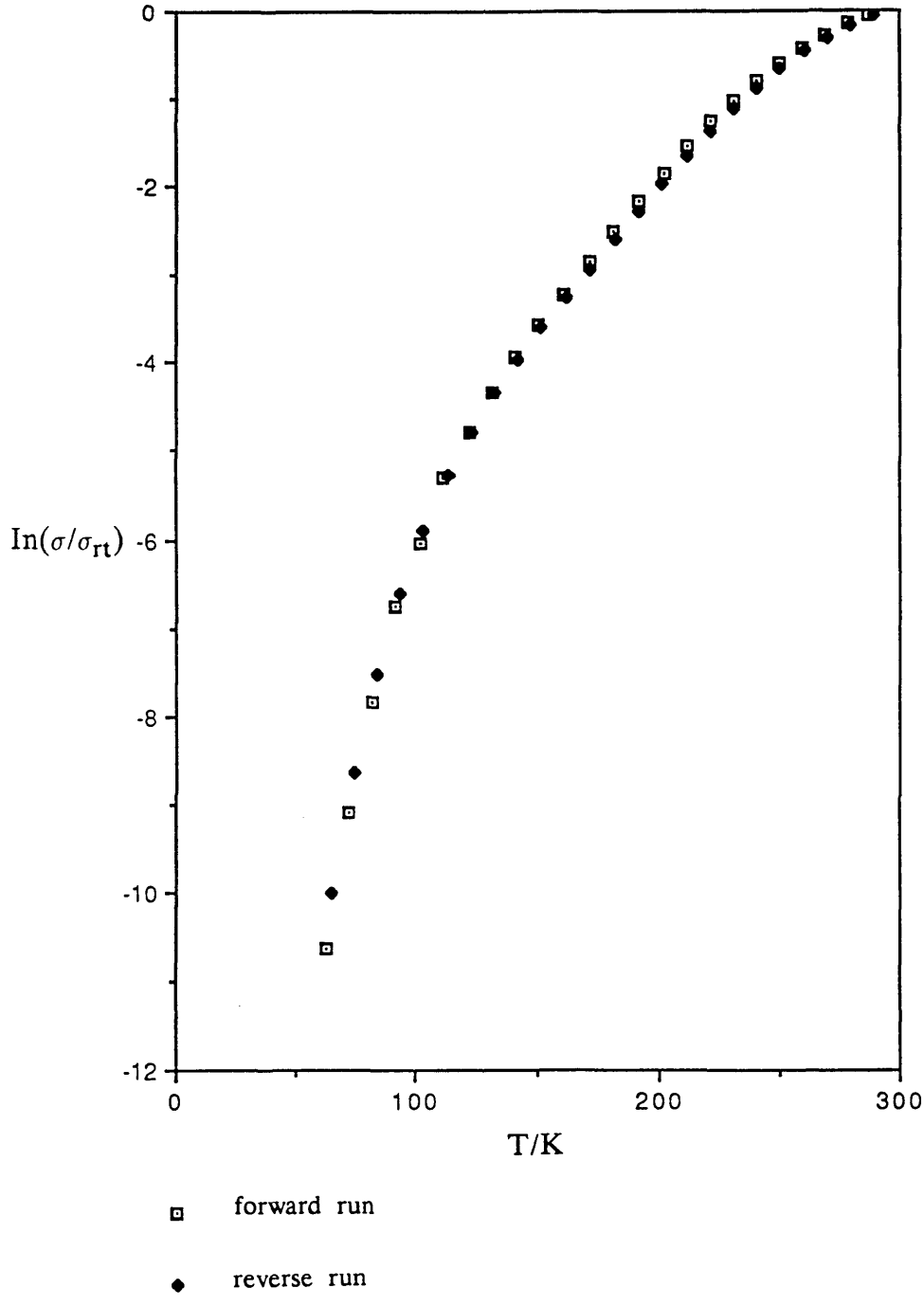
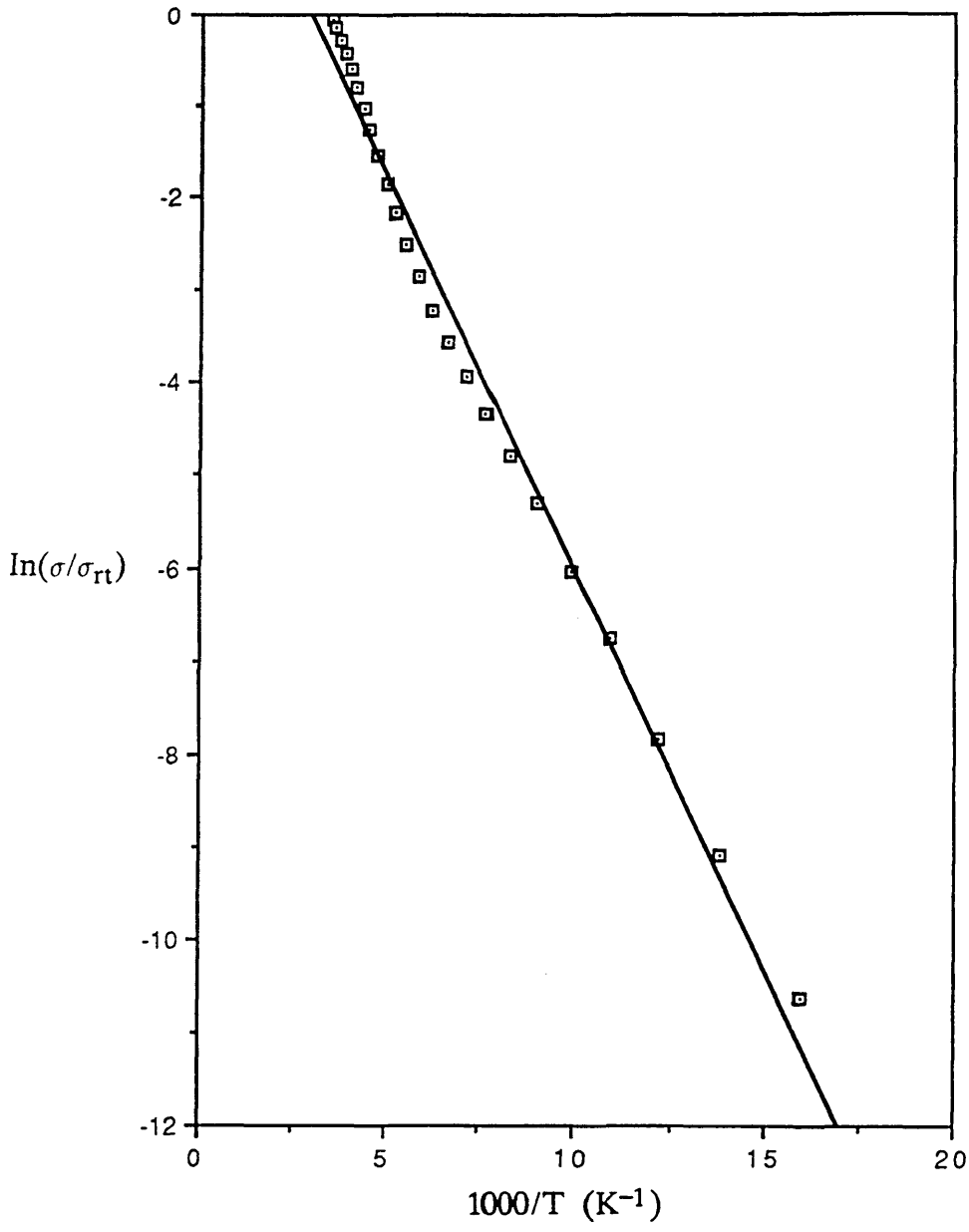


fig., **2.3.25.**

Plot of $\ln(\sigma/\sigma_{rt})$ versus 1000/T for $[ET]_5HgBr_3$



2.4.1. FT–IR Absorption Spectra of Polycrystalline Pressed Samples of Organic Metals

Many reflectance measurements have been published (see review by J R Ferraro and J M Williams[66], and references cited within), but very few absorption data are reported. The optical properties are valuable tools to characterize the charge–transfer (CT) excitations in these solids, which are indicative of electronic correlations[135]. Absorption spectroscopy can provide information on the bulk phonons without interference of possible defects and impurities at the surface. It allows us to recognize electron–molecular vibrational (e–mv) interactions, which activate forbidden a_g vibrations as explained by Yartsev *et al.* in the case of quasi–isolated dimers[136,137] or, more generally, when the translational symmetry in a 1–D stack is lost. Often measurements can only be made on pulverised materials diluted in compressed pellets of CsI or KBr, as very thin crystals are required for single crystal measurements, which is not always possible. The question arises as to the validity of the measurements, as organic metals often undergo a phase transition[138] during the preparation of pellets under pressure.

The recent discovery of superconductivity in polycrystalline pressed samples of organic metals[138] makes the study of such pellets very interesting.

Experimental

The samples (prepared by electrocrystallisation) were ground in an agate mortar together with dry KBr. The weight concentration of the organic metals in the pellet was ca.5%. Special care was taken to achieve homogenous pellets of good optical quality and were prepared with a pressure of 10^4 $Kgcm^{-2}$. Spectra in the range 7200–250 cm^{-1}

were obtained using a Perkin–Elmer FT–1720X spectrometer, at a resolution of $2cm^{-1}$. A good signal to noise ratio was obtained by accumulating 500 scanning interferograms.

Discussion

As can be seen from the figures (*figs.*, 2.4.1.–2.4.5.), the spectra of the materials are very similar and the spectral range can be roughly divided into two regions: the first one from 6000 cm^{-1} to the sharp increase in absorption at 1500 cm^{-1} and the second from 1500 cm^{-1} to 250 cm^{-1}. In the first area, a very broad absorption peak with a maximum at around 3000 cm^{-1} is observed for ET and HMTTeF salts, which is characteristic of the CT "A" band for a mixed valence state in these types of salts[139,140,141]. In the case of the TTF salts, the broad maxima is observed at approximately 5700 cm^{-1}. In addition, the spectra of the Pt(mnt)$(CN)_2$–donor salts show two sharp doublets assigned to the C≡N vibrations of the dithiolene and metal bonded cyanide.

It is well known that in such systems[142] the totally symmetric modes (a_g) of the intramolecular vibrations give rise to a coupling to the conduction electrons. The broad peak at 3000 cm^{-1} is generally assigned to electronic interband transitions between split bands, whereby the splitting is due to strong intermolecular interactions between the donors and the anions[143,144]. The peaks at 2965 and 2918 cm^{-1} can be attributed to C–H stretching modes.

The sharp increase in absorption at around 1500 cm^{-1} marks the beginning of the vibronic pattern which can be attributed to the interaction between conduction electrons and molecular (phonon) vibrations. A similar sharp absorption increase at nearly the same frequency was observed in the absorption of single crystals and

powdered samples of α-$[ET]_2I_3$[143], in pressed pellets of α-$[ET]_2NO_3$ and α-$[ET]_2(ClO_4)_3$[145], in reflectance data on α-$[ET]_2I_3$[146,147] and β-$[ET]_2I_3$[148,149], as well as in reflectance data with polarization along the a, b and c axes in κ-$[ET]_2Cu(NCS)_2$[144,150,151].

From Raman measurements of the donor molecule BEDT-TTF (ET)[143,152] as well as of the organic metals $[ET]_2Br$[153], β-$[ET]_2I_3$ [154] and κ-$[ET]_2Cu(NCS)_2$[155], it is known that the totally symmetric vibrational modes (a_g) of the rings and central C=C bonds occur in the region between 1500 and 1400 cm^{-1}. It was further observed that in all the organic metals a shift to lower energies with respect to the neutral donor ET ($\sim$ 1500 cm^{-1}) appears. The shift is smaller in the case of β-$[ET]_2I_3$[154], than in κ-$[ET]_2Cu(NCS)_2$[155] or $[ET]_2Br$[153]. It is well known from theory[143,156,157] that in the IR vibronic spectra the shift to lower energies with repect to Raman data is determined by the strength of the e-mv coupling and that the shift can be of the order of 200 cm^{-1}[158]. Therefore the bands between 1400 and 1335 cm^{-1} can be described by the coupling of electrons with the C=C stretching mode of the central carbons of the ET cations and corresponds to an increase in the length of the central C=C bond. It is interesting to note that in the case of the deuterated κ-$[ET]_2Cu(NCS)_2$, the band is shifted by 30 cm^{-1} (1320 to 1290 cm^{-1}) to lower energies, indicating a somewhat stronger e-mv coupling; a higher superconducting transition temperature (T_c= 11K) is observed for the deuterated compound with respect to protonated samples[52,86], in contrast to theoretical expectations- the reason for which is unclear. Bands at 1455 and 1415 cm^{-1} can be related in the same way to the antisymmetric (b_{1u}) C=C stretching mode of the ring carbons, which may be tentatively used to explain the existence of two different donor dimers in κ-$[ET]_2Cu(NCS)_2$[150,172] which show a nearly perpendicular crystallographic arrangement. A

similar, but more complicated situation is observed in polycrystalline pressed samples of β–$[ET]_2I_3$. Single crystals of β–$[ET]_2I_3$ contain only one type of dimerized donor stack. It is known that the β–phase undergoes a phase transition during the preparation of the pressed samples, since Raman measurements show two independent I_3^- anions[159] and an onset to superconductivity is observed at 9K. Therefore two types of donor cation are likely to exist in pressed samples of β–$[ET]_2I_3$ with two bands at 1455 and 1415 cm^{-1} tentatively assigned to C=C stretching modes[160].

The bands at 1280 to 1260 cm^{-1} and 1180 to 1170 cm^{-1} can be correlated to CH_2, C–C–H and H–C–H vibrations. This attribution is supported by spectra for deuterated compounds, where those bands disappear and are shifted to lower energies (1114 cm^{-1} and 1024 cm^{-1})[160] in contrast to the band at 1320 cm^{-1} which appears in the deuterated case in about the same position (1290 cm^{-1}), supporting the assignment as a C=C stretching mode of the central bond. A similar observation is noted in reflectance spectra, where a dip (i.e., splitting of bands) occurs at 1302 and 1280 cm^{-1} for κ–$[ET]_2Cu(NCS)_2$[66] which is correlated to the interaction of the –C–C–H bending vibration with the anion moiety. Upon deuteration, the dip disappears; the results also indicate the presence of two non–equivalent ET molecules. The position of the δ–C–C–H frequency (dip) in reflectance spectra has also been related to the electronegativity of the halogen atom; in PT salts studied the δ–C–C–H vibrations occur 5–10 cm^{-1} lower than in the ET salts, indicative of slightly stronger H···X interactions in the cavity (decrease in lattice softness) for the ET salts vs. the PT salts[66]. However the insensitivity of the δ–C–C–H vibration in relation to the halogen in the ET series prevents one from determining if this suggestion is valid.

Small dips at 1293 and 1181 cm^{-1} have been correlated to methylene vibrations[143,150,161], and especially a C–C–H bending mode for the 1293 cm^{-1} band. Similar narrow dips attributed to methyl group deformations have been previously observed in the infra-red spectra of $[TMTT(S)F]_2X$ conductors[158,162,163]. A splitting in the dips is observed for κ-$[ET]_2Cu(NCS)_2$ which agrees with two types of ET cations with slightly different hydrogen–anion interactions[150].

The bands at 880 and 490 to 440 cm^{-1} can be assigned to an e–mv coupling with C–S modes[143,147], namely the ν_{10} mode for the former and the ν_{12} and ν_{13} modes for the latter. An estimation of the relative strength of the coupling is in the order $\nu_4 > \nu_{12} > \nu_{10}$, based on the intensity of the related vibronic features, in agreement with that observed for corresponding modes of TTF[164,165] and TMTTF[158,166]. In deuterated samples these bands are shifted slightly to higher frequencies supporting the fact of a stronger e–mv coupling. For organic conductors it was usually considered that only totally symmetric a_g modes can couple with electrons[167]. An alternative mechanism of e–mv coupling proposed for TTF compounds[165] suggests that the electronic overlap of an out–of–plane vibration of TTF molecules can be modulated leading to finite IR activity. A similar mechanism has been discussed for ET and DIMET salts[168]. Based on theoretical calculations of the e–mv coupling constant[147], it has been proposed that the band at 440 cm^{-1} is due to an out–of–plane deformation of the ET cations since the ET molecule has an out–of–plane deformation of symmetry b_{2g} at the frequency close to 430 cm^{-1}. The band at 460 cm^{-1} can be assigned to ν_{12} totally symmetric vibrations of the ET molecule activated through linear coupling with electrons. A small peak at 643 cm^{-1} may be related to the ν_{11} ethylenedithio (EDT) C–S and C–C stretching vibrations,

observed in the Raman spectra of neutral ET at 656 cm^{-1}[143].

The absorption spectrum for $[ET]_4[Pt(mnt)(CN)_2]$ (*fig.*, 2.4.1.) reveals a rich vibronic pattern comprising of both donor and anion stretching vibrations. Sharp peaks are observed for the cyanide stretching vibrations of the anion i.e., 2205, 2195 cm^{-1} for $\nu(C{\equiv}N)_{mnt}$ and 2125, 2114 cm^{-1} for $\nu(C{\equiv}N)_{Pt}$. Similarly peaks for $[Pt(mnt)(CN)_2]^{2-}$ are observed in the vibronic pattern, previously described in 1.3.3. i.e., 1152 cm^{-1}, $\nu(C{\cdots}S)_{asym}$; 1011 cm^{-1}, π(CCN); 802 cm^{-1}, $\nu(C{\cdots}S)_{sym}$; 511 cm^{-1}, ring deformation + δ(CCN) and 316 cm^{-1}, ν(Pt–S) + ring deformation. The ν(C=C) vibration of the dithiolene occurs in the same region as the asymmetric b_{1g} vibration of the outer ring C=C bond of the ET cation (1466 cm^{-1}).

Vibrations characteristic of the ET cation occur at: 1466, 1406 and 1344 cm^{-1} ν(C=C); 1262 and 1175 cm^{-1} $\delta(CH_2)$; 1283 cm^{-1} δ(CCH); 881 and 773 cm^{-1} ν(C–S); 643 cm^{-1}, EDT external C–S and ring C–C stretch; 473, 437 and 395 cm^{-1} e–mv coupling with C–S modes of ET.

The room temperature absorption spectra reported for $[ET]_4[M(CN)_4]$ (M = Ni or Pt)[169] exhibit the typical vibronic pattern observed in organic metals with the most intense lines being the $a_g\nu_4$ ν(C=C) mode at 1345 and 1338 cm^{-1} respectively. A peak at 1280 cm^{-1} is assigned to a CH_2 deformation mode of the ethylene protons. The coupling of the ν(C=C) mode in the TTF pentamers of $[TTF]_5[Pt(CN)_4]$ is responsible for 3 centrosymmetric vibrations in the Raman and two non–centrosymmetric vibrations in the IR observed at 1348 and 1411 cm^{-1}.

A plot of the integrated intensities for the a_g ν(C=C) vibronic mode versus temperature and the position (frequency) for the ET salts reveal an inflexion point at 200K for the Ni salt and *ca.*, 250K for the Pt analogue indicative of a phase transition. However it is noted, that

the detected phase transition is not similar to that already described in $[TMTSF]_2X$ salts[141], where an increase in both intensity and frequency of the a_g ν(C=C) mode is noted.

The cyanide stretching frequencies in $[HMTTeF]_3[Pt(mnt)(CN)_2]$ (*fig.*, 2.4.1.) are shifted slightly with respect to the ET salt; 2212 and 2198 cm^{-1} for $\nu(C{\equiv}N)_{mnt}$ and 2112 and 2104 cm^{-1} for $\nu(C{\equiv}N)_{Pt}$. The peak at 1506 cm^{-1} may be tentatively assigned to ν(C=C) of the dithiolene. Further dithiolene vibrations occur at 1150, 509 and 326 cm^{-1}, the assignments of which correlate to the ET salt.

Symmetric stretching vibrations (a_{1g}) of the central C=C bond of the TTeF portion are located at 1436, 1353 and 1328 cm^{-1}. Important CH_2, δ(CCH) and H–C–H vibrations are found at 1298, 1282, 1197 and 1021 cm^{-1} while the CH_2 stretching vibrations are slightly different to the ET molecule i.e., 2938, 2885 and 2825 cm^{-1}. The weak peak at 391 cm^{-1} may be tentatively assigned to ν(C$\cdots$Te) (HMTTeF; ν(C$\cdots$Te) 413 cm^{-1}).

Vibrational assignments and normal coordinate analysis[170,171] for neutral TTF have been detailed (*fig.*, 2.4.6.). The absorption spectra for $[TTF]_2[Pt(mnt)(CN)_2]$ and $[TTF]_5[AuBr_4]$ (*fig.*, 2.4.2.) can be assigned by comparison with the infra–red spectra of solution or solid state systems containing the dimerized species $[TTF]_2^{+\cdot}$ which showed absorptions of vibronic origin were observed at 1360, 749 and 492 cm^{-1}[164].

The ethylenic C–H stretches of the TTF radical cation are located at 3073 cm^{-1} (b_{1u}, ν_{13}) and 3058 cm^{-1} (b_{2u}, ν_{22}). It has been noted that the coupling of electrons with the C–H stretching frequency is vanishingly small, since the intensity of the absorption does not vary significantly with temperature[165]. The cyanide stretching frequencies for the TTF–Pt salt found at 2203, 2192 and 2183 and 2121, 2110 cm^{-1}

are as previously assigned.

Peaks in the region 1511 to 1473 cm^{-1} are assigned to a_g ν_2(C=C) stretches and experience weak e–mv coupling. The bands at 1476 in the case of the TTF–Au (i) complex and 1481, 1473 cm^{-1} for the TTF–Pt complex (ii) correspond also to the b_{1u} ν_{14}(C=C) stretch. The doublet which occurs at 1377, 1366 cm^{-1} (i) relates to the vibronic intensity enhancement of the a_g ν_3 modes of $TTF^{+\cdot}$ clearly recognised in the infra–red spectrum of the $[TTF]_2^+$ dimer in solution at 1360 cm^{-1}[164]. A similar doublet is noted in the spectra of (ii) at 1350 and 1341 cm^{-1}. A sharp absorption at 1235 cm^{-1} for both compounds relates to the antisymmetric in–plane b_{2u} ν_{23}(C–C–H) bend. The weak e–mv coupling associated with the totally symmetric a_g ν_4(C–H) bend occurs at 1074 and 1067 cm^{-1} for (i) but appears to be absent in (ii); the absorption at 1146 cm^{-1} for (ii) corresponds to the asymmetric (C–S) stretch of the dithiolene, while the b_{1u} in–plane ν_{15}(C–H) bending mode may be tentatively assigned to the absorption at 1106 cm^{-1} (c.f., ν_{15} $TTF^{+\cdot}$: 1072 cm^{-1})[164].

A doublet at 885, 873 cm^{-1} and single peak at 870 cm^{-1} in (i) and (ii) respectively, of weak intensity, comply with the b_{2u} ν_{24}(C–S) and C–H stretches and ring SCC bend of the TTF^+ molecule. A triplet of peaks for (i) occur at 838, 831 and 824 cm^{-1}, of which the first two are b_{1u} ν_{16}(C–S) bending modes and the third assigned to a b_{2u} ν_{25}(C–S) mode; only a single peak is observed in (ii) at 830 cm^{-1}. Similarly a peak at 748 cm^{-1} compares to the doublet at 752, 748 cm^{-1} in (i) which relates to the a_g ν_5(C–S) and b_{1u} ν_{17}(C–S) modes. The splitting of these bands is characterised by a common pattern consisting of two very close components at higher frequency and a well separated component at lower frequency. As a consequence the doublet at 712 and 697 cm^{-1} in (i), assigned to the b_{3u} out–of–plane ν_{34}(C–H) bend,

resolves into three components at 715, 713 and 698 cm^{-1}, as previously observed[164]. Only one single peak is observed at 689 cm^{-1} in (ii).

Further evidence of vibronic intensity enhancement is observed at 486 and 490 cm^{-1} in (i) and (ii) respectively, which corresponds to the a_g ν_6(C=C) mode, with smaller peaks observed at 510 cm^{-1}. Thus not only are totally symmetric a_g vibrations effective in the vibronic mechanism of intensity enhancement, but the coupling of some out–of–plane molecular modes may occur by modulation of the electron transfer integral i.e., the b_{3u} ν_{34}(C–H) bending mode at 712, 697 cm^{-1} which is reported to undergo considerable intensity enhancement as the temperature is lowered.

Finally, weak absorption peaks at 459, 429 and 466, 432 cm^{-1} for (i) and (ii) repectively, relate to b_{1u} ν_{18}(C–S) stretching and CSC bending modes; slightly more intense absorptions at 361 and 353 cm^{-1} for (i) and (ii) relate to the out–of–plane oscillation of the sulphur atoms of the TTF radical cations. The vibrational assignment of the TTF molecule is not detailed enough to allow a definite correlation to a specific molecular mode in this case; however, the sharpness of the band does not favour the assignment of an overtone of an intermolecular lattice mode and intensity enhancement at low temperatures suggests e–mv coupling.

A comparison of the absorption spectra for ET salts with the anions $AuBr_2^-$ and $AuBr_4^-$ reveal similar details with the characteristic vibronic region mentioned previously. The symmetric a_{1g} ν(C=C) stretching mode of the central carbons for α'–$[ET]_2[AuBr_2]$, the product from ET and $[Bu_4N][AuBr_4]$ in benzonitrile and $[ET]_3[AuBr_4]$ (*fig.*, 2.4.3.) are found at 1338, 1343 and 1399 cm^{-1} respectively. The bands at 1430, 1411 and 1413 cm^{-1} for the three salts may be similarly ascribed to the C=C stretching mode of the ring carbons. The higher

frequency of the a_{1g} ν(C=C) vibration for $[ET]_3[AuBr_4]$ indicates a lengthening of the C=C bond; crystallographic evidence reveals two independent ET cations with bond lengths 1.327 and 1.370Å. Bands at 1284 to 1262 cm^{-1} and 1175 cm^{-1} are correlated to CH_2, C–C–H and H–C–H vibrations, while evidence of e–mv coupling to C–S modes is found at 880 and 460, 435 cm^{-1}. It is interesting to note that a doublet is observed at 460, 435 cm^{-1} for α'-$[ET]_2[AuBr_2]$ and ET/$AuBr_4$ (benzonitrile) while only a sharp single peak is found in $[ET]_3[AuBr_4]$ (thf) at 479 cm^{-1}. Peaks at 1125 and 1010, 1005 cm^{-1} may be assigned to a combination of C–H and C–C stretching vibrations; the peak at 1024 cm^{-1} for $[ET]_3[AuBr_4]$ (thf) is shifted by ~ 15 Hz. From conductivity measurements, $[ET]_3[AuBr_4]$ was found to undergo a phase transition at 125K; therefore the absorption spectra is likely to be related to this new phase due to the preparation of the compressed disc. Any lattice distortion involving the organic sheets would cause an enhancement of the asymmetry of the electron transfer interactions among the ET molecules. It has been observed that the vibronic features become more prominent at low temperatures and has been related to the effects of lattice distortion[143]. Thus the enhancement of the vibronic features in $[ET]_3[AuBr_4]$ (1413, 1399 cm^{-1}; 916–812 cm^{-1}; 479 cm^{-1}) may be related to a new (insulating) phase, as a result of lattice distortion.

The ν(Au–Br)[173] stretching vibration (254 cm^{-1}) was not observed for any of the ET–gold salts (KBr disc or nujol mull on CsI plates).

The absorption spectra for $[ET]_3[NiCl_4].H_2O$ and the microcrystalline materials from $[Ph_4As]_2[MCl_4]$ (M = Ni, Co) (*fig.*, 2.4.4.) and ET in benzonitrile provide a useful comparison for the gold–ET systems.

The ring C=C and central a_g ν(C=C) stretches are found as single

peaks at 1404 cm^{-1} in the Ni–systems, while peaks at 1408, 1398 cm^{-1} and 1354, 1325 cm^{-1} occur in the Co–donor salt. Small absorption peaks for CH_2, C–C–H and H–C–H vibrations are observed at 1260 and 1174 cm^{-1}; the metallic $[ET]_3[NiCl_4].H_2O$ provides evidence of the C–C–H bending mode at 1290 and 1187 cm^{-1} with single peaks at 1284 cm^{-1} for the Ni and Co–ET systems. The values of the C–H and C–C stretching vibrations (1132 to 1126 cm^{-1} and 1010 cm^{-1}) are the same as those noted in the Au–ET salts. Small peaks in the region 880 cm^{-1} correspond to e–mv coupling with C–S modes, with only single peaks observed at 472 cm^{-1} for the Ni salts; the $CoCl_4^{2-}$ salt displays a greater number of peaks with values 491–480 and 447 cm^{-1}– the latter value attributed to an out–of–plane deformation of the ET cations.

The band at 591, 580 cm^{-1} in $[ET]_3[NiCl_4].H_2O$ may possibly be a vibrational rocking mode of the water molecule[174].

A nujol mull of the cobalt salt on CsI plates reveal Co–Cl stretches (308, 297, 288 and 269 cm^{-1}) which corresponds closely to the values given for $[Et_4N][CoCl_4]$ (ν_3: 311, 291 cm^{-1} and ν_1: 269 cm^{-1})[175].

The absorption spectra for $ET/Pd_2X_6^{2-}$ (X = Cl, Br) and $ET/Pt_2Cl_6^{2-}$ (*fig.*, 2.4.5.) reveal the same vibronic envelope observed for ET salts: 1451 to 1338 cm^{-1}, ring C=C and central C=C stretching vibrations; 1284 and 1174 cm^{-1}, CH_2, C–C–H and H–C–H vibrations; 1125 and 1021 to 1003 cm^{-1}, C–H and C–C vibrations; 890–882 cm^{-1}, e–mv coupling with C–S modes. All three display a strong e–mv coupling in the region 490–472 and 449 cm^{-1}.

Metal–halogen stretches are observed for Pd–Cl (319 cm^{-1}) and Pt–Cl (329, 318 cm^{-1}) but are unable to provide information on the geometry of the metal–halide species i.e., $[M_2X_6^{2-}]$[178] or $[MX_4^{-}]$[176,177] due to the weakness of the absorption. Similarly, no metal–halogen

stretches are observed in the nickel ($NiCl_4^{2-}$, ν_3: 294, 280 and ν_1: 264 cm^{-1})[175,179] ET salts.

The ET/HgBr species, obtained from electrocrystallisation of ET and K[$Hg(CN)_2Br$]/18–crown–6 in benzonitrile, are all characterised by the disappearence of the cyanide stretch (K[$Hg(CN)_2Br$], 2187 cm^{-1}) (*fig.*, 2.4.1.) and the absence of nitrogen in the elemental analysis. Vibrations characteristic of the ET cation occur at: 1404, 1385, 1344 and 1317 cm^{-1}, centre and outer ring ν(C=C) stretches; 1275 and 1173 cm^{-1}, $\delta(CH_2)$, C–C–H and H–C–H vibrations; 1114 and 1023 cm^{-1}, C–H and C–C stretches; 880–775 cm^{-1} and 535–476 cm^{-1}, e–mv coupling with ν(C–S) modes.

It was not possible to distinguish between the platelets ($[ET]_5HgBr_3$), obtained initially, and the needles ($[ET]_5Hg_3Br_{11}$) which were formed after 1 month, except for small deviations in the frequencies of the ν(C=C) and ν(C–C–H) vibrations (for the latter: 1395, 1338 and 1282 cm^{-1}; c.f., reflectance spectra for $[ET]_5Hg_3Br_{11}$[66]).

Conclusions

The room temperature absorption spectra are in good agreement with previously reported infra–red and reflectance spectra. The effects of electron molecular vibrational coupling for ET salts have been found to be in common with TTF salts with the most strongly coupled modes related to the stretching of the central C=C (ν_3, ν_4), C–S (ν_{10}) and external C–S bonds (ν_{12}, ν_{13}) of the TTF skeleton in the order of decreasing strength. In comparison, vibronic coupling effects for TTF salts is most significant for the stretching of C=C (ν_2, ν_3 and ν_{14}), C–S (ν_{16}) and the out–of–plane bending of the C–H bonds (ν_{34}).

The effects of phase transitions on the infra–red spectra may be identified by increases in intensity at lower temperatures; an

interpretation of the temperature dependence shows that e–mv interaction plays a relevant role in the stabilization of the low temperature semiconducting or insulating phases. Similarly, the effects of pressure during the preparation of KBr discs is likely to result in a phase change, as observed for the $[ET]_3[AuBr_4]$ salt. The above observations do not suffice to identify a specific structural change. However they indicate some of its features (i) It should cause a loss of some symmetry element and (ii) induce a widening of the band gap.

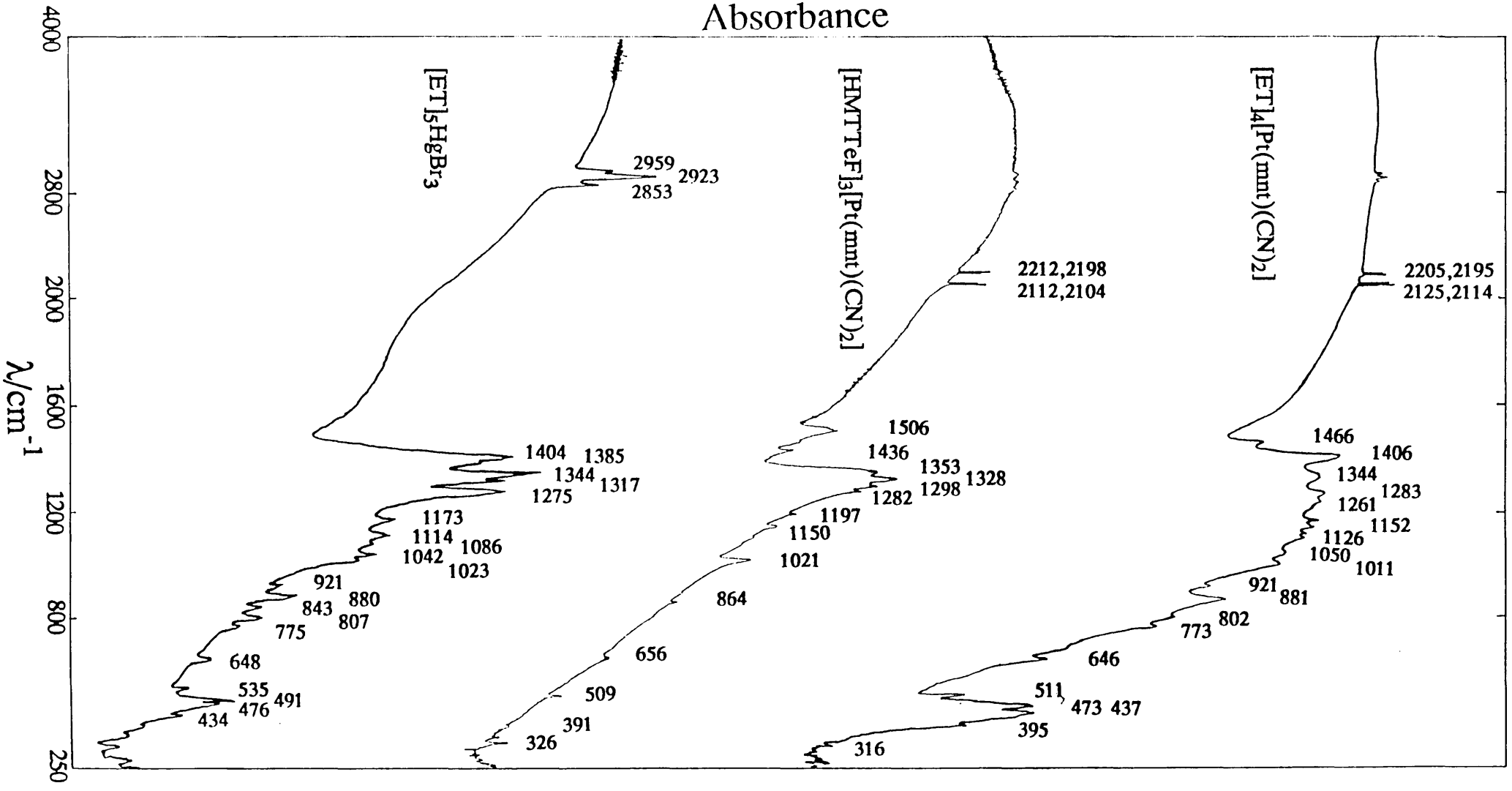


fig., 2.4.1. Absorption spectra for $[ET]_4[Pt(mnt)(CN)_2]$, $[HMTTeF]_3[Pt(mnt)(CN)_2]$ and $[ET]_5HgBr_3$

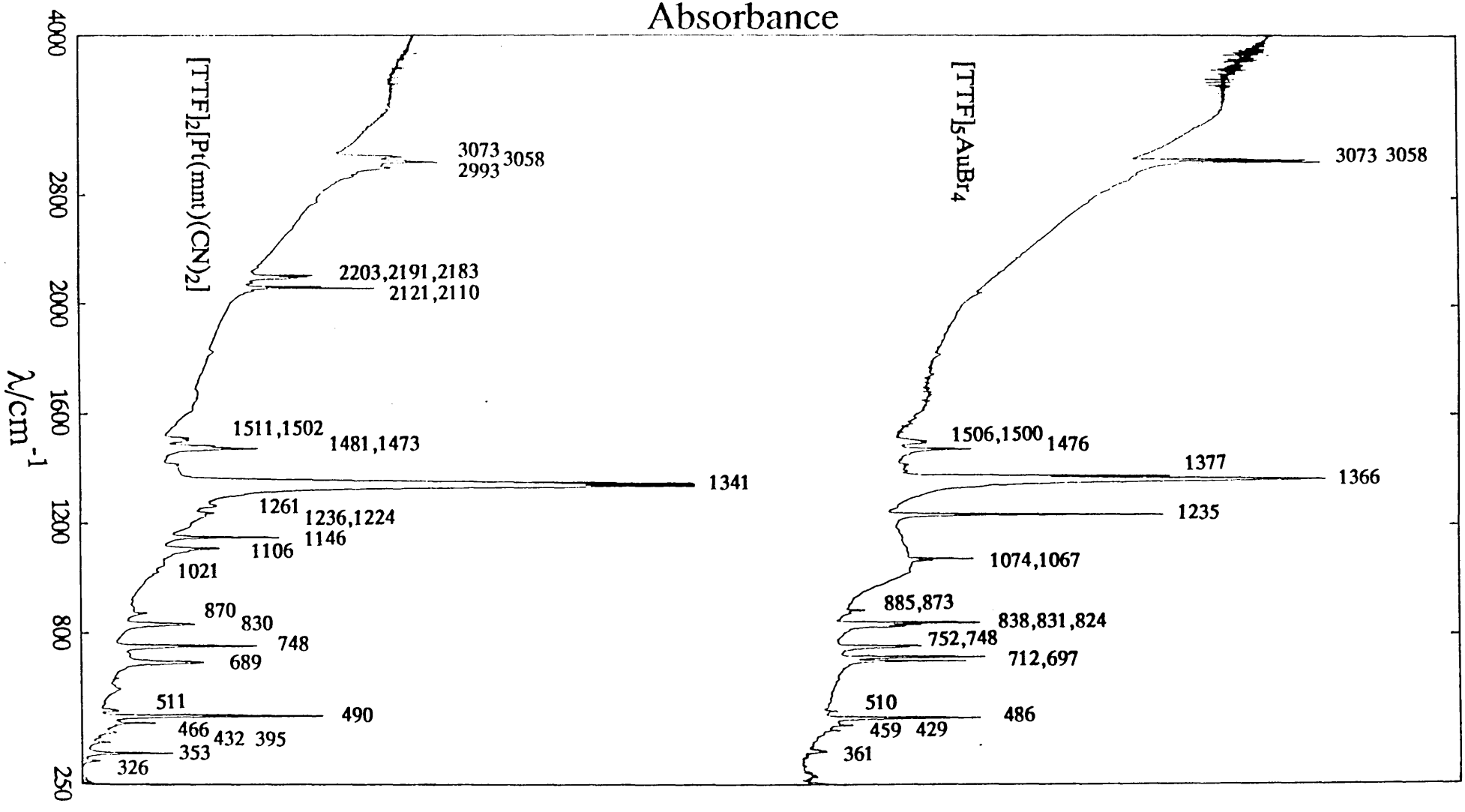


fig., **2.4.2.** Absorption spectra for $[TTF]_5AuBr_4$ and $[TTF]_2[Pt(mnt)(CN)_2]$

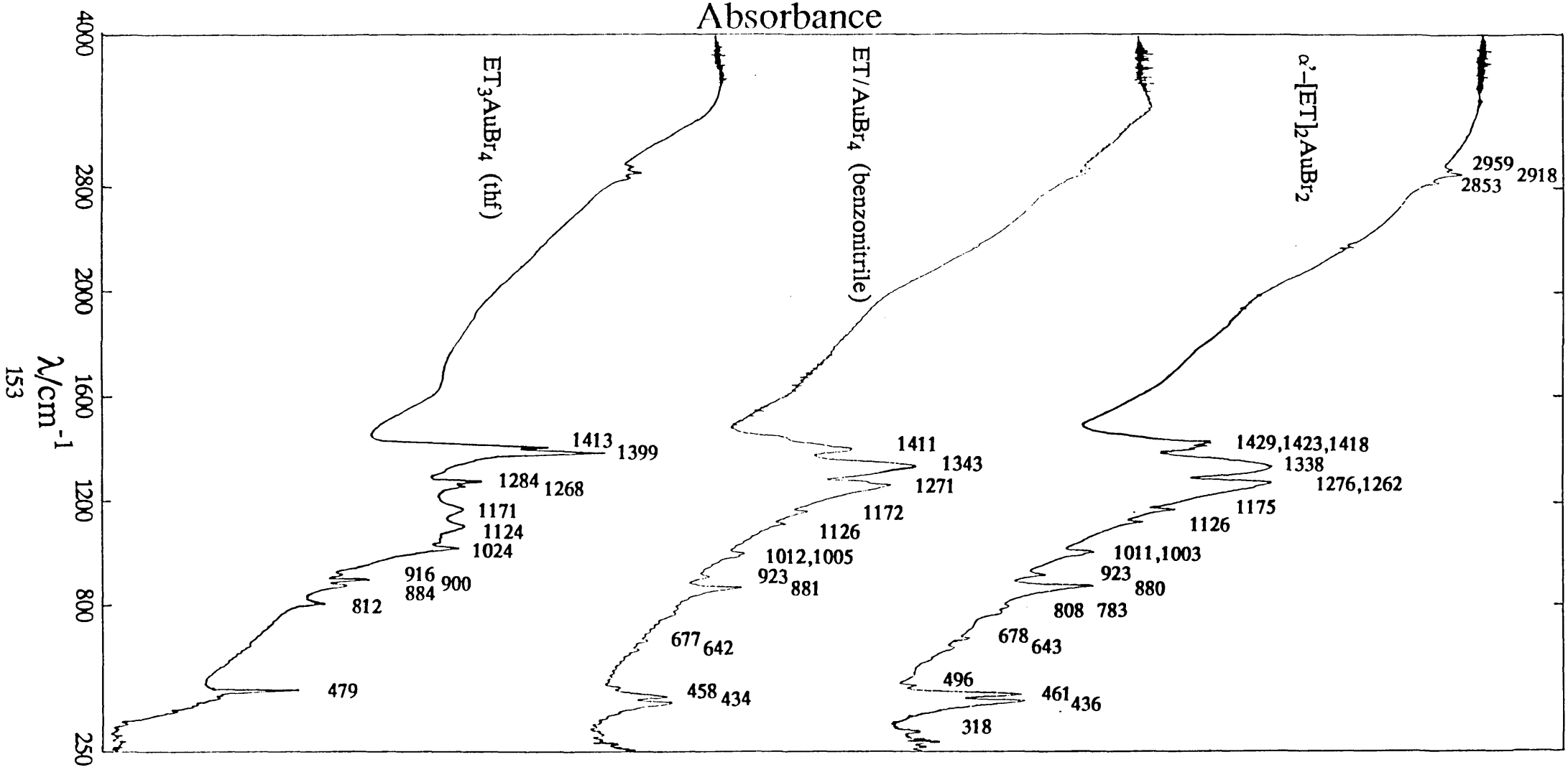


fig., 2.4.3. Absorption spectra for α'–$[ET]_2AuBr_2$, $ET/AuBr_4$ (benzonitrile) and ET_3AuBr_4 (thf)

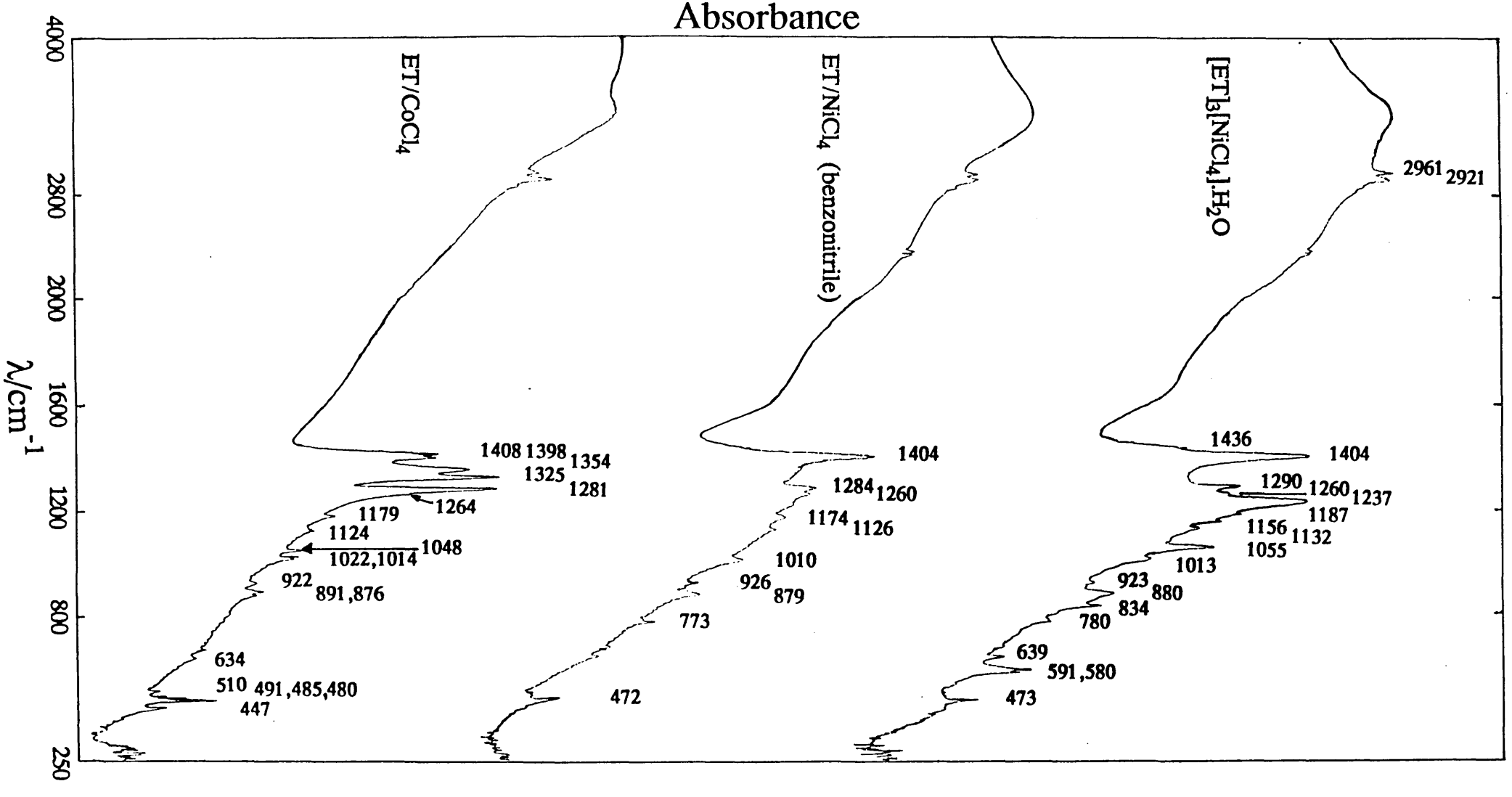


fig., 2.4.4. Absorption spectra for $[ET]_3[NiCl_4].H_2O$, $ET/NiCl_4$ (benzonitrile) and $ET/CoCl_4$

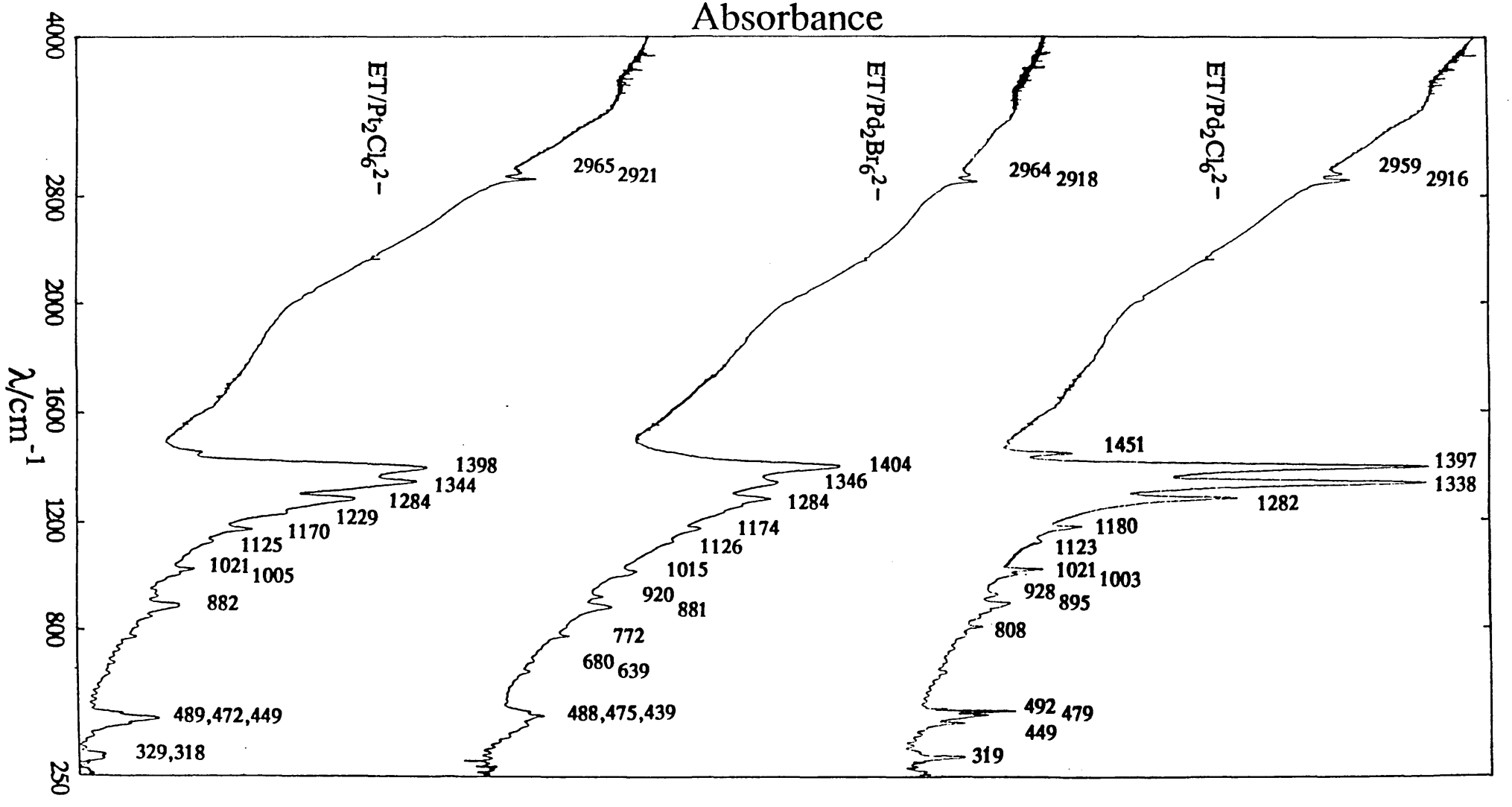
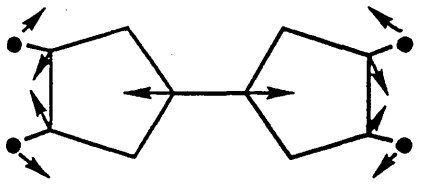
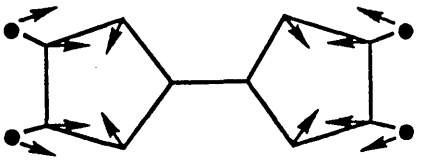


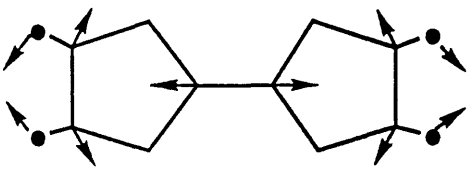
fig., 2.4.5. Absorption spectra for $ET/Pd_2Cl_6^{2-}$, $ET/Pd_2Br_6^{2-}$ and $ET/Pt_2Cl_6^{2-}$



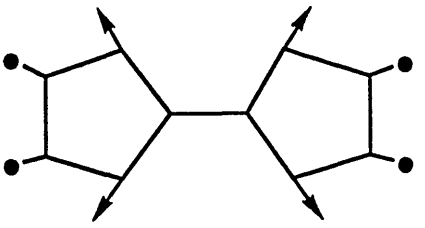
ν_2 1555 cm^{-1}



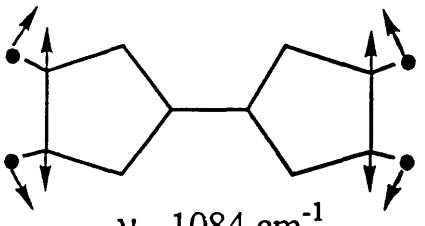
ν_5 737 cm^{-1}



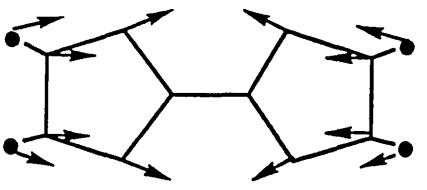
ν_3 1500 cm^{-1}



ν_6 463 cm^{-1}



ν_4 1084 cm^{-1}



ν_7 236 cm^{-1}

fig., **2.4.6.** a_g vibrational modes of neutral TTF observed in infra-red

Molecular and Crystal Structures

2.5.1. *$[ET]_3[NiCl_4].H_2O$*

The structure of an ET molecule is shown in *fig.*, **2.5.1.**. Views down the three crystallographic axes are given in *figs.*, **2.5.2.** to **2.5.4.**. Tables., **2.5.1.** to **2.5.3.** list the structural parameters. The structure consists of stacks of ET molecules separated by sheets of $NiCl_4^{2-}$ anions. The asymmetric unit contains three ET molecules and one $NiCl_4^{2-}$ anion. The anions are situated in an "anion" cavity formed by the ethylene groups of the ET molecules. Within the stacks, the ET molecules are parallel with each other. Looking down onto the mean plane of the ET cations, two of the ET molecules lie with adjacent molecules above in the conventional a mode (as defined by Williams[51] - where ET molecules stack uniformly with a relative displacement ΔY along the long in-planar molecular axis of one of the ET molecules). Whereas the third ET molecule is partway between a and b modes and forms part of the Z type sheet in the interstacking mode (i.e., the ET molecules are staggered with respect to the local z axis).

Molecular orbital calculations have shown that increasing the positive charge on the ET molecule results in an increase in the central C=C and decrease in C–S bond lengths[92,93]. The ratio b/a, where b is the C–S bond length of the TTF portion of the ET molecule and a is the central C=C bond length, provides an approximate indication of the charge on the ET cation.

Thus the three ET molecules in $[ET]_3NiCl_4.H_2O$, due to slightly different geometries, can be classified by their degree of partial oxidation. For ET molecules (1) and (3) (see bond lengths and angles tables), a is 1.364Å and b 1.738Å i.e., b/a = 1.27(5). For molecule (2) (a = 1.376Å and b = 1.730Å), b/a = 1.25(7), which by correlation

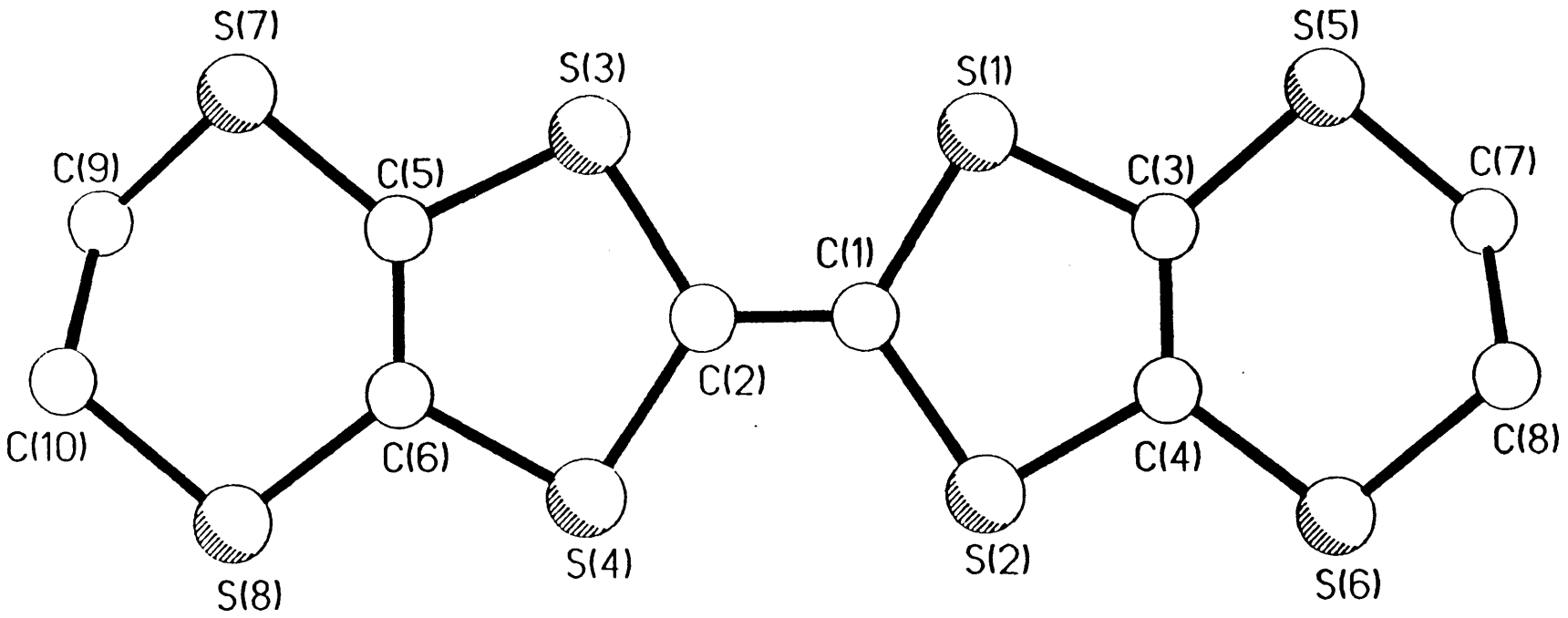


fig., **2.5.1.** Structure of ET molecule and numbering scheme

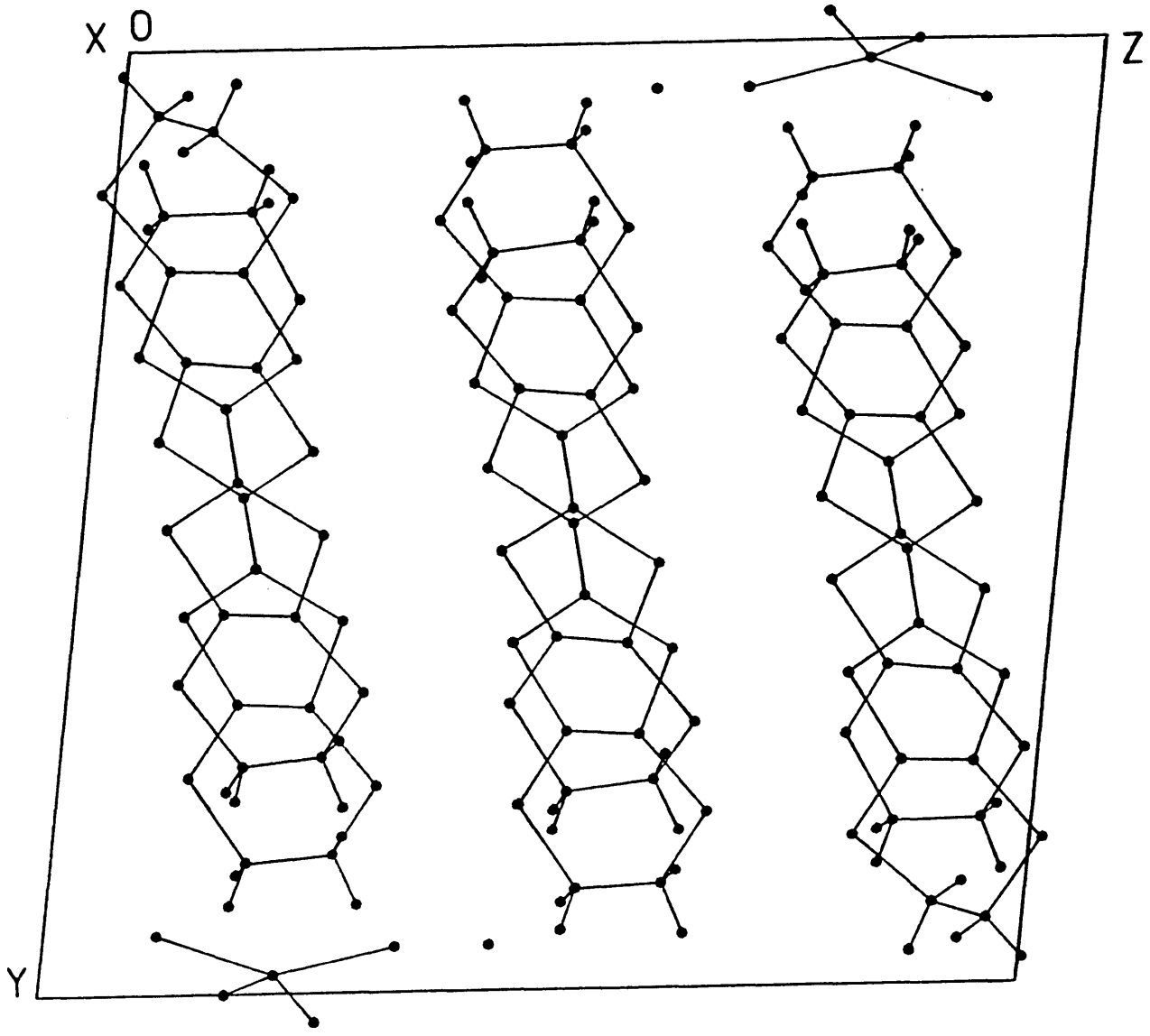


fig., **2.5.2.** View down crystallographic a axis in $[ET]_3[NiCl_4].H_2O$

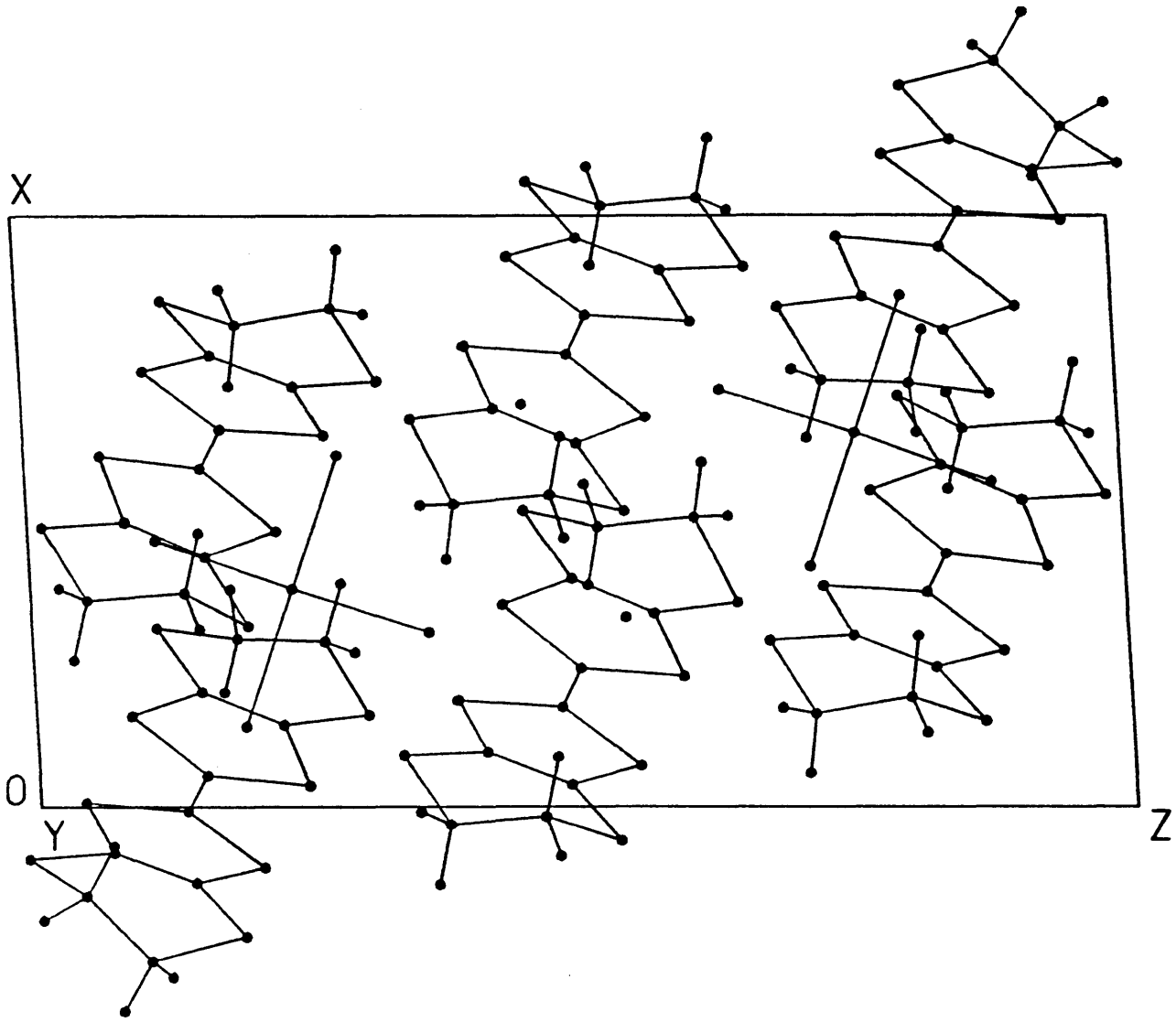


fig., **2.5.3.** View down crystallographic b axis in $[ET]_3[NiCl_4].H_2O$

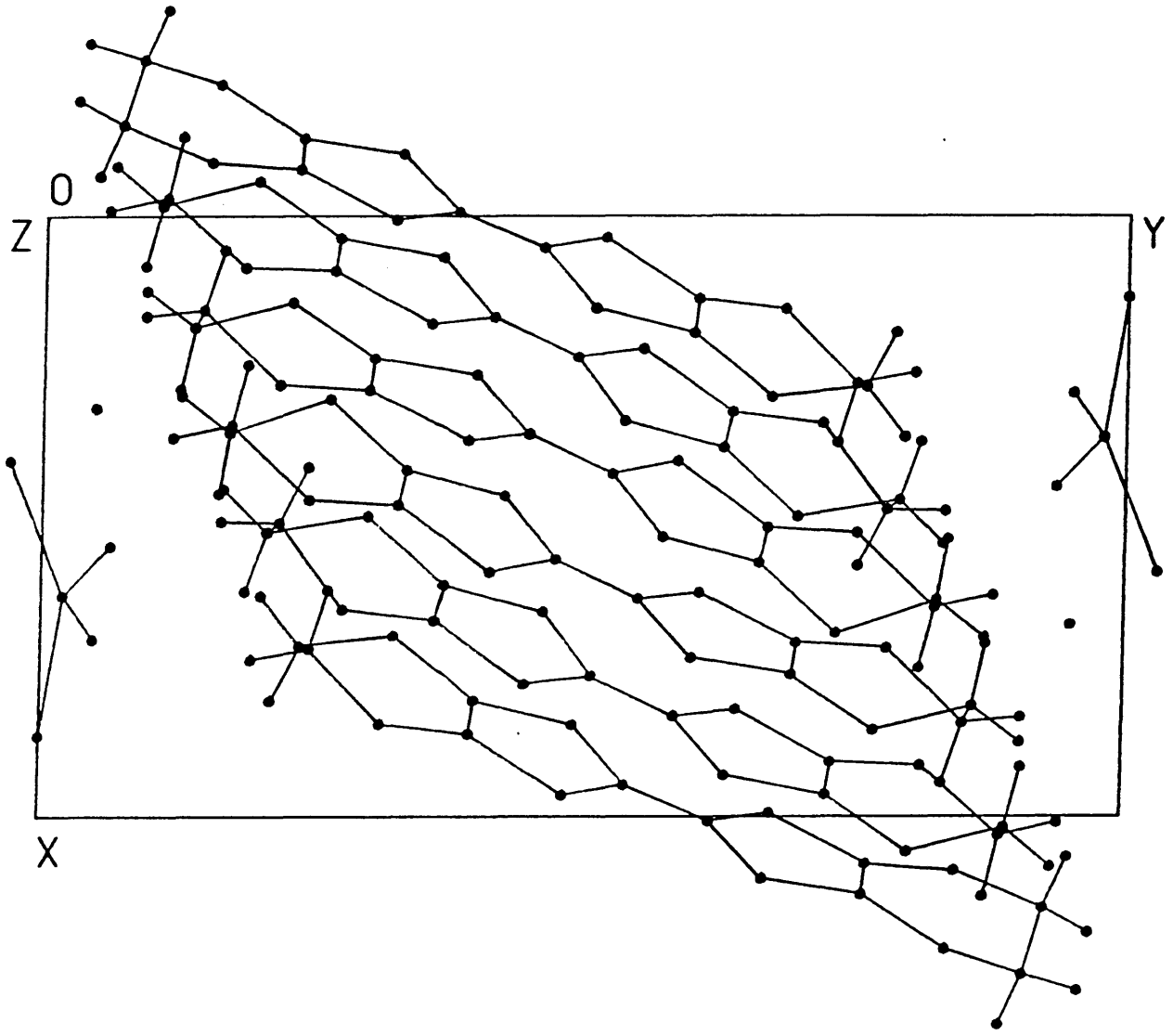
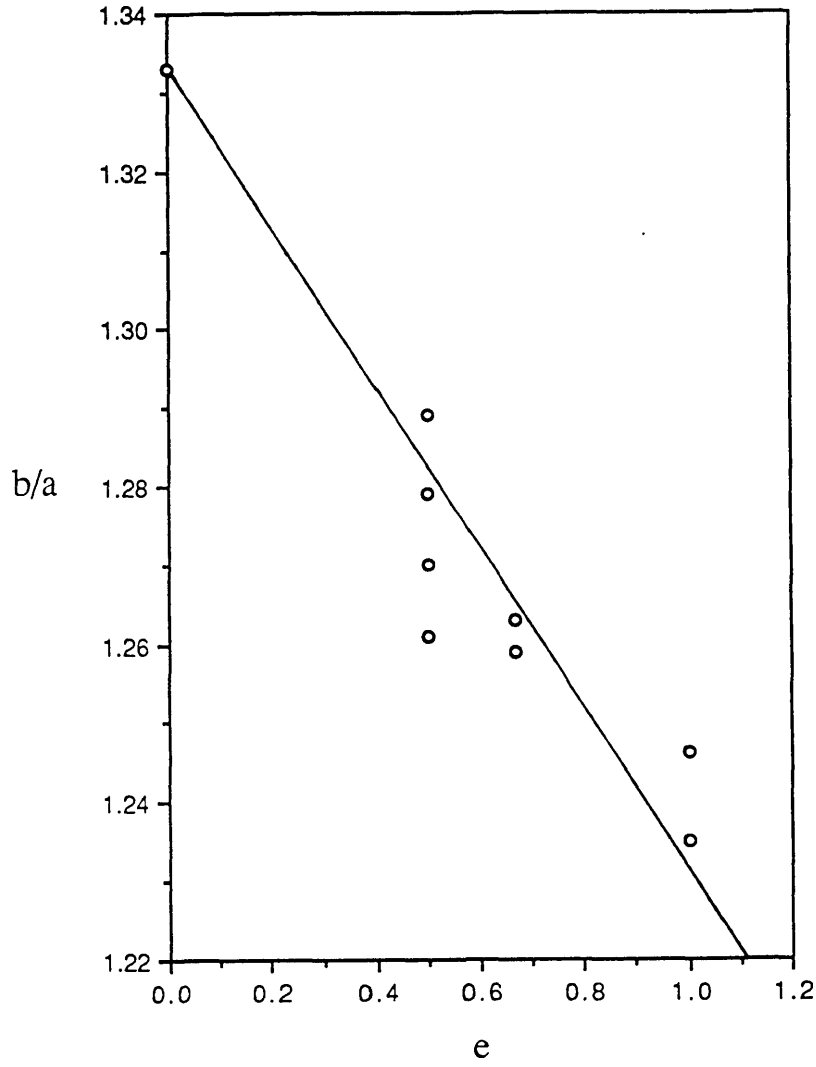


fig., **2.5.4.** View down crystallographic c axis in $[ET]_3[NiCl_4].H_2O$

with other values for ET salts (*fig.*, **2.5.5.**), indicates a marginally higher degree of oxidation compared to molecules (1) and (3).



o: See Appendix **2.6.1.**

fig., **2.5.5.** Graphical representation of the ratio b/a (C–S/C=C bond lengths for the central TTF portion of ET) versus e (charge) for known ET salts

There are significant CH_2···Cl interactions. The majority of the methylene hydrogen···Cl distances are in the range 2.70–2.90 Å; however there are two especially short distances (Cl(4)···H(7"B) 2.55, Cl(4)···C(7) 3.47, Cl(4)···H(10C) 2.53 and Cl(4)···C(10) 3.46 Å). Within the ET sheets, there are close S···S contacts (S(A) are sulphurs within

5-membered and S(B) are sulphurs within 6-membered rings) of S(A)···S(A) 4.0 Å, S(B)···S(B) 3.36 Å and S(A)···S(B) 3.41 Å. Within the ET stacks, the S(A)···S(A) distances are 4.0 Å and S(B)···S(B) 4.3 Å. Finally, an interesting feature of this structure is the geometry of the $NiCl_4^{2-}$ anion which is intermediate between square planar and tetrahedral (∠Cl-Ni-Cl 150°); there are also significantly short Ni-Cl distances of 2.24Å compared to the more regular tetrahedral $NiCl_4^{2-}$ salts.

A regular tetrahedral geometry is observed in $[MePh_3As]_2[NiCl_4]$ (Ni-Cl 2.27Å; ∠Cl-Ni-Cl 109.5°)[185] while a somewhat flattened pseudotetrahedral geometry exists in $[Me_4N]_2[NiCl_4]$[186] (2.26, 2.28Å; ∠Cl-Ni-Cl 107.8, 114.4°).

2.5.2. *[ET]$_3$[AuBr$_4$]*

Views down the three crystallographic axes are shown in *figs.*, **2.5.6.** to **2.5.8.**. Tables **2.5.4.** to **2.5.5.** list the structural parameters. Perspective views of the unit cell are shown in *fig.*, **2.5.9.**. The asymmetric unit contains 1.5 ET molecules and 0.5 of a $AuBr_4^-$ anion. There are two crystallographically independent molecules, the second of which is symmetry generated (hence 1.5 ET molecules) with central C=C (C-S in parentheses) bond lengths of 1.327 (1.747)Å and 1.370 (1.730)Å, respectively.

For the first ET molecule, b/a = 1.31(7), which corresponds closely to neutral ET (C=C, 1.32Å; C-S, 1.76Å, b/a = 1.33). The second (1/2) molecule gives a value of b/a = 1.26(3), which by comparison with other ET salts (γ-$[ET]_3[ClO_4]_2$; b/a = 1.26) corresponds to a charge of +2/3. This indicates that only a small positive charge resides on the first ET molecule, with most of it located on the second molecule.

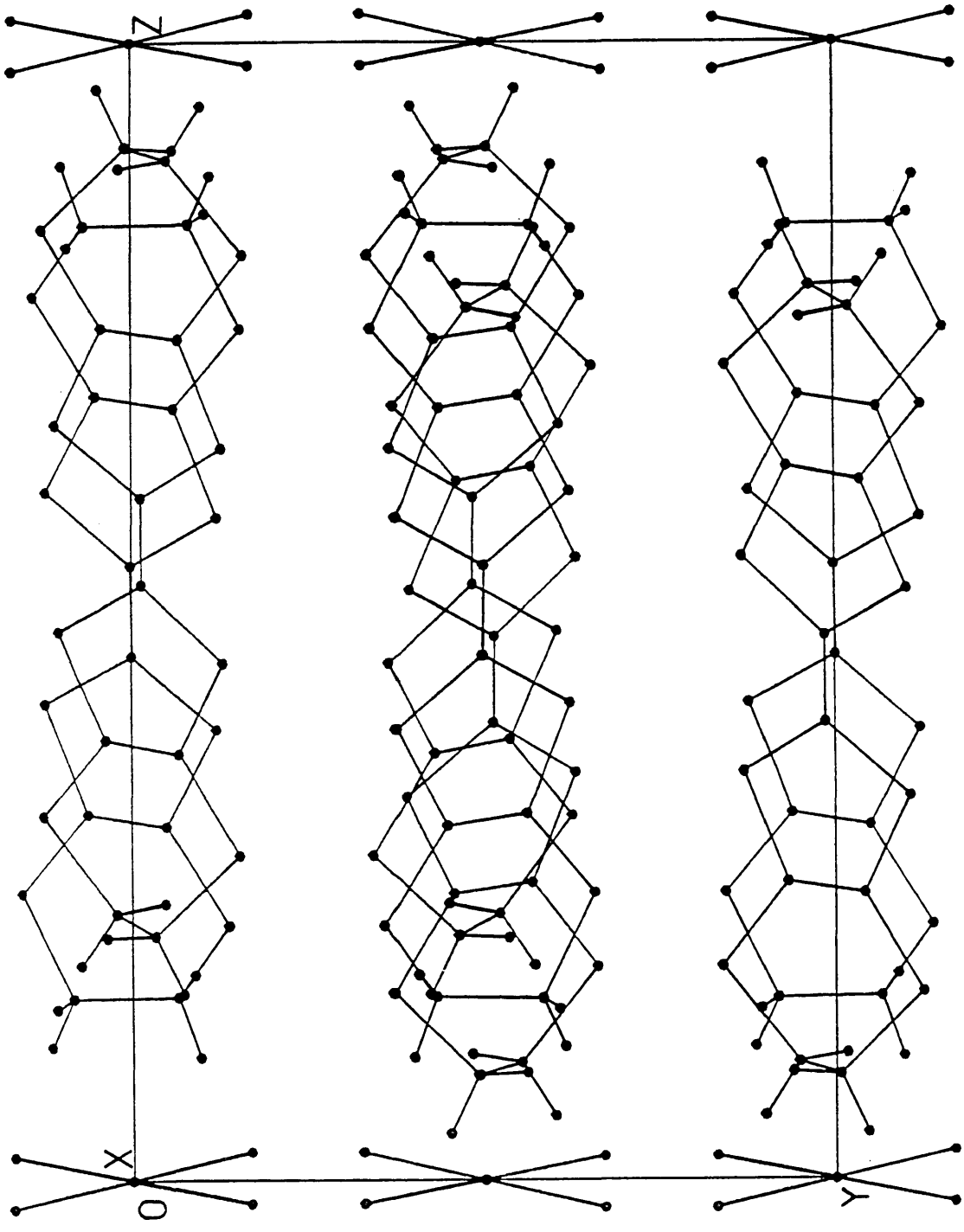


fig., **2.5.6.** View down crystallographic a axis in $[ET]_3AuBr_4$

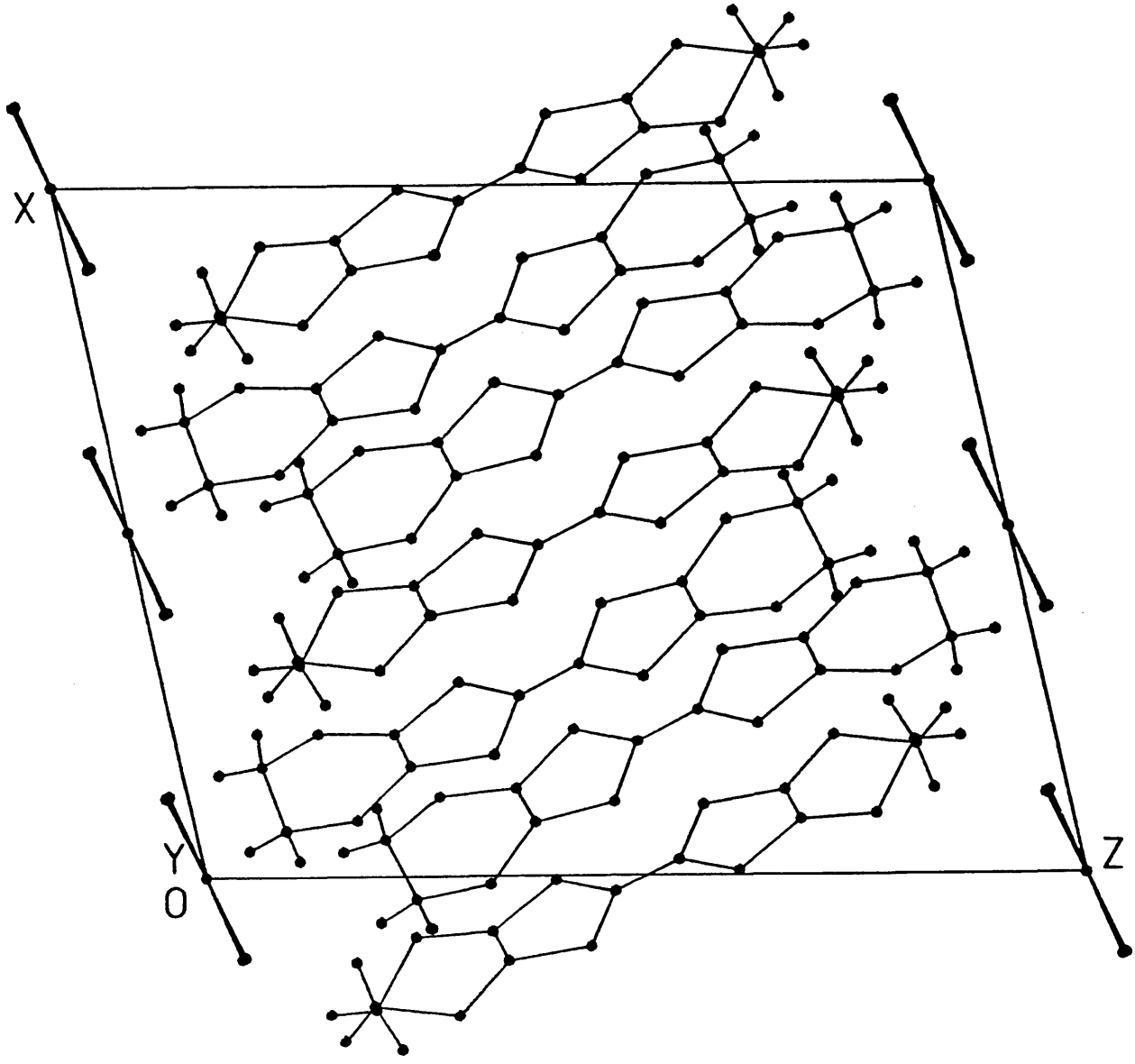


fig., 2.5.7. View down crystallographic b axis in $[ET]_3AuBr_4$

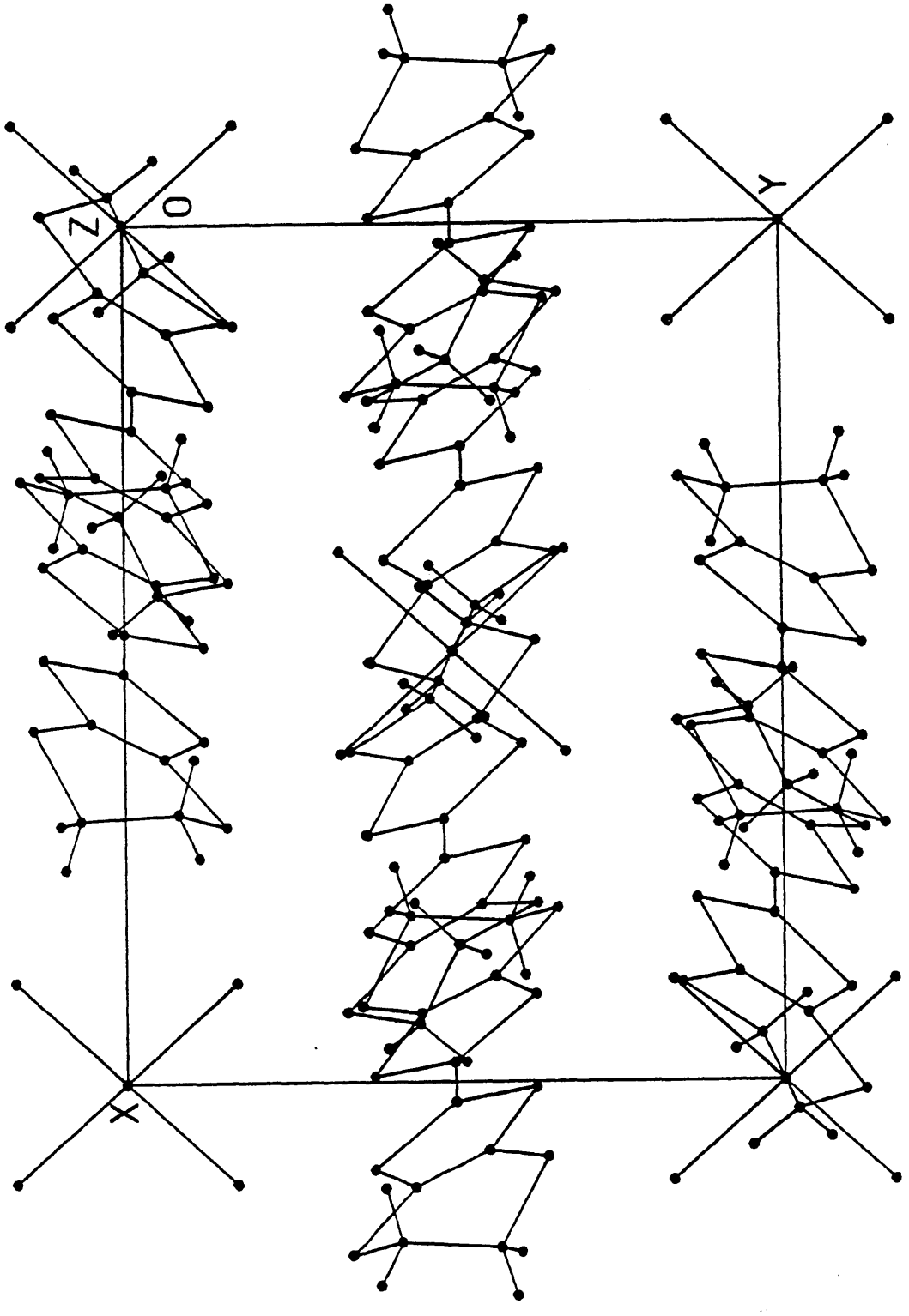


fig., 2.5.8. View down crystallographic c axis in $[ET]_3AuBr_4$

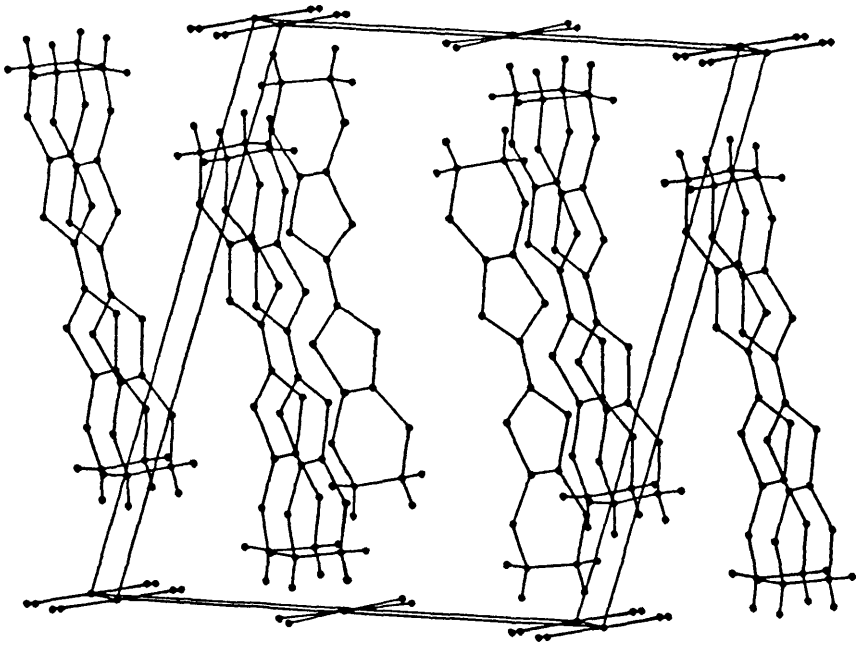
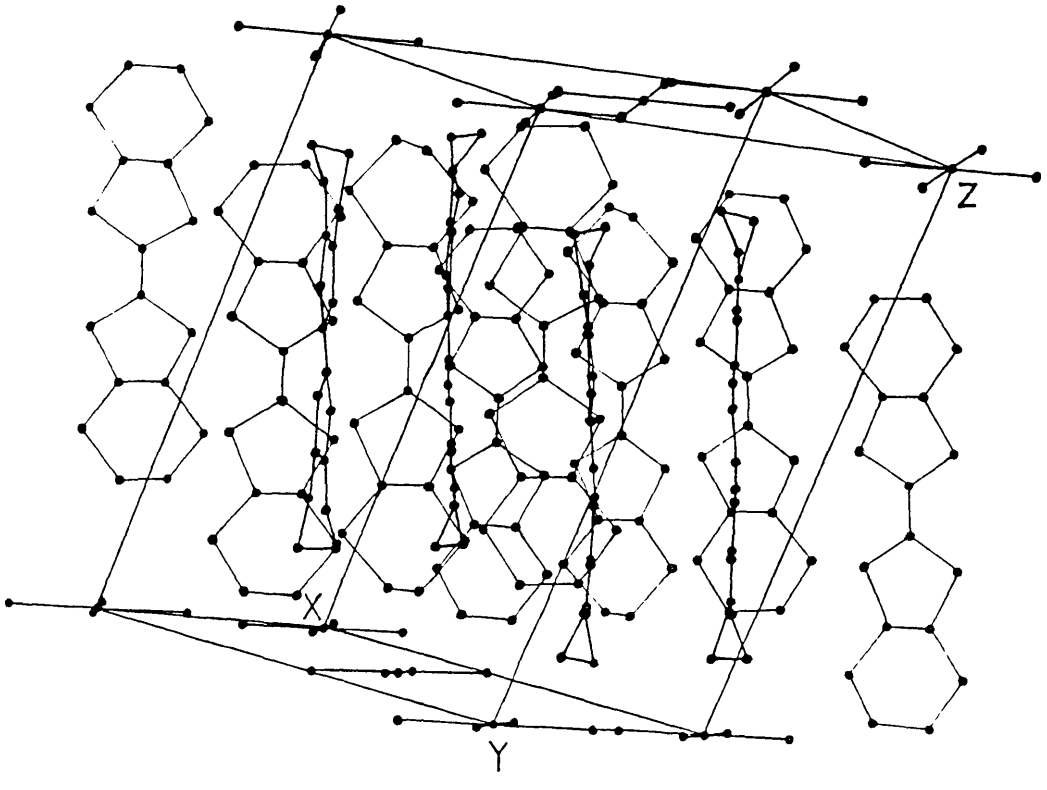


fig., **2.5.9.** Perspective views of $[ET]_3AuBr_4$ in the unit cell



The ET molecules pack in the b and Z mode. There are Br···H contacts of *ca.* 2.9 Å, whilst the shortest S···Br contacts are 3.8 Å (c.f., ι–$[ET]_2AuBr_2$[134]: one S···Br contact of 3.70Å occurs per ET molecule, which is shorter than the sum of the Van der Waals radii (3.8Å); the twist stacks of t–$[ET]_2AuBr_2$ exhibit two short S···Br contacts (3.54 and 3.79Å) per ET molecule). The interstacking S···S distances are S(A)···S(A) 3.82, 3.77 Å and S(B)···S(B) 4.01, 4.21 Å.

2.5.3. Important structural characteristics of donor molecules

The packing arrangement in neutral BEDT–TTF comprises of (i) short C–H···S and C–H···C(sp^2) contacts between adjacent molecules (ii) a π–framework which is bent (fig., $\theta \simeq 15^{\circ}$) and (iii) one six–membered ring of BEDT–TTF has a staggered conformation (a) while the other ring has a conformation similar to an eclipsed one (d) (*fig.*, 2.5.10.).

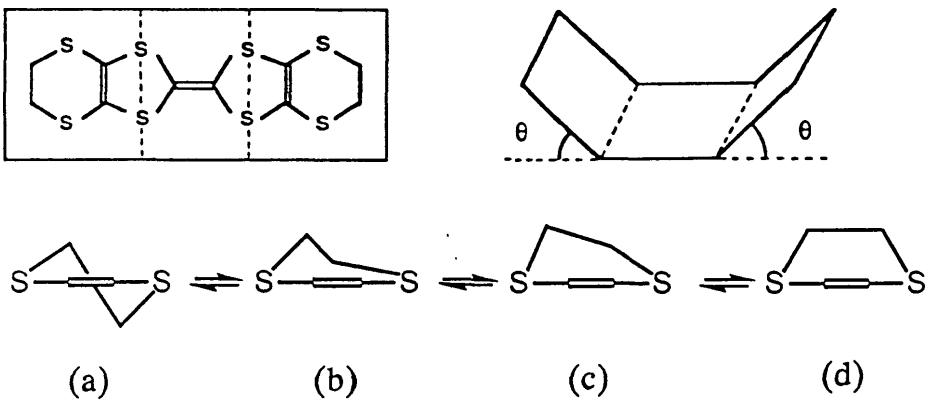


fig., 2.5.10. The π–framework of neutral ET and ethylene conformations of the six–membered ring

The six–membered ring conformation (a) is converted to (d) via the intermediates (b) and (c). In (b), one of the methylene carbon atoms lies on the π–plane, while in (c) both methylene atoms are above the π–plane with one half the height of the other. When a

methylene group lies above the π–plane, one C–H bond is almost perpendicular to the π–plane while the other is approximately parallel. The occurrence of such conformations must arise from external forces associated with short intermolecular contacts.

In the case of the salts $[ET]_3AuBr_4$ and $[ET]_3NiCl_4.H_2O$, we note that the π–framework of BEDT–TTF is nearly flat, the donor molecules have a range of six–membered ring conformations (a) to (d) and there are short C–H···anion, C–H···C(sp^2), C–H···S contacts which lead to attractive interactions and provide the energy for the π–framework bending of the neutral donor molecule[90].

In $[ET]_3AuBr_4$, there are (two) similar, but different, types of ET molecules. Molecule (1) (which is only partially oxidised) has one ethylene conformation (c) of the six–membered ring above the π–plane while the other lies below the π–plane with a conformation approaching that of (d). The second ET molecule (which is more partially oxidised) has the six–membered ring conformation (d).

There are three types of BEDT–TTF molecule in $[ET]_3NiCl_4.H_2O$. Molecules (3) and (1) (designated from the tables for bond lengths and angles) are very similar in respect to the degree of partial oxidation. However the ethylene conformations are slightly different; one of the six–membered ring conformations (comprising of S(5) and S(6)–see *fig.*, **2.5.1.**) in (1) lies slightly out of the π–plane with a conformation very close to (b) while the ring conformation for S(7), S(8) lies in the π–plane with the ethylene conformation intermediate between (c) and (d). In molecule (3), the six–membered ring conformation (containing S(5) and S(6)) has an ethylene conformation, intermediate between (c) and (d), below the π–plane; the other conformation is close to (c) and lies above the π–plane.

The second BEDT–TTF molecule (2) is different due to a slightly

larger degree of partial oxidation; the conformation of the six–membered rings is also different, since both lie above the π–plane with ethylene conformations (b) and (d).

The staggered ethylene group conformations has been correlated to higher superconducting temperatures (β^*–$[ET]_2I_3$; $T_c\sim$ 8K, 0.5Kbar), compared to β–$[ET]_2X$ (X^- = IBr_2, (T_c= 2.8K) and AuI_2(T_c= 5K)) which possess lower T_c's and eclipsed ethylene group conformations[66].

While the staggered conformation is the most energetically stable, the potential surface is very soft towards conformational change and the stabilisation energy associated with C–H···donor contacts is greater than the destabilisation energy associated with π–framework bending, the adoption of the eclipsed conformation, and repulsive S···S contacts[90]. Thus, the eclipsed vs. staggered conformations are not intrinsic properties of the ET molecule but result from the packing arrangement, rather than determining it.

2.5.4. Crystallographic Data

Computations were carried out on an Eclipse S140 computer using the SHELXTL program system (see 1.4.1.., ref 118).

3[$C_{10}H_8S_8$]$NiCl_4$.H_2O: M = 1372.6, triclinic, a = 9.016(2), b = 16.269(3), c = 16.696(2) Å, α = 96.87(1) β = 93.22(1), γ = 90.81(2)°, U = 2427 Å^3, space group P$\bar{1}$, Z = 2, D_c = 1.88 gcm^{-3}. Crystal dimensions 0.10 × 0.10 × 0.36 mm, μ(Cu–K_α) = 125 cm^{-1}, λ = 1.54178 Å, F(000) = 1388.

Data collection and processing: Nicolet R3m diffractometer, ω–scan method, ($2\theta \leq 116^o$), graphite monochromated Cu–K_α radiation; 6547 independent measured reflections, 4808 observed [$|F_o| > 3\sigma(|F_o|)$], corrected for Lorentz and polarisation factors; numerical absorption

correction (face indexed crystal), maximum and minimum transmission factors 0.412 and 0.135 respectively.

Structure analysis and refinement: The structure was solved by direct methods and the non-hydrogen atoms refined anisotropically. A $\Delta\underline{F}$ map revealed the presence of a water molecule, on which the protons were not located. The positions of the hydrogen atoms were idealised (C-H = 0.96 Å), assigned isotropic thermal parameters $\underline{U}(H) = 1.2\underline{U}eq(C)$ and allowed to ride on their parent carbons. Refinement was by block-cascade full-matrix least squares to $\underline{R} = 0.066$, $\underline{R}_w = 0.066$ ($w^{-1} = \sigma^2(\underline{F}) + 0.00050\underline{F}^2$). The maximum and minimum residual electron densities in the final $\Delta\underline{F}$ map were 0.98 and -0.59 $e\text{Å}^{-3}$ and the mean and maximum shifts/error in the final refinement cycle were 0.006 and 0.026 respectively.

$3[C_{10}H_8S_8]AuBr_4$: $\underline{M}$ = 1670.6, monoclinic, $\underline{a}$ = 13.919(4), $\underline{b}$ = 10.292(4), $\underline{c}$ = 17.216(4) Å, β = 102.39(2)°, $\underline{U}$ = 2409 Å^3, space group $\underline{P}2_1/\underline{a}$, $\underline{Z}$ = 2 (the molecule is disposed about a centre of symmetry), $\underline{D}_c$ = 2.30 gcm^{-3}. Crystal dimensions 0.13 × 0.18 × 0.23 mm, μ(Cu-$\underline{K}_\alpha$) = 197 cm^{-1}, λ = 1.54178 Å, $\underline{F}$(000) = 1614.

Data collection and processing: Nicolet R3m diffractometer, ω-scan method, ($2\theta \leq 100°$), graphite monochromated Cu-$\underline{K}_\alpha$ radiation; 2467 independent measured reflections, 2158 observed [$|\underline{F}_o| > 3\sigma(|\underline{F}_o|)$], corrected for Lorentz and polarisation factors; numerical absorption correction (face indexed crystal), maximum and minimum transmission factors 0.199 and 0.057 respectively.

Structure analysis and refinement: The structure was solved by direct methods and the non-hydrogen atoms refined anisotropically. The positions of the hydrogen atoms were idealised (C-H = 0.96 Å),

assigned isotropic thermal parameters $\underline{U}(H) = 1.2\underline{U}eq(C)$ and allowed to ride on their parent carbons. Refinement was by block-cascade full-matrix least squares to $\underline{R} = 0.044$, $\underline{R}_w = 0.050$ ($w^{-1} = \sigma^2(\underline{F}) + 0.00100\underline{F}^2$). The maximum and minimum residual electron densities in the final $\Delta\underline{F}$ map were 0.94 and -0.97 $e\dot{A}^{-3}$ and the mean and maximum shifts/error in the final refinement cycle were 0.007 and 0.035 respectively.

Table., 2.5.1.

Bond lengths (Å) with e.s.d's in parentheses.

Ni–Cl(1)	2.266(2)	Ni–Cl(2)	2.244(3)
Ni–Cl(3)	2.244(2)	Ni–Cl(4)	2.279(3)

Molecule 1.

C(1)–C(2)	1.361(10)	C(1)–S(1)	1.742(7)
C(1)–S(2)	1.738(8)	C(2)–S(3)	1.742(8)
C(2)–S(4)	1.729(7)	S(1)–C(3)	1.755(8)
S(2)–C(4)	1.744(7)	S(3)–C(5)	1.742(7)
S(4)–C(6)	1.752(7)	C(3)–C(4)	1.344(11)
C(3)–S(5)	1.740(7)	C(4)–S(6)	1.749(8)
C(5)–C(6)	1.345(10)	C(5)–S(7)	1.743(8)
C(6)–S(8)	1.751(7)	S(5)–C(7)	1.813(8)
S(6)–C(8)	1.789(8)	S(7)–C(9)	1.795(8)
S(8)–C(10)	1.802(8)	C(7)–C(8)	1.512(11)
C(9)–C(10)	1.501(11)		

Molecule 2.

C(1')–C(2')	1.376(9)	C(1')–S(1')	1.726(7)
C(1')–S(2')	1.733(8)	C(2')–S(3')	1.732(8)
C(2')–S(4')	1.729(7)	S(1')–C(3')	1.745(7)
S(2')–C(4')	1.744(7)	S(3')–C(5')	1.755(7)
S(4')–C(6')	1.748(7)	C(3')–C(4')	1.345(10)
C(3')–S(5')	1.750(7)	C(4')–S(6')	1.746(8)
C(5')–C(6')	1.341(10)	C(5')–S(7')	1.737(8)
C(6')–S(8')	1.735(7)	S(5')–C(7')	1.775(10)

S(6')–C(8')	1.782(9)	S(7')–C(9')	1.782(9)
S(8')–C(10')	1.742(12)	C(7')–C(8')	1.427(15)
C(9')–C(10')	1.361(14)		

Molecule 3.

C(1")–C(2")	1.365(9)	C(1")–S(1")	1.736(7)
C(1")–S(2")	1.739(8)	C(2")–S(3")	1.736(8)
C(2")–S(4")	1.735(7)	S(1")–C(3")	1.742(7)
S(2")–C(4")	1.746(7)	S(3")–C(5")	1.757(7)
S(4")–C(6")	1.750(7)	C(3")–C(4")	1.350(10)
C(3")–S(5")	1.748(7)	C(4")–S(6")	1.740(8)
C(5")–C(6")	1.358(10)	C(5")–S(7")	1.736(8)
C(6")–S(8")	1.744(7)	S(5")–C(7")	1.787(9)
S(6")–C(8")	1.803(8)	S(7")–C(9")	1.775(9)
S(8")–C(10")	1.799(9)	C(7")–C(8")	1.493(12)
C(9")–C(10")	1.446(12)		

Table., **2.5.2.**

Bond angles (°) with e.s.d.'s in parentheses.

Cl(1)–Ni–Cl(2)	93.9(1)	Cl(1)–Ni–Cl(3)	92.4(1)
Cl(2)–Ni–Cl(3)	149.9(1)	Cl(1)–Ni–Cl(4)	150.1(1)
Cl(2)–Ni–Cl(4)	93.9(1)	Cl(3)–Ni–Cl(4)	95.2(1)

Molecule 1.

C(2)–C(1)–S(1)	122.6(6)	C(2)–C(1)–S(2)	122.8(6)
S(1)–C(1)–S(2)	114.6(4)	C(1)–C(2)–S(3)	122.7(6)
C(1)–C(2)–S(4)	122.4(6)	S(3)–C(2)–S(4)	114.9(4)
C(1)–S(1)–C(3)	95.9(4)	C(1)–S(2)–C(4)	95.5(4)
C(2)–S(3)–C(5)	95.3(3)	C(2)–S(4)–C(6)	95.7(3)
S(1)–C(3)–C(4)	116.0(5)	S(1)–C(3)–S(5)	114.3(4)
C(4)–C(3)–S(5)	129.6(6)	S(2)–C(4)–C(3)	117.8(6)
S(2)–C(4)–S(6)	115.2(4)	C(3)–C(4)–S(6)	126.9(6)
S(3)–C(5)–C(6)	117.5(5)	S(3)–C(5)–S(7)	114.5(5)
C(6)–C(5)–S(7)	128.0(5)	S(4)–C(6)–C(5)	116.3(5)
S(4)–C(6)–S(8)	115.1(4)	C(5)–C(6)–S(8)	128.6(6)
C(3)–S(5)–C(7)	103.0(4)	C(4)–S(6)–C(8)	99.9(4)
C(5)–S(7)–C(9)	101.4(4)	C(6)–S(8)–C(10)	102.3(3)
S(5)–C(7)–C(8)	115.2(5)	S(6)–C(8)–C(7)	114.3(6)
S(7)–C(9)–C(10)	114.8(5)	S(8)–C(10)–C(9)	114.3(5)

Molecule 2.

C(2')–C(1')–S(1')	122.6(6)	C(2')–C(1')–S(2')	122.7(5)
S(1')–C(1')–S(2')	114.6(4)	C(1')–C(2')–S(3')	122.0(5)
C(1')–C(2')–S(4')	122.4(6)	S(3')–C(2')–S(4')	115.5(4)
C(1')–S(1')–C(3')	96.0(3)	C(1')–S(2')–C(4')	95.8(3)

C(2')–S(3')–C(5')	95.3(3)	C(2')–S(4')–C(6')	95.3(3)
S(1')–C(3')–C(4')	116.6(5)	S(1')–C(3')–S(5')	115.0(4)
C(4')–C(3')–S(5')	128.4(6)	S(2')–C(4')–C(3')	116.8(6)
S(2')–C(4')–S(6')	114.5(4)	C(3')–C(4')–S(6')	128.7(5)
S(3')–C(5')–C(6')	116.7(5)	S(3')–C(5')–S(7')	114.6(4)
C(6')–C(5')–S(7')	128.6(5)	S(4')–C(6')–C(5')	117.1(5)
S(4')–C(6')–S(8')	114.9(4)	C(5')–C(6')–S(8')	128.0(6)
C(3')–S(5')–C(7')	102.0(4)	C(4')–S(6')–C(8')	100.0(4)
C(5')–S(7')–C(9')	101.0(4)	C(6')–S(8')–C(10')	102.2(4)
S(5')–C(7')–C(8')	117.0(7)	S(6')–C(8')–C(7')	120.1(7)
S(7')–C(9')–C(10')	121.1(7)	S(8')–C(10')–C(9')	122.8(8)

Molecule 3.

C(2")–C(1")–S(1")	123.5(6)	C(2")–C(1")–S(2")	121.8(5)
S(1")–C(1")–S(2")	114.8(4)	C(1")–C(2")–S(3")	123.0(5)
C(1")–C(2")–S(4")	122.2(6)	S(3")–C(2")–S(4")	114.7(4)
C(1")–S(1")–C(3")	95.7(3)	C(1")–S(2")–C(4")	95.7(3)
C(2")–S(3")–C(5")	96.0(3)	C(2")–S(4")–C(6")	96.0(3)
S(1")–C(3")–C(4")	117.1(5)	S(1")–C(3")–S(5")	114.9(4)
C(4")–C(3")–S(5")	128.0(6)	S(2")–C(4")–C(3")	116.7(6)
S(2")–C(4")–S(6")	114.9(4)	C(3")–C(4")–S(6")	128.4(5)
S(3")–C(5")–C(6")	116.2(5)	S(3")–C(5")–S(7")	115.9(4)
C(6")–C(5")–S(7")	127.9(5)	S(4")–C(6")–C(5")	116.8(5)
S(4")–C(6")–S(8")	114.4(4)	C(5")–C(6")–S(8")	128.8(6)
C(3")–S(5")–C(7")	101.7(4)	C(4")–S(6")–C(8")	101.5(4)
C(5")–S(7")–C(9")	101.4(4)	C(6")–S(8")–C(10")	102.2(4)
S(5")–C(7")–C(8")	115.8(6)	S(6")–C(8")–C(7")	113.0(6)
S(7")–C(9")–C(10")	118.4(6)	S(8")–C(10")–C(9")	117.7(6)

Table., **2.5.3.**

Torsion angles (˚) with e.s.d.'s in parentheses.

Molecule 1.

S(1)–C(1)–C(2)–S(3)	-5.7(10)	S(1)–C(1)–C(2)–S(4)	175.2(4)
S(2)–C(1)–C(2)–S(3)	176.8(4)	S(2)–C(1)–C(2)–S(4)	-2.3(10)
C(2)–C(1)–S(1)–C(3)	180.0(7)	S(1)–C(1)–S(1)–C(3)	-2.3(5)
C(2)–C(1)–S(2)–C(4)	-179.4(7)	S(1)–C(1)–S(2)–C(4)	2.8(5)
C(1)–C(2)–S(3)–C(5)	-173.8(7)	S(4)–C(2)–S(3)–C(5)	5.4(5)
C(1)–C(2)–S(4)–C(6)	172.7(7)	S(3)–C(2)–S(4)–C(6)	-6.5(5)
C(1)–S(1)–C(3)–C(4)	0.5(7)	C(1)–S(1)–C(3)–S(5)	177.4(4)
C(1)–S(2)–C(4)–C(3)	-2.6(7)	C(1)–S(2)–C(4)–S(6)	177.6(5)
C(2)–S(3)–C(5)–C(6)	-1.6(7)	C(2)–S(3)–C(5)–S(7)	177.5(4)
C(2)–S(4)–C(6)–C(5)	5.5(6)	C(2)–S(4)–C(6)–S(8)	-176.4(4)
S(1)–C(3)–C(4)–S(2)	1.4(9)	S(1)–C(3)–C(4)–S(6)	-178.8(5)
S(5)–C(3)–C(4)–S(2)	-174.9(5)	S(5)–C(3)–C(4)–S(6)	5.0(12)
S(1)–C(3)–S(5)–C(7)	178.7(4)	C(4)–C(3)–S(5)–C(7)	-5.0(9)
S(2)–C(4)–S(6)–C(8)	153.5(5)	C(3)–C(4)–S(6)–C(8)	-26.3(8)
S(3)–C(5)–C(6)–S(4)	-2.7(8)	S(3)–C(5)–C(6)–S(8)	179.6(4)
S(7)–C(5)–C(6)–S(4)	178.3(4)	S(7)–C(5)–C(6)–S(8)	0.5(11)
S(3)–C(5)–S(7)–C(9)	-163.8(4)	C(6)–C(5)–S(7)–C(9)	15.2(8)
S(4)–C(6)–S(8)–C(10)	-168.1(4)	C(5)–C(6)–S(8)–C(10)	9.7(8)
C(3)–S(5)–C(7)–C(8)	35.2(7)	C(4)–S(6)–C(8)–C(7)	56.1(7)
C(5)–S(7)–C(9)–C(10)	-49.2(7)	C(6)–S(8)–C(10)–C(9)	-43.3(6)
S(5)–C(7)–C(8)–S(6)	-65.9(7)	S(7)–C(9)–C(10)–S(8)	68.2(7)

Molecule 2.

S(1')–C(1')–C(2')–S(3')	2.3(9)	S(1')–C(1')–C(2')–S(4')	-179.1(4)
S(2')–C(1')–C(2')–S(3')	-177.8(4)	S(2')–C(1')–C(2')–S(4')	0.8(9)
C(2')–C(1')–S(1')–C(3')	-175.7(6)	S(1')–C(1')–S(1')–C(3')	4.4(5)
C(2')–C(1')–S(2')–C(4')	176.0(6)	S(1')–C(1')–S(2')–C(4')	-4.1(5)
C(1')–C(2')–S(3')–C(5')	178.0(6)	S(4')–C(2')–S(3')–C(5')	-0.7(5)
C(1')–C(2')–S(4')–C(6')	-178.8(6)	S(3')–C(2')–S(4')–C(6')	0.0(5)
C(1')–S(1')–C(3')–C(4')	-3.0(6)	C(1')–S(1')–C(3')–S(5')	178.8(4)
C(1')–S(2')–C(4')–C(3')	2.1(6)	C(1')–S(2')–C(4')–S(6')	-177.7(5)
C(2')–S(3')–C(5')–C(6')	1.5(7)	C(2')–S(3')–C(5')–S(7')	-179.5(4)
C(2')–S(4')–C(6')–C(5')	1.1(7)	C(2')–S(4')–C(6')–S(8')	-179.3(4)
S(1')–C(3')–C(4')–S(2')	0.6(8)	S(1')–C(3')–C(4')–S(6')	-179.6(4)
S(5')–C(3')–C(4')–S(2')	178.5(4)	S(5')–C(3')–C(4')–S(6')	-1.7(11)
S(1')–C(3')–S(5')–C(7')	-171.3(5)	C(4')–C(3')–S(5')–C(7')	10.8(8)
S(2')–C(4')–S(6')–C(8')	-167.2(5)	C(3')–C(4')–S(6')–C(8')	13.0(8)
S(3')–C(5')–C(6')–S(4')	-1.9(8)	S(3')–C(5')–C(6')–S(8')	178.6(5)
S(7')–C(5')–C(6')–S(4')	179.3(5)	S(7')–C(5')–C(6')–S(8')	-0.2(11)
S(3')–C(5')–S(7')–C(9')	-167.9(5)	C(6')–C(5')–S(7')–C(9')	10.9(9)
S(4')–C(6')–S(8')–C(10')	-172.9(5)	C(5')–C(6')–S(8')–C(10')	6.6(9)
C(3')–S(5')–C(7')–C(8')	-39.8(8)	C(4')–S(6')–C(8')–C(7')	-43.9(8)
C(5')–S(7')–C(9')–C(10')	-36.8(12)	C(6')–S(8')–C(10')–C(9')	-33.5(11)
S(5')–C(7')–C(8')–S(6')	62.7(10)	S(7')–C(9')–C(10')–S(8')	53.2(15)

Molecule 3.

S(1")–C(1")–C(2")–S(3")	-2.9(10)	S(1")–C(1")–C(2")–S(4")	178.4(4)
S(2")–C(1")–C(2")–S(3")	176.4(4)	S(2")–C(1")–C(2")–S(4")	-2.2(9)
C(2")–C(1")–S(1")–C(3")	-179.0(7)	S(1")–C(1")–S(1")–C(3")	1.6(5)
C(2")–C(1")–S(2")–C(4")	-179.8(6)	S(1")–C(1")–S(2")–C(4")	-0.3(5)
C(1")–C(2")–S(3")–C(5")	-174.7(7)	S(4")–C(2")–S(3")–C(5")	4.1(5)
C(1")–C(2")–S(4")–C(6")	173.8(6)	S(3")–C(2")–S(4")–C(6")	-5.0(5)
C(1")–S(1")–C(3")–C(4")	-2.9(7)	C(1")–S(1")–C(3")–S(5")	178.4(4)
C(1")–S(2")–C(4")–C(3")	-1.6(7)	C(1")–S(2")–C(4")–S(6")	179.0(4)
C(2")–S(3")–C(5")–C(6")	-1.2(6)	C(2")–S(3")–C(5")–S(7")	178.0(4)
C(2")–S(4")–C(6")–C(5")	4.3(6)	C(2")–S(4")–C(6")–S(8")	-175.7(4)
S(1")–C(3")–C(4")–S(2")	3.1(8)	S(1")–C(3")–C(4")–S(6")	-177.6(6)
S(5")–C(3")–C(4")–S(2")	-178.3(4)	S(5")–C(3")–C(4")–S(6")	0.9(11)
S(1")–C(3")–S(5")–C(7")	167.8(4)	C(4")–C(3")–S(5")–C(7")	-10.8(8)
S(2")–C(4")–S(6")–C(8")	162.9(5)	C(3")–C(4")–S(6")–C(8")	-16.4(8)
S(3")–C(5")–C(6")–S(4")	-2.1(8)	S(3")–C(5")–C(6")–S(8")	177.8(4)
S(7")–C(5")–C(6")–S(4")	178.8(4)	S(7")–C(5")–C(6")–S(8")	-1.3(11)
S(3")–C(5")–S(7")–C(9")	-163.2(5)	C(6")–C(5")–S(7")–C(9")	15.9(8)
S(4")–C(6")–S(8")–C(10")	-172.5(4)	C(5")–C(6")–S(8")–C(10")	7.6(8)
C(3")–S(5")–C(7")–C(8")	45.3(7)	C(4")–S(6")–C(8")–C(7")	49.0(7)
C(5")–S(7")–C(9")–C(10")	-45.8(9)	C(6")–S(8")–C(10")–C(9")	-37.0(8)
S(5")–C(7")–C(8")–S(6")	-69.3(8)	S(7")–C(9")–C(10")–S(8")	61.4(10)

Table., **2.5.4.**

Bond lengths (Å) with e.s.d.'s in parentheses

Au–Br(1)	2.482(1)	Au–Br(2)	2.476(1)
Au–Br(1a)	2.482(1)	Au–Br(2a)	2.476(1)

Molecule 1

C(1)–S(1)	1.755(9)	C(1)–S(2)	1.750(10)
C(1)–C(2)	1.327(12)	S(1)–C(3)	1.747(9)
S(2)–C(4)	1.737(8)	C(3)–C(4)	1.319(14)
C(3)–S(5)	1.757(9)	C(4)–S(6)	1.753(9)
S(5)–C(7)	1.805(10)	S(6)–C(8)	1.811(10)
C(7)–C(8)	1.451(15)	C(2)–S(3)	1.740(9)
C(2)–S(4)	1.741(9)	S(3)–C(5)	1.748(9)
S(4)–C(6)	1.750(8)	C(5)–C(6)	1.335(14)
C(5)–S(7)	1.734(10)	C(6)–S(8)	1.766(8)
S(7)–C(9)	1.770(10)	S(8)–C(10)	1.807(10)
C(9)–C(10)	1.477(16)		

Molecule 2

C(1')–S(1')	1.734(10)	C(1')–S(2')	1.727(10)
C(1')–C(1'a)	1.370(18)	S(1')–C(3')	1.747(9)
S(2')–C(4')	1.750(8)	C(3')–C(4')	1.331(14)
C(3')–S(5')	1.745(9)	C(4')–S(6')	1.747(9)
S(5')–C(7')	1.815(11)	S(6')–C(8')	1.788(9)
C(7')–C(8')	1.536(15)		

Table., **2.5.5.**

Bond Angles (°) with e.s.d.'s in parentheses

Br(1)–Au–Br(2)	89.6	Br(1)–Au–Br(1a)	180.0
Br(2)–Au–Br(1a)	90.4	Br(1)–Au–Br(2a)	90.4
Br(2)–Au–Br(2a)	180.0	Br(1a)–Au–Br(2a)	89.6

Molecule 1

S(1)–C(1)–S(2)	113.6(5)	S(1)–C(1)–C(2)	122.1(7)
S(2)–C(1)–C(2)	124.3(7)	C(1)–S(1)–C(3)	95.6(4)
C(1)–S(2)–C(4)	95.5(4)	S(1)–C(3)–C(4)	117.0(6)
S(1)–C(3)–S(5)	113.1(5)	C(4)–C(3)–S(5)	129.9(7)
S(2)–C(4)–C(3)	118.2(6)	S(2)–C(4)–S(6)	114.5(6)
C(3)–C(4)–S(6)	127.3(6)	C(3)–S(5)–C(7)	101.3(4)
C(4)–S(6)–C(8)	100.1(5)	S(5)–C(7)–C(8)	115.0(7)
S(6)–C(8)–C(7)	114.6(7)	C(1)–C(2)–S(3)	121.6(7)
C(1)–C(2)–S(4)	123.8(7)	S(3)–C(2)–S(4)	114.6(5)
C(2)–S(3)–C(5)	95.9(4)	C(2)–S(4)–C(6)	95.1(4)
S(3)–C(5)–C(6)	116.3(7)	S(3)–C(5)–S(7)	114.4(5)
C(6)–C(5)–S(7)	129.2(7)	S(4)–C(6)–C(5)	117.9(6)
S(4)–C(6)–S(8)	114.6(5)	C(5)–C(6)–S(8)	127.5(7)
C(5)–S(7)–C(9)	100.7(5)	C(6)–S(8)–C(10)	100.7(4)
S(7)–C(9)–C(10)	113.8(8)	S(8)–C(10)–C(9)	114.4(7)

Molecule 2.

S(1')–C(1')–S(2')	115.3(5)	S(1')–C(1')–C(1'a)	121.3(10)
S(2')–C(1')–C(1'a)	123.4(10)	C(1')–S(1')–C(3')	95.1(5)
C(1')–S(2')–C(4')	95.4(4)	S(1')–C(3')–C(4')	117.4(6)
S(1')–C(3')–S(5')	113.8(6)	C(4')–C(3')–S(5')	128.8(7)
S(2')–C(4')–C(3')	116.8(6)	S(2')–C(4')–S(6')	114.3(5)
C(3')–C(4')–S(6')	128.9(6)	C(3')–S(5')–C(7')	101.1(5)
C(4')–S(6')–C(8')	100.9(4)	S(5')–C(7')–C(8')	113.1(7)
S(6')–C(8')–C(7')	112.6(6)		

Table., **2.5.6.**

Torsion angles (°) with e.s.d.'s in parentheses.

Molecule 1.

S(2)–C(1)–S(1)–C(3)	1.7(6)	C(2)–C(1)–S(1)–C(3)	-177.7(9)
S(1)–C(1)–S(2)–C(4)	-1.0(6)	C(2)–C(1)–S(2)–C(4)	178.3(9)
S(1)–C(1)–C(2)–S(3)	-2.1(13)	S(1)–C(1)–C(2)–S(4)	179.2(6)
S(2)–C(1)–C(2)–S(3)	178.6(6)	S(2)–C(1)–C(2)–S(4)	-0.1(13)
C(1)–S(1)–C(3)–C(4)	-2.1(9)	C(1)–S(1)–C(3)–S(5)	179.6(6)
C(1)–S(2)–C(4)–C(3)	-0.4(9)	C(1)–S(2)–C(4)–S(6)	-179.8(6)
S(1)–C(3)–C(4)–S(2)	1.7(11)	S(1)–C(3)–C(4)–S(6)	-179.0(6)
S(5)–C(3)–C(4)–S(2)	179.7(6)	S(5)–C(3)–C(4)–S(6)	-1.0(15)
S(1)–C(3)–S(5)–C(7)	-173.8(6)	C(4)–C(3)–S(5)–C(7)	8.1(11)
S(2)–C(4)–S(6)–C(8)	-162.5(6)	C(3)–C(4)–S(6)–C(8)	18.2(10)
C(3)–S(5)–C(7)–C(8)	-42.1(9)	C(4)–S(6)–C(8)–C(7)	-52.2(8)
S(5)–C(7)–C(8)–S(6)	69.4(9)	C(1)–C(2)–S(3)–C(5)	176.5(9)
S(4)–C(2)–S(3)–C(5)	-4.6(6)	C(1)–C(2)–S(4)–S(6)	-176.0(9)
S(3)–C(2)–S(4)–C(6)	5.2(6)	C(2)–S(3)–C(5)–C(6)	2.0(9)
C(2)–S(3)–C(5)–S(7)	-175.9(6)	C(2)–S(4)–C(6)–C(5)	-4.0(9)
C(2)–S(4)–C(6)–S(8)	175.5(5)	S(3)–C(5)–C(6)–S(4)	1.4(11)
S(3)–C(5)–C(6)–S(8)	-178.1(6)	S(7)–C(5)–C(6)–S(4)	178.9(6)
S(7)–C(5)–C(6)–S(8)	-0.6(15)	S(3)–C(5)–S(7)–C(9)	161.9(6)
C(6)–C(5)–S(7)–C(9)	-15.7(11)	S(4)–C(6)–S(8)–C(10)	170.3(6)
C(5)–C(6)–S(8)–C(10)	-10.2(10)	C(5)–S(7)–C(9)–C(10)	51.0(8)
C(6)–S(8)–C(10)–C(9)	45.6(8)	S(7)–C(9)–C(10)–S(8)	-71.9(8)

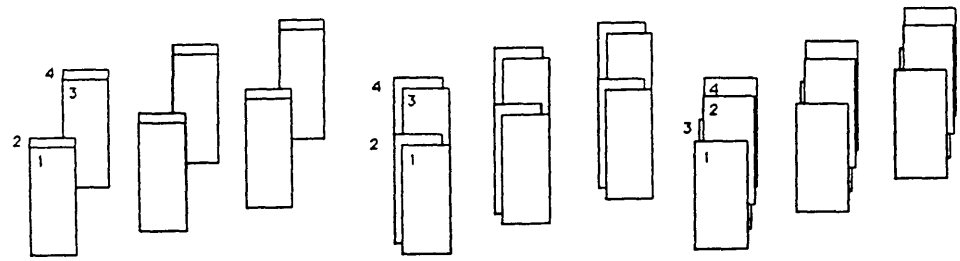
Molecule 2.

S(2')–C(1')–S(1')–C(3')	-3.0(7)	C(1a')–C(1')–S(1')–C(3')	176.4(12)
S(1')–C(1')–S(2')–C(4')	2.7(7)	C(1a')–C(1')–S(2')–C(4')	-176.7(13)
C(1')–S(1')–C(3')–C(4')	2.1(9)	C(1')–S(1')–C(3')–S(5')	-179.4(6)
C(1')–S(2')–C(4')–C(3')	-1.3(9)	C(1')–S(2')–C(4')–S(6')	179.5(6)
S(1')–C(3')–C(4')–S(2')	-0.6(11)	S(1')–C(3')–C(4')–S(6')	178.5(6)
S(5')–C(3')–C(4')–S(2')	-178.8(6)	S(5')–C(3')–C(4')–S(6')	0.3(15)
S(1')–C(3')–S(5')–C(7')	169.6(6)	C(4')–C(3')–S(5')–C(7')	-12.2(11)
S(2')–C(4')–S(6')–C(8')	163.1(5)	C(3')–C(4')–S(6')–C(8')	-16.0(11)
C(3')–S(5')–C(7')–C(8')	46.9(8)	C(4')–S(6')–C(8')–C(7')	50.5(8)
S(5')–C(7')–C(8')–S(6')	-71.8(9)		

2.5.5. Discussion

The structure of $[ET]AuCl_4AuCl_2$[24] comprises of donor–$AuCl_2$ networks which are separated from each other by the $AuCl_4^-$ sheets. While the structure of $[ET]_2AuBr_4AuBr_2$ or $[ET]_2AuBr_4$ would provide a more useful comparison (but as yet unpublished), it is interesting to note the alternation of Au–Cl bond lengths in relation to the oxidation state of the gold atom[24]. In β'–$[ET]_2Au(I)Cl_2$[180], the distance is 2.271Å, and for $[ET]Au(II)Cl_2$, 2.30Å (out–of–sheet) and 2.25Å (in–sheet). The salt of stoichiometry 1:1:1, has values of 2.269Å for $AuCl_2$ and 2.284Å for $AuCl_4^-$ which suggests that the existence of $HAuCl_2$ cannot be excluded. The structure of $[ET]AuCl_4AuCl_2$ comprises of slipped, tilted stacks which was found to preclude close interstack S···S interactions (closest: 3.773Å involving only the outer sulphurs of the ET molecules).

A comparison of the various types of packing motifs has been made for salts of the type β–$[ET]_2X$ and β–$[ET]_2AuCl_4$[23]. By considering the ET molecule as planar, the packing array of sheets can be visualised, as shown in *fig.*, **2.5.11.**, where each rectangle represents an ET molecule viewed perpendicular to the π–framework of the ET molecule. The β–$[ET]_2X$ salts can be divided into Type I (quasi–1D metals; $X^- = ICl_2$, BrICl) and Type II (superconductors; $X^- = I_3$, AuI_2, IBr_2) salts in which the intra– and interstack packing motifs are b and L–modes and a and L–modes respectively; Type III salts refer to β–$[ET]_2X$ salts ($X^- = AuCl_4^-$). While $[ET]_3AuBr_4$ possesses three donor molecules per repeat distance and is not strictly comparable to the β–type salts, the type I salts can be regarded as strongly dimerized along the stacking direction, whereas the stacking is more uniform in the type II and III salts.



Type I Type II Type III

fig., **2.5.11.** Packing arrangements in β–$[ET]_2X$ and β–$[ET]_2AuCl_4$ salts

Most planar anions have yielded ET–salts of stoichiometry different from 2:1, with the exception of $[ET]_2C(CN)_3$[37], which contains the trigonal planar tricyanomethanide anion. Recently the crystal structures for β–$[ET]_2AuCl_4$ and $[ET]_2Au(CN)_2Cl_2$ have been reported[23]. Both salts were obtained as lustrous blocks, in the case of the former, and as square–like plates in the latter, from thf. The crystal packing in β–$[ET]_2AuCl_4$ consists of ET donor layers in the ab–plane, separated by the layers of $AuCl_4^-$ anions along the c direction. The plane of each anion is not parallel to the ab–plane but inclined with a dihedral angle of 35.1°. Therefore the donor sheets are more separated in β–$[ET]_2AuCl_4$ than in β–$[ET]_2X$ salts with linear triatomic anions.

The crystal structure, semiconducting properties ($\sigma_{rt} \sim 0.05$ Scm^{-1}, $E_a \simeq 180meV$) and temperature dependent esr parameters for $[ET]_2Au(CN)_2Cl_2$ were found to be very similar to $[ET]_2QF_6$ (Q = Sb, As); all undergo a broad phase transition near or slightly below room temperature[23].

Recently the tetrahedral anionic complexes $[ET]_2FeCl_4$ and $[ET]FeBr_4$ have been reported[36]. While the former was found to be a semiconductor ($\sigma_{rt} \sim 10^{-2}$ Scm^{-1}, E_a 210meV), the latter was a poor semiconductor ($\sigma_{rt} \sim 10^{-6}$ Scm^{-1}). The chloro complex consisted of

dimerized stacks of ET molecules separated by sheets of tetrahedral $FeCl_4^-$ anions, with the shortest intermolecular S···S distances being in the range 3.42–3.52Å; the α and β forms of $[ET]_2[PF_6]$ have nearly identical interstack interactions. This contrasts with the corrugated sheet network of $[ET]_2[ReO_4]$[20] and $[ET]_2[BrO_4]$[19].

The absence of stacks and planes of closely spaced ET molecules and coulombic repulsion between relatively large charges in the $FeBr_4^{2-}$ salt may explain the low conductivity. Intradimer overlap is of the a type, while the anion has short intermolecular contacts to 2 ET molecules but is isolated from any other short interactions.

Of interest, is the comparison which can be made with $[ET]_3NiCl_4.H_2O$ and the crystalline salts obtained from electrocrystallisation of ET and $[Ph_4As]_2[MCl_4]$ (M= Ni, Co). Tetrachloro–nickelate (II) salts are known only to exist in the tetrahedral geometry. Since $[ET]_3NiCl_4.H_2O$ was obtained by chance, possibly due to chlorine abstraction from 1,1,2–tce, the formation of the $NiCl_4^{2-}$ ion and it's geometry may be determined by the interaction of the donor molecules and short donor H···Cl contacts, which are known to exist. Hence the unusual (distorted) tetrahedral geometry of $NiCl_4^{2-}$ allows important interactions to occur, which is reflected in the electrical properties; metallic behaviour is observed to reasonably low temperatures (120K) with moderate conductivity at room temperature (σ_{rt}= 20 Scm^{-1}). Another unusual feature, but not totally uncommon, is the incorporation of a water molecule in the structure (c.f., κ–$[ET]_2Ag(CN)_2.H_2O$[34]; metallic to 150K); though the role of the water molecule cannot be distinguished with regard to the molecular structure, it may represent an important structural or electronic modification.

A comparison with the salt obtained from $[Ph_4As]_2NiCl_4$ and ET in

benzonitrile indicates that the latter is likely to contain $NiCl_4^{2-}$ in the more typical tetrahedral geometry. While crystals were of insufficient quality for X-Ray analysis, conductivity measurements show the compound to be of poor metallic nature with a transition to a semiconducting state at approximately 140K. Conductivity measurements on ET/$CoCl_4$, are as yet, undetermined.

$Hg(CN)_2Br$/ET salts

The enhancement of the superconducting transition temperature T_c is correlated with "soft" C–H···X contacts found in large anions containing terminal halide ligands[66]. The iodine atom is the largest and most polarisable halogen atom and it's bonds with late–period main group metals are among the largest covalent bonds known. Soft C–H···X anion contacts are expected from a large, polarisable anion, but such an anion may prevent the formation of a 2:1 salt. Thus a balance of polarisability and size appears to be crucial in obtaining a 2:1 salt with soft C–H···anion contacts.

Suitable candidates were considered to be the potassium/sodium salts of $Hg(CN)_2X^-$ (X^-: Cl, Br, I), which contain 2D polymeric networks necessary for the formation of a 3D metal. The presence of the complex–forming diamagnetic metal ion mercury, in conjunction with the bridging anion ligand CN^- (as linear $Hg(CN)_2$ molecules) and the polarisable halide X represents the desired features for electrocrystallisation with organic donors. Electrocrystallisation of K[$Hg(CN)_2Br$]/ 18–crown–6 with ET yields very thin, brown coloured diamond shaped platelets, similar in shape to that obtained for [ET]Ag_4CN_5. Long needle shaped crystals grew on the anode after 1 month.

Elemental analysis as well as the absorption spectra revealed that

the cyanide ligands were no longer bonded to mercury, and that the salt was likely to be an ET–polymeric mercury bromide species.

Since the discovery of the superconductor κ–$[ET]_4Hg_{3-x}Br_8$[49,71], other ET–Hg–Br phases have been identified during the electrocrystallisation of ET, Bu_4NBr and $HgBr_2$ in tce[181], including $[ET]HgBr_3$[120], ι–$[ET]_3[HgBr_3]_2$[182], $[ET]_5Hg_3Br_{11} \equiv [ET]_5[HgBr_4]_2[HgBr_3]$[120] and $[ET]_4Hg_2Br_6(tce)$[181].

$[ET]HgBr_3$ behaves as a semiconductor ($\sigma_{rt}\sim 1.7\times10^{-4}$ Scm^{-1}, $E_a=$ 300meV) while $[ET]_5Hg_3Br_{11}$ shows metallic behaviour ($\sigma_{rt}\sim 50$ Scm^{-1}) with a metal to semiconductor transition at 100K. The structure of ι–$[ET]_3[HgBr_3]_2$ ($\sigma_{rt}\sim 9$ Scm^{-1}; $E_a=$ 9meV) is related to ι–$[ET]_2AuBr_2$[134] and ι–$[ET]_4[Mo_6Cl_8]Cl_6(thf)$[21]. Thus the ET–Hg–Br system contains a wide variety of modifications depending on the crystal growth conditions.

The elemental analysis for the platelets indicated a high ET to $HgBr_x$ ratio (analyses as $[ET]_5HgBr_3$) and conductivity measurements on a compressed disc revealed semiconductor behavior ($\sigma_{rt}\sim 0.3$ Scm^{-1}, $E_a=$ 75meV) (*fig.*, 2.3.24. and 2.3.25.).

Crystallographic analysis (unit cell parameters) of the needles revealed the compound to be $[ET]_5Hg_3Br_{11}$, which has previously been obtained from $[Et_4N]_2HgBr_3$ and ET in benzonitrile[120]. The anion unit of the molecular structure comprises of a central planar triangular $HgBr_3^-$ and two nearly tetrahedral $HgBr_4^-$ which are weakly bonded to the central unit. The unit cell consists of 3 type "II" ET molecules (with charges close to +2, they are considered not to be related to the conduction process), 7 type "1" (which have an even charge distribution of +4/7) and two $Hg_3Br_{11}^{5-}$ units.

Further crystalline long plates of $[ET]_5Hg_3Br_{11}$ were obtained after two months. Obviously, there are a variety of ET–Hg–Br species,

which can be obtained over a period of time, depending on the bromine concentration.

An alternative strategy would be to electrocrystallise ET and $Hg(CN)_2$/KBr/18–crown–6 in benzonitrile, to discover if the cyanide ligands are labile in this system. It was a surprise to discover the loss of cyanide from mercury, since the Hg–C bond is expected to be stronger than Hg–halide bonds, if the heats of formation of gaseous $HgCl_2$, $HgBr_2$, HgI_2 and $Hg(CN)_2$ are considered[183]: Hg–CN > Hg–Cl > Hg–Br > Hg–I.

Similarly, the formation constant for $Hg(CN)_2$ in aqueous solution is high.

Similar linear chain systems which should be investigated, include $Hg(CN)_2.Ag(NO_3).2H_2O$ (–Ag–NC–Hg–CN–Ag–) and $Hg(CN)(NO_3)$[184].

Very little has been studied on the combination of two successful principles in the solid state, ie., the properties of the "inorganic" 1D molecular metals of interest because of their potential to form 1D interacting transition metal ion chains and the often pronounced 2D properties of metallic, organic solids containing radical cations such as ET^+. The crystal structures of these two types of compounds contain linear segregated mixed valence stacks of planar organic radical cations and planar platinum complexes[124].

The mixed valence systems $[D_x]^{2+}[A]^{2-}$ with D = TTF, TMTTF, TMTSF, ET and A = $M(CN)_4$; M = Ni or Pt have been recently synthesized with conductivities ($\sigma\sim$ 0.1–10 Scm^{-1}) at room temperature. $[TMTT(S)F]_3[M(CN)_4]$ molecules are present in stacks of parallel centrosymmetric trimers with an irregular stacking mode indicated by short intra–trimer Se···Se contacts (3.66–3.78Å) (shorter than observed in $[TMTSF]_2X$), while inter–trimer Se···Se contacts are

longer than the corresponding 4Å Van der Waal's radii. The three donor molecules are almost identical with a formal charge of +2/3e. $[ET]_4[M(CN)_4]$ has donor molecules arranged as sheets of tetramers in a given plane leading to a 2D network. Intrastack S···S contacts are greater than the corresponding 3.8Å Van der Waals separations, while the interstack S···S contacts are less than 3.8Å. The sheet–like network packing and formal charge of +0.5e on each ET molecule is similar to those observed in ET salts with monoanions.

Common structural features are: (i) bond lengths in the $Pt(CN)_4$ unit agree well with those observed in $K_2Pt(CN)_4.3H_2O$, (ii) the Pt atoms are fully oxidised indicated by the fact that they are not stacked and (iii) the $Pt(CN)_4^{2-}$ dianions form a dihedral angle of ~70° with the organic radical cation.

In the $[TTF]_5[Pt(CN)_5].2MeCN$ salt, TTF molecules are organised in centrosymmetric isolated pentamers in two perpendicular directions with strong S···S interactions (3.32–3.61Å). The isolated $Pt(CN)_4^{2-}$ anions are separated by disordered acetonitrile molecules and together with varying charges on the TTF molecules, the material behaves as an insulator.

This summary reveals that compounds of the type $[D_x]^{2+}[A]^{2-}$ with D= ET, HMTTeF and TTF and A= $Pt(mnt)(CN)_2$ resemble their donor:tetracyanoplatinate counterparts with similar stoichiometries and electrical properties. While the crystal structure of $[ET]_4[Pt(mnt)(CN)_2]$ could not be determined due to poor crystal quality, it is probably similar to $[ET]_4[Pt(CN)_4]$. The conduction process in these compounds arises largely via the interstack interactions of the donor molecules; hence the room temperature conductivity (σ_{rt}~ 10^{-1} Scm^{-1}) is of comparable magnitude (the Pt atoms in $Pt(CN)_4^{2-}$ are fully oxidised). The crystal structure of $[ET][Ni(mnt)_2]$ revealed

that there are no sulphur–sulphur contacts between the donor and acceptor molecules. There are significant S···S intermolecular contacts (3.524 and 3.528Å) between ET cations and S–S distances of 3.70Å between $[Ni(mnt)_2]$ ions.

In comparison, $[ET]_4[Pt(C_2O_4)_2]$[187] was found to be a metal (σ_{rt} ~ 20 Scm^{-1}) with a metal–metal phase transition at 200K and a second broad phase transition to a semiconducting state at 60K. The structure contains sheets of ET cations separated by sheets of $Pt(C_2O_4)_2^{2-}$ counterions with short intermolecular S···S contacts observed between the donor molecules.

Concluding Remarks

Further advancement in the value of the superconducting transition temperature may be achieved, in principle, by considering donor salts of the fully substituted–oxo derivative of ET. The electron–phonon mechanism for superconductivity predicts that an increase in T_c may be attained by a diminishment of the molecular mass or increase of the electron–phonon coupling matrix constant (2.1.1.) The synthesis of the donor constituent is dependent on the flexibility of organic chemistry. Early attempts to couple the 2–thiomethoxy–1,3–dioxolium cation has only led to an intractable material[188]. An alternative strategy would be treatment of the 1,3–dioxolium cation with triphenylphosphine which leads to the phosphonium salt; deprotonation with butyllithium at -78°c and coupling with another cation would yield the precursor. Treatment with triethylamine could afford the oxo–derivative of TTF.

A variety of donor salts have been decribed within, most notably $[ET]_3NiCl_4.H_2O$, which contains an unusual distorted (from tetrahedral geometry) $NiCl_4^{2-}$ ion. The processes by which these salts are formed is not understood and deserves further investigation. Variation of the solvent is one of the major factors which governs the formation of crystals of donor salts.

Current interest has centred upon ET salts with polymeric metal halide (pseudohalide) species, as a result of the highest T_c value observed to date for κ–$[ET]_2Cu[N(CN)_2]Br$ (12.5K, 0.3kbar). There are undoubtedly further advances to be made in this field of study.

2.6.1. Appendix 1

e	*b/a*	
0	1.333	ET^0
+1/2	1.289	β–$[ET]_2I_3$, α–$[ET]_2IBr_2$
+1/2	1.279	β–$[ET]_2PF_6$
+1/2	1.270	α–$[ET]_2I_3$, $[ET]_2ReO_4$, $[ET]_2BrO_4$, β–$[ET]_2IBr_2$
+1/2	1.261	$[ET]_2[BrO_4]$.1/2tce
+2/3	1.263	γ–$[ET]_3[ClO_4]_2$
+2/3	1.259	γ–$[ET]_3[BrO_4]_2$
+1	1.246	$[ET]FeBr_4$, $[ET][ReO_4]$.1/2thf
+1	1.235	$[ET][Ni(mnt)_2]$

2.7.1. References

1. D S Acker, R J Harder, W R Hertler, W Mahler, L R Melby, R E Benson and W E Mochel, J.Am.Chem.Soc., 1960, 82, 6408

2. F Wudl, G M Smith, E J Hufnagel, J.Chem.Soc.,Chem.Commun., 1970, 1453

3. J Ferraris, D O Cowan, V W Walatka Jr., and J H Perlstein, J.Am.Chem.Soc., 1973, 95, 948

4. L B Coleman, M J Cohen, D J Sandman, F G Yamagishi, A F Garito and A J Heeger, Solid.State.Commun., 1973, 12, 1125

5. D Jerome and H Schulz, Adv.Phys., 1982, 31, 299

6. L N Bulaevskii, "High Temperature Superconductivity", 1982, e.d., V L Ginzberg and D A Kirzhnits, New York.

7. E M Engler and V V Patel, J.Am.Chem.Soc., 1974, 96, 7376

8. A N Bloch, D O Cowan, K Bechgaard, R E Pyle, R H Banks and T O Poehler, Phys.Rev.Lett., 1975, 34, 1561

9. C S Jacobsen, K Mortensen, J R Andersen and K Bechgaard, Phys.Rev.B.Solid State., 1978, 18, 905

10. D Jerome, A Mazaud, M Ribault and K Bechgaard, J.Phy.Lett.(Les Ulis,Fr)., 1980, 41, L195

11. R Brusetti, M Ribault, D Jerome and K Bechgaard, J.Phys., 1982, 13, 801

12. K Bechgaard, K Carneiro, M Olsen, F B Rasmussen, C S Jacobsen, Phys.Rev.Lett., 1981, 46, 852

13. J M Williams, M A Beno, E H Appelman, F Wudl, E Aharon-Shalom and D Nalewajek, Mol.Cryst.Liq.Cryst., 1982, 79, 319

14. K Bechgaard, K Carneiro, M Olsen, G Rindorf, C S Jacobsen, H J Pedersen and J C Scott, J.Am.Chem.Soc., 1981, 46, 852

15. G Saito, T Enoki, K Toriumi and H Inokuchi, Solid.State.Commun., 1982, 42, 557

16. J M Williams, H H Wang, M A Beno, T J Emge, L M Sowa, P T Copps,

F Behroozi, L N Hall, K D Carlson and G W Crabtree, Inorg.Chem., 1984, 23, 3839

17. J M Williams, T J Emge, H H Wang, M A Beno, P T Copps, L N Hall, K D Carlson and G W Crabtree, Inorg.Chem., 1984, 23, 2558

18. S S P Parkin, E M Engler, R R Schumaker, R Lagier, V Y Lee, J C Scott and R L Greene, Phys.Rev.Lett., 1983, 50, 270

19. J M Williams, M A Beno, H H Wang, P E Reed, L J Azevedo, J E Schirber, Inorg.Chem., 1984, 23, 1790

20. J F Kwak, L J Azevedo, J E Schirber, J M Williams amd M A Beno, Mol.Cryst.Liq.Cryst., 1985, 125, 365

21. E Amberger, H Fuchs and K Polborn, Synth.Met., 1987, 19, 605

22. A Penicaud, C Lenoir, P Batail, C Coulon and A Perrin, Synth.Met., 1989, 32, 25

23. U Geiser, B A Anderson, A Murray, C M Pipan, C A Rohl, B A Vogt, H H Wang, J M Williams, D B Kang and M.–H Whangbo, Mol.Cryst.Liq.Cryst., 1990, 181, 105

24. T Mori and H Inokuchi, Chem.Lett., 1986, 2069

25. L C Porter, H H Wang, M A Beno, K D Carlson, C M Pipan, R B Proksch and J M Williams, Solid.State.Commun., 1987, 64, 387

26. H Kobayashi, A Kobayashi, Y Sasaki, G Saito, and H Inokuchi, Chem.Lett., 1983, 759

27. H Kobayashi, T Mori, R Kato, A Kobayashi, Y Sasaki, G Saito and H Inokuchi, Chem.Lett., 1983, 581

28. T Mori, A Kobayashi, Y Sasaki, R Kato, and H Kobayashi, Solid.State.Commun., 1985, 53, 627

29. J M Williams and K Carneiro, Adv.Inorg.Chem.Radiochem., 1985, 29, 249

30. M A Beno, G S Blackman, P C W Leung, K D Carlson, P T Copps, and J M Williams, Mol.Cryst.Liq.Cryst., 1985, 119, 409

31. A Kobayashi, A Kob, Y Sasaki, G Saito and H Inokuchi, Chem.Lett., 1984, 183

32. H Kob, R Kato, T Mori, A Kob, Y Sasaki, G Saito, T Enoki and H Inokuchi, Chem.Lett., 1984, 179

33. K Carneiro, J C Scott and E M Engler, Solid.State.Commun., 1984, 50, 477

34. S S P Parkin, E M Engler, V Y Lee and R R Schumaker, Mol.Cryst.Liq.Cryst., 1985, 119, 375

35. M A Beno, D D Cox, J M Williams and J F Kwak, Acta.Cryst., 1984, C40, 1334

36. T Mallah, C Hollis, S Bott, M Kurmoo, P Day, M Allan and R H Friend, J.Chem.Soc.Dalton Trans., 1990, 859

37. M A Beno, H H Wang, L Soderholm, K D Carlson, L N Hall, L Nuñez, H Rummens, B Anderson, J A Schlueter, J M Williams, M.-H. Whangbo and M Evain, Inorg.Chem., 1989, 28, 150

38. A Weber, H Endres, H J Keller, E Gogu, I Heinen, K Bender, D Schweitzer, Z.Naturforsch., 1985, 40B, 1658

39. U Geiser, H H Wang, L E Gerdom, M A Firestone, L M Sowa, J M Williams, J.Am.Chem.Soc., 1985, 107, 8305

40. U Geiser, H H Wang, K M Donega, B A Anderson, J M Williams, J F Kwak, Inorg.Chem., 1986, 25, 401

41. M Kurmoo, D R Talham, K L Pritchard, P Day, A M Stringer and J A K Howard, Synth.Met., 1988, 27, A177

42. U Geiser, M A Beno, A M Kini, H H Wang, A J Schultz, B D Gates, C S Cariss, K D Carlson, J M Williams, Synth.Met., 1988, 27, A235

43. U Geiser, H H Wang, P R Rust, L M Tonge, J M Williams, Mol.Cryst.Liq.Cryst., 1990, 181, 117

44. R P Shibaeva and R M Lobkovskaya, Kristallografiya., 1988, 33, 408; Sov.Phys.-Crystallogr.(Engl.Trans)., 1988, 33, 241

45. A M Kini, U Geiser, H H Wang, K D Carlson, J M Williams, W K

Kwok, K G Vandervoort, J E Thompson, D L Stupka, D Jung, M.–H Whangbo, Inorg.Chem., 1990, 29, 2557

46. J M Williams, A M Kini, H H Wang, K D Carlson, U Geiser, L K Montgomery, G J Pyrka, D M Watkins, J M Kommers, S J Boryschuk, A V S Crouch, W K Kwok, J E Schirber, D L Overmyer, D Jung, M.–H Whangbo, Inorg.Chem., 1990, 29, 3274

47. U Geiser, H H Wang, S Kleinjan, S M Budz, J M Williams and M.–H Whangbo: to be published

48. U Geiser, H H Wang, S M Budz, M J Lowry, J M Williams, J Ren and M.–H Whangbo, Inorg.Chem., 1990, 29, 1611

49. R N Lyubovskaya, E I Zhilyaeva, S I Pesotskii, R B Lyubovskii, L O Atovmyan, O A Dyachenko and T G Takhirov, JETP.Lett., 1988, 46, 188

50. R P Sibaeva and L P Rozenberg, Sov.Phys.Crystallogr., 1988, 33, 834

51. J M Williams, H H Wang, T J Emge, U Geiser, M A Beno, K D Carlson, R J Thorn, A J Schultz and M.–H Whangbo, Prog.Inorg.Chem., 1987, 35, 51

52.H Urayama, H Yamochi, G Saito, K Nozawa, T Sugano, M Kinoshita, S Sato, K Oshima, A Kawamoto and J Tanaka, Chem.Lett., 1988, 55

53. K D Carlson, U Geiser, A M Kini, H H Wang, L K Montgomery, W K Kwok, M A Beno, J M Williams, C S Cariss, G W Crabtree, M.–H Whangbo and M Evain, Inorg.Chem., 1988, 27, 965

54. S Gärtner, E Gogu, I Heinen, H J Keller, T Klutz and D Schweitzer, Solid.State.Commun., 1988, 65, 1531

55. I D Parker, R H Friend, M Kurmoo, P Day, C Lenoir and P Batail, J.Phys.Condens.Matter., 1989, 27, 4479

56. A Kobayashi, R Kato, H Kobayashi, S Moriyama, Y Nishio, K Kajita and W Sasaki, Chem.Lett., 1987, 459, 507

57. G C Papavassiliou, G A Mousdis, J S Zambounis, A Terzis, A Hounkas, B Hilti, C W Mayer and J Pfeiffer, Synth.Met., 1988, 27, B379

58. K Kikuchi, Y Honda, Y Ishikawa, K Saito, I Ikemoto, K Murata, Y Anzai, I Ishiguro and K Kobayashi, Solid.State.Commun., 1988, 66, 405

59. P J Nigrey, B Morosin, J F Kwak, E L Venturini and R J Baughman, Synth.Met., 1986, 16, 1

60. R P Shibaeva and L P Rozenberg, Kristallografiya., 1988, 33, 1402;

61. R N Lyubovskaya, R B Lyubovskii, R P Shibaeva, M Z Aldoshina, L M Goldenberg, L P Rozenberg, M L Khidekel, Y F Schulpyakov, Pis'ma.Zh.Eksp.Teor.Fiz., 1985, 42, 380; JETP.Lett., 1985, 46, 188

62. J M Williams, H H Wang, A M Kini, K D Carlson, M A Beno, U Geiser, M.–H Whangbo, D Jung, M Evain and J J Novoa, Mol.Cryst.Liq.Cryst., 1990, 181, 59

63. M.–H Whangbo, J M Williams, A J Schultz, T J Emge and M A Beno, J.Amer.Chem.Soc., 1987, 109, 90

64. J R Ferraro, H H Wang, J Ryan and J M Williams, Appl.Spectrosc., 1987, 41, 1377

65. W L McMillan, Phys.Rev., 1968, 167, 331

66. J R Ferraro and J M Williams, Mol.Cryst.Liq.Cryst., 1990, 181, 253

67. E G Yagubskii, I F Shchegolev, V N Laukhin, P A Kononovich, M V Kartsovnik, A V Zvarykina, L I Baravov, JETP Lett.Engl.Transl., 1984, 39, 12

68. M Tokumoto, H Bando, H Anzai, G Saito, K Murata, K Kajimura and T Ishiguro, J.Phys.Soc.Jpn., 1985, 54, 869

69. H H Wang, M A Beno, U G Geiser, M A Firestone, K S Webb, L Nuñez, G W Crabtree, K D Carlson, J M Williams, L J Azevedo, J F Kwak and J E Schirber, Inorg.Chem., 1985, 24, 2465

70. K D Carlson, G W Crabtree, L Nuñez, H H Wang, M A Beno, U Geiser, M A Firestone, K S Webb and J M Williams, Solid.State.Commun., 1986, 57, 89

71. E V Yagubskii, I F Shchegolev, R P Shibaeva, D N Fedutin, L P Rozenberg, E M Sogomonyan, R M Lobkovskaya, V N Laukhin, A A Ignat'ev, A V Zvarykina and L I Buravov, Zh.Eksp.Teor.Fiz.Pis'ma Red., 1985, 42, 167

72. R N Lyubovskaya, E I Zhilyaeva, S I Pesotskii, R B Lyubovskii, L O Atovmyan, O A Dyachenko and T G Takhirov, Pis'ma Zh.Exp.Teor.Fiz., 1987, 46, 149

73. R P Shibaeva, V F Kaminskii and E B Yagubskii, Mol.Cryst.Liq.Cryst., 1985, 119, 361

74. E B Yagubskii, I F Shchegolev, S I Pesotskii, V N Laukhin, P A Kononovich, M V Kartsovnik and A V Zvarykina, JETP Lett., 1984, 39, 328

75. K D Carlson, G W Crabtree, L N Hall, F Behroozi, P T Copps, L M Sowa, L Nuñez, M A Firestone, H H Wang, M A Beno, T J Emge and J M Williams, Mol.Cryst.Liq.Cryst., 1985, 125, 159

76. H Kobayashi, R Kato, A Kobayashi, Y Nishio, K Kajita, W Sasaki, Chem.Lett., 1986, 789

77. K Murata, M Tokumoto, H Anzai, H Bando, G Saito, K Kajimura, T Ishiguro, J.Phys.Soc.Jpn., 1985, 54, 1236

78. V N Laukin, E E Kostyuchenko, Y V Sushko, T F Shchegolev, E B Yagubskii, Pis'ma.Zh.Eksp.Teor.Fiz., 1985, 41, 68; JETP.Lett., 1985, 41, 81

79. T Mori and H Inokuchi, Solid.State.Commun., 1987, 64, 335

80. T Mori and H Inokuchi, Chem.Lett., 1987, 1657

81. M J Rosseinsky, M Kurmoo, D R Talham, P Day, D Chasseau, D Watkin, J.Chem.Soc.Chem Commun., 1988, 270

82. J Bardeen, L N Cooper and J R Schrieffer, Phys.Rev., 1957, 106, 162, 108, 1175

83. F Wudl, H Yamochi, T Suzuki, H Isotalo, C Fite, H Kasmai, K Lion and G Srdanov, J.Amer.Chem.Soc., 1990, 112, 2461

84. C M Varma, "Superconductivity in d– and f–band Metals", 1982, Karlsruhe, pg 603

85. M A Beno, H H Wang, K D Carlson, A M Kini, G M Frankenbach, J R Ferraro, N Larson, G D McCabe, J Thompson, C Purnama, M Vashon, J M Williams, D Jung and M.–H Whangbo, Mol.Cryst.Liq.Cryst., 1990, 181, 145

86. D Schweitzer, K Polychroniadis, T Klutz, H J Keller, I Hennig, I Heinen, U Haeberlen, E Gogu and S Gärtner, Synth.Met., 1989, 27, A465

87. C P Heidmann, K Andres and D Schweitzer, Physica.B., 1986, 143, 357

88. K Andres, H Schwenk and H Veith, Physica.B., 1986, 143, 334

89. M A Beno, H H Wang, A M Kini, K D Carlson, U Geiser, W K Kwok, J E Thompson, J M Williams, J Ren and M.–H Whangbo, Inorg.Chem., 1990, 29, 1599

90. J J Novoa, M.–H Whangbo and J M Williams, Mol.Cryst.Liq.Cryst., 1990, 181, 25

91. (a) A Bondi, J.Phys.Chem., 1964, 68, 441

(b) L Pauling, 'The Nature of the Chemical Bond', Cornell University Press, Ithaca, NY, 1960

92. T Mori, A Kobayashi, Y Sasaki, H Kobayashi, G Saito and H Inokuchi, Chem.Lett., 1984, 957

93. T Mori, A Kobayashi, Y Sasaki, H Kobayashi, G Saito and H Inokuchi, Bull.Chem.Soc.Jpn., 1984, 51, 627

94. J P Pouget, R Moret, R Comes, K Bechgaard, J M Fabre and L Giral, Mol.Cryst.Liq.Cryst., 1982, 79, 129

95. J P Pouget, G Shirane, K Bechgaard and J M Fabre, Phys.Rev.B Condens.Matter., 1983, 37, 5203

96. M A Beno, G S Blackman, P C W Leung and J M Williams, Solid.State.Commun., 1983, 48, 99

97. K Bender, I Hennig, D Schweitzer, K Dietz, H Endres and H J Keller, Mol.Cryst.Liq.Cryst., 1984, 108, 359

98. T J Emge, H H Wang, M A Beno, P C W Leung, M A Firestone, K S Webb, K D Carlson, J M Williams, E L Venturini, L J Azevedo and J E Schirber, Mol.Cryst.Liq.Cryst., 1986, 132, 363

99. T J Emge, H H Wang, P C W Leung, P R Rust, J D Cook, P L Jackson, K D Carlson, J M Williams, M.–H. Whangbo, E L Venturini, J E Schirber, L

J Azevedo and J R Ferraro, J.Am.Chem.Soc., 1986, 108, 695

100. T J Emge, H H Wang, M A Beno, P C W Leung, M A Firestone, H C Jenkins, J D Cook, K D Carlson, J M Williams, E L Venturini, L J Aze

101. G Saito, H Urayama, H Yamochi, K Oshima, Synth.Met., 1988, 27, A331

102. M Mizuno, A F Garito and M P Cava, J.Chem.Soc.Chem Commun., 1978, 18

103. S Wawzonek and S M Heilmann, J.Org.Chem., 1974, 39, 511

104. G Steimecke, H Sieler, R Kirmse and E Hoyer, Phos.and.Sulf., 1979, 7, 49

105. K S Varma, A Bury, N J Harris and A E Underhill, Synthesis., 1987, 9, 837

106. R Kato, A Kobayashi, Y Sasaki and H Kobayashi, Chem.Lett., 1984, 993

107. H Poleschner, W John, G Kempe, E Hoyer and E Fanghänel, Z.Chem., 1978, 18, 345

108. R R Schumaker and E M Engler, J.Am.Chem.Soc., 1977, 99, 5521

109. R R Schumaker, V Y Lee and E M Engler, J.Org.Chem., 1984, 49, 564

110. P Braunstein and R J H Clarke, J.Chem.Soc.Dalton Trans., 1973, 1845

111. R Uson, J Vicente and J Oro, Inorg.Chim.Acta., 1981, 52, 29

112. D M L Goodgame, M Goodgame and F A Cotton, J.Am.Chem.Soc., 1961, 83, 4160

113. F A Cotton, D M L Goodgame and M Goodgame, ibid., 1961, 83, 4690

114. A K Agrawal and R C Mehrota, Z.Anorg.Allgem.Chem., 1965, 336, 66

115. J P Fackler and D Coucouvanis, J.Am.Chem.Soc., 1966, 88, 3913

116. C M Harris, S E Livingstone and N C Stephenson, J.Chem.Soc, 1958, 3697

117. D M Adams, P J Chandler and R G Churchill, J.Chem.Soc A., 1967, 1272

118. L B Coleman, Rev.Sci.Instrum., 1975, 46, 1125

119. M A Beno, M A Firestone, P C W Leung, L M Sowa, H H Wang, J M Williams and M.–H Whangbo, Solid.State.Commun., 1986, 57, 735

120. M Kurmoo, D R Talham, P Day, J D Parker, R H Friend, A M Stringer, J A K Howard, Solid.State.Commun., 1987, 61, 459

121. T Mori, P Wang, K Imaeda, T Enoki and H Inokuchi, Solid.State.Commun., 1987, 64, 733

122. T Sugano, G Saito and M Kinoshita, Phys.Rev.B., 1986, 34, 117

123. A A Galimzyanov, A A Ignat'ev, N D Kushch, V N Laukin, M K Makova, V A Merzhanov, L P Rozenberg, R P Shibaeva and E B Yagubskii, Synth.Met., 1989, 33, 81

124. L Ouahab, J Padiou, D Grandjeau, C Garrigou–Lagrange, P Delhaes and M Bencharif, J.Chem.Soc.Chem Commun., 1989, 1038

125. A E Underhill, J S Tonge and P I Clemenson, Mol.Cryst.Liq.Cryst., 1985, 125, 439

126. M Gurvitch, Phys.Rev.Lett., 1986, 56, 647

127. D Ziman, "Electrons and Phonons", 1960, Oxford

128. I N Bulaevskii, Adv.Phys., 1988, 37, 443

129. K Bechgaard, C S Jacobsen, K Mortensen, J H Pedersen and N Thorup, Solid.State.Commun., 1980, 33, 1119

130. M Weger, M Kaveh and H Gutfreund, Solid.State.Commun., 1981, 37, 421

131. (a) A J Epstein, E M Conwell, D J Sandman and J S Miller, Solid.State.Commun., 1977, 23, 355

(b) A J Epstein and E M Conwell, ibid., 1977, 24, 627

132. T Mori, F Sakai, G Saito and H Inokuchi, Chem.Lett., 1986, 1037

133. T Mori, F Sakai, G Saito and H Inokuchi, Chem.Lett., 1986, 1589

134. E Amberger, K Polborn and H Fuchs, Angew.Chem.Int.Ed.Engl., 1986, 25, 727, 729

135. J B Torrance, "Low Dimensional Conductors and Superconductors, NATO ASI Series, Series B: Physics", 1987, Vol 155, eds. D Jérôme and L G Caron, Plenum NY, pg 113

136. M J Rice, Solid.State.Commun., 1979, 31, 93

137. M J Rice, V M Yartsev and C S Jacobsen, Phys.Rev., 1980, B21, 3437

138. D Schweitzer, S Gärtner, H Grimm, E Gogu and H J Keller,

Solid.State.Commun., 1989, 69, 843

139. C Garrigou–Lagrange, S A Rozanski, M Kurmoo, F L Pratt, G Maceno, P Delhaes, M Lequan and R M Lequan, Solid.State.Commun., 1988, 67, 481

140. G Maceno, C Garrigou–Lagrange, P Delhaes, F Bechtel, G Bravic, J Gaultier, M Lequan and R M Lequan, Synth.Met., 1988, B57, 27

141. C Garrigou–Lagrange, A Graja, C Coulon and P Delhaes, J.Phys.C, 1984, 17, 5437

142. C B Duke, Ann.N.Y.Acad.Sci., 1978, 313, 166

143. M Meneghetti, R Bozio and C Pecile, J.de.Physique., 1986, 47, 1377

144. A Ugawa, G Ojima, K Yakushi and H Kuroda, Phys.Rev., 1988, B38, 5122

145. R Swietlik, D Schweitzer and H J Keller, Material.Science., in press

146. K Yakushi, H Kanbara, H Tajima, H Kuroda, G Saito and T Mori, Bull.Chem.Soc.Jpn., 1987, 60, 4251

147. V Zelezny, J Petzelt, R Swietlik, D Schweitzer and H J Keller, J.de.Physique., 1990, 51, 869

148. H Tajima, H Kanbara, K Yakushi, H Kuroda and G Saito, Solid.State.Commun., 1986, 57, 911

149. H Tajima, K Yakushi, H Kuroda and G Saito, Solid.State.Commun., 1985, 56, 159

150. J R Ferraro, H H Wang, U Geiser, A M Kini, M A Beno, J M Williams, S Hill, M.–H Whangbo and M Evain, Solid.State.Commun., 1988, 68, 917

151. T Sugano, H Hayashi and H Takenouchi, Phys.Rev., 1988, B37, 9100

152. M E Kozlov, K I Pokhodnia and A A Yurchenko, Spectrochim.Acta., 1987, 43, 323

153. M E Kozlov, K I Pokhodnia and A A Yurchenko, Spectrochim.Acta., in press

154. S Sugai and G Saito, Solid.State.Commun., 1986, 58, 759

155. R Zamboni et al, to be published

156. M J Rice, Phys.Rev.Lett., 1976, 37, 36

157. M J Rice, L Pietronero and P Brüesch, Solid.State.Commun., 1977, 21, 757

158. R Bozio, M Meneghetti and C Pecile, J.Chem.Phys., 1982, 76, 5785

159. R Zamboni, D Schweitzer and H J Keller, Solid.State.Commun., 1990, 73, 41

160. R Zamboni, D Schweitzer, H J Keller, C Taliani, Z.Naturforsch., 1989, 44a, 295

161. J R Ferraro, H H Wang, J Ryan and J M Williams, Appl.Spectr., 1987, 41, 1377

162. R Bozio, C Pecile, K Bechgaard, F Wudl and D Nalewajek, Solid.State.Commun., 1982, 41, 905

163. C S Jacobsen, D B Tanner and K Bechgaard, Phys.Rev., 1983, B28, 7019

164. R Bozio, I Zanon, A Girlando and C Pecile, J.Chem.Phys., 1979, 71, 2282

165. R Bozio and C Pecile, J.Phys.C., 1980, 13, 6205

166. M Meneghetti, R Bozio, I Zanon, C Pecile, C Ricotta and M Zanetti, J.Chem.Phys., 1984, 80, 6210

167. C B Duke, N O Lipari and L Pietronero, Chem.Phys.Lett., 1975, 30, 415

168. R Swietlik, D Schweitzer and H J Keller, Mat.Sci., 1988, 14, 39

169. C Garrigou–Lagrange, L Ouahab, D Grandjeau and P Delhaes, Synth.Met., 1990, 35, 9

170. R Bozio, A Girlando and C Pecile, Chem.Phys.Lett., 1977, 52, 502

171. A J Berlinsky, Y Hoyano and L Weiler, Chem.Phys.Lett., 1977, 45, 419

172. H Urayama, H Yamochi, G Saito, S Sato, A Kawamoto, J Tanaka, T Mori, Y Maruyama and H Inokuchi, Chem.Lett., 1988, 463

173. Y N Bosworth and R J H Clark, J.Chem.Soc.Chem Commun., 1975, 381

174. K Ichida, Y Kuroda, D Nakamara and M Kubo, Spectrochim.Acta., 1972, 28A, 2433

175. H G M Edwards, L A Woodward, M J Gall and M J Ware, Spectrochim.Acta., 1970, 26A, 287

176. P L Goggin and J Mink, J.Chem.Soc.Dalton Trans., 1974, 1479

177. P J Hendra, J.Chem.Soc.A, 1967, 1298; Spectrochim.Acta., 1967, 23A, 2871

178. P L Goggin, J.Chem.Soc.Dalton Trans., 1974, 1483

179. A Sabatini and L Sacconi, J.Am.Chem.Soc., 1964, 86, 17

180. T Mori and H Inokuchi, Solid.State.Commun., 1987, 62, 525

181. U Geiser, H H Wang, S Kleinjan and J M Williams, Mol.Cryst.Liq.Cryst., 1990, 181, 125

182. H Müller, H P Fritz, C.–P Heidmann, F Gross, H Veith, A Lerf, K Andres, H Fuchs, K Polborn and W Abriel, Synth.Met., 1988, 27, A257

183. J J Christensen, R M Izatt and D Eatough, Inorg.Chem., 1965, 4, 1278

184. C Mahon and D Britton, Inorg.Chem., 1971, 10, 586, 2331

185. P Pauling, Inorg.Chem., 1966, 5, 1498

186. J R Weisner, R C Srivastava, C H L Kennard, M.di Vaira and E C Lingafelter, Acta.Cryst., 1967, 23, 565

187. S Gärtner, I Heinen, D Schweitzer, B Nuber and H J Keller, Synth.Met., 1989, 31, 199

188. R D Braun and D C Green, J.Electroanal.Chem., 1977, 79, 381